Investigating the influence of retinal pigment epithelium on retinal function with a view to studying RPE cell transplantation.

Aisling Lynch

Institute of Ophthalmology

University College London

Submitted in part fulfilment for the degree of

Doctor of Physiology

Faculty of Brain Science

University College London

October 2017

I, Aisling Lynch, confirm that the work presented in this thesis is my own. Where information has been derived from other sources, I confirm that this has been indicated in the thesis.

Abstract

Age-related macular degeneration (AMD) is a debilitating disease and the leading cause of blindness in the developed world. It is a disease of the retinal pigment epithelium (RPE), the support cells for rods and cones. Currently there are no approved methods of treating the failing RPE, however, RPE transplantation is proving to be a promising therapy. The royal college of surgeons (RCS) rat has been extensively studied as a model for RPE transplantation, although, it does not model RPE death, as RPE remain intact in this disease model. In this thesis, I examine two alternative mouse models and their suitably for RPE transplantation. The first model uses sodium iodate to selectively kill off the RPE, which results in rapid retinal degeneration. Chemically removing the RPE frees Burch's membrane for donor RPE attachment. It was discovered that this model results in severe loss of outer-retinal photoreceptor function and function was unable to be restored with human embryonic stem cell-derived RPE (hESC-RPE) transplantation.

The second model is the *rd12* mouse, which has a mutation in *rpe65*, arresting the visual cycle. Thus, improvements in visual function would be specific to the visual cycle. This model, showed slow retinal degeneration and an ability for retinal function rescue with synthetic chromophore and hESC-RPE transplantation, though, no surviving grafted hESC-RPE were found in the retina. This study also examines the effects of RPE on melanopsin function. Melanopsin labelling and function was significantly reduced in *rd12* mice. It was shown that supplementing chromophore significantly restored the intrinsic pupillary light reflex (iPLR) in *rd12* and that this requires retina attached to the iris/ciliary body. Restoring *rpe65* gene function improves melanopsin function when the gene is

placed subretinally and expressed by the RPE and no effect is seen when the gene is placed intravitreally.

Impact Statement

This thesis introduces two alternative modes for examining RPE cell transplantation. The choice of retinal degenerative model used for studying RPE cell grafting has a large impact on what improvements in retinal function can be measured. This study draws attention to the benefits and difficulties with the $NaIO_3$ and *rd12* models for restoring retinal function. This will undoubtedly affect the choice of using these models in further studies and how they achieve the greatest functional recovery.

This study has also highlighted melanopsin function as an additional retinal readout. The discovery of this photoreceptor is relatively new, and so far, underutilised for the assessment of RPE function. This study has shown the reliance of the melanopsin system on the RPE visual cycle. It is an important retinal function and its restoration should be considered along with outer-retinal photoreceptors. It is hoped that this will encourage further studies to examine melanopsin function when ascertaining improvements in retinal function following RPE cell transplantation.

Determining the significance of the role of RPE on melanopsin function should impact patient care. Patients with AMD or a mutation affecting RPE function may have deficits in melanopsin function. This can leave the patient susceptible to a plethora of conditions such as seasonal affective disorder and disfunctions in their sleep/wake cycle and also it has been linked to cancer, obesity and mental illness.

Contents

List of Figures

List of tables

Publications arising from the work of this thesis

Poster Presentation: Characterisation of a mouse model for testing the efficacy of transplanted human RPE cells. Lynch A, Semo M, Aslan, J, Vugler A. Society for Neuroscience November 2016; 238.04

Poster Presentation: Chromophore acts on the retina to restore the intrinsic pupillary light reflex to isolated *rd12* mouse eyes. Society for Neuroscience November 2016; 240.24

Paper Presentation: RPE65 Fuels the intrinsic pupillary light reflex in mice. Lynch A, Sprogyte L, Semo M, Carr A J, Vugler A. ARVO May 2015; 1710. This talk was selected as a “hot topic”.

Glossary of abbreviations

AAV	Adeno-associated virus
ABCA4	ATP-binding cassette transporter A4
AMD	Age-related macular degeneration
ANOVA	Analysis of variance
BLA	Behavioural light aversion
BRB	Blood retinal barrier
Brn3b	Brain-specific homeobox 3b
cGMP	Cyclic guanosine monophosphate
CMZ	Ciliary marginal zone
CRALBP	Cellular retinaldehyde binding protein
CRBP	Cellular retinal binding protein
DA-AC	Dopaminergic amacrine cell
DMEM	Dulbecco’s modified eagle’s medium
DRS	DMEM cell re-suspension solution
EGF	Epidermal growth factor
ERG	Electroretinogram
FAK	Focal adhesion kinase
GABA	Gamma-aminobutyric acid
GAP	GTPase accelerating protein
GC	Guanylate cyclase
GCAP	Guanylate cyclase activating protein
GCL	Ganglion cell layer
GDP	Guanosine diphosphate
GTP	Guanosine triphosphate

GPCR	G-protein coupled receptor
hESC	Human embryonic stem cells
hESC-RPE	Human embryonic stem cell-derived RPE
HSC	Haematopoietic stem cells
iCa^{2+}	Intracellular calcium
INL	Inner nuclear layer
IP	Intraperitoneal
IPC	Interplexiform cell
IPL	Inner plexiform layer
ipRGC	Intrinsically photoresponsive retinal ganglion cell
iPSC	Induced pluripotent stem cells
iPSC-RPE	Induced pluripotent stem cell-derived RPE
IRBP	Inter-photoreceptor retinal-binding protein
IVT	Intravitreally
K^+	Potassium
LCA	Leber’s congenital amaurosis
LGN	Lateral geniculate nucleus
LRAT	Lectin retinol acyltransferase
MerTK	Mer proto-oncogene, tyrosine kinase
MFG-E8	Milk fat globule-EGF 8
M/L-opsin	Medium – long wavelength opsin
Na^+	Sodium ion
NDS	Normal donkey serum
ONL	Outer nuclear layer
OPL	Outer plexiform layer
OPN	Olivary pretectal nucleus

PACAP	Pituitary adenylate cyclase-activating polypeptide
PBS	Phosphate buffer saline
Pde6b	Phosphodiesterase 6B
PEDF	Pigment epithelium-derived factor
PFA	Paraformaldehyde
PIS	Photoreceptor inner-segments
PLR	Pupillary light reflex
PNA	Peanut agglutinin
POS	Photoreceptor outer-segments
PS	Phosphatidylserine
RBP-1	Retinol-binding protein 1
RCS	Royal college of surgeons
RDH	Retinal dehydrogenase
REH	Retinyl ester hydrolase
RGR	RPE-retinal G protein-coupled receptor
RGS9	Regulator of G-protein Signalling 9
RPE	Retinal pigment epithelium
RPE65	Retinal pigment epithelium-specific 65 kDa protein
SBR	Subretinally
SCID	Severe combined immunodeficiency
SCN	Suprachiasmatic nucleus
SNP	Single nucleotide polymorphism
S-opisn	Short wavelength opsin
TBS	Tris buffer saline
UV	Ultraviolet
VGLUT2	Vesicle glutamate transporter 2

WT	Wild type
ZT	Zeitgeber time

Chapter 1 Introduction

1.1 The Retina

1.1.1 Structure of the retina

The retina is a neuronal layer at the back of the eye, which absorbs and processes light (Figure 1.1). Photoreceptors are the cells that absorb light, two types of which, rods and cones lie at the back of the neural retina and are most important for image forming vision. They hyperpolarise in the presence of light. This signal is relayed via horizontal and bipolar cells in the inner nuclear layer, which carry out preliminary sorting and pooling of the visual signal. The inner nuclear layer contains horizontal cells, bipolar cells, amacrine cells and Müller glial cells. Horizontal cells and some amacrine cells are involved in lateral connections across the retina. Horizontal cells feedback information to both the photoreceptor and the bipolar cell. Amacrine cells are the most diverse cell type in the retina and feedback information to bipolar cells. Bipolar cells and amacrine cells send the photoreceptor signal on to the ganglion cell layer (GCL) via axons in the inner plexiform layer (IPL). Ganglion cells have long axons which lie at the vitreal aspect of the retina and send the signal to the brain via the optic nerve. A subset of the ganglion cells make-up the third photoreceptor type, called the intrinsically photosensitive retinal ganglion cells (ipRGC). Interplexiform cells (IPCs) are GABAergic neurons which provide feedback information from amacrine cells in the IPL to bipolar cell dendrites in the OPL (Kolb and West, 1977, Nakamura et al., 1980).

1.1.2 Pooling of signal

Pooling of the electrical signal allows for fewer axons sending information to the brain. The density ratio of rods to rod bipolar cells is roughly 10:1. Around 16-20 rods converge on one bipolar cell and average divergence is less than 2 bipolar cells (Freed et al., 1987). Ganglion cells collect excitatory inputs from several bipolar cells (Barlow, 1953), allowing for a high degree of convergence onto a single ganglion cell. The number of bipolar cells that converge to a ganglion cell depends on the ganglion cell receptive field. In addition to this, inhibitory interactions mediated by horizontal and amacrine cells also contribute to the structure of the receptive field by lateral interactions, which provide spatial information.

1.1.3 Centrifugal innervation

Information from the brain is also sent to the retina, these are called centrifugal innervations. Axons from the hypothalamus containing histamine enter the retina via the optic nerve, some run around the peripheral retina and terminate in the IPL, occasionally alongside retinal blood vessels and others circle the primate fovea in the optic fibre layer and appear to return to the optic disc (Gastinger et al., 1999). It is believed that these neurons play a circadian role, as their activity is highest in the morning. It has been shown that mouse dopaminergic amacrine cells (DA-AC) respond to histamine (Frazao et al., 2011). Dopaminergic processes have been shown to project to the GCL and to the OPL. Dopaminergic pre-synaptic terminals have been imaged next to horizonal cells in the OPL (Frederick et al., 1982) and ipRGCs in the GCL (Vugler et al., 2007b). It is

hypothesised that dopaminergic cells in the retina are involved in a feedback loop from the SCN and ipRGCs.

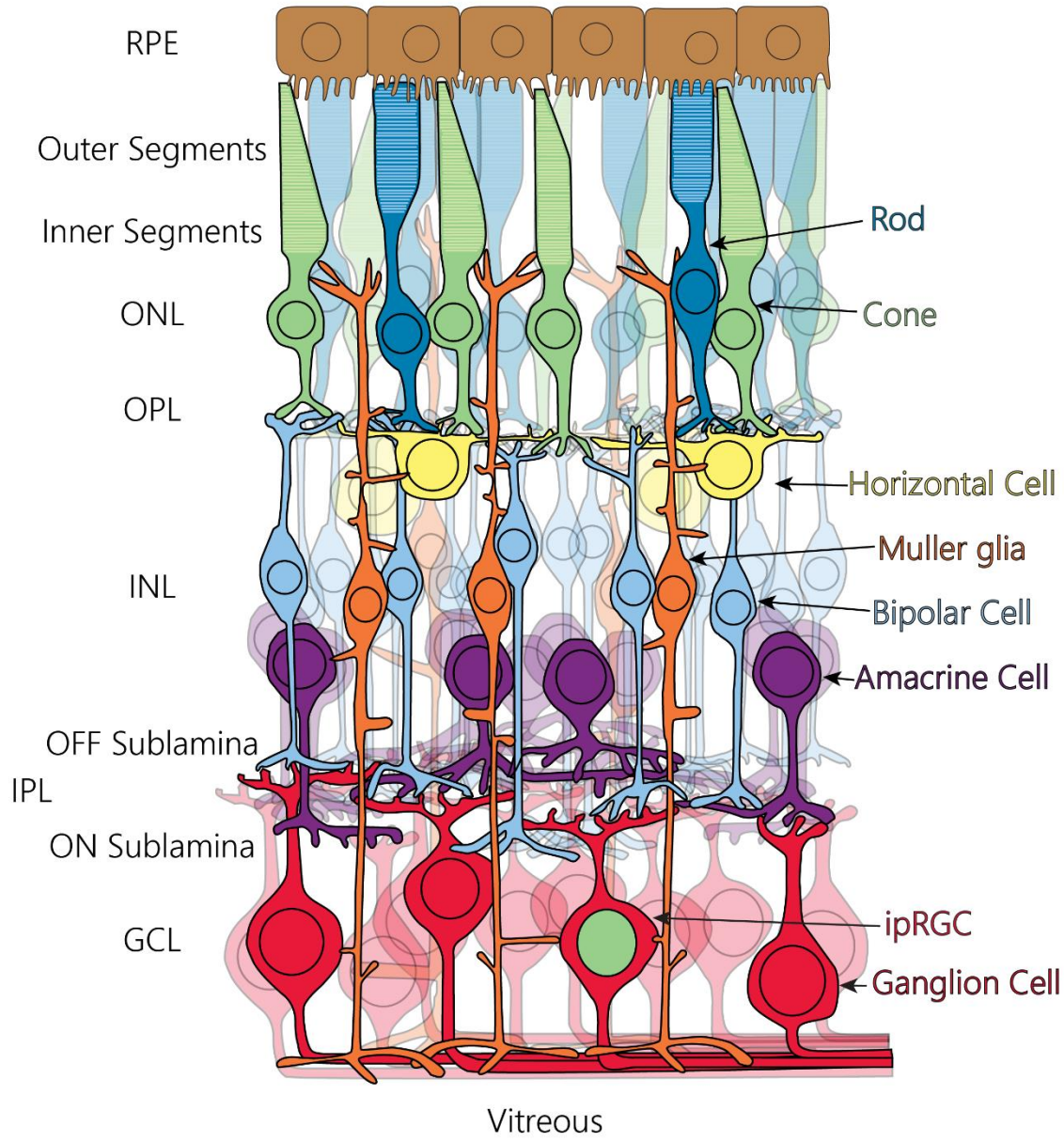

Figure 1.1 Layers of the retina
Rods and cones absorb light at the back of the neural retina. This signal is then sent to horizontal, bipolar and amacrine cells which sort and pool signals and send the signal to the ganglion cells. This layer of cells further pool and sort the signals and project the signal to the brain via the optic nerve. RPE: Retinal pigment epithelium; ONL: outer nuclear layer; OPL: outer plexiform cells; INL: inner nuclear layer: IPL: Inner plexiform layer; GCL: ganglion cell layer; ipRGC: intrinsically photosensitive retinal ganglion cell.

1.2 Phototransduction

1.2.1 In the dark

Phototransduction is the process in which light is absorbed by photoreceptors and converted into an electrical signal. In darkness, photoreceptors are depolarised, which is controlled by the flow of ion currents. There is an outward K^+ current through non-gated channels. There is a Na^+ influx through cyclic GMP (cGMP)-gated channels, depolarising the cell (Hagins et al., 1970). This inward current is made up mostly (~85%) of Na^+, as Na^+ is the predominant external cation, although Ca^{2+} and a small amount of Mg^{2+} also enter the non-selective channel (Chen et al., 2003). This is call the dark current and maintains the cell at around -40 mV. cGMP levels are high in darkness to maintain these open channels. This depolarisation opens voltage-gated calcium channels, resulting in increased intracellular calcium (iCa^{2+}), which causes glutamate release. Glutamate, though usually excitatory, inhibits the excitation of post-synaptic rod bipolar cells. In on-centre bipolar cells, glutamate binds to metabotropic glutamate receptors, causing cation channels to close and hyperpolarises the cell. In off-centre bipolar cells, glutamate binds to ionotropic glutamate receptors resulting in an inward current and depolarisation of the cell. To maintain an ionic balance an energy dependant pump in the photoreceptor inner segments (PIS) pumps out Na+ and pumps K+ into the cell. In the photoreceptor outer segments (POS), Ca2+ is exported by a Na+/Ca2+, K+ exchanger, which trades one Ca2+ and one K+ for four inward Na+ (Figure 1.2).

1.2.2 Illumination

The visual pigment consists of an opsin, which is a seven trans-membrane domain, with a chromophore, 11-cis retinal, that sits in the opsin and is located in disk outer-membranes. In darkness, 11-cis retinal acts as an inverse agonist to lock rhodopsin in an inactive state. The absorption of a photon isomerases 11-cis retinal to all-trans retinal, activating the photopigment by a conformational change to form metarhodopisn II. Metarhodopsin II is unstable and splits to form a free opsin and all-trans retinal. This is the start of the phototransduction cascade.

The opsin binds transducin, a G-protein heterotrimer and catalyses the exchange of guanosine triphosphate (GTP) for guanosine diphosphate (GDP) on the α-subunit (see Figure 1.2). The α-subunit now bound to GTP dissociates from the transducin photopigment complex, and binds to the inhibitory γ-subunit of cGMP phosphodiesterase (PDE) (Hurley and Stryer, 1982). The photopigment can now activate additional transducin molecules. PDE is anchored in the disk membrane by its α- and β-subunits (Baehr et al., 1979). Activated α-subunit-GTP-PDE complex hydrolyses cGMP resulting in cGMP-gated channels to close. These channels are responsible for cation influx (Hagins et al., 1970), thus their closure stops this influx. This causes rods and cones to hyperpolarise. Ca^{2+} is continually exported through the Na^{+}/Ca^{2+}, K^{+} exchanger. This lowers iCa^{2+} (Polans et al., 1996) and terminates the release of glutamate as it is required for glutamate vesicles to fuse with the cell membrane. Also, the increased levels of extracellular Na^{+} triggers the uptake of extracellular glutamate by RPE cells (Miyamoto and Del Monte, 1994). This loss of glutamate results in depolarisation of on-centre bipolar cells and hyperpolarisation of cone off-centre bipolar cells. Cones have a much faster photo-response and a quicker termination of phototransduction. This

rapid photo-response and recovery allows cones to detect a high temporal frequency achieved by faster clearance of Ca^{2+} as their channels are twice as permeable.

1.2.3 Amplification

Rods and cones have adapted this process to cover vision over nine orders of luminance magnitude. Rods have adapted to work well under dim light and bleach at high light intensities. The larger rod outer-segment, contains much more rhodopsin than opsin in cones, which allows a much higher sensitivity. Activation of a single rhodopsin molecule can activate 500 phosphodiesterase and hydrolyse 4×10^5 cGMP (Yee and Liebman, 1978). Activation of transducin is the first amplification step, where a single activated opsin can activate ~20 transducin molecules in mouse rods (Krispel et al., 2006, Leskov et al., 2000). In contrast to this, activation of PDE is not amplified, although, activated PDE has strong catalytic power and hydrolyses cGMP at a high rate. Thus rods can convert a single photon into an electrical response (Baylor et al., 1979), due to amplification in the phototransduction cascade and a longer photo-response. This sensitivity comes at a price of low temporal frequency. Cones, on the other hand, have a reduced amplification and thus are not sensitive to low light intensities (Tachibanaki et al., 2001).

1.2.4 Deactivation of the phototransduction cascade

Following light activation, the dark current is recovered by deactivation of the phototransduction cascade. This recovery requires inactivation of each of the activated component of the phototransduction cascade and re-opening of the cGMP-gated channels. Low iCa^{2+} play an important role in recovering from the

phototransduction cascade. The loss of iCa^{2+} causes Ca-recoverin-rhodopsin kinase to dissociate into Ca^{2+}, recoverin and rhodopsin kinase. Activated rhodopsin is phosphorylated by rhodopsin kinase (GRK1), which partially supresses the activity of the active rhodopsin. Arrestin then binds to the phosphorylated rhodopsin stopping any residual activity (Wilden et al., 1986, Kuhn and Wilden, 1987).

Reduced iCa^{2+} also enables deactivation of transducin. Ca^{2+} is also bound to a GTPase accelerating protein (GAP), regulator of g protein signalling 9 (RGS9). With low iCa^{2+}, RGS9 is dissociated and interacts with the α-subunit of transducin causing it to hydrolyse GTP to GDP. In rods, the recovery kinetics of transducin is 2.5 times slower than active rhodopsin (Krispel et al., 2006), thus, the recovery of transducin determines the recovery kinetics of a single photon. RGS9 is more plentiful in cones (Cowan et al., 1998, Zhang et al., 2003), and allows for faster recovery. The dissociation of transducin α-subunits results in the inactivation of α-subunit-GTP-PDE complex, stopping the hydrolysis of cGMP.

Low iCa^{2+} also results in the re-opening of cGMP-gated channels. Guanylate cyclase activating protein (GCAP) is a Ca-binding protein and as iCa^{2+} levels decrease, GCAP dissociates from Ca^{2+} and interacts with guanylate cyclase (GC) to activate it. GC then transforms GTP to cGMP, replenishing the cGMP levels needed for opening the cGMP-gated channels and the restoration of the dark current (Figure 1.2). Also, the low iCa^{2+} increases the sensitivity of the cGMP-gated channels via the Ca^{2+}-calmodulin complex in the cGMP-gated channels, thus, opening the channels in low cGMP levels (Hsu and Molday, 1993).

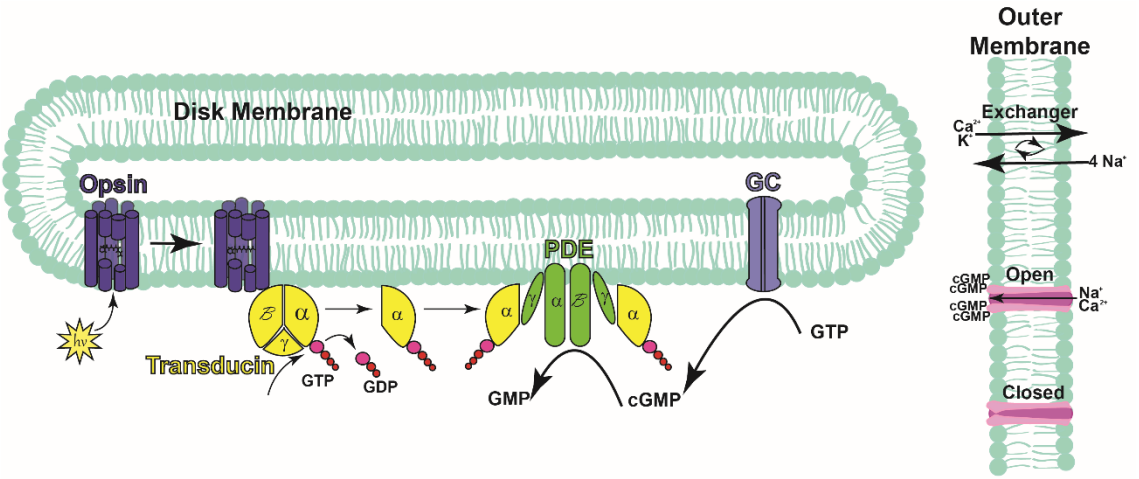

Figure 1.2 Phototransduction Cascade.
A photon (hv) is absorbed by opsin, in the disk membrane, containing 11-cis retinal, which changes to all-trans retinal once activated by light. Activated opsin binds transducin, and dissociates from GDP and binds GTP. The α-subunit and GTP complex dissociates and binds to the γ-subunit of PDE, forming a complex that hydrolyses cGMP to a non-cyclic form, GMP. The loss of cGMP causes cGMP-gated channels in the outer membrane to close, stopping the influx of Na^+ ions, causing rods and cones to hyperpolarise and signal to cells in the INL. During the light phase, Ca^{2+} is continually pumped out and lowers the iCa^{2+}. The loss of iCa^{2+} feeds back negatively and results in the activation of GC which transforms GTP to cGMP, replenishing the cGMP levels to re-open the cGMP-gated channels restoring the dark current. Image modified from (Leskov et al., 2000).

1.2.5 Light adaptation

The human eye functions from dim to very bright light levels, spanning nine orders of magnitude. Yet, at any given moment, contrast ratio can only distinguish around 3 orders of magnitude. Thus, an adaptation occurs at the level of the retina adjusting to a new definition of what is black, to the surrounding visual environment. It can take 20-30 minutes for the eye to fully adapt to darkness and around 5 minutes to adapt to bright sunlight. Cones operate at higher light intensities than rods and can differentiate between wavelengths, allows for colour vision at light levels within the cone sensitivity.

A major player in light adaptation is the recycling of chromophore. Chromophore is required for the detection of light, and following light detection all-*trans* retinal

is transported to the RPE for recycling into the usable form of 11-*cis* retinal. This process of using up available 11-*cis* retinal is called bleaching. Along with faster phototransduction and recovery, cones have also been shown to have an alternative source of regenerated chromophore, allowing for a faster recovery of bleached opsin (Goldstein and Wolf, 1973).

Modifications to the elements in the phototransduction cascade also lead to light adaptation. In darkness, transducin α- and β-subunits are found predominantly in rod outer-segments, but translocate to the PIS and the INL under bright light (Kassai et al., 2005, Sokolov et al., 2002). It is thought that this translocation process protects rods under bright light conditions and also contributes to light adaptation in rods (Elias et al., 2004). Cone transducin α-subunit was not found to translocate (Coleman and Semple-Rowland, 2005, Elias et al., 2004), except, at much higher light levels (Chen et al., 2007). This may be due in part to the different transducin subtypes found in rods and cones (Fung et al., 1992, Lee et al., 1992).

The reduction of iCa^{2+} under illumination, triggers negative feedback and contributes to light adaptation. Low iCa^{2+} helps photoreceptors recover from the phototransduction cascade and also increases the sensitivity of the cGMP-gated channels, resulting in the activated α-subunit-GTP-PDE complex being required to hydrolys more cGMP to achieve closed cGMP-gated channels (Hsu and Molday, 1993).

1.2.6 Colour Vision

There are three cone types in humans L-, M- and S-cones, named by the wavelength of light that they are more sensitive to: long (565 nm), medium (545 nm) and short (440 nm) wavelengths. The human and old world primate fovea is

rich in M- and L- cones. Blue cones compose of less than 6% of the total primate cone population (Roorda et al., 2001) and are absent from the fovea, limiting the resolution to outside 20-30 degrees of eccentricity (Curcio et al., 1991). A large proportion of short-wavelength light is filtered out by the cornea and lens before reaching the retina, diminishing the contribution of blue cones for human vision. In the mouse retina, cones make up about 3% of the outer-retinal photoreceptor population (Carter-Dawson and LaVail, 1979, Jeon et al., 1998). Most new world primates and non-primate mammals do not have a gene for L-opsin and are dichromatic (Dulai et al., 1999). S- and M- opsin in rodents have a maximum spectral sensitivity at 359 nm and 510 nm, respectively (Applebury et al., 2000, Jacobs et al., 1991).

1.3 Electroretinogram

The electrogram (ERG) is a method of measuring retinal function. It gives a reading of the electrical wave that is sent through the retina, from the photoreceptors to the nerve fibres, due to the absorption of light. It is used to diagnose abnormalities in the retinal signalling. It is non-invasive, making it extremely useful for reporting measurements that evaluate changes in progressive disease forms. It is amendable for use in a wide range of species, including humans, and as such bridges human clinical evaluations and animal models of retinal disease. The earliest age at which ERG photoresponses can be measured reproducibly in mice is 3 weeks (Pang et al., 2006). An ERG is made up of different components, first described by Granit in 1933 (Granit, 1933). The two main components studied in this thesis are the a- and the b-wave (Figure 1.3).

1.3.1 The a-wave

The a-wave is an initial fast negative wave, representing a light-evoked hyperpolarisation of the rod membranes (Brown, 1968, Heynen and van Norren, 1985, Hood and Birch, 1990, Hood and Birch, 1995). The latency of the a-wave is measured from the light onset to the peak of the a-wave. Rodents under photopic conditions do not usually produce an a-wave, due to small cone counts.

1.3.2 The b-wave

The b-wave is a large positive wave that follows the a-wave. It is created by depolarisation of cells in the inner retina. Its generation is from the input of many neurons, including Müller cell processes (Miller and Dowling, 1970, Xu and Karwoski, 1994). The amplitude of the b-wave is measured from the trough of the a-wave to the peak of the b-wave. The implicit time of the b-wave is a measurement taken from the flash of light onset to the peak of the b-wave.

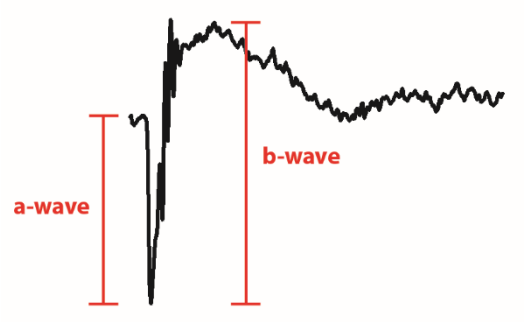

Figure 1.3 Scotopic ERG waveform
The a-wave is a rapid negative wave, representing the hyperpolarisation of rod membranes. This is followed by the positive b-wave, representing the depolarisation of cells in the inner retina.

1.4 Retinal pigment epithelium

The RPE is a monolayer of pigmented epithelial cells, which lie in the outer-retina adjacent to POS and acts as a support cell for outer-retinal photoreceptors. It has

a neuroectodermal origin and is therefore considered to be part of the retina. RPE cells have an apical and basal polarisation. The basal membrane is a component of Bruch's membrane and interacts with the choroid. The apical membrane has large microvilli, which extend to surround the photoreceptor outer-segments (POS). This is important to facilitate close communication between RPE cells and photoreceptors to optimise the RPE's functions that enhance photoreceptor performance (Figure 1.4).

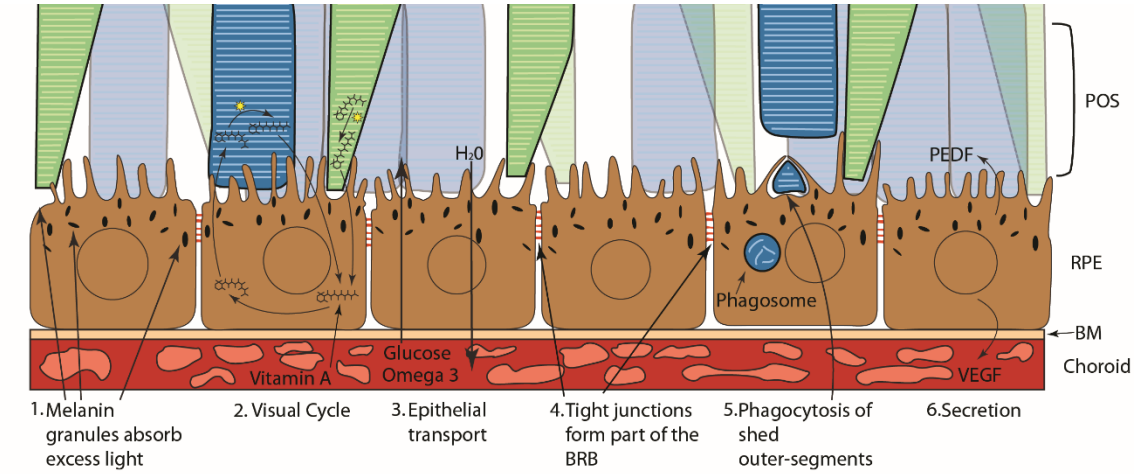

Figure 1.4 Functions of the RPE.
The RPE has many functions which are necessary for vision and maintaining retinal health. 1) Melanin granules in the RPE give the RPE their dark colour and absorb excess light preventing light scatter. 2) Vitamin A is sourced from the diet, converted to 11-cis retinal by the RPE and transported to photoreceptors for phototransduction. Absorption of light causes 11-cis retinal to be converted to all-trans retinal and transported back to the RPE where it is recycled to 11-cis retinal for phototransduction. 3) The RPE selectively takes up glucose and nutrients and transport them to the photoreceptors and pumps out water and ions to the choroid to maintain visual clarity. 4) Tight junctions make diffusion between cells difficult and contribute to the blood retinal barrier (BRB). 5) Rods and cones shed the tip of their outer-segments daily which are phagocytosed and digested by the RPE. 6) The RPE produces and secretes growth factors, including PEDF into the retina and VEGF into the choroid.

1.4.1 Blood retinal barrier

Blood is supplied to the photoreceptors by the choroid, which is separated from the retina by the RPE (Tornquist et al., 1990). The RPE acts as part of the blood retinal barrier (BRB) preventing blood leaking and the infiltration of immune cells,

and controlling the transport across the barrier. RPE cells have tight junctions on their lateral side, connected to neighbouring RPE cells, making diffusion between cells difficult. This tightly controlled barrier facilitates the immune privilege status of the eye.

1.4.2 Transport Epithelium

The RPE selectively takes up nutrients such as glucose, ascorbic acid and fatty acids from the blood and transports these nutrients to the photoreceptors. To transfer glucose, the RPE contains many glucose transporters on both the apical and basolateral membranes. Omega-3 fatty acid is transported because it is required for membrane structure of neurons but cannot be synthesised by neural tissue.

The RPE transports ions and water out of the retina. A large volume of water is produced in the retina and intraocular pressure leads to a movement of water from the vitreous towards the retina (Moseley et al., 1984). Müller cells are thought to transport water through the retina (Nagelhus et al., 1999), which is pumped out of the retina by the RPE. Na^+-K^+-ATPase is located on the apical membrane and provides the energy for this transepithelial transport (Ostwald and Steinberg, 1980). This flow of water acts as an adhesion force between the neural retina and the RPE. Maintaining the retina in a proper state of hydration is also important for visual clarity.

1.4.3 Excess light absorption

The retina is exposed to high levels of light throughout the day and can lead to photo-oxidative reactions, which can be toxic to neural cells. The RPE contains many melanin granules, which give it the dark colour. These pigments absorb

excess light. This, not only protects the neural retina, but also the absorption of excess light provides clearer vision by preventing light scatter.
The RPE also contains high levels of antioxidants, which counterbalance the high oxidative stress in the retina created by its high oxygen consumption.

1.4.4 Secretion

The RPE produces and secrets a variety of growth factors into the retina or choroid. Pigment endothelium-derived factor (PEDF) is secreted into the neural retina, which inhibits the growth of blood vessels and prevents apoptosis (Cayouette et al., 1999). Vascular endothelial growth factor (VEGF) is secreted basally (Adamis et al., 1993). It prevents endothelial cell apoptosis and acts as a permeability factor stabilising the fenestrations of the endothelium (Roberts and Palade, 1995).

1.4.5 Shedding of outer-segments

Rods and cones have a very high metabolic rate and accumulate toxic photo-oxidative compounds due to the high light exposure. Thus, rods and cones renew their outer-segments continually (Young, 1967, Young and Droz, 1968). Photoreceptors synthesise new outer-segment disks at the base of the POS and the oldest disks at the tip of the POS are shed daily and phagocytosed by the RPE (Young and Bok, 1969). The shedding and phagocytosing of POS is controlled by both light and circadian rhythm (Goldman et al., 1980, LaVail, 1980). Rod outer-segments are shed at light onset (LaVail, 1976), while the timing of cone outer-segment shedding varies by species. In nocturnal rodents, cones undergo POS shedding at lights on (Bobu and Hicks, 2009), while gold fish, chick

and squirrel cones shed their POS early in the dark phase (O'Day and Young, 1978, Young, 1978, Long et al., 1986).

RPE cells phagocytose more material over a lifetime than any other cell type in the body. There are three stages to this phagocytic process: recognition, internalisation and digestion of shed POS (Figure 1.5). It is understood that these processes are like those observed in macrophages.

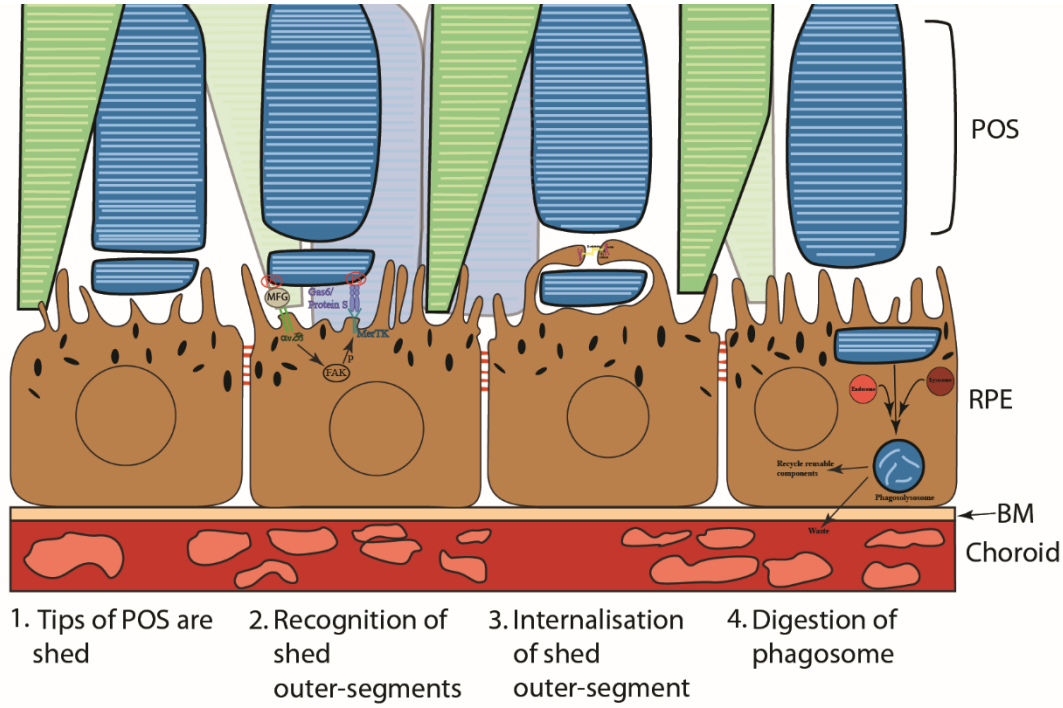

Figure 1.5 Shedding of POS
Rods and cones shed the tip of their outer-segments diurnally (1). The exposed plasma membrane is recognised by the apical microvilli (2). The shed outer-segment is engulfed by the apical appendages, which form around it (3). The phagocytosed outer-segment becomes fused with endosomes and lysosomes which break down the contents (4). Waste is excreted to the choroid and re-usable contents are recycled.

Recognition of shed outer-segment

Shed POS are identified by the disruption of the plasma membrane. In an intact plasma membrane, phospholipids containing terminal primary amino groups, such as phosphatidylserine (PS), are localised in to the cytoplasmic surface (Figure 1.6). After disruption of the plasma membrane, PS becomes exposed

extracellularly, allowing for recognition of shed outer-segment (Fadok et al., 2001). PS interacts with secreted binding proteins, milk fat globule-EGF 8 (MFG-E8) (Hanayama et al., 2002), growth arrest-specific gene 6 (Gas6), (Hall et al., 2001, Nagata et al., 1996, Nakano et al., 1997) and protein S (Hall et al., 2005). MFG-E8 interacts with integrin αvβ5, and Gas6 and protein S are ligands for MerTK on RPE cells (Finnemann et al., 1997, Nandrot et al., 2004). The binding of the MFG-E8 to avβ5 mobilises a pool of focal adhesion kinase (FAK), to the apical RPE and triggers autophosphorylation. This then causes MerTK phosphorylation (Finnemann, 2003).

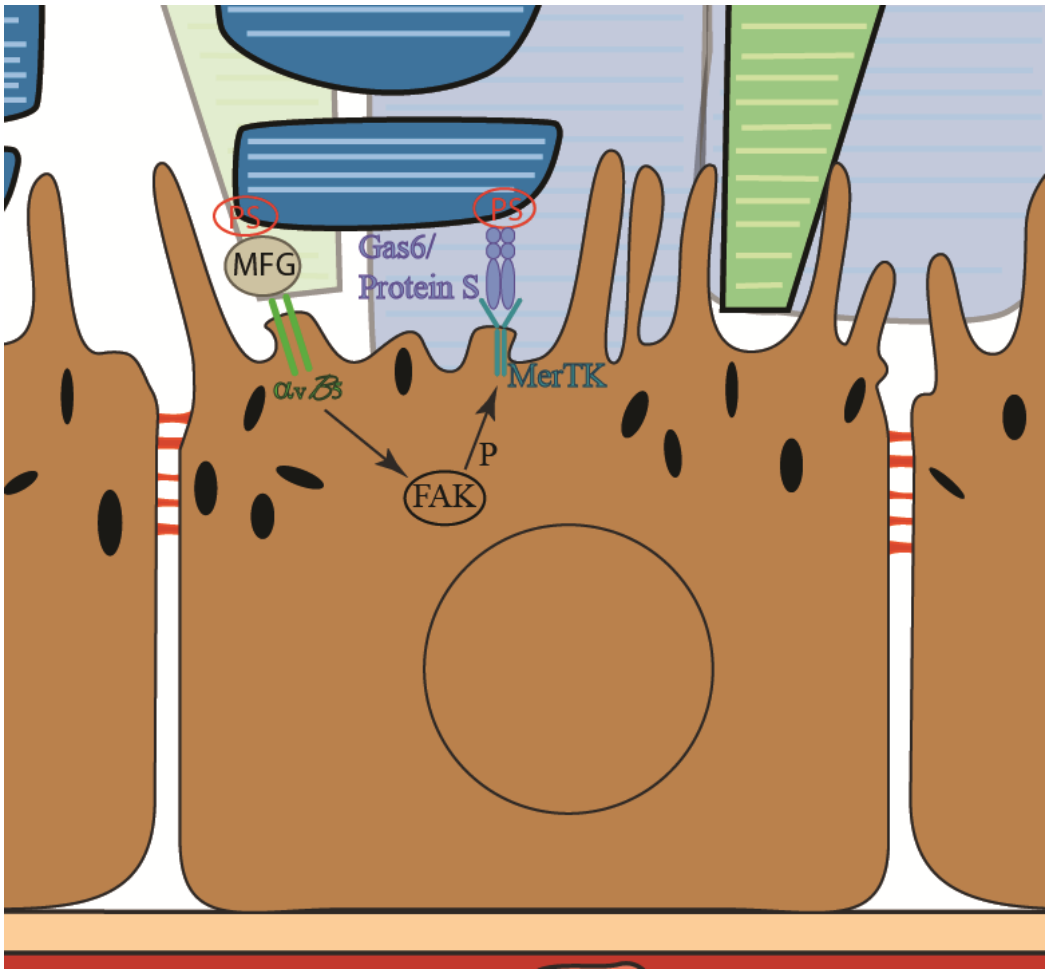

Figure 1.6 Recognition of shed outer-segments
The exposure of phospholipids such as PS, following the disruption of the plasma membrane are recognised by secreted binding proteins MFG-E8 (MFG), Gas6 and protein S. MFG interacts with integrin αvβ5 on RPE. Gas6 and protein S interact with MerTK on RPE. The activation of αvβ5 mobilises a pool of FAK which phosphorylates MerTK. This initiates the internalisation of the shed outer-segment.

Internalisation of shed outer-segment

MerTK phosphorylation then initiates internalisation of shed POS by mobilising myosin II from the RPE periphery and re-arranges the cytoskeleton (Strick et al., 2009). The cytoskeleton re-arrangement forms pseudopods which engulf the shed outer-segment and must fuse together around it (Figure 1.7). Cadherins are a class of membrane-bound protein which bind to other cadherins on adjacent membranes, forming adherens junctions (Hulpiau and van Roy, 2009). Catenins are another class of protein which lie on the cytoplasmic end of cadherins and form a protein complex with the actin cytoskeleton (Ozawa et al., 1989). The reorganisation of actin results in the formation of mature adherens junctions and fusion of the two membranes. This has not been demonstrated in RPE cells, still, it is the most likely approach to engulfing the shed POS.

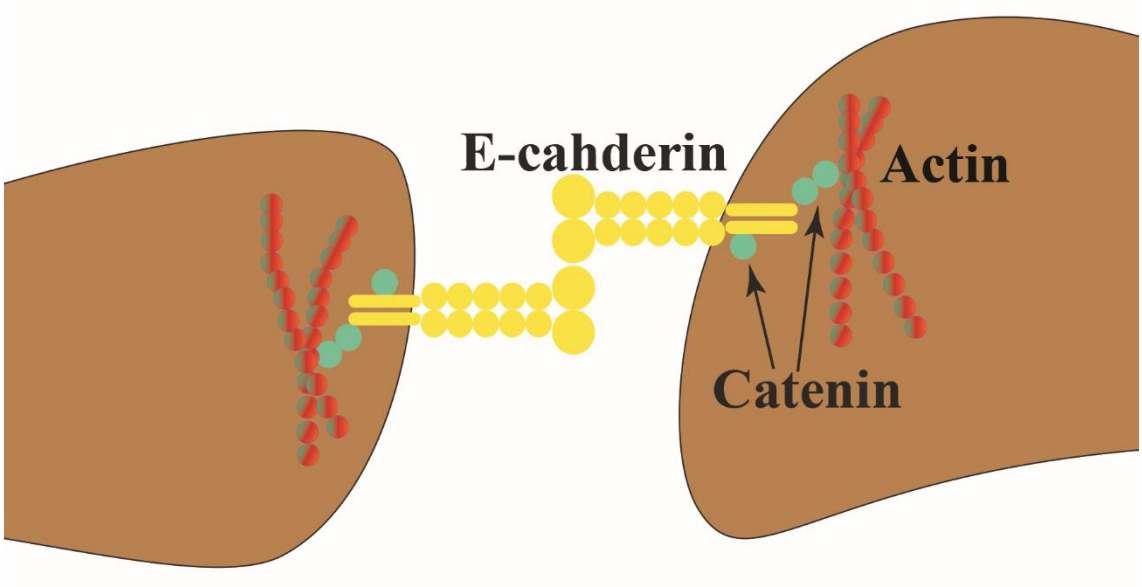

Figure 1.7 Joining of pseudopods.
Pseudopods engulf the shed outer-segment and fuse together around it. Membrane-bound cadherins bind to cadherins on adjacent membranes. Catenins lie on the cytoplasmic side of the membrane and form a complex with cadherins and actin to form a mature adherens junction and result in the fusion of the two membranes.

Once engulfed, the phagosome fuses with endosomes and lysosomes to form a phagolysosome, breaking down the contents and recycling re-usable components and removing waste to the choroid (Figure 1.8).

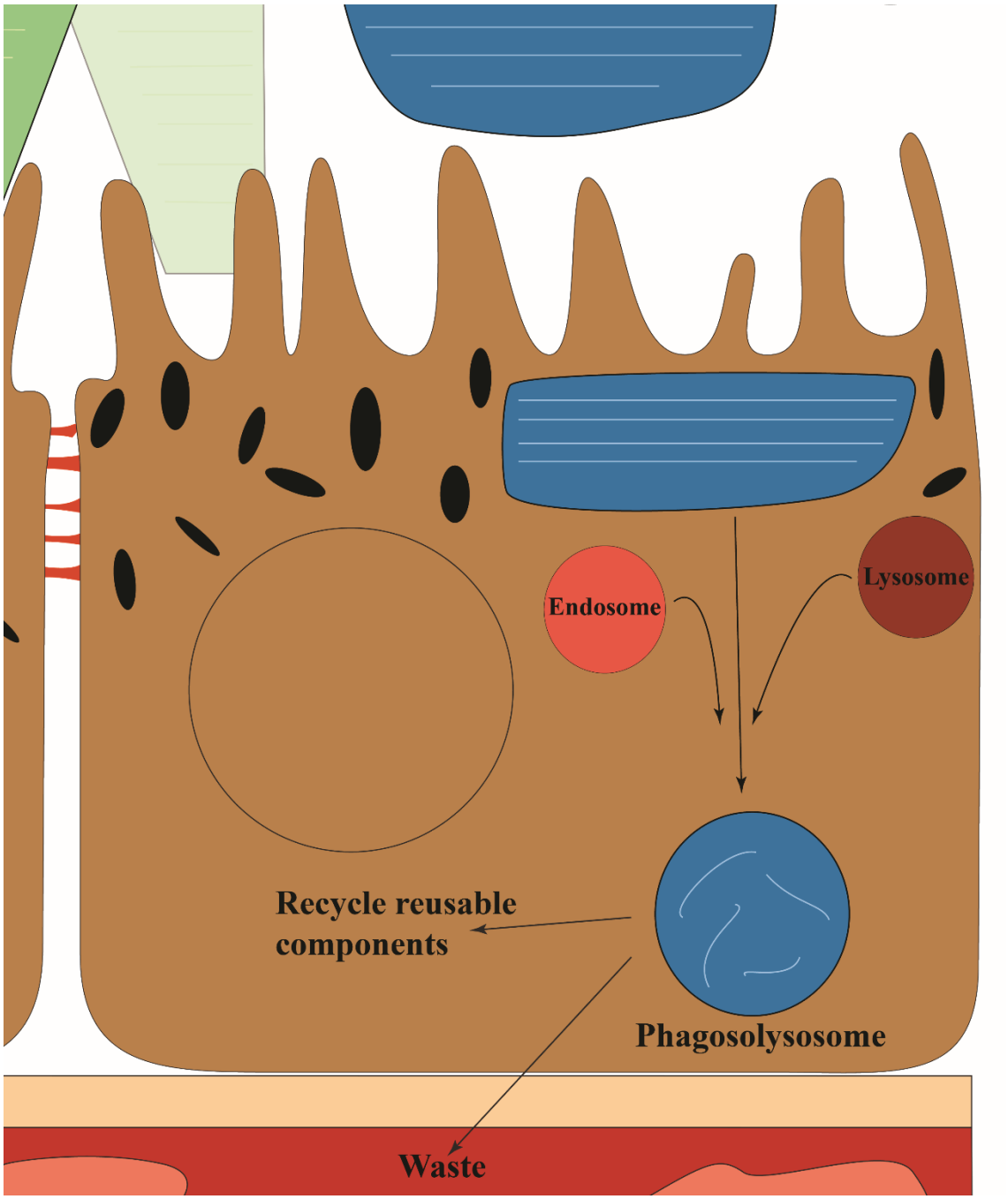

Figure 1.8 Digestion of phagosome.
The phagosome fuses with endosomes and lysosomes to form a phagolysosome. Useful components are recycled and waste is excreted to the choroid for clearance.

1.4.6 The visual cycle

The RPE plays a crucial role in vision by recycling vitamin A (all-*trans*-retinol) to 11-*cis* retinal, which when combined with opsin forms the visual pigment in photoreceptors. All-*trans*-retinol is sourced from the diet transported to the RPE via the choroid. Here, it binds to cellular retinal binding protein (CRBP) and becomes esterfied by lecithin retinol acyltransferase (LRAT) to all-*trans*-retinyl ester (Figure 1.9). This is then hydrolysed and isomerised by retinal pigment epithelium-specific protein 65 KDa (RPE65) (Redmond et al., 1998) to form 11-*cis*-retinol. This then binds to cellular retinaldehyde binding protein (CRALBP) where it can be stored to allow a quick conversion from dark to light phase or it can be oxidised by 11-*cis* retinal dehydrogenase to form 11-*cis* retinal. 11-*cis* retinal is transported to the rods and cones via inter-photoreceptor retinal-binding protein (IRBP). In the photoreceptor, 11-*cis*-retinal sits in the opsin to form the visual pigment. Upon illumination, 11-*cis*-retinal changes to all-*trans*-retinal and is then reduced by retinal dehydrogenase (RDH) to form all-*trans*-retinol, at which point is transported back to the RPE via IRBP for recycling.

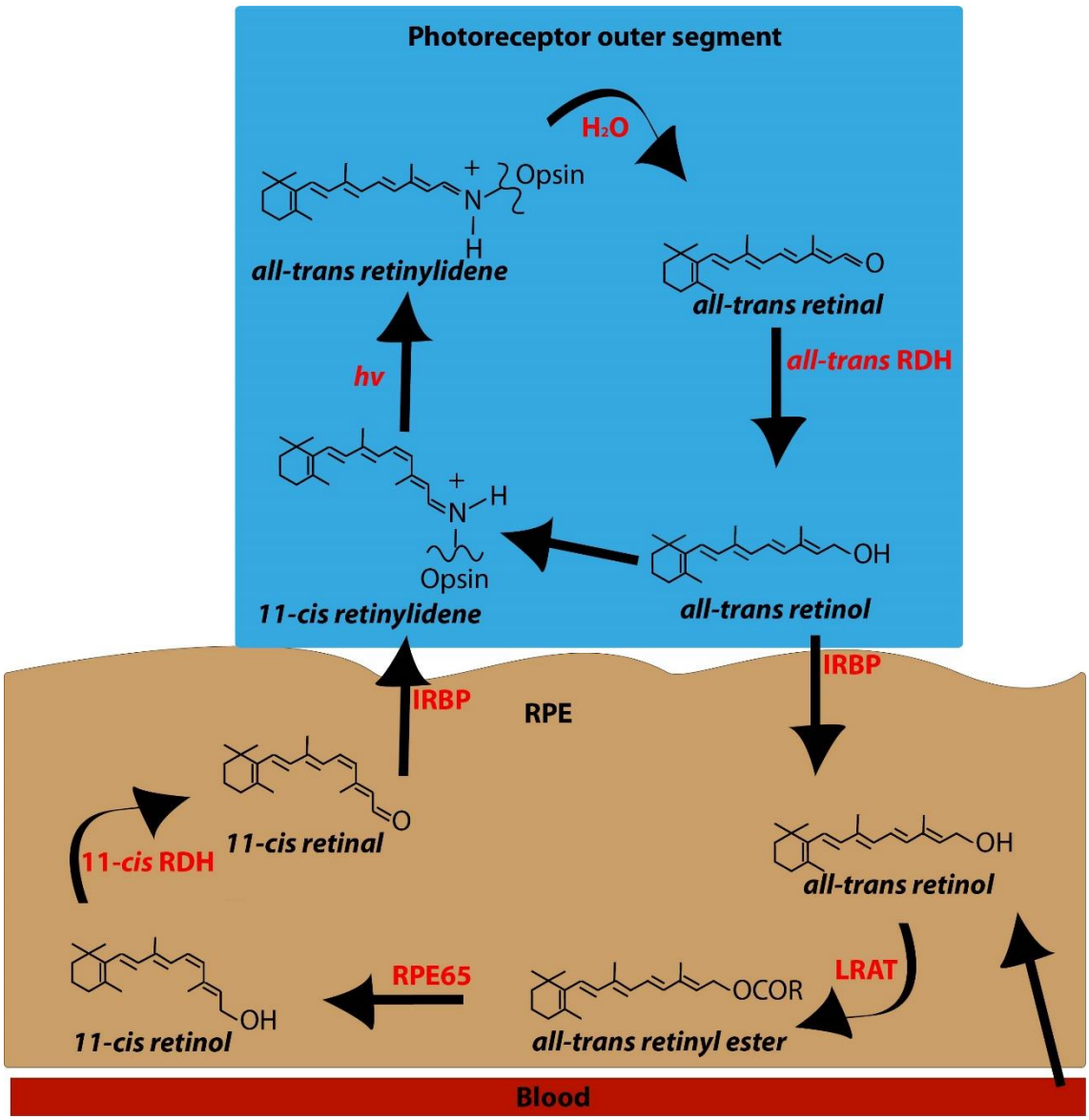

Figure 1.9 The Visual Cycle
All-trans retinol enters the RPE from the choroid blood supply and becomes esterified by LRAT to form all-trans retinyl ester. It then undergoes hydrolysis and isomerisation by RPE65 to form 11-cis retinol. 11-cis retinol can then be oxidised by 11-cis dehydrogenase to become 11-cis retinal and can now enter the photoreceptor via IRBP where it is taken up by a vacant opsin forming 11-cis retinylidene. Upon illumination, a photon (hv) is absorbed by the opsin-chromophore complex resulting in a conformational change, and converting the 11-cis retinylidene to all-trans retinylidene and activating transducin, which initiates the phototransduction cascade. The chromophore is then released from the opsin by hydrolysis and is then reduced by RDH forming all-trans retinol which can then be transported back to the RPE via IRBP for recycling.

This visual cycle between photoreceptor cells and the RPE is not the complete story as M- and L-cone opsin can be regenerated in isolated retina (Goldstein and Wolf, 1973). One possible mechanism is provided by Müller cell's ability to

produce 11-*cis*-retinol (Das et al., 1992, Fleisch and Neuhauss, 2010). This may be necessary to compete with the high turnover of chromophore in cones. RPE65, the enzyme responsible for hydrolysing and isomerising all-*trans* retinal ester to 11-*cis* retinol (Jin et al., 2005, Moiseyev et al., 2005, Redmond et al., 2005) has been reported in L- and M-cones but not in S-cones, rods nor Müller glia (Znoiko et al., 2002, Tang et al., 2011, Ma et al., 1998). Rods are very sensitive and can respond from absorbing just one photon (Baylor et al., 1979), while cones need a lot of chromophore activation to elicit a response (Ingram et al., 2016). It has been proposed that RPE65 acts as a retinoid binding protein to stabilise 11-*cis* retinol and shuttles it along the M- and L-cone outer-segments (Tang et al., 2011).

It has also been discovered that rods, but not cones, can function without REP65 in mice, albeit at higher luminosity (Seeliger et al., 2001). *Rpe65*$^{-/-}$ mice have a small but robust visual response in photopic conditions, which is now known to be rod generated. Comparing ERG or optokinetic responses shows that visual responses for *rpe65*$^{-/-}$ mice and *rpe65*$^{-/-}$*Cnga3*$^{-/-}$ (also knocking out cone function), mice are comparable. While, also knocking out rod function (*rpe65*$^{-/-}$*rho*$^{-/-}$) resulted in no detectable response (Cachafeiro et al., 2010, Seeliger et al., 2001). The lack of RPE65 is thought to enable rods to respond under conditions that would normally bleach rods, due to the decreased sensitivity of rods with limited chromophore. It has been discovered through spectral absorbance that the visual pigment in *rpe65*$^{-/-}$ mice is isorhodopsin. This uses 9-*cis* retinal as it's chromophore supported by 9-*cis* retinal found in dark-reared *rpe65*$^{-/-}$ mice. It was not possible to determine if these levels are also present in wild type (WT) mice reared under normal light dark cycles (Fan et al., 2003).

RPE65

RPE65 is necessary for converting all-*trans* to 11-*cis* retinal, established through *rpe65*$^{-/-}$ mouse where 11-*cis* retinal was absent and all-*trans* retinyl-esters accumulated (Redmond et al., 1998). In rodents, *rpe65* mRNA is first detected at E18, while protein levels become detectable at P4, this accumulates gradually until P12, when it reaches steady state levels (Manes et al., 1998). *Rpe65* has a daily cyclic expression, with mRNA peaking at ZT14 (2 hours after lights off) in the chick retina (Bailey et al., 2004). In contrast to this, as rodents are nocturnal, the rat cyclic expression of *rpe65* mRNA peaks at lights on (Beatrice et al., 2003). Mutations in *rpe65* can result in many retinal degenerative diseases, such as retinitis pigmentosa and Leber's congenital amaurosis (LCA) (Morimura et al., 1998, Marlhens et al., 1997).

LRAT

LRAT is another enzyme in the visual cycle, which catalyses the esterification of all-*trans* retinol into all-*trans* retinyl ester. Mutations in LRAT are responsible for a small percentage of LCA cases (Sweeney et al., 2007). The phenotype of patients with mutations in LRAT is similar to that of patients with mutations in *rpe65* (Fan et al., 2008, Senechal et al., 2006).

RGR

RPE-retinal G protein-coupled receptor (RGR) is an opsin which is a member of the rhodopsin-like receptor subfamily of GPCR. RGR is expressed in the RPE and Müller glia (Jiang et al., 1993). After all-*trans*-retinol is esterfied by LRAT to form all-*trans*-retinyl ester, it is either stored in lipid droplets or goes to a smaller isomerase pool to continue the visual cycle via RPE65. All-*trans*-retinyl esters in

the storage pool can be hydrolysed by all-*trans*-retinyl ester hydrolase to re-form all-*trans*-retinol and re-enter the visual cycle (Figure 1.10). In the dark, RGR contains all-*trans*-retinal (Hao and Fong, 1999) and inhibits all-trans-retinyl ester hydrolase and partially inhibits LRAT promoting all-*trans*-retinyl ester storage. Upon light exposure, all-*trans*-retinal is isomerised to 11-cis-retinal and RGR no longer inhibits all-*trans*-retinyl ester hydrolase or LRAT (Radu et al., 2008). Thus, all-*trans*-retinyl ester hydrolase can hydrolyse all-*trans*-retinal esters to all-*trans*-retinol which then enters the visual cycle and is re-esterfied by LRAT to form all-*trans*-retinal ester and converted by RPE65 to 11-*cis*-retinol. This is then subsequently oxidised by 11-*cis*-retinal dehydrogenase to form 11-*cis*-retinal which is taken up by photoreceptor opsins to detect light. RGR has also been associated with retinitis pigmentosa (Bernal et al., 2003, Morimura et al., 1999).

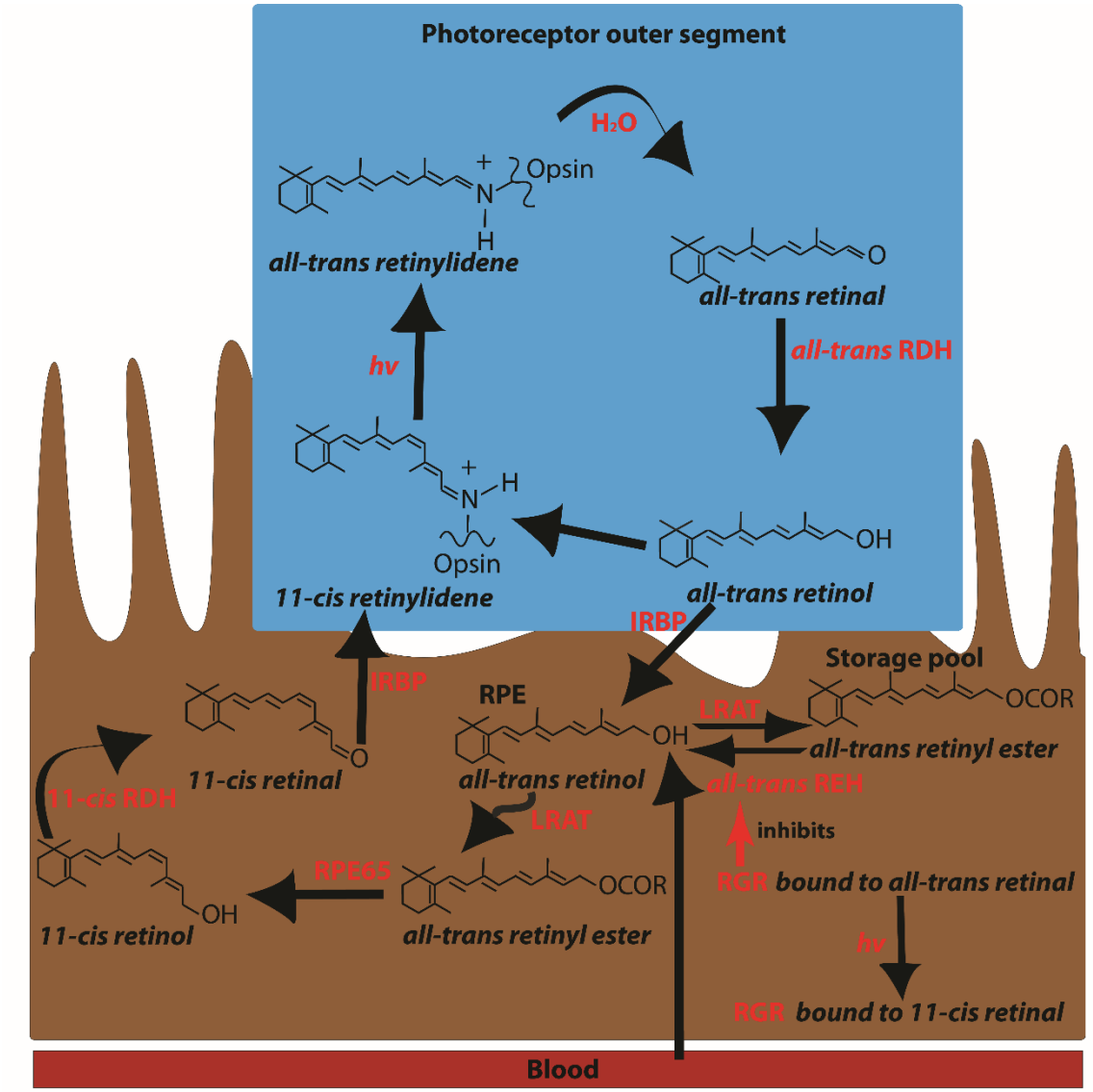

Figure 1.10 RGR is an opsin that controls the visual cycle.
All-trans retinol is taken up by the RPE and becomes esterified by LRAT to form all-trans retinyl ester. This then either becomes hydrolysed and isomerised by RPE65 and continues with the visual cycle or it becomes stored in lipid droplets. In the dark, RGR is bound to all-trans retinal and strongly inhibits all-trans retinyl ester hydrolase (REH), which is needed to release all-trans retinyl ester from the storage pool. RGR-all-trans retinal also partially inhibits LRAT but promotes the storage of all-trans retinyl esters. Upon illumination (hv), RGR-all-trans retinal absorbs a photon which isomerises all-trans retinal to 11-cis retinal stopping the inhibitory action of RGR. This accelerates the hydrolysis and release of all-trans retinly esters from the storage pool by all-trans retinyl ester hydrolase to form all-trans retinol. This is then re-esterfied by LRAT and released into a smaller pool which feeds into the visual cycle.

IRBP

IRBP, also known as retinal binding protein 3 (RBP3), is found in the inter-photoreceptor matrix between outer-retinal photoreceptors and the RPE. It is a

large glycoprotein synthesised by photoreceptors. It transports 11-*cis*-retinal from the RPE to the outer-retinal photoreceptors for phototransduction and IRBP transports all-*trans*-retinol back to the RPE following photon absorption (Liou et al., 1982). IRBP is also important for fatty acid transport.

1.5 Intrinsically photoresponsive retinal ganglion cells (ipRGCs)

IpRGCs are a subset of ganglion cells that are inner retinal photoreceptors (Berson et al., 2002), required for non-image forming vision in mice (Guler et al., 2008). The opsin used by ipRGCs is melanopsin (*opn4)* (Panda et al., 2005, Provencio et al., 2000) and is found in about 2% of ganglion cells (Provencio et al., 2000, Hattar et al., 2002). In mice, the melanopsin system is functional from birth (Sekaran et al., 2005). *Opn4* mRNA reaches peak expression in the retina in the early morning (ZT0-4) in chick (Chaurasia et al., 2005) and at early night (ZT14) in nocturnal rodents (Sakamoto et al., 2004). These ipRGCs also can be identified by the presence of neurotransmitter pituitary adenylate cyclase-activating polypeptide (PACAP) (Hannibal et al., 2001) and vesicle glutamate transporter 2 (VGLUT2) (Purrier et al., 2014). All ipRGCs have intrinsic sustained melanopsin responses, but also extrinsic responses from the photoreceptors in the outer retina. This creates an initial rapid component of light-evoked inward current via inhibitory input from amacrine cells and excitatory input from bipolar cells (Zhao et al., 2014, Dacey et al., 2005, Schmidt et al., 2008, Weng et al., 2013, Zhang et al., 2008). Thus, even in the absence of melanopsin, where ipRGCs lose their intrinsic photosensitivity, still innervate the correct brain regions and can convey rod and cone input (Lucas et al., 2003, Wong et al., 2007) to drive non-image forming visual functions (Lucas et al., 2003, Mrosovsky and Hattar, 2003).

1.5.1 Subdivision of ipRGCs

IpRGCs can be subdivided into five subtypes, M1, M2, M3, M4 and M5 (Figure 1.11). M1 ipRGCs rely on intrinsic responses more than extrinsic (Schmidt and Kofuji, 2010). They have a lower threshold, higher amplitude, faster response than the 4 other subtypes, M2-M5. They are the only sub-type to stratify in the OFF sublamina of the IPL, which may mediate retrograde visual signalling (Zhang et al., 2012, Zhang et al., 2008). Around 1% M1 IpRGCs in mice are displaced in the INL (Hattar et al., 2002). M1 ipRGCs are not a uniform population but have at least 2 sub-populations defined by the presence or absence of POU transcription factor, Brn3b. All non-M1 ipRGCs express Brn3b. The first known function of ipRGCs was the entrainment of the circadian clock (Berson et al., 2002, Provencio et al., 2000, Lucas et al., 2003, Lupi et al., 1999). This is mostly by Brn3b-negative M1 ipRGCs, which make up 10% of all ipRGCs and project into the suprachiasmatic nucleus of the hypothalamus, the primary pacemaker in mammals (Baver et al., 2008, Chen et al., 2011). It is now known that some but not many Brn3b positive ipRGCs also innervate the SCN, although they are not necessary for fully functioning circadian photoentrainment (Chen et al., 2011). Brn3b-negative ipRGCs also have projections from the retina into the ciliary body in mice (Semo et al., 2014), this may mediate the intrinsic pupillary light reflex (iPLR). M2-M5 have centre-surround-organised receptive fields allowing spatial sensitivity (Zhao et al., 2014). They rely on extrinsic synaptic responses more than intrinsic (Schmidt and Kofuji, 2010). Non-M1 ipRGCs have been shown to send axons to the lateral geniculate nucleus (LGN) where spatial and temporal information is sorted. This information is then sent to the visual cortex and to the superior colliculus which acts as the visual reflex centre (Brown et al., 2010, Ecker

et al., 2010) and the olivary pretectal nucleus, which control the PLR (Chen et al., 2011).

M2 cells have large dendritic arbores that branch in the ON sublayer. M3-5 ipRGCs have much weaker melanopsin immunoreactivity (Berson et al., 2010). IpRGCs have also been reported to respond to a wide range of motion speeds, with M1-M4 classes having different motion speed sensitivity, allowing the detection of speed, but not motion direction (Zhao et al., 2014). It has also been demonstrated that melanopsin contributes to brightness discrimination (Brown et al., 2012) and M4 ipRGCs have been found to enhance contrast sensitivity in image forming vision (Schmidt et al., 2014, Allen et al., 2014).

Topographically, the dorsal and temporal retina is most rich with ipRGCs in mice (Vugler et al., 2015). This is likely associated with the horizontal visual streak of high RCG-density just dorsal to the optic nerve (Ortin-Martinez et al., 2010, Salinas-Navarro et al., 2009). Rodents also have a melanopsin rich plexus in the ciliary marginal zone (CMZ) (Vugler et al., 2008b, Semo et al., 2014). In primates, ipRGCs increase in density towards the fovea and form a ring around it (Dacey et al., 2005).

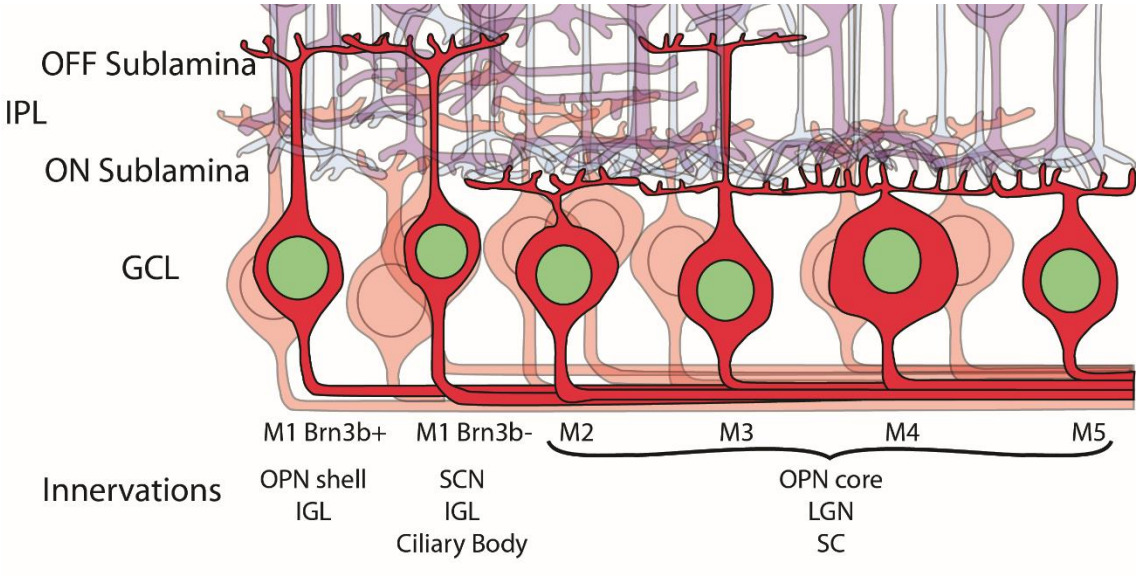

Figure 1.11 ipRGC sub-populations.
This Schematic diagram illustrates the different subtypes of ipRGCs and their projections. M1 ipRGCs stratify in the off sublamina. M2, M4 and M5 ipRGCs stratify in the on sublamina. M3 ipRGCs stratify in both on and off subliamina. M1 have the smallest cell bodies and M4 have the largest cell bodies. M1 ipRGCs are subdivided into two populations based on the expression of Brn3b transcription factor. Brn3b$^+$ M1 ipRGCs project to the shell of the OPN, which controls the PLR. Brn3b$^-$ M1 ipRGCs project to the SCN, to control circadian photoentrainment and, also, have been found to project into the ciliary body. Both Brn3b$^+$ and Brn3b$^-$ M1 ipRGCs project to the intergeniculate leaflet (IGL) of the LGN. All non-M1 ipRGCs express Brn3b and project to image forming areas of the brain such as the LGN and the super colliculus (SC) and to the core of the OPN. A few Brn3b$^+$ also project to the SCN. M2-M5 ipRGCs rely more on input from the outer retina than intrinsic responses. For simplicity, M1 ipRGCs which are displaced in the INL are not depicted in this diagram.

1.5.2 Pupil Light Reflex

Melanopsin also contributes to the pupillary light reflex (PLR) by Brn3b-positive ipRGCs innervating the olivary pretectal nucleus (OPN) shell (Hattar et al., 2002, Morin et al., 2003, Hattar et al., 2003, Lucas et al., 2003, Chen et al., 2011, Baver et al., 2008, Guler et al., 2008, Lucas et al., 2001). They signal to the sphincter muscles of the iris via the OPN. The human pupil diameter can change from 7.9 mm to 2 mm to protect the inner eye against bright light and relaxing to maximise the amount of light entering the eye. Cones bleach and compensate for high levels of light, this means that they do not communicate irradiance levels.

Melanopsin can communicate high irradiance levels much more accurately and is necessary for a complete PLR (Lucas et al., 2003).

An intrinsic pathway also controls the PLR in rodents, bypassing the OPN. This was first seen in fish (Seliger, 1962) but also found in amphibians (Barr and Alpern, 1963), birds (Tu et al., 2004) and more recently reported in mice (Semo et al., 2014, Vugler et al., 2015, Xue et al., 2011). Melanopsin is required to drive the iPLR (Xue et al., 2011) and the iPLR is particularly sensitive following dark-adaptation (Vugler et al., 2015). It has been shown that an intact CMZ is necessary for a complete iPLR response, as damage to the CMZ significantly reduces the iPLR in axotomized eyes (Semo et al., 2014). The iPLR cannot be generated by cones and is unaffected by cone loss, while rod function and pigmentation (non-albino) appear to be essential for normal iPLR development in mice (Vugler et al., 2015). Also, aged mice have a significantly reduced peak constriction compared to adults (Vugler et al., 2015).

The iPLR develops progressively from P21-49 in mice (Vugler et al., 2015) much later than the PLR, which develops from P7-P10, concomitant with outer-retinal signalling (McNeill et al., 2011). This may be due to late maturation of Brn3b-negative M1 ipRGCs, which innervate the ciliary body, as it is known that these Brn3b-negative M1 ipRGCs mature their projections into the SCN around P21 (McNeill et al., 2011).

1.5.3 Does Melanopsin require the visual cycle?

Melanopsin requires chromophore

Melanopsin also uses 11-*cis* retinal to capture light energy and converts the 11-*cis* retinal to all-trans retinal. This is supported by the action spectrum of ipRGCs

fitting to the absorption spectrum of a vitamin A-based photopigment with a peak absorbance (λmax) around 480nm (Berson et al., 2002, Lucas et al., 2001). Also, mice with an inhibited visual cycle have attenuated melanopsin functions (Doyle et al., 2006). In ipRGCs, light causes a depolarisation and an increase of intracellular calcium, (Hartwick et al., 2007) similar to rhabdomeric photoreceptors found in invertebrates. It is not clear how ipRGCs get 11-*cis* retinal as they are located in the inner retina and are separated by several layers of cells from the RPE in the outer retina, the classic site of 11-*cis* retinal isomerisation. Perhaps, 11-*cis* retinal diffuses through the retina. Another possibility is that Müller cells, which have been recognised to play a role in opsin recycling for cones (Wang and Kefalov, 2011), regenerate chromophore and/or transport chromophore to the inner retina. It has been reported that Müller cells are closely associated with ipRGCs but not non-melanopsin ganglion cells (Viney et al., 2007).

Melanopsin can act as a bi-stable pigment

Melanopsin has also been reported to work as a bi-stable pigment. It has photoisomerase capacity generating 11-*cis* retinaldehyde from all-trans retinaldehyde upon exposure to long wavelength light (Melyan et al., 2005, Fu et al., 2005). This intrinsic photoisomerisation is also seen in many invertebrate rhabdomeric photopigments. Phylogenically, melanopsin shows more kinship to invertebrate pigment, some of which are bistable, than to rod and cone pigments (Provencio et al., 1998). Another potential source of chromophore is 9-*cis*-retinal. In the absence of 11-cis-retinal, it has been shown that rods can use isorhodopsin, with the chromophore 9-*cis*-retinal, in the absence of the visual cycle (Fan et al., 2003). Hence, this is a candidate for chromophore in ipRGCs.

But, 9-*cis* retinal is produced at a much slower rate than 11-cis retinal in a normal retina and is unlikely to be produced in sufficient quantities to support a fully functioning melanopsin system. Furthermore, 9-*cis* retinal production may be a result of build-up of all-trans retinyl esters in retinas lacking visual cycle enzymes, which does not occur in wild-type retina (Imanishi et al., 2004).

Effects of the visual cycle on melanopsin

It is known that *rpe65*$^{-/-}$ mice have attenuated phase shifting responses (Doyle et al., 2006) and mice with *rpe65*$^{-/-}$ or *lrat*$^{-/-}$ have a less sensitive PLR than WT (Tu et al., 2006). The *rpe65*$^{-/-}$ and *lrat*$^{-/-}$ mice have a PLR less sensitive than that of an *rdta or rd1 mice* (Tu et al., 2006). *Rdta* mice express the gene for an attenuated diphtheria toxin under the control of a portion of the rhodopsin promotor. This eliminates the majority of the ONL by P7, which corresponds closely to the onset rhodopsin expression at P5 in the mouse retina (McCall et al., 1996). *rd1* mice have a mutation in *Pde6B* needed for phototransduction and see loss of photoreceptors by 1 month (Bowes et al., 1990, Pittler and Baehr, 1991). *Rdta* mice, with selective deletion of rods exhibited an increased magnitude of circadian phase shift compared to WT controls and displayed tonic activation of RGCs (Lupi et al., 1999). Furthermore, selectively knocking out rods along with visual cycle (*rpe65*$^{-/-}$*:*rdta or *lrat*$^{-/-}$*:rd1*) improves circadian photosensitivity and knocking out rods and *rpe65* or *lrat* improves the PLR compared to *rpe65*$^{-/-}$ or *lrat*$^{-/-}$ alone (Tu et al., 2006), perhaps freeing up some chromophore, which otherwise would be taken up by rods. This is supported by Doyle et al., which showed that selectively eliminating rods in an *rpe65*$^{-/-}$, via *rdta* transgene, can restore circadian photosensitivity and knocking out *opn4* and *rpe65* results in a loss of photoentrainment (Doyle et al., 2006).

Rods and cones may influence melanopsin expression in ipRGCs. Royal college of surgeons (RCS) dystrophic rat retina has a significant (>90%) reduction of melanopsin mRNA and protein levels. This model has a mutation in *MerTK*, resulting in loss of phagocytosis of rod and cone outer-segments and melanopsin expression starts to fall after P21, following photoreceptor degeneration (Sakamoto et al., 2004). Perhaps the loss of melanopsin expression in the RCS dystrophic rat is due to the lack of chromophore being recycled and the separation of the RPE from the neural retina by the debris zone of unphagocytosed POS tips. IpRGCs are capable of phototransduction in new born mice, prior to rod and cone function which occurs after P10 (Hannibal and Fahrenkrug, 2004, Sekaran et al., 2005) so ipRGCs may not need rod and cone function at this stage of development.

The melanopsin system is often not considered when assessing visual function in retinal degeneration, even though, it has the clear potential to provide additional readouts on retinal and RPE function. In this thesis, I will employ functional readouts of both outer-retinal function and inner retinal function to assess improvements by RPE cell replacement.

1.6 The iris

1.6.1 Function of the iris

The iris is responsible for controlling the size of the pupil and thus, the amount of light entering the retina. In darkness, the pupil dilates, to allow more light to be captured, while, in bright light, the pupil constricts to help reduce the brightness to an optimal level. Additionally, excessive sun exposure can cause irreversible retinal damage (Glickman, 2011). The other effect of the pupil is to control depth

of field, which is the distance from nearest to the farthest objects that appear focused. A constricted pupil increases the degrees of freedom, as light does not hit the outside of the lens, reducing the spherical aberration. A dilated pupil allows light to enter the eye at the outer lens, which results in increased refraction, and thus, a loss of focus.

1.6.2 Structure of the iris

The front of the iris is a pigmented fibrovascular tissue known as the stroma and behind this are 2 layers of pigmented epithelial cells. The high levels of pigment prevent light passing through the iris. Iris colour is due to variable amounts of eumelanin (brown) and pheomelanin (red/yellow) pigments. The outer edge of the iris, known as the root, is attached to the sclera and anterior ciliary body. Two different muscles are responsible for the constriction and dilation of the pupil, the sphincter and dilator muscles, respectively (Figure 1.12).

1.6.3 Dilator muscles

Dilator muscles runs radially in the iris and contracts to dilate the pupil (Figure 1.12). Myoepithial cells of the dilator muscles are stimulated by the sympathetic nervous system. Thus, when the fight or flight response is activated, the pupil dilates, temporarily allowing more light to enter the retina.

1.6.4 Sphincter muscle

The sphincter muscle lies on the inside of the iris and contracts in a circular motion, causing the pupil to constrict (Figure 1.12). It is innervated by the parasympathetic fibres.

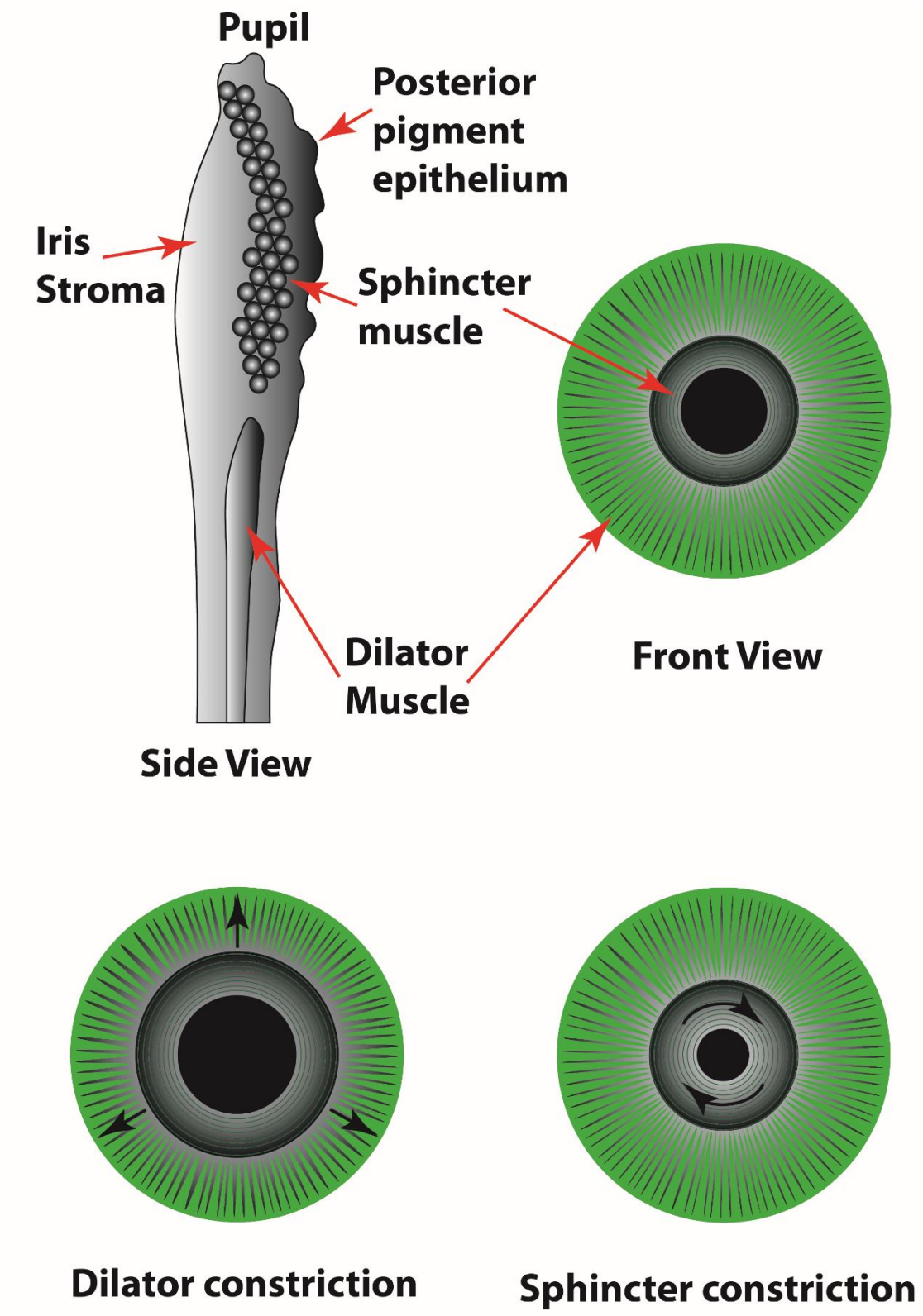

Figure 1.12 The muscles in the iris

The stroma lies at the front of the iris and the posterior consists of pigmented epithelial cells. Two muscles control the constriction and dilation of the iris. The dilator is radial and is the outer muscle. It constricts with sympathetic stimulation, causing the pupil to enlarge. The sphincter muscle lies on the inside of the iris circulating the pupil. It constricts with parasympathetic stimulation, reducing the size of the pupil.

1.7 Bruch's membrane

Bruch's membrane lies between the RPE and the choroid. It consists of five layers: the basement membrane of the RPE, the inner collagenous zone, elastic fibre layer, outer collagenous zone and the basement membrane of the choriocapillaris. The elasticity of Bruch's membrane accommodates changes in intraocular pressure and changes in choroidal blood volume. The thickness of Bruch's membrane increases with age from 2 to 4.7 microns (Ramrattan et al., 1994).

1.8 Blood supply to the eye

The ophthalmic artery branches off the carotid artery and supplies blood to the eye. This then branches into the central retinal artery, the short and long posterior ciliary arteries and the anterior ciliary arteries. The retina is supplied by the central retinal artery and the short posterior ciliary artery. The central retinal artery enters the retina at the optic nerve and branches to supply the layers of the retina (Figure 1.13). Humans have an avascular zone at the fovea as veins branch around this region. Rodents, which do not have a fovea have a radial branching of the retinal vasculature. Retinal veins coalesce into the central vein which exits the eye at the optic nerve.

The short posterior ciliary arteries pierce the sclera around the optic nerve and then arborize to form the arteries of the choroid, which supply lobules of the choriocapillaries which lie under Bruch's membrane. These then drain into venules which coalesce into one of the vortex veins that pierce the sclera at the equator of the eye (Figure 1.13).

The vortex veins and central vein merge with the superior and inferior ophthalmic vein, this is connected to the cavernous sinus, the pterygoid venous plexus and the facial vein. In rodents, the orbital veins form a sinus behind the eye.

The iris and the ciliary body is supplied by the anterior ciliary arteries, the long posterior ciliary arteries and connections to the anterior choroid. The anterior ciliary arteries travel along the extraocular muscles and pierce the sclera near the limbus and feeds an arterial circle in the iris. The long posterior ciliary arteries pierce the sclera at posterior of the eye and travel between the sclera and the choroid and then join the arterial circle of the iris. The arterial circle then further branches into the iris and ciliary body. Venous draining is directed anteriorly into the choroid.

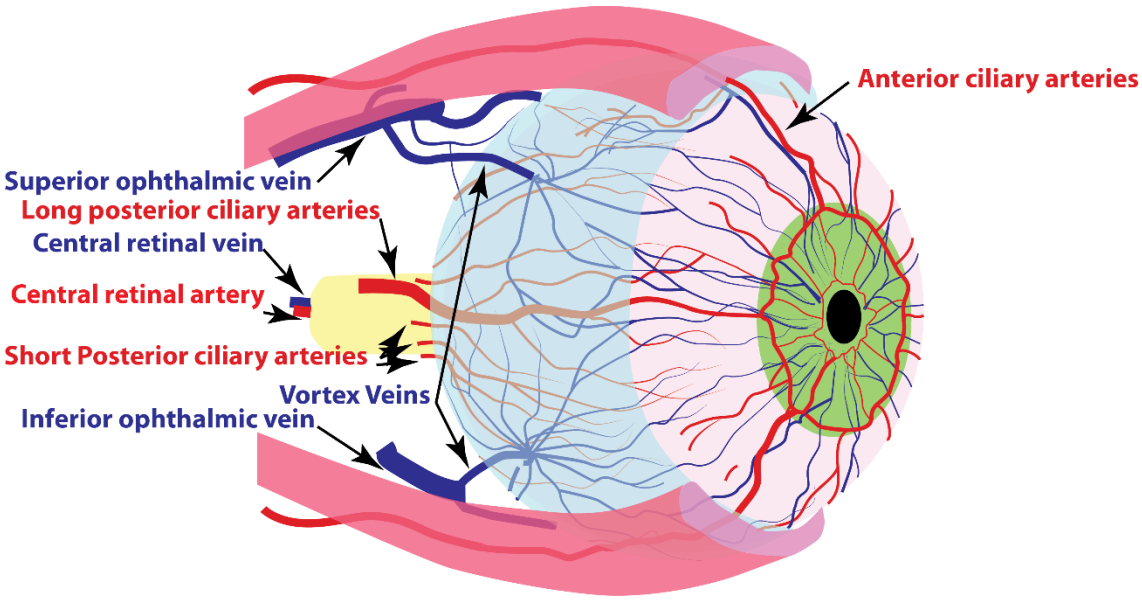

Figure 1.13 Blood supply of the eye
The ophthalmic artery branches into the central retinal artery, the long posterior arteries and the short posterior arteries. The central retinal artery enters the retina at the optic nerve and then branches in the retina. Veins in the retina coalesce and exit the eye at the optic nerve as the central retinal vein. The short posterior ciliary arteries pierce the sclera around the optic nerve and feed the choroid. Choroidal veins drain at the equator of the eye as the vortex veins, which merge to form the superior and the inferior ophthalmic vein. The iris is fed by the long posterior arteries and the anterior ciliary arteries. The long posterior artery pierces the sclera at the back of the eye and travels between the sclera and the choroid and feed the arterial circle in the iris. The anterior ciliary arteries travel along the extraocular muscles and pierce the sclera near the limbus.

1.9 RPE transplantation for the treatments of retinal degenerative diseases

With such a strong dependence on the RPE for photoreceptor function it is unsurprising that many diseases, resulting in photoreceptor degeneration, are primarily diseases of the RPE. Also, many genes involved in the visual cycle can result in blindness. For example, mutations in *rpe65* or *RDH* cause LCA, and mutations in *lrat* can cause juvenile retinitis pigmentosa, both resulting in early on-set blindness. Additionally, with LCA alone, there are 12 genes, including *rpe65*, associated with forms of LCA (http://www.sph.uth.tmc.edu/Retnet). With numerous genes which can result in either recessive or dominant RPE diseases, developing a single therapy that can address each individual case is an appealing approach. Replacing patient RPE cells with gene corrected RPE cells is a possible therapy for correcting all RPE genetic diseases.

Unfortunately, the large degree of genetic heterogeneity raises significant problems with developing new treatments. The frequency of LCA occurrence is around 1:80,000 (Stone, 2007), therefore, each of the 12 identified genes correspond to a relatively small number of affected patients, thus, techniques which are broadly applicable, and, to some extent mutation-independent, may be much more feasible in treating large numbers of patients. For some diseases, such as dry age-related macular degeneration (AMD), there are many genes associated with the development of this disease but no single mutation will directly result in the development of AMD. Thus, genetic therapy may not be a suitable approach and there are no current treatments available to those with dry AMD (90% AMD patients). Replacement of cells using a regenerative medicine

approach to produce replacement RPE cells from stem cells may be the only option, and this is currently being validated for efficacy (Schwartz et al., 2012).

1.9.1 AMD

AMD is the leading cause of blindness in the developed world and is recognised as a disease of the RPE. Degeneration of RPE cells is a fundamental element in AMD, which also affects the choroid and Bruch's membrane. The exact cause and pathology of AMD is not fully understood. There are many genetic and environmental factors that contribute to the risk and severity of the disease. It is believed that, lipofuscin, a by-product of phagocytosis of rod and cone outer-segments, accumulates with age to form drusen deposits between RPE cells and Bruch's membrane. Lipids also accumulate in Bruch's membrane, resulting in thickening of the membrane, exacerbated by dysregulation of the complement system. AMD results in the loss of RPE cells, which lead to rod and cone death (Jackson et al., 2002). This advances in 10-15% of patients to wet AMD, where leaky blood vessels proliferate into the retina, from choroidal neovascularisation (Klein et al., 1997). Monthly injections of anti-vascular endothelial growth factor has become the standard treatment for preventing blood vessel growth, but, there is no current standard treatment for RPE cell death and the resulting photoreceptor loss (Del Priore et al., 2006). It is hoped that stem cells could provide a potential therapy by replacing RPE cells (Vugler et al., 2007a). Replacement of RPE cells using stem cells is currently being validated as a suitable treatment for AMD (Schwartz et al., 2012, Carr et al., 2013, Nommiste et al., 2017, Kamao et al., 2014, Reardon and Cyranoski, 2014), with positive results seen in patients in initial trials (da Cruz et al., 2018).

1.9.2 Immune environment of the eye

The eye has a unique environment which aids the prolonged survival of incompatible grafts (Medawar, 1948). This is because the eye is immune privileged. It has a tightly controlled BRB, which prevents cellular migration from the blood. Immune privilege means that the introduction of foreign antigens are more readily tolerated and less likely to elicit an inflammatory response. Medawar and colleagues showed that skin allografts transplanted to the anterior chamber survive without rejection even when the recipient is previously immunized against the alloantigens. This immune privilege is only maintained while the BRB is intact (Medawar, 1948). The BRB is supported by tight junctions in RPE cells and inner retinal vessels.

This does not mean that the eye is void of immune cells as the eye has resident macrophage-like microglia, similar to those in the brain (Ajami et al., 2007, Albini et al., 2005, Ginhoux et al., 2010, Paques et al., 2010). The BRB allows the eye to form a microenvironment which supresses inflammation and promotes immune tolerance. Soluble factor in the aqueous humour (Goslings et al., 1998, Taylor et al., 1992, Taylor et al., 1994, Taylor and Yee, 2003, Taylor et al., 1998) and on pigmented epithelium (Ishida et al., 2003, Kawazoe et al., 2012, Sugita et al., 2006, Sugita et al., 2009, Wenkel and Streilein, 2000, Jorgensen et al., 1998) regulate this anti-inflammatory environment. Differences in immune privilege exist within the eye. It has been shown that injection of an adeno-associated viral (AAV) vector into the vitreous, resulting in vector expression in the inner retina, produced a humoral immune response against the AAV capsid. This prevented the vector expression when re-administered into the vitreous of the partner eye. In contrast to this, when the vector was re-administered into the subretinal space of the partner eye, vector expression was not affected by the first injection.

Alternatively, administering the first injection into the subretinal space did not produce a rise in anti-AAV antibodies in the serum and did not inhibit vector expression when re-administered either intravitreally or subretinally in to the partner eye (Li et al., 2008, Li et al., 2009).

Survival of RPE cell allografts in the dystrophic RCS rat has been seen up to 12 months without immunosuppression (Li and Turner, 1991). Donor RPE cells came from Long-Evan rats and could sustain the ONL for 6 months before a gradual decline in ONL thickness, but, this gradual loss of ONL matched that seen in healthy Sprague-Dawley rats (Li and Turner, 1991). Matching of major histocompatibility complexes (MHC) has been shown to be important in RPE cell allograft survival (Zhang and Bok, 1998). Immunosuppressants are administered to help prevent rejection in xenografted RPE cells. Spontaneously immortalised human RPE cell line ARPE19 transplanted into immunosuppressed RCS rats showed surviving ONL and visual function beyond 6 months (Coffey et al., 2002). Preservation of retinal function and ONL is seen in many studies, albeit, often only a small percentage of cells survive (Wang et al., 2005).

1.9.3 Potential sources of replacement RPE cells

The eye is an ideal testing ground for stem cell therapies, since it exhibits relative immune privilege (Grisanti et al., 1997) and it is readily accessible for monitoring and imaging purposes. RPE cells are also the most ideal retinal cell for replacement as unlike retinal neurons they do not require synaptic reconnection and can be easily grown as a monolayer of cells for transplantation. RPE cell transplant studies were first reported in the 1980s, showing that dissociated RPE cells could attach to Bruch's membrane in primate retina (Gouras et al., 1985) and that they could prevent photoreceptor degeneration in the RCS rat (Li and

Turner, 1988).

Stem cells provide a means of regenerative medicine by replacing damaged or lost tissue. Stem cells are undifferentiated cells, which have the capability of reproducing by mitosis, to produce more stem cells, and are able to differentiate into a specialised cell. There are many sources of stem cells. Some are found in the adult body such as haematopoietic stem cells (HSCs). HSCs are extracted from healthy bone marrow and used to reconstitute the immune system after leukaemia, lymphoma, various blood or autoimmune disorders and have been used in transplants for over 40 years. Unfortunately, these adult stem cells are limited in population and their capacity to differentiate. They are multipotent; meaning they can only differentiate into a small number of similarly specified cells.

Human embryonic stem cells

Human embryonic stem cells (hESC) are stem cells derived from the inner cell mass of a blastocyst, an early-stage embryo (5 days post fertilisation). These cells are pluripotent and as such, can develop into any cell type in the body (Thomson et al., 1998) bar the sex cells. They are also renewable, such that stem cells derived from one blastocyst can produce cells to treat many patients, while avoiding any genetic defects inherited in autologous RPE cells. HESC-RPE cells' shape and organisation are almost identical to that of human macular RPE cells (Vugler et al., 2008a). Unfortunately, hESC are associated with ethical controversy and although they may suffer rejection from the host, when administered with an immunosuppressant hESC-RPE cells have survived subretinally in RCS rats for more than 7 months (Lu et al., 2009).

Induced pluripotent stem cells

One way of overcoming rejection is by using induced pluripotent stem cells (iPSC), as these can be autologous. These cells can be formed from somatic cells from the patient or from a relative, treated with a cocktail of transcription factors to re-program the cells to a pluripotent state (Takahashi and Yamanaka, 2006). These can then be differentiated to form the cell type of interest. Unfortunately, as RPE cells derived from iPSC are patient specific, time to prepare the cells will be a factor, whereas, hESC-RPE cells can be available as needed. iPSC-derived RPE (iPSC-RPE) cells are also likely to incur more costs as there are more steps involved and each RPE cell preparation is developed for the individual patient.

ARPE-19 cell line

Another source of RPE cells is ARPE-19, a spontaneously immortalised human adult RPE cell line. They were once thought to be a viable source of cells for therapy with less ethical issues associated compared to hESC, but, they may pose a greater risk of rejection following transplantation. This cell line is a valuable source of RPE cells for studying and transplantations of RPE cells (Wang et al., 2005, Coffey et al., 2002).

The feasibility of this has been demonstrated by autologous transplantation of RPE cells and choroid from periphery to macula (van Meurs and Van Den Biesen, 2003, da Cruz et al., 2007). This has paved the way for clinical trials. The first of which is using human embryonic stem cells (hESC) in suspension injected subretinally in AMD and Stargardt's disease patients (Schwartz et al., 2012, Schwartz et al., 2015). The London Project are also carrying out a clinical trial where RPE cells are transplanted in a monolayer on a polyester membrane and

have treated two patients to date (Carr et al., 2013, Nommiste et al., 2017, da Cruz et al., 2018). RPE cells derived from iPSC are also being tested in a clinical trial (Kamao et al., 2014, Reardon and Cyranoski, 2014).

1.9.4 How to culture RPE cells

There are many protocols for producing cells with an RPE-like phenotype. These protocols have been developed through trial and error. These protocols also change depending on the cell source. In general, ARPE-19, hESC and iPS cells have a fibroblast shape. When they are first plated they will multiply fast. The addition of serum, amino acids and growth factors ensures this. The incubation temperature is controlled at 37°C and the CO_2 is maintained at 5%, mimicking that of mammalian blood. Once the dish is confluent or covered with new cells, growth factors are removed to help the cells to develop and the fibroblast phenotype is lost. Growing stem cells on a plate often see the spontaneous growth of patches of pigmented cells. These are then isolated to create a pure pigmented dish with RPE characteristics. Once this new dish is confluent the serum levels are reduced. The medium that these cells are developed in is rich in nutrients for cells with a high energy demand, such as L-glutamine and amino acids.

1.9.5 Disease models for testing the function of transplanted RPE stem cells

To date, the majority of RPE transplant studies have been carried out on the RCS rat, a model of retinal dystrophy with progressive and early photoreceptor loss (Dowling and Sidman, 1962). The RCS rat has a mutation in *mertk.* Mer tyrosine kinase is a transmembrane protein involved in the phagocytosis of POS. Phagocytosis of POS by RPE follows a daily rhythm with a peak of activity 1.5-2

h after light onset for rod photoreceptors (LaVail, 1980). Mutations in *mertk* are associated with autosomal recessive retinitis pigmentosa (Ksantini et al., 2012, Wang et al., 2001). The mutation in RCS rats result in failure to phagocytose shed POS (Edwards and Szamier, 1977, D'Cruz et al., 2000). This results in accumulation of shed POS, creating a debris zone between photoreceptors and RPE. This separation of RPE from the neural retina results in fast photoreceptor degeneration (D'Cruz et al., 2000). From P21 the ONL is reduced to 2 rows of cells and only 1 row at 4 months (Girman et al., 2005). At P60 opsin mRNA is undetectable (Agarwal et al., 1992).

This model of retinal degeneration was discovered almost 80 years ago, and it is a well-studied model. Yet, the RCS rat is a less than ideal model for studying the effects of RPE transplantation due to the early onset and fast rod and cone degeneration, making visual rescue difficult. The death of RGCs in the RCS rat is also quite extensive and to date transplantation has failed to prevent RGC pathology (Klassen et al., 2001), and RGC stability is an important consideration when attempting to restore vision. Photoreceptor preservation in RCS rats and improvements in the visual function of these animals can be achieved by an array of cells, including hESC-RPE (Idelson et al., 2009, Zhu et al., 2013), iPSC-RPE (Carr et al., 2009, Krohne et al., 2012), human RPE (Little et al., 1996), rat RPE (Jiang and Hamasaki, 1994), ARPE-19 cells (Coffey et al., 2002), but also, neural progenitors (Wang et al., 2008) and Schwann cells (Lawrence et al., 2000). Thus, identifying RPE-specific therapeutic effects is complicated as many studies show photoreceptor survival are likely due to trophic effects. This is supported by areas of photoreceptor rescue larger than the graft of hRPE (Wang et al., 2005), suggesting the diffusion of trophic factors is responsible for cell survival.

Despite these drawbacks of using the RCS rat model to examine the therapeutic effects of RPE transplantation, it is still widely used as a pre-clinical efficacy model in the development of cellular therapies for retinal degenerations including AMD. AMD is a complicated disease to model and so far, no animal model which fully recapitulates the human macular disease has been identified. AMD has a very late onset, complex genetics and environmental risk factors. Fortunately, there are new models of retinal degeneration with a slower degeneration, which may prove more useful in studying the therapeutic effects of RPE transplantation, such as the *rd12* mouse.

1.10 *Rd12*: A model of LCA2

1.10.1 Identification of the *rd12* mouse

To study a disease in depth and to develop and investigate the efficacy of therapies it is useful to have a reliable model of the disease. In 2005, a naturally occurring mouse model of LCA 2 was discovered (Pang et al., 2005), which has a mutation in *rpe65*, also seen in LCA2 patients (refSNP cluster report: rs368088025), making it a clinically relevant model. LCA2 is characterised by early onset of central vision loss, sensory nystagmus, amaurotic pupils and absent signals on ERG. It is one of the earliest and severe forms of inherited retinal dystrophies. In these mice, retinal degeneration is caused by a naturally occurring nonsense mutation in exon 3 of *rpe65*. A substitution of a single cytosine nucleotide to thymine results in a premature stop codon at position 44 (Pang et al., 2005). Aminoglycosides were administered to *rd12* mice as a readthrough therapy. This allows the translation of mRNA to bypass a premature stop codon, to produce a full protein. Despite this, the *rd12* did not respond to this

therapy (Guerin et al., 2008) and it is now understood *rpe65* mRNA fails to bind to ribosomes to initiate translation in *rd12* mice. The mRNA is appropriately spliced and is exported to the cytoplasm and is bound to ribosome free messenger ribonucleoproteins but is not associated with translating polyribosomes (Wright et al., 2014). Thus, the mRNA does not undergo non-sense mediated decay. The *rd12* mice were repeatedly backcrossed to a WT, C57BL/6J, to make a congenic inbred strain and C57BL/6J are used as a WT control when assessing *rd12* mice (Pang et al., 2005). The *rd12* mouse has a very similar phenotype to *rpe65*$^{-/-}$ mice. Although, *rd12* mice develop distinctive white dots throughout the retina that become apparent at around 5 months of age, similar to those seem in LCA2 patients (Pang et al., 2005), which are not found in *rpe65*$^{-/-}$ mice. This characteristic of *rd12* mice makes it a better model for human LCA2, as they are more likely to simulate the actual disease mechanism.

1.10.2 Pathology

The first sign of the *rd12* morphology is seen at 3 weeks when lipid-like droplets are found in the RPE. At 6 weeks, occasional voids start to appear in the POS and by 3 months these voids become obvious, and much larger lipid-like droplets appear (Pang et al., 2005). Small punctuate white spots on fundus examination appear at 5 months of age, similar to those seen in human LCA. By 7 months, the ONL is reduced by 40%, with only 6-7 layers of cells remaining and the POS are obviously shorter (Pang et al., 2005, Wright et al., 2014). After 2 years, the POS are almost absent and the ONL reduced to just 3-4 layers of cells. At this stage, RPE cells are atrophied and hypopigmented (Pang et al., 2005).

Cones are lost early in the *rd12* mouse; by P21, PNA-lectin positive cone count is reduced to 55% that of WT, though, cones lose opsin before cone death (Li et

al., 2011), so surviving cones may no longer be functional. By P90 PNA-positive cone counts are reduced to 16% of WT, and only 15% of these express M/L-opsin while there is no S-opsin. Regionally, cones are first lost from the central and ventral-nasal region of the retina, where S-cones are most highly populated, and survive longer in the dorsal-temporal region (Li et al., 2011). RPE65 in WT rat development reaches its peak and steady state expression around P10-P12. This coincides with peak opsin expression in rat and mouse (Bowes et al., 1988, Manes et al., 1998, Hamel et al., 1993) and development of the ERG (Bakall et al., 2003). This could help explain the initiation of dramatic cone loss after P14, when cones are more demanding for chromophore, while at P14 PNA-positive cone counts are similar to WT (Li et al., 2011).

As early as 3 weeks, the scotopic ERG starts to diminish in *rd12* mice. The photopic ERG responses are significantly more robust, although amplitudes under both dark- and light-adapted conditions decrease with age (Pang et al., 2005, Pang et al., 2006). Although the photopic ERG responses are more robust, it is known that this is rod driven (Seeliger et al., 2001, Cachafeiro et al., 2010, Dai et al., 2015). The lack of RPE65 in *rd12* mice allows rods to function at brighter light intensities without bleaching. More evidence to suggest that the remaining visual signal is rod driven, comes from work showing that *rd12* mice respond to visually evoked potentials at low temporal frequencies whilst responses to high frequency stimuli spatially and temporally are lost as early as P18 (Nusinowitz et al., 2006). In the *rpe65*$^{-/-}$ mouse it was shown that the likely candidate for the visual pigment used in the residual rods is isorhodopsin, created with 9-*cis*-retinal, perhaps as a result of the excess retinyl esters (Fan et al., 2003).

Positive masking is an increase in activity in response to dim light. This is usually seen in nocturnal rodents, but, *rd12* mice do not have this positive masking response. The visual system in *rd12* mice are not sensitive enough to react to a dim light. Negative masking is a suppression of activity in bright light, seen in WT mice. *Rd12* mice actually have increased activity in bright lights. *Rd1* mice have no outer-retinal-derived visual function and still have a negative masking affect (Mrosovsky et al., 1999, Thompson et al., 2008). Thus, it is not just rod and cone function that determines negative masking. IpRGCs can maintain negative masking in the absence of outer-retinal photoreception, thus, ipRGCs are also affected by the loss of the visual cycle, in *rd12* mice (Thompson et al., 2008). It has been shown that *rpe65*$^{-/-}$ mice have a shifted circadian behaviour, commencing nightly activity about 2 hours before WT (Doyle et al., 2006). However, when illumination was increased, *rpe65*$^{-/-}$ mice were able to phase shift, suggesting that entrainment is possible at high light intensities (Doyle et al., 2006).

1.10.3 Treating the *rd12* disease

Many studies show that early intervention in the *rd12* animal has the most hope for a significant retinal rescue, as there is very early cone loss (Nusinowitz et al., 2006, Li et al., 2011, Pang et al., 2010). Pang et al initiated gene therapy at P14 with a rAAV5-CBA-hRPE65 vector, which resulted in RPE65 expression over large areas of the RPE. Rhodopsin levels, measured by spectral absorbance, rose to 70% WT level and ERG signals to approximately 66% of normal when assayed at 7-months of age (Pang et al., 2006). Treatment with gene therapy has been shown to keep remaining cones alive and to rescue opsin expression in these cones (Li et al., 2011). In animal models of RPE65 deficiency, rods undergo

a slow progressive degeneration, which is why restoration of rod vision appears to be possible over a broad range of ages.

The *rd12* mouse is an under-utilised animal for cellular transplants. Chaudhry et al injected ESC and ESC-derived neuroprogenitors into the *rd12* mouse. The undifferentiated ESC proliferation was robust and resulted in the disruption of the retinal structure and the formation of teratomas beyond 6 weeks of post-implantation. However, the neuroprogenitors proliferated slowly and differentiated and integrated further, although, more neuroprogenitor cells integrated into the neural retina than the RPE. This may be due to early loss of photoreceptors (Chaudhry et al., 2009). Li et al injected iPSC-RPE cells subretinally into 2-day old albino *rd12* and showed the presence of pigment in the RPE at 5 months although it cannot be determined if these are viable transplanted cells, or pigment from the transplants phagocytosed by host RPE. iPSC-RPE cells were also injected into *rd12* mice crossed with $Prkdc^{scid}/Prkdc^{scid}$ mice for a double homozygous with both severe combined immunodeficiency (SCID) and *rpe65* mutation. While increased b-wave amplitude was seen, the a-wave was still absent (Li et al., 2012b).

Most single nucleotide polymorphisms (SNPs) identified in the human *rpe65* gene are autosomal recessive mutations (Gu et al., 1997, Hanein et al., 2004, Philp et al., 2009, Stone, 2007). Thus naturally, the *rd12* mutation was first thought to be recessive. However, it was shown to have semi-dominant characteristics (Wright et al., 2014). Mice with the *rd12* mutation lose all visual acuity measured by optokinetic tracking by P90, which is a quicker decline than an $rpe65^{-/-}$ mouse, which still has visual acuity until P120. A mouse with one copy of the *rd12* allele will have slight reductions in the a- and b-wave and some cone loss (Wright et al., 2014). Also, $rpe65^{-/-}$ mice do not exhibit the small white dots observed in the

retinal fundus of the *rd12* mouse and seen in LCA2 patients (Pang et al., 2005). Thus, the *rd12* mouse is a much closer model to LCA2 in humans, than *rpe65*$^{-/-}$ mice, which will be useful in studying the disease and the ability to treat the disease. Also, even though *rd12* is a model of LCA, stem cell work on this model can be translated to many other forms of retinopathy, such as testing RPE cell transplantation for application in age-related macular degeneration. While the *rd12* mouse is not a model of AMD, it has many advantageous characteristics for studying RPE cell replacement therapies, such as a slow rod degeneration and a visual cycle specific disease.

1.10.4 The benefit of using the *rd12* mouse over other *rd* models

The *rd1* mouse was the first inherited mouse model of retinal degeneration. It has a non-sense mutation in the gene encoding the beta subunit of rod cGMP-phosphodiesterase, *Pde6b* (Bowes et al., 1990). Pde6B is needed for phototransduction, to hydrolyse cGMP on rods and hence, close cGMP-gated channels. This mutation results in rod degeneration from P8 until 4 weeks when there are no surviving photoreceptors (Bowes et al., 1990, Pittler and Baehr, 1991). The *rd10* mouse also has a mutation in *Pde6b*, however, this is a missense mutation and while it has rapid degeneration of the photoreceptors, its retinal degeneration is milder than that of the *rd1* (Chang et al., 2007, Rivas and Vecino, 2009). While the young *rd10* retina has better function than the *rd12* retina, it has a much more aggressive degeneration (Hasegawa et al., 2016).

The *rd2* mouse, first known as *rd slow* or *rds*, has a mutation in the gene for peripherin 2, *Prph2*. It is a transmembrane glycoprotein found in rod and cone outer-segments. It is thought that peripherin 2 works as an adhesion molecule in the stabilization of outer-segment disks and maintaining the curvature of the disk

rim. ONL starts degenerating at 2 weeks and by 12 months there is no ONL cells (Sanyal et al., 1980).

The mutation in *rd3* is not yet known, although, it is important for stable expression of guanylate cyclase in photoreceptors (Dizhoor et al., 2016) and the mutation causes LCA12. It has a much faster retinal degeneration than *rd12* (Chang, 2016). ERG is lost by 7 weeks (Chang et al., 1993).

The *rd4* mutation is autosomal dominant, which is homozygous lethal. The ONL is lost by 6 weeks in the heterozygotes. At 4 weeks there is retinal vessel attenuation, pigment spots and optic atrophy in the fundus (Roderick et al., 1997). The mutation occurs in Gnb1, the gene encoding transducin beta1-subunit, necessary for phototransduction (Kitamura et al., 2006).

The homozygous *rd5* mouse is a model of Usher syndrome type I. The mutation is not yet known. By 5 weeks the POS look disorganised and start to degenerate. By 8 months the ONL is lost (Heckenlively et al., 1995).

The autosomal recessive *rd6* mutation sees macrophage appear in the subretinal space around 8 weeks and with time show to contain lipofuscin and pigment. An abnormal ERG is detected around 1 month and photoreceptors slowly degenerate (Hawes et al., 2000). The mutation occurs in the *Mfrp* gene which encodes membrane frizzled-related protein.

The autosomal recessive *rd7* mutation is a frame shift mutation causing a pre-mature stop codon in *Nr2e3*, which codes for a photoreceptor-specific nuclear receptor. This disorder is unusual as it shows increased S-cones at the expense of rods and M/L-cones, which leads to retinal rosetting and a slow degeneration (Milam et al., 2002).

The *rd8* mutation is a slow retinal degeneration, which is first detected in the ventral retina. Degeneration and pseudo-rosettes can be seen at 8 weeks. The

rd8 mutation occurs in *crb1*, coding for Crumbs homolog 1 and locates in photoreceptor inner-segements (PIS) (Mattapallil et al., 2012).

Rd9 is a semidominant X-linked mutation in the gene encoding retinitis pigmentosa GTPase regulator, resulting in pigment loss and a slow degeneration of the ONL. Rhodopsin and transducin in rod outer-segments are reduced and cone opsins are mislocalised. ERG amplitudes are attenuated and degenerate with age up to 24 months (Thompson et al., 2012).

The *rd11* mutation occurs in *Lpcat1*, the gene encoding lysophosphatidlycholine acetyltransferase-1 (LPCAT1), resulting in a truncated protein. This localises in the PIS and promotes the conversion of palmitoyl-lysophosphatidylcholine (LPC) to dipalmitoylphosphatidylcholine (DPPC). This causes rapid photoreceptor dysfunction and degeneration. By P31 the ONL is reduced by 60% and by P47 this is further reduced to a single row (Friedman et al., 2010).

The mutation in the *rd13* mouse is not yet known, although it has been mapped to the distal 4 Mb of chromosome 15. This mutation causes a reduction in cell number in ONL containing only 2-3 layers at P12, which, did not seem to have reduced further by P40 (Buchner et al., 2004).

The *rd14* is an autosomal recessive mutation on chromosome 18. Large cells appear in the subretinal space and blood is observed on some retinas which decreased ERG recordings, otherwise the ERG is normal (Zhang et al., 2005).

The *rd15* mutation has been mapped to chromosome 7 and is an autosomal recessive mutation. At 4 weeks there is no rod ERG b-wave and a severely reduced cone response, yet, retinal degeneration is slow and seen around 9 months (Hawes et al., 2005).

The *rd16* mouse has an autosomal recessive mutation in *CEP290*, which is associated with LCA10 and important for centrosome and cilia development in

photoreceptors. Retinal degeneration is seen at 3 weeks after which the ERG response worsens and cannot be detected at 2 months. This mutation results in a much faster degeneration than the *rd12* mouse (Chang, 2016).

From this list, the *rd12* mouse has the advantage of a slow degeneration allowing time to halt the degeneration but also retinal function is severely affected from early on so any restoration to function can be observed. The *rd12* is also advantageous due to mutation being known and that the mutation is RPE specific, which is the cell type of interest. Also, this allowed us to investigate the effects of the RPE on ipRGCs.

1.11 Sodium Iodate: The selective RPE killer

1.11.1 Benefits of removing the RPE prior to transplantation

A major issue with RPE cell transplantation is achieving cell integration. Many animal models do not mirror RPE cell loss seen in diseases of the RPE like dry AMD, in which photoreceptors die subsequent to RPE cell loss. In many studies involving sub-retinal transplantation into rodent models where host RPE cells remain, the grafted RPE clump together to form a bolus of cells and do not sit down in a monolayer (Carido et al., 2014, Li and Turner, 1991, Seaton and Turner, 1992, Sheedlo et al., 1991, Carr et al., 2009). Studies have shown that RPE cells undergo apoptosis in the absence of a suitable substrate to attach to (Tezel and Del Priore, 1997, Tezel et al., 2004). This is known as anoikis. Thus, space on Bruch's membrane needs to be made available for donor RPE cells to survive transplantation. In human, it is possible to surgically remove RPE cells and this occurs with AMD progression in the form of geographic atrophy. Unfortunately, due to the small size of a rodent eye, physical removal of the host

RPE cells prior to grafting is unfeasible, with chemical removal of RPE cells being a more realistic approach. The loss of RPE cells prior to transplantation will damage the BRB (Wenkel and Streilein, 1998) which can complicate donor cell survival, but, this is an important factor to address, as this BRB breech is seen in AMD patients. Other animal models used for RPE cell transplantation such as the RCS rat do not simulate this challenge.

1.11.2 Discovery of Sodium Iodate

Sodium iodate ($NaIO_3$) is a drug, which is selectively toxic to the RPE and causes RPE cell necrosis. Between 1926 and 1934, seven cases of blindness were reported after the administration of an antiseptic, Septojod. The active chemical in Septojod, which when isolated resulted in blindness was identified as sodium iodate (Sorsby, 1941). The selective death of RPE cells is followed by photoreceptor cell apoptosis. Benefits of using $NaIO_3$ to create a model of retinal degeneration include its selective effects on RPE cells after a single administration of $NaIO_3$ and the rapid onset of RPE cell death. Oedema has been observed 1 hour after administration via the tail vein (Hariri et al., 2013).

1.11.3 Method of toxicity

It is not yet fully understood how $NaIO_3$ is toxic to RPE cells nor why its toxicity is specific to RPE cells, despite this, there are many well-supported theories. Anstadt et al showed that the tight junctions remain relatively stable and that gaps in the RPE layer are a result of direct RPE cell destruction (Anstadt et al., 1982). RPE death is due to necrosis, suggesting a chemical or physical injury.

The choroid, which lies beneath Bruch's membrane and the RPE, has the highest rate of blood flow in the body, needed to supply the retina, the most metabolically

active tissue in the body. This high blood flow is also needed for cooling retinal tissue, with the choroid acting as a heat sink. It is hypothesised that $NaIO_3$ specifically affects RPE cells due to this high blood flow and the uptake of $NaIO_3$ by the RPE. This is supported by studies showing more severe degeneration in the central retina (Redfern et al., 2011). The central retina has the highest choroidal blood flow and all major blood vessels of the retina and choroid enter and exit the eye at the optic nerve head. Nishimura et al. 1990 injected $NaIO_3$ into primate carotid artery, severe RPE damage was seen in the ipsilateral eye but did not affect the contralateral eye (Nishimura et al., 1990). This showed varied results, with a dose of 10 mg/Kg, with some eyes only showing damage at the posterior pole and others showing complete fundus deterioration. Another property of the choroid which leave the RPE susceptible to $NaIO_3$ damage is its permeability to sodium. It is at least 50 times more permeable than skeletal muscle (Tornquist et al., 1990).

It is known that Iodate is a powerful oxidising agent, and causes denaturation of proteins and co-administering $NaIO_3$ with anti-oxidants reduces the damage to the RPE (Heike and Marmor, 1990). Yet, the effects of iodate on the RPE are unlikely attributed solely to oxidation as similar oxidising agents such as sodium perchlorate and potassium bromate are non-toxic (Baich and Ziegler, 1992). Why the RPE is particularly susceptible to oxidative stress is not understood. One theory is that $NaIO_3$ reacts with the melanin in the RPE to produce harmful toxins via oxidation (Baich and Ziegler, 1992). It is thought that $NaIO_3$ may bring about its toxic effect by disrupting the melanosome membrane via oxidation and result in the release of potentially toxic melanin and its metabolites. Conflicting this theory is that melanin is not specific to the RPE, and $NaIO_3$ has been reported to be effective on albino RPE cells (Chowers et al., 2017), which should have a null

effect if melanin was necessary. Kiuchi et al claimed that $NaIO_3$ had an identical response in pigmented WT mice and albinos (Kiuchi et al., 2002, Chowers et al., 2017). Another study by Redfern et al., states that albino rats were, in fact, more sensitive to sodium iodate (Redfern et al., 2011).

Another theory is that the RPE is susceptible to photooxidative damage from bisretinoid flurophores that form in photoreceptor cells and accumulate with age as lipofuscin in RPE cells. ATP-binding cassette transporter (ABCA4) is important for transporting all-*trans* retinaldehyde back to the RPE for recycling, following phototransduction. Mutations in *Abca4* are known to cause autosomal-recessive Stargardt's macular dystrophy. A build-up of all-*trans* retinaldehyde occurs in POS which are then shed and phagocytosed by RPE cells and form the toxin A2E. *Abca4*$^{-/-}$ mice have an accumulation of these toxic bisretinoids and this makes them more susceptible to the toxic effects of $NaIO_3$. This is supported by a reduced effect of $NaIO_3$ in *rd12* mice, which have low levels of bisretinoids (Zhao et al., 2017).

Other theories suggest that $NaIO_3$ is not specific to RPE cells. Wang et al., 2014 administered 10, 20 or 30 mg/Kg $NaIO_3$ retro-orbitally in C57 mice and suggested a direct effect of $NaIO_3$ on photoreceptors 5 days after $NaIO_3$ administration at 20 or 30 mg/Kg $NaIO_3$. Although, it cannot be concluded that these effects were not a secondary effect of RPE cell death. Also, the effects $NaIO_3$ *in vitro* were examined using ARPE19 cells versus 661W cells, a cell line with characteristics of cone photoreceptors. It showed that higher concentrations of $NaIO_3$ were needed to kill the APRE-19 cells than 661W cells (Wang et al., 2014). Although, the ARPE-19 cells used were only 5 days post-confluency, a time point at which these cells do not show characteristics of RPE cells such as shape, protein expression or even melanin (Ahmado et al., 2011). Another study suggested

direct effects of $NaIO_3$ on dopaminergic neurons. Two weeks after $NaIO_3$ administration, dendritic fields of DA-ACs, horizontal cells and ipRGCs are decreased, but again, there is no evidence to exclude attributing this to secondary effects of RPE cell death (Tao et al., 2013). It has been shown by Carido and colleagues that bipolar cell dendrites become hypertrophic, along with a loss in the number of Pax-6 positive amacrine cells from day 14 after $NaIO_3$. Arguably, this is a secondary effect of $NaIO_3$ on RPE cells (Carido et al., 2014).

$NaIO_3$-induced retinal toxicity has been studied in a wide variety of animals such as rabbits (Heike and Marmor, 1990, Yoon and Marmor, 1993), sheep (Nilsson et al., 1977), pig (Mones et al., 2016), rats (Chen et al., 2009, Garcia-Layana et al., 2009, Gong et al., 2008, Ohtaka et al., 2006) as well as mice (Machalinska et al., 2011, Redfern et al., 2011, Carido et al., 2014).

1.11.4 Time course of pathology

The effects of sodium iodate are very rapid, with changes seen within 1 hour of $NaIO_3$ administration; RPE cell nuclei become defragmented, fluid accumulates between the POS, causing tearing of the POS from the RPE (Hariri et al., 2013). Adhesion is reduced between the RPE and Bruch's membrane (Yoon and Marmor, 1993). RPE cytoplasmic organelles start to swell. The basement membrane degenerates. Apical microvilli are lost and the POS become disorganised. The separation of the RPE and POS, caused by fluid accumulation, starts to reduce between 3-12 hours after $NaIO_3$ administration (Hariri et al., 2013). At this stage, the RPE is necrotic and the retinal layers are not fully defined. RPE cells are flattened and devoid of nuclei within 12 hours of $NaIO_3$ administration (Machalinska et al., 2010). RPE markers Otx2, RPE65 and ZO-1 are lost by 24 hours (Carido et al., 2014). By day 3, the RPE has disintegrated,

nuclei defragmented, with a thin layer of melanin remaining, loss of apical microvilli and tight junction and macrophage infiltration (Carido et al., 2014, Machalinska et al., 2010). The 3rd day also marks the peak of photoreceptor apoptosis (Machalinska et al., 2010). Scotopic ERG responses are abolished (Carido et al., 2014). After 1 week, the thickness of the ONL is significantly less and the length of the POS and PIS are shortened (Machalinska et al., 2010). Hariri et al found that there was a strong variation in timing of morphological changes between animals, though, this variation was reduced when the $NaIO_3$ was administered with an additional subcutaneous saline injection. It also helped reduce side effects of drug toxicity such as blood in urine (Hariri et al., 2013).

1.11.5 Effects of dose and route of administration

The severity and time delay in pathology depends greatly on dose and route of administration. Also, at a low dose of $NaIO_3$, the RPE in the central retina can be selectively targeted, and the peripheral RPE relatively spared.

Administration via the Orbital Venous plexus

$NaIO_3$ administered via the orbital venous plexus (the retro orbital sinus) has an extremely rapid and severe response. At a dose of 40 mg/kg in mice the whole RPE is destroyed within 24 hours and the scotopic and photopic ERG is completely diminished by day 3. While, at 20 mg/kg, the peripheral retina is much less severely degenerated, with healthy polygonal cells remaining and a small remaining photopic b-wave is observed. RPE cells are absent in the centre of the eye cup and the remaining peripheral RPE cells become more irregular in shape towards the centre. Their border curvature and area increase as they get closer to the eyecup centre as the cells rearrange to try cover the area from shed cells.

These cells lose their characteristics such as polygonal shape and RPE65, which was not recovered 1 month after $NaIO_3$ (Machalinska et al., 2010, Xia et al., 2011, Wang et al., 2014). No effect was seen at a dose of 10mg/Kg (Wang et al., 2014).

Administration via the tail vein

Administering $NaIO_3$ via the caudal tail vein requires a higher dose to achieve similar results as those via the orbital region. Enzmann and colleagues claimed that there is no significant effect on the RPE or ONL with a dose of 35mg/kg and very few disruptions to the overall morphology even up to 14 days (Enzmann et al., 2006). Redfern et al showed that the peripheral retina has less marked degeneration than central retinal and closely resembled normal retina after 50 mg/kg sodium iodate. There was a clear recovery of the peripheral retina 2 weeks post-dose and at 4 weeks head tracking tests showed visual acuity had recovered to normal levels in Han Wistar rats (Redfern et al., 2011). Carido et al. reported that at 70 mg/Kg, RPE was retained at the periphery for longer but the peripheral RPE had damaged nuclei and did not label positive for Otx2 (Carido et al., 2014). Enzmann et al. demonstrated that at 70mg/kg $NaIO_3$, RPE cells across the whole retina were destroyed by day 3 after $NaIO_3$ administration (Enzmann et al., 2006).15 mg/kg $NaIO_3$ still causes rapid RPE cell loss, even though, the number of cell in the ONL does not fall to a significant level until 3 months after the $NaIO_3$ injection. Whereas, a dose of 25 mg/kg and 35 kg/mg, result in significant loss of ONL cells by 14 days and 3 days respectively (Franco et al., 2009). 15 mg/kg NaIO3 significant reduces the optokinetic response (OKR) response in mice, which decreases until day 7, yet the mice are still capable of performing in the water maze (WM) task. After 25 mg/kg the OKR is absent on day 3 but improves over the next 3 months, and 35 mg/kg reduces performance in WM on day 14 but

OKR is lost by day 3. The RPE benefits from partial recovery 3 months after $NaIO_3$, observed by an increase in autofluorescence in whole eye flatmount preparations (Franco et al., 2009). RPE cells and Müller glial cells can proliferate in response to acute injury, because of this, $NaIO_3$-induced retinopathy can improve over time. At a higher dose of 70mg/Kg no recovery of retinal function is seen. ERG responses are completely lost by day 14 and OKR is lost by day 21 (Carido et al., 2014).

Administration via the intraperitoneal route

A dose of 100mg/kg $NAIO_3$ administered via the intraperitoneal (IP) route also provided rapid necrosis of RPE cells after 6 hours; some RPE cells remained after 7 days, although, it affected central and peripheral retina equally. No differences were reported between male and female mice (Kiuchi et al., 2002). Major blood vessels of the choroidal and retinal circulation enter and exit the eye at the optic nerve and have their largest diameter there, thus delivery of and perhaps damage from sodium iodate is greatest in this region. Peripheral regions may also be repaired more rapidly due to the presence of progenitor cells in this region (von Leithner et al., 2010). Caution must be exercised when using published data for planning an experiment. It is difficult to extrapolate from different studies due to different doses, route of administration, time points, strain of animals, age of animal and the examination methods. These results are important when considering a suitable model to investigate a regenerative therapy. Additionally, it was reported that a dose of 100 mg/Kg administered via the IP route resulted in systemic toxicity and high mortality in C57 and BALBc mice (Chowers et al., 2017). Although, this is much lower than the LD50 (lethal dose for 50% of population), which is 505 mg/Kg (Sigma).

Table 1 Effects of route of administration and dose of $NaIO_3$ on RPE and retinal function

Dose	Retro-orbitally	Intravenously	Intraperitoneally
10-15 mg/Kg	No changes in fundus or OCT. RPE marker expression unchanged. Normal ERG (Wang et al., 2014)	Loss of RPE and decrease in OKR (Franco et al., 2009)	
20-25 mg/Kg	Relative sparing of peripheral RPE, but loss of RPE markers. ERGs reduced but not flatlined (Machalinska et al., 2010, Wang et al., 2014).	Loss of RPE and transient loss of OKR (Franco et al., 2009)	Inconsistent results. Histology and ERGs ranged from near normal to severe (Chowers et al., 2017).
30-35 mg/Kg	Relative sparing of peripheral RPE, but loss of RPE markers. Complete loss of scotopic and photopic b-wave (Wang et al., 2014)	No significant changes in autofluoresence or ONL thickness (Enzmann et al., 2006). Significant loss of RPE and loss of OKR (Franco et al., 2009).	
40 mg/Kg	Total eye cup affected. ERG flatlined (Machalinska et al., 2010).		
50 mg/Kg		Central RPE loss, which grew with time (Enzmann et al., 2006).	ERG significantly reduced and loss of RPE markers by 24 h. Total loss of RPE markers and ERG flatlined by 4 weeks (Chowers et al., 2017).
70 mg/Kg		Total eye cup affected. OKR and ERG responses eliminated (Carido et al., 2014, Enzmann et al., 2006)	
100 mg/Kg			RPE death (Kiuchi et al., 2002). High mortality rate (Chowers et al., 2017).

Evidence of proliferation and retinal recovery

Expression of markers for mitosis peak 2-3 days after $NaIO_3$ administration (Redfern et al., 2011). 3 days after $NaIO_3$ administration there is evidence of Müller cell proliferation, macrophage migration and RPE cell regeneration (Kiuchi et al., 2002). It was shown that stem or progenitor cells in the blood start homing into the retina 3 days after NaIO3 injection. Despite this, functional recovery is not achieved by these stem cells (Machalinska et al., 2011) and synaptophysin, a marker for synaptic vesicles in the PIS, is depleted, even after 6 weeks (Redfern et al., 2011). Thus, the natural process of cell replacement and proliferation is too late and ineffective at preventing photoreceptor loss.

1.11.6 Cell studies using the $NaIO_3$ model

The $NaIO_3$ model has been used to study transplantation of bone-marrow derived stem cells (Harris et al., 2006), mesenchymal stem cells (Gong et al., 2008), hESC-derived retinal progenitors (Amirpour et al., 2012) and hESC-RPE cells (Carido et al., 2014). Atmaca-Sonmez et al carried out a study to decide the optimum time for cell transplantation following 50 mg/Kg $NaIO_3$ injected intravenously. Using GFP^+ bone marrow-derived and haematopoietic stem cells, optimum transplantation times were observed by transplanting these cells in to the tail vein in a range of days following $NaIO_3$-treatment. Their results showed that 5-7 days after $NaIO_3$ is best for bone marrow-derived and haematopoietic stem cell incorporation and survival in the subretinal space (Atmaca-Sonmez et al., 2006). These GFP+ cells stained positive for RPE65. It was shown that stem or progenitor cells in the blood homing into the retina 3 days after NaIO3 injection (Atmaca-Sonmez et al., 2006). The same group mobilised bone marrow-derived stem cells and directed them to the retina three days after an intravenous injection

of 25 mg/Kg $NaIO_3$ in mice. They saw significant improvements in the OKR 21 and 28 days after $NaIO_3$ administration (Enzmann et al., 2017).

hESC-RPE cell transplantation

Between 100-200,000 hESC-RPE cells were transplanted subretinally into C57 mice 1 week after 70 mg/Kg NaIO3 administered via the tail vein. The hESC-RPE cells formed extensive monolayers in the sub-retinal space, attached to Bruch's membrane, highlighting the value of removing host RPE cells prior to transplantation. The transplanted RPE cells had correct apical-basolateral organisation, with basal nuclei and apical melanosomes and microvilli. While there was evidence of phagocytosis by the grafted HESC-RPE cells and preservation of the ONL, no functional recovery was observed by ERG. Cells were not transplanted until 7 days post $NaIO_3$, when there was already a significant reduction in photoreceptors and a complete loss of all normal ERG responses (Carido et al., 2014). $NaIO_3$ is a fast-acting chemical; it has been reported that RPE cell death occurs within 12 hours and by 3 days the RPE cells are destroyed (Hariri et al., 2013, Machalinska et al., 2010). It is possible that although the grafted hESC-RPE cells could phagocytose rhodopsin positive debris, these cells were not sufficiently differentiated to perform the visual cycle. In support of this, there was no confirmation that the hESC-RPE cells used in the study by Carido and colleagues could express visual cycle markers either *in vitro* or *in vivo* (Carido et al., 2014). It is also important to consider the possibility that the number of surviving human RPE cells was insufficient to significantly improve the ERG (which is a fields potential) in the study by Carido and colleagues. A review of the literature suggests that the clearance rate of $NaIO_3$ is unknown. $NaIO_3$ is likely to be cleared quickly as time frames for cell death are similar

regardless of the dose used and at smaller doses of $NaIO_3$ the peripheral RPE is spared.

Another study on albino rabbits transplanted 50,000 hESC-RPE cells subretinally in to eyes treated with 50 µL 1mM $NaIO_3$ subretinally. They found that hESC-RPE cells did not integrate into areas of degenerated outer-retina but were located in areas with preserved photoreceptor nuclei and POS. 2 months post transplantation the pigmented donor RPE did not label positive for RPE65, although, by 8 months RPE65 was expressed in these cells (Petrus-Reurer et al., 2017).

The $NaIO_3$ model of retinopathy is very useful for the study of RPE stem cells transplant as no naturally occurring models of RPE death in adult animals are available. The $NaIO_3$ model is a rapid model to generate, with effects seen after a single injection. It has a powerful rapid effect and loss of RPE cells is dose dependent. It is also cheaper than inducible knock out models, which are expensive and difficult to produce (Longbottom et al., 2009). It is not yet known if lasting retinal recovery from $NaIO_3$ toxicity is possible but this would be an important pre-clinical readout for RPE stem cell therapy. This model could also be used in conjunction with the *rd12* model to clear RPE cells, to give space for the transplanted RPE cells to settle down. Still, caution should be exercised when comparing acute retinal injury to a chronic disease such as AMD. A key difference between this model and naturally occurring retinopathy is that $NaIO_3$ is a fast-acting, once off insult, while most retinopathies are slow and progressive.

Aims and objectives of the Thesis

Given the shortcomings of the RCS rat described above, the aim of this thesis is to investigate two alternative models for studying RPE cell transplantation and to determine the importance of the RPE on the function of the melanopsin system.

The first model uses $NaIO_3$ to chemically remove RPE cells prior to grafting RPE cells into the subretinal space and may have a benefit of clearing Bruch's membrane to allow transplanted cells to anchor. The second model is the *rd12* mouse, which has a mutation in *rpe65*, resulting in the loss of the visual cycle. The possible benefit of this model is that any improved functional effects are likely to be visual cycle specific. The value of these models for studying RPE cell transplantation is determined by examining residual retinal function and histology, and determining if retinal function can improve with synthetic chromophore prior to assessing retinal function improvements with grafted hESC-RPE cells.

The reliance of the melanopsin system on the RPE will be examined by assessing the effect of chemically removing RPE cells and the loss of the visual cycle on melanopsin function and if either synthetic chromophore or *rpe65* gene restoration can improve melanopsin function in the *rd12* mouse.

Chapter 2 Methods

2.1 Animal housing

All procedures were conducted according to the Home Office (UK) regulations, under the Animals (Scientific Procedures) Act of 1986, and with local (UCL-Institute of Ophthalmology, London, UK) ethics committee approval. C57BL/6 (C57) mice and *rd12* mice were used in this study. All animals were housed under a 12:12 hour light dark cycle (lights on a 7 a.m.), with food and water available *ad libitum.* All studies were age and sex matched.

2.2 Functional Assessment of animal visual responses

2.2.1 Electroretinography

To record an ERG, Animals were dark adapted for overnight and anesthetised under dim red light with Ketamine (6 mg/100g; Narketan® 10, vétoquinol) and Medetomidine Hydrochloride (0.1 mg/100 g; Domitor, Orion Pharma) in injection water (Norbrook, Newry, UK) via IP route 20 minutes before retinal recording. Pupils were dilated, to allow maximum light stimulus, with 1% tropicamide (Bausche and Lomb, Kingston-on-Thames, UK) and 2.5% phenylephrine (Bausche and Lomb, Kingston-on-Thames, UK). Tropicamide is an anti-muscarinic drug, which prevents the iris sphincter muscle from contracting. Phenylephrine is an α_1-adrenergic receptor agonist, which activates the pupil dilator muscle. Viscotears® (Alcon) was applied to the cornea to maintain hydration. Active gold loop electrodes, were placed on the corneas and held in position with Viscotears®. The reference electrode was inserted subcutaneously

on the head between the ears. The ground electrode was inserted subcutaneously on the back of the animal. ERGs were recorded from both eyes under scotopic and photopic conditions. Scotopic flash intensity range was -5 to 1 lg cd/s/m^2 in a ganzfeld colour dome by LED stimulator. In order to investigate the rod response at high intensities, some animals were also recorded from a high intensity scotopic protocol with flash intensity from -4.5 to 3.5 lg cd/s/m^2. After light adaption for 15 minutes, photopic responses were recorded at a background light intensity of 20 cd/m^2 and increasing flash intensities of -1 to 1.5 lg cd/s/m^2. The responses were measured using espion Diagnosys software. Where the wave was absent in the recording the amplitude was recorded as zero and the latency/implicit time was omitted from results. Where both eyes are treated equally, they are analysed as separate subjects. Animals were recovered from medetomidine hydrochloride with antipamezole (0.1 mg/100 g; Antisedan, Vétoquinol) in injection water (Norbrook, Newry, UK) via the IP route. All ERG recordings were carried out between 9 a.m. and 4 p.m. with animals alternated from control or experimental group where to possible to counter act effects of circadian changes in the recordings. While, the use of candelas as a recording of light intensity may pose controversy as it is weighted by the sensitivity of the human eye to different wavelengths, this is the measurement generally reported in studies using rodents (Carido et al., 2014, Li et al., 2011, Li et al., 2012b, Machalinska et al., 2010, Nusinowitz et al., 2006, Pang et al., 2010, Pang et al., 2005, Pang et al., 2006, Wang et al., 2014, Wright et al., 2014).

2.2.2 Behavioural Light Aversion (BLA)

Normally mice will prefer to be in dark or dim light and would choose this over bright light when presented with the choice. Melanopsin alone can drive this

effect, but it is not required for this effect to occur, although with melanopsin the behavioural light aversion increases with time (Semo et al., 2010). Methods to assess BLA have previously been reported in Semo et al., 2010. In brief, an open field arena was used, illustrated in Figure 2.1, with a closed back half that is kept in darkness and an open front half which is either illuminated (600 μW/cm^2/1,300 Lux) or also in darkness. This arena allowed a mouse to pass to either side easily. A naïve mouse was placed in the open front half and monitored for 31 minutes where it travelled using infrared light. The first minute was always discounted, to give the mouse time to acclimatise to the new surroundings. Comparisons were made between groups and within a group comparing animals in an arena with the front half under a bright light compared to a completely dark arena. Total time spent in the dark was analysed by a one-tailed Mann Whitney U t-test. Time spent in the dark was also analysed in 5-minute bins by two-way repeated measures ANOVA with post-hoc Holm-Sidak's multiple comparisons test and linear regression. All BLA tests were run between 9 a.m. and 12 p.m. and animals were alternated from control and experimental groups to counteract effects of circadian changes in behaviour.

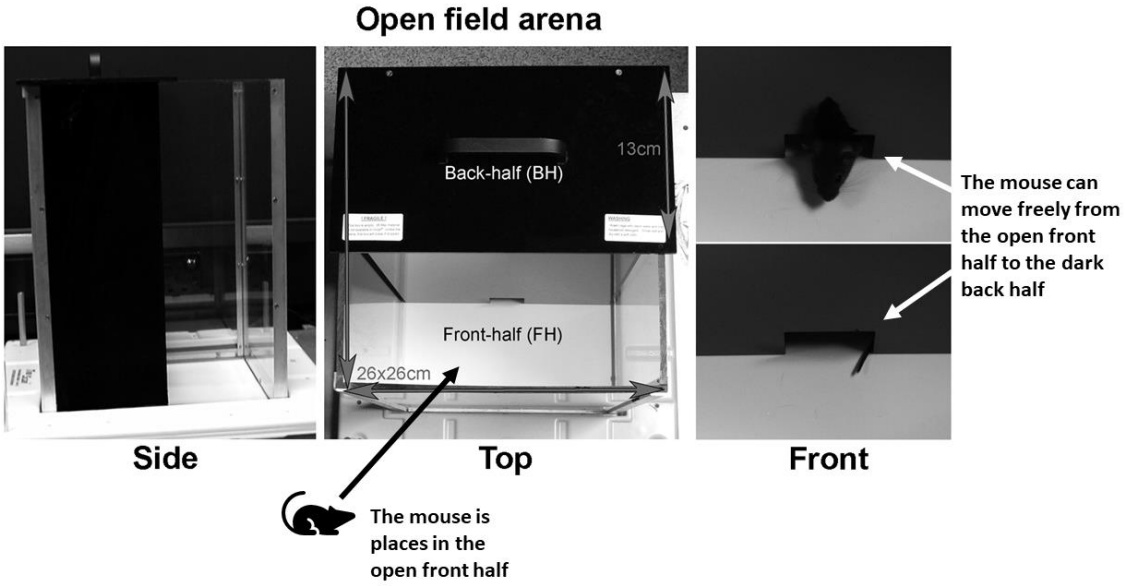

Figure 2.1 Open Field Arena for testing Behavioural Light Aversion
A mouse placed in the open front half could move freely between the open front half and the dark back half, by an opening in the centre. Comparisons were made between behaviours when the front half was illuminated with behaviours when both halves were under complete darkness. Figure adapted from Semo et al., 2010.

2.2.3 Pupillary Light Reflex

The PLR is used to measure both outer-retinal photoreceptor and ipRGC function in live animals. The PLR was measured in un-anaesthetised mice dark-adapted for at least 2 hours. Equipment used to record the PLR was previously descried in Semo et al., 2010. Eyes were illuminated with infra-red light and stimulated with a broad-spectrum white light from a xenon-arc lamp (Lambda DG-4, Linton Instrumentation) which was heat filtered for wavelengths >600 nm and guided through a fibre optic cable which terminated 5 cm from the eye. Animals were recorded and stimulated for 60 s by white light. A range of light intensities were used to assess the PLR. The 30 s prior- and 60 s post-light stimulus were also recorded. Spatially binned (2x2) frames at 4 Hz were collected. Pupil area was estimated off-line by an observer using customized MATLAB software at frame times -30, -25, -20, -15, -10, -5, 0, 1, 2, 3, 4, 5, 7, 11, 15, 20, 30, 40, 50, 60, 61,

69, 77, 85, 93, 101, 109, 117, 125, 133, 141 and 149s, where T0 indicated the point at which the light is stimulated. Measurements of pupil area are expressed as normalised to pupil area at T0. Two-way ANOVA and post-hoc Holm-Sidak's multiple comparisons test were carried out on PLR constriction traces. Repeated measures were not applied to the ANOVA as these recordings were on live animals and some time-points during the recording were not captured as the pupil was out of focus. Maximum pupil constriction was defined by the lowest point of constriction within the first 30 seconds of lights on. Two-way ANOVA was used to analyse the maximum constriction over the different light powers. Latency to 90% peak constriction was also analysed by two-way ANOVA. Baseline pupil area at time zero was analysed by two-tailed Mann Whitney t-test.

All PLR recordings were carried out between 10 a.m. and 3 p.m. and animals alternated from control and experimental group to counteract effects of circadian changes. A group is determined to have a constriction if the average pupil size during light on is significantly less than 1 (pupil area at time 0).

2.2.4 Intrinsic pupillary light reflex

The iPLR is used to measure isolated melanopsin function. While ipRGC function can be recorded in the PLR, these recordings are an output of both ipRGC and outer-retinal photoreceptors (Chen et al., 2011, Guler et al., 2008, Hattar et al., 2003, Lucas et al., 2001, Lucas et al., 2003). Using the PLR to assess ipRGC function in a model of inhibited visual cycle may make it difficult to distinguish ipRGC from outer-retinal photoreceptor function. Thus, recording the iPLR allows the isolation of melanopsin function (Semo et al., 2014, Xue et al., 2011). To record this the eye must not receive input from the brain, thus eyes are excised from culled animals. This means that this procedure is a final functional recording

and may not be appropriate when perfusion is the preferred method of fixation. Methodology for recording iPLR in whole eyes was previously described in Vugler et al., 2015 and recordings in isolated anterior chamber were described previously by Semo et al., 2014. In brief, mice were dark adapted overnight. Mice were culled swiftly under dim red light by cervical dislocation and the eyes enucleated and placed in Neurobasal® culture medium (12348-017; Invitrogen) which had been pre-heated to 37°C. Eyes were illuminated with infra-red light and stimulated with a broad-spectrum white light as described in PLR methodology. The fibre optic cable terminated 1.5 cm from the cornea, delivering 40 mW/cm^2 to the eye. Baseline video recording of pupil was made for 30 seconds using infrared camera followed by light stimulation for 60 seconds and then 60 seconds in darkness to monitor pupil recovery. Recordings and analysis are as described in the PLR methodology. iPLR recordings were all carried out between 9 a.m. and 12 p.m. and animals alternated between control and experimental groups to counteract the effects of circadian changes.

2.3 Histology

2.3.1 Fixation of tissue

Animals were first perfused to fix the tissue and remove background auto-fluorescence from blood. Animals were euthanised by a 10 ml/Kg injection of Sodium Pentobarbital. Once reflexes were lost, a cut was made along the sternum, then the diaphragm was cut along the bottom and the ribs were cut up towards the head on the outside of the lungs to expose the heart. The left ventricle was cut to allow the cannula to enter the ascending aorta. Once the cannula tip was visible in the aorta, the cannula was clamped into place. The right atrium was

then punctured, allowing the return circulation to escape. 0.1M phosphate buffer saline (PBS, approximately 50 mL) was pumped through the cannula and into the aorta, this was then followed by 4% paraformaldehyde (PFA), until the body becomes stiff (approximately 100 mL). The eyes were then removed, the cornea punctured and placed in 4% PFA at 4°C to allow further fixation. All perfusions were carried out at the same time of day and alternated between control and experimental animals to counteract effects of circadian changes to protein expression.

2.3.2 Sectioning and immunostaining retinas

Eyes were fixed in 4% PFA overnight, then cryoprotected in 30% sucrose in 0.1 M PBS overnight at 4°C. Corneas and lenses were removed from the eyes, which were frozen in tissue-Tek® O.C.T (VWR) and stored at -80°C. The eyes were cut in 16 µm sections along the sagittal axis from the middle third of the eye using the cryostat (Leica CM1850). Cut sections were thaw-mounted onto Superfrost Plus slides (BDH, Poole, UK) and allowed to dry at room temperature overnight and stored at -80°C.

To label the protein with fluorescent marker, the sections were incubated in 5% normal donkey serum (NDS) in 0.3% triton X-100 (BDH Cat#366324N) in PBS for 1 h. The sections were then incubated overnight at room temperature with the primary antibody diluted in 1 % NDS in 0.3% Triton X-100 in PBS. Contol slides were treated identically, except the primary antibody was omitted. Slides were washed multiple times in PBS before secondary antibodies were applied. Secondary antibodies were diluted in 2% NDS in 0.3% Triton X-100 in PBS and were incubated with the sections in the dark for 1 h. the sections were then incubated with 0.02% DAPI in PBS for 1 minute, after which the slides were

washed multiple times with PBS and then multiple times with tris-buffered saline (TBS), mounted with Vectashield (Vector Laboratories) and coverslipped.

2.3.3 Flatmounting and immunostaining

Depending on the protein of interest, retinas were flatmounted to get a composite view of the retina. After perfusion, eyes were fixed for 2 h in 4% PFA at 4°C. Each eye was then pinned to a wax plate and the cornea and lens removed. Cuts were made in the dorsal, nasal, ventral and temporal retina. The retina was teased away from the RPE and cut away from the optic nerve and placed in 4% PFA. The retina was then placed on a slide with the inner retina facing up. A non-fibrous paper was then placed on top of the retina, which sticks to it, due to the presence of the vitreous. This was then placed in 4% PFA for 20 minutes followed by a wash in PBS where the retina floats off the paper removing the vitreous. The retina or RPE was blocked for 2 h in 5% NDS in 3% Triton X-100 in PBS on a shaker. Primary antibodies were prepared in 1% NDS in 3% Triton X-100 in PBS and the samples were incubated with this preparation overnight on a shaker. After multiple washes in PBS, secondary antibody was made up in 2% NDS in 0.3% Triton X-100 in PBS and incubated with the samples for 2 h in darkness on a shaker. The tissue was then incubated with 0.02% DAPI (4',6-diamidino-2-phenylindole, Sigma Aldrich) in PBS for 1 minute in the dark. After this the tissue was washed multiple times in PBS then multiple times in TBS, then mounted in vectashield and coverslipped.

2.3.4 Imaging and Analysis of flatmounted retinal tissue

Confocal images were taken on either a Zeiss LSM 710 or 700 microscope. For flatmount analysis of melanopsin, Brn3a, Fos and TH, regions covering 399.72

µm x 399.72 µm were sampled from four retinal quadrants: superior-temporal (ST); superior-nasal (SN); inferior-nasal (IN) and inferior-temporal (IT). Z-stacks were taken to ensure capture of displaced cells. The maximum intensity projection was then used for analysis. Confocal files were coded and a single observer made counts of melanopsin and Brn3a cells. Soma counts, size and staining intensity were analysed using MATLAB which could define the boundaries of each soma. Staining intensity was measured in grey level (0-255). Melanopsin-positive neurites were assessed in a programme written in MATLAB described previously in Semo et al., 2016, where images were filtered to enhance elongated structures and only neurites with a length >20 pixels were considered for quantification. A range of thresholds of normalized greylevel were applied to images to identify both weakly and strongly stained neurites (low threshold of 0.02) or to isolate strongly stained neurites (high threshold of 0.1).

2.4 Ocular Treatments

2.4.1 Administration of $NaIO_3$ by IP and retro-orbital route

$NaIO_3$ was dissolved in sterile saline and either injected via IP or retro-orbitally. Animals which received $NaIO_3$ retro-orbitally were anaesthetised with Ketamine (12 mg/100g; Narketan® 10, vétoquinol) and Medetomidine Hydrochloride (0.07 mg/100 g; Domitor, Orion Pharma) in injection water (Norbrook, Newry, UK) via the IP route. $NaIO_3$ was made up at a concentration of 20 mg/mL and a dose of 40 mg/Kg was administered into the orbital plexus of the right eye. Viscotears® (Alcon) was applied to the cornea to maintain hydration. Animals were recovered from medetomidine hydrochloride with antipamezole (0.3 mg/100 g; Antisedan, Vétoquinol) in injection water (Norbrook, Newry, UK) via the IP route.

2.4.2 Administration of replacement chromophore

9-*cis* retinal is widely used in vision experiments as it is easily synthesised and more stable than 11-*cis* retinal. Under dim red light, 25mg 9-*cis*-Retinal (sigma) was dissolved in 250 µL ethanol and then diluted in 10% Bovine Serum albumin (Sigma), 0.9% NaCL to a concentration of 1 mg/100 µL. 9-*cis* retinal was omitted for a saline control. 1 mg 9-*cis* retinal solution (9-*cis*) was injected via IP into animals under dim red light and animals were placed in the dark for 16 hours. This method is an amalgamation of two previous published methods (Fu et al., 2005, Tu et al., 2006).

2.4.3 RPE cell transplantation

To investigate the ability of RPE cell suspension to integrate into mouse retina Shef 6 hESC-RPE cells were transplanted in to the subretinal space in mouse retina. Shef 6 hESC-RPE cells (Passage 2) were incubated with accutase at 37˚C for 80 minutes, until the cells become round. They were then put through a cell strainer. A sample was taken to look at cell viability by mixing 1:1 cell solution:trypan blue. Trypan blue is a dye which healthy cells, with intact cell membranes will not absorb, but it can transverse the membrane of a dead cell. Thus, the number of dead cells in a sample can be counted to determine viability of the cells. Cells were spun down and re-suspended in Dulbecco's modified eagle's medium (DMEM) cell resuspension solution (DRS: 0.005% DNase1, 0.5mM NAC in DMEM F12) to a concentration of 50,000 cell/µl. Animals were anesthetised with Ketamine (12 mg/100g; Narketan® 10, vétoquinol) and Medetomidine Hydrochloride (0.07 mg/100 g; Domitor, Orion Pharma) in injection water (Norbrook, Newry, UK) via the IP route. Pupils were dilated, to allow the

observation of the back of the eye, with 1% tropicamide (Bausche and Lomb, Kingston-on-Thames, UK) and 2.5% phenylephrine (Bausche and Lomb, Kingston-on-Thames, UK). Observing the back of the eye during this procedure aids the delivery of the cells to the correct retinal layer and the success of the surgery is determined visually, by observing retinal detachment and no retinal bleeding. Viscotears® (Alcon) was applied to the cornea to maintain hydration. 1.5 µl cell suspension was injected into the sub-retinal space and a counter-punch was delivered to the cornea to relieve pressure and avoid reflux of cells out of the eye. Animals were recovered from medetomidine hydrochloride with antipamezole (0.3 mg/100 g; Antisedan, Vétoquinol) in injection water (Norbrook, Newry, UK) via the IP route. Mice had been given 170mg/L cyclosporine (Norvartis) in the drinking water three days prior to the transplantation. Animals remained on the immunosuppressant for the remainder of the experiment.

2.4.4 *rpe65* gene therapy

Animals were anesthetised with Ketamine (12 mg/100g; Narketan® 10, vétoquinol) and Medetomidine Hydrochloride (0.07 mg/100 g; Domitor, Orion Pharma) in injection water (Norbrook, Newry, UK) via IP route. Pupils were dilated with 1% tropicamide (Bausche and Lomb, Kingston-on-Thames, UK) and 2.5% phenylephrine (Bausche and Lomb, Kingston-on-Thames, UK). Viscotears® (Alcon) was applied to the cornea to maintain hydration. 1.5 µL virus preparation (1×10^{12} particles/ml) was injected into the sub-retinal space between the RPE and photoreceptors of the Left eye and 2 µL was injected into the vitreous of the right eye, using a 32-gauge needle attached to a Hamilton syringe. A counter-punch was delivered to the cornea to relieve pressure and avoid reflux of virus. Animals were recovered from medetomidine hydrochloride with antipamezole

(0.3 mg/100 g; Antisedan, Vétoquinol) in injection water (Norbrook, Newry, UK) via IP route.

2.5 Statistical Analysis

All statistics were analysed using graphPad Prism (Graphpad Software, San Diego, CA). For comparing two groups with one variable a non-parametric Mann Whitney test was used and or more than two groups a non-parametric Kruskal-wallis test and post-hoc Dunn's multiple comparisons test was used. For two-variables Two-way Analysis of variance (ANOVA) was calculated followed by Holm-Sidak's multiple comparisons test as this is a powerful test. Where data was missing and an ANOVA was not possible to be carried out, the Holm-Sidak comparisons test was used to analyse the data. All graphs plot the mean ± SEM.

Chapter 3 $NaIO_3$: Model of AMD

3.1 Introduction

In this chapter, $NaIO_3$ will be used to selectively kill RPE cells to mirror the death of RPE cells seen in dry AMD. The aim is to look at the potential benefits and examine the limitations of using this model for studying RPE cell transplantation. One of the exciting possibilities of this model is the anchoring of donor RPE on Bruch's membrane seen in mice (Carido et al., 2014) and rabbits (Petrus-Reurer et al., 2017). In studies where host RPE remain, grafted RPE cells can be found as clumps in the subretinal space (Carido et al., 2014, Li and Turner, 1991, Seaton and Turner, 1992, Sheedlo et al., 1991, Carr et al., 2009). Based on published work, it is hypothesised that $NaIO_3$ will create conditions similar to those seen in dry AMD and will be a useful model for studying RPE cell transplantation.

But, before using the model for transplanting RPE cells, an optimum dose and route of administration of $NaIO_3$ must first be determined. There is much variation in the literature surrounding the route of administration, dose of $NaIO_3$ given and the time delay following $NaIO_3$ administration, with severity and time delay in pathology depending greatly upon dose/route of administration. Therefore, the overall aim in this chapter is to determine optimal parameters for creating an RPE cell deficient retinal environment, which retains the ability of effectively signal the restoration of photoreceptor function following RPE cell transplantation.

3.2 Validating the toxic effect of $NaIO_3$ on the retina

3.2.1 Introduction

Comparing the literature there are 3 common methods used for delivering $NaIO_3$: intravenous, IP and retro-orbital. While administering $NaIO_3$ via the caudal tail vein requires a higher dose to achieve similar results to those obtained via the orbital plexus (Enzmann et al., 2006, Machalinska et al., 2010, Redfern et al., 2011), animals require general anaesthesia for retro-orbital injection. General anaesthetic is not required for either IP or intravenous injection. Anaesthetising animals involves the risk of poor recovery and it is desirable to avoid this extra procedure if possible. $NaIO_3$ administered via the tail vein has a more powerful effect on the RPE than IP injection. 70 mg/Kg injected into the tail vein resulted in RPE cell loss in the whole retina (Carido et al., 2014, Enzmann et al., 2006), whereas, 100 mg/Kg administered via IP did not result in total loss of RPE cells (Kiuchi et al., 2002). After our preliminary attempts to administer saline via the tail vein, it was realised that this method was quite difficult and hence too dangerous for me to preform, therefore, $NaIO_3$ was administered via IP in the first instance in a small pilot study to confirm the functioning of the chemical.

3.2.2 Methods

$NaIO_3$ Administration

A 25g mouse was administered 60 mg/Kg $NaIO_3$ in sterile 0.9% NaCl IP at a volume of 200 µL. Two control mice, weighing 24-25g, were also injected IP with 200 µL sterile 0.9% NaCl. RPE cell death was reported 3 days post $NaIO_3$

administered via IP injection (Enzmann et al., 2006), thus this is the time point chosen to be examined in this experiment.

ERGs

Scotopic and Photopic ERGs were recorded 3 days after $NaIO_3$ treatment as described in chapter 2 (page 93). As this was a small pilot experiment, perfusion was not performed, instead, following ERG recordings, animals were culled by cervical dislocation and their eyes excised, the cornea pierced and placed in 4% paraformaldehyde overnight.

Flatmounts

After fixation, the retina was removed from the left eye cup and the RPE was stained with DAPI (1:5000 in PBS).

Rhodopsin staining

Right eyes were cryoprotected, sectioned and stained as described in Chapter 2 page 99. The primary antibody used was anti-rhodopsin raised in rabbit diluted 1:1000 (abcam) and the secondary was donkey anti-rabbit FITC, diluted at 1:200 (Jackson Immuno Research, West Grove, PA, USA). Images were captures on the Zeiss 700 confocal microscope.

3.2.3 Results

Effect of 60 mg/Kg $NaIO_3$ on the ERG

ERG responses were reduced in $NaIO_3$-treated mice and the wave was often negative (Figure 3.1). In saline-treated mice, the b-wave is seen at -5 Lg cd.s/m^2,

and the a-wave appears at -2 Lg cd.s/m^2. These waves are not identifiable in the $NaIO_3$-treated mouse.

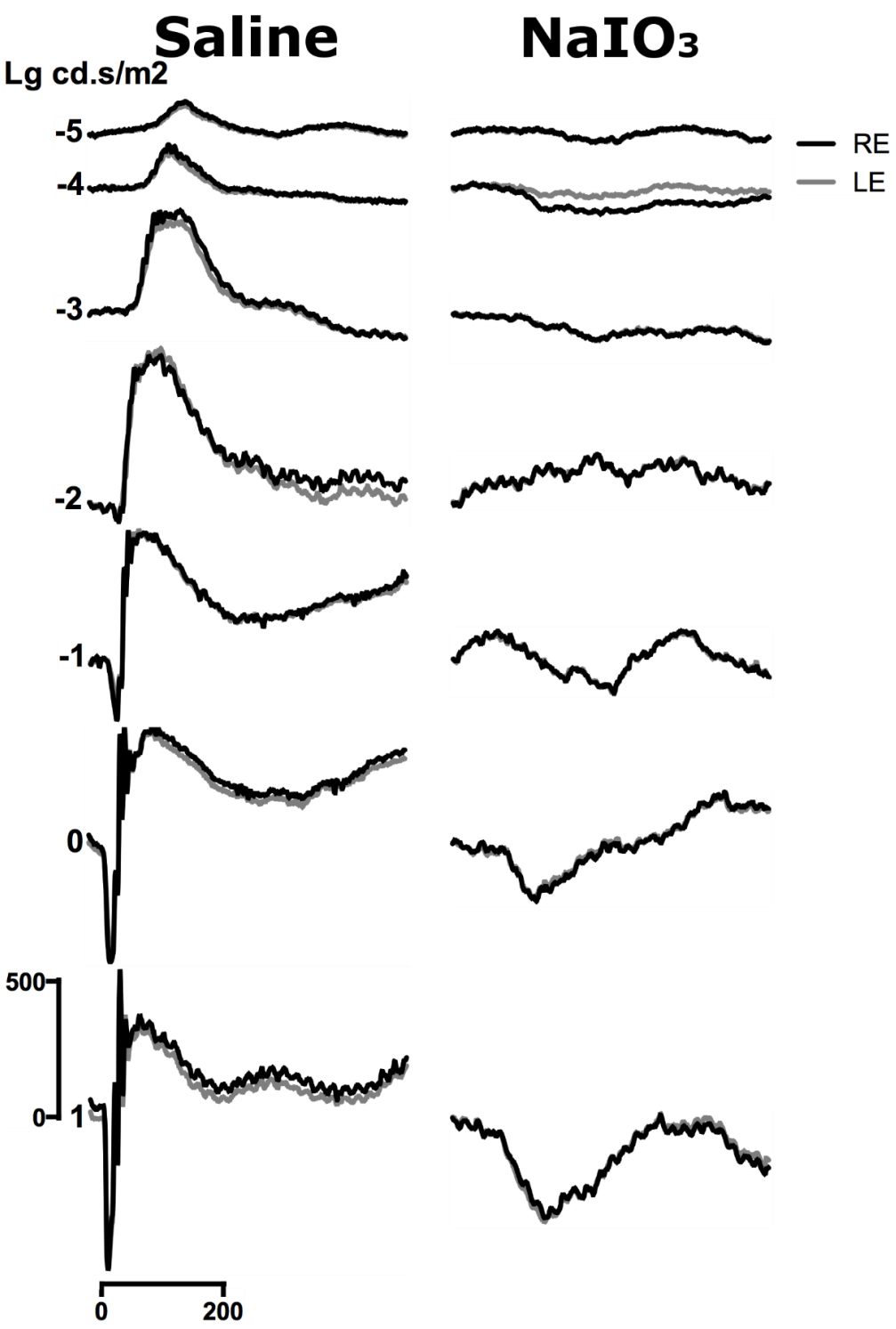

Figure 3.1 Scotopic ERG 3 days following 60 mg/Kg $NaIO_3$.
This figure displays scotopic ERG traces from a saline-treated mouse and $NaIO_3$-treated mouse from -5 to 1 Lg cd.s/m^2. $NaIO_3$-treated mice do not have an obvious a- and b-wave but show a negative ERG at higher light intensities. Both right (RE, black) and left (LE, grey) eye traces are displayed. The vertical scale indicates 500 µV and the horizontal scale indicates 200 ms.

The photopic b-wave is also strikingly reduced and appears negative at the higher light intensity (Figure 3.2).

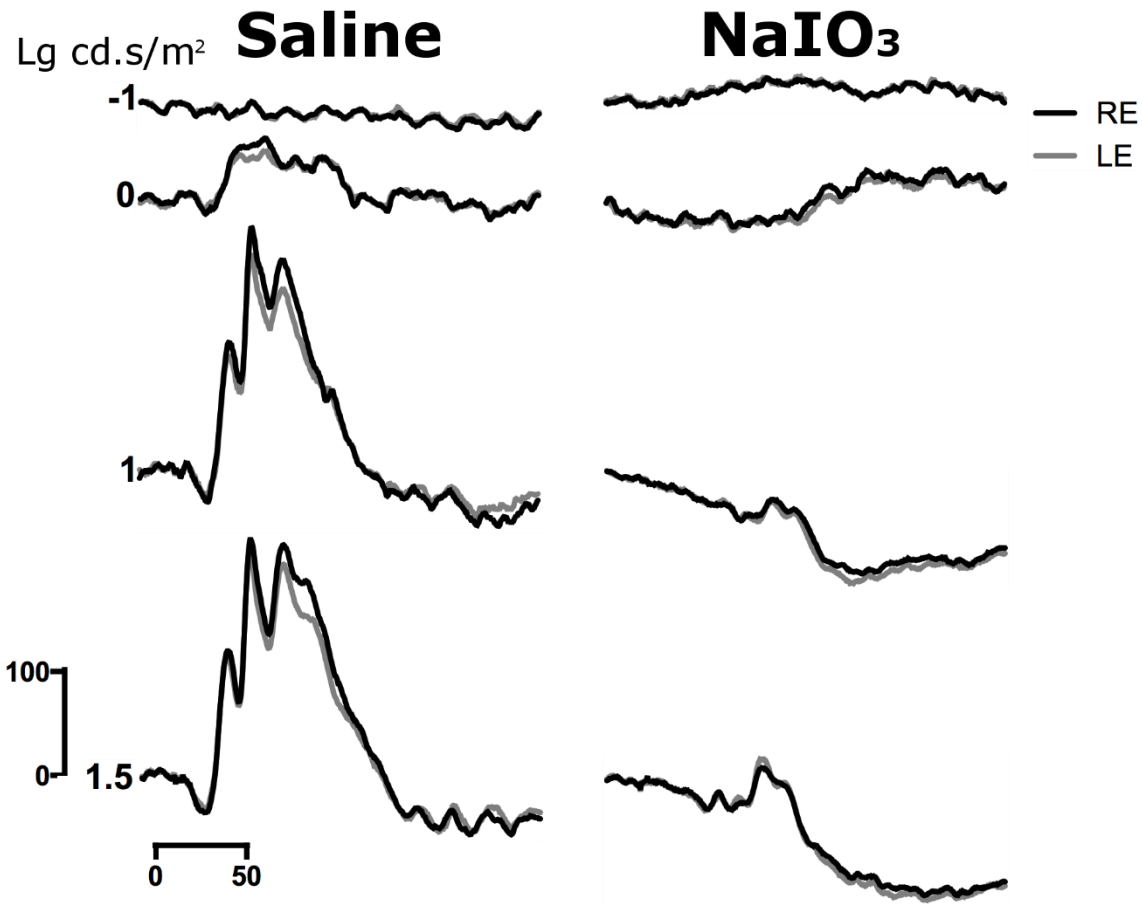

Figure 3.2 Photopic ERG 3 days following 60 mg/Kg NaIO3.
This figure displays photopic ERG traces from a saline-treated mouse and $NaIO_3$-treated mouse from -1 to 1.5 lg cd.s/m^2. $NaIO_3$-treated mice still have a b-wave at high light intensities, though, it is markedly reduced and appears on a negative wave. Both right (RE, black) and left (LE, grey) eye traces are displayed. The vertical scale indicates 100 µV and the horizontal scale indicates 50 ms.

Death of RPE cells following 60 mg/Kg $NaIO_3$

RPE nuclei have mostly disappeared 3 days following $NaIO_3$-treatment and those remaining appear swollen (Figure 3.3).

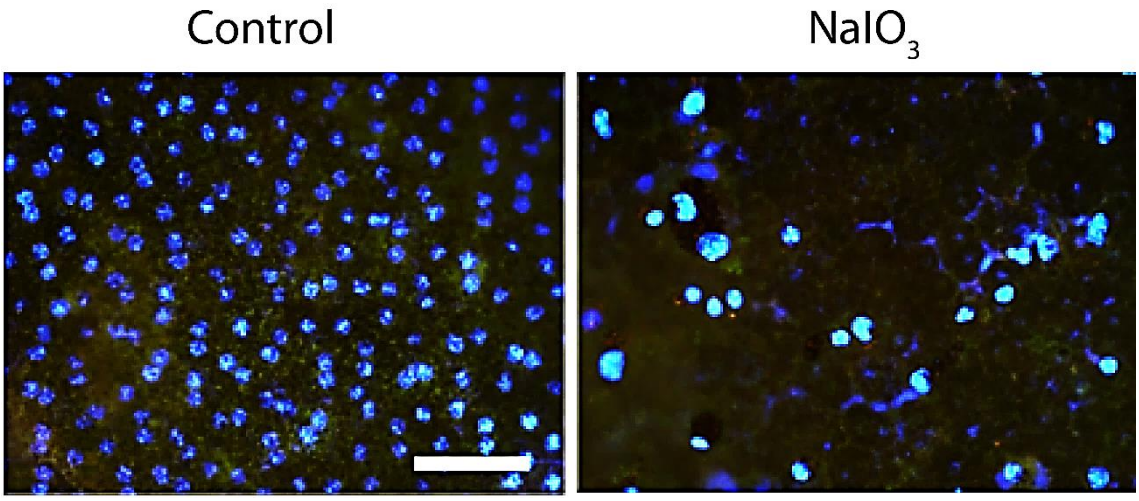

Figure 3.3 Nuclear labelling in flatmount RPE 3 days following 60mg/Kg $NaIO_3$. Nuclei (blue) in the RPE have mostly disappeared. Remaining nuclei appear swollen. Scale bar represents 50 µm.

Effects of 60 mg/Kg $NaIO_3$ on rods

Rhodopsin labelling in $NaIO_3$-treated animals was disorganised and not restricted to POS compared to control animals (Figure 3.4). 3 days following $NaIO_3$ treatment POS are disorganised as well as ONL, which has reduced layers of cells.

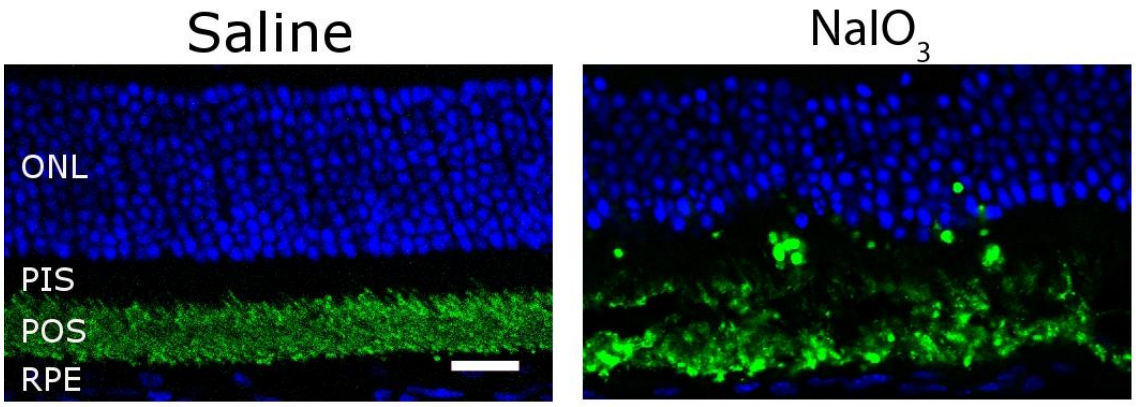

Figure 3.4 Rhodopsin labelling 3 days following 60mg/Kg $NaIO_3$.
While rhodopsin labelling (green) is present, 3 days after $NaIO_3$-treatment, the POS are disorganised and rhodopsin labelling is also found in the PIS. The ONL is also disorganised and has a reduction in the number of layers. Scale bar: 20 µm.

3.2.4 Discussion

During preliminary work, it was decided that administering $NaIO_3$ via the tail vein was an unsafe method of administration and thus, the IP route was then examined for the injection $NaIO_3$. This pilot experiment aimed to validate $NaIO_3$ as an effective toxin to ablate RPE cells and the IP route as a suitable method of administration. At 3 days post $NaIO_3$ treatment the ERG recordings are strikingly reduced, RPE cells are lost and rod degeneration can clearly be seen. Following these results, it is concluded that IP injection appears to be an effective route of delivering $NaIO_3$ and the next step is to expand on these results and investigate the impact on retinal function by a range of $NaIO_3$ doses delivered IP.

3.3 Dose response of $NaIO_3$ injected IP

3.3.1 Introduction

Having established that $NaIO_3$ is effective delivered IP and that a dose of 60 mg/Kg had a marked effect on both RPE cell death and retinal function, a range of doses up to 60 mg/Kg were then investigated for their ability to suppress retinal function as measured by ERG. As not many studies deliver $NaIO_3$ via the IP route, a dose response study was helpful in determining a good dose with would offer maximum RPE death. The death of RPE cells was assessed qualitatively in eyecup wholemounts.

3.3.2 Methods

Doses of 0, 15, 30 or 60 mg/Kg $NaIO_3$ diluted in 0.9% NaCL were given to animals weighing 24 – 35g (100 µL IP). Scotopic and Photopic ERGs were recorded 3 days after $NaIO_3$ treatment as described in 2.2.1.

Statistical Analysis

a-wave and b-wave peaks were attained from the diagnosys software and analysed by repeated measures two-way ANOVA and Holm-sidak multiple comparisons test. Each eye was an individual entry, n = 8 for each dose.

Flatmounts

Following ERGs animals were culled by cervical dislocation and their eyes were fixed in 4% PFA overnight. Animals were not perfused to reduce the time delay following ERGs and this study focused on visual function and not much histology was carried out. Left eyes had the retina removed and the RPE was stained with DAPI for 1 minute (1:5000 in PBS).

3.3.3 Results

Effects of $NaIO_3$ dose response on ERG

The effects of $NaIO_3$ after 3 days has had a significant reduction on the scotopic b-wave amplitude, but the scotopic a-wave was present. The scotopic a-wave amplitude in $NaIO_3$-treated animals increased in amplitude with increased light intensity (Figure 3.5), similar to control animals. There is not a significant effect of the dose of $NaIO_3$ on the scotopic a-wave (Table 2), except at the highest light

intensity, which shows untreated animals have a greater a-wave amplitude compared to $NaIO_3$-treated animals.

While the scotopic b-wave amplitude also shows a trend of increasing amplitude with light intensity (Figure 3.5), this increasing amplitude is significantly reduced in $NaIO_3$-treated animals. There is a clearer dose effect of $NaIO_3$ on the scotopic b-wave amplitude, with the smaller dose of 15 mg/Kg $NaIO_3$ having a greater amplitude than the higher doses of 30 and 60 mg/Kg (Figure 3.5).

Table 2 Two-way ANOVA of Scotopic ERG 3 days after $NaIO_3$ at different doses

Two-way RM ANOVA	Scotopic A-wave		Scotopic B-wave	
	F (DFn, DFd)	P-value	F (DFn, DFd)	P-value
$NaIO_3$ Dose	F (3, 28) = 0.04172	P = 0.9884	F (3, 28) = 12.87	P < 0.0001
Light Intensity	F (6, 168) = 90.20	P < 0.0001	F (6, 168) = 35.96	P < 0.0001
Interaction	F (18, 168) = 1.945	P = 0.0155	F (18, 168) = 5.591	P < 0.0001
Subjects matching	F (28, 168) = 3.717	P < 0.0001	F (28, 168) = 6.407	P < 0.0001

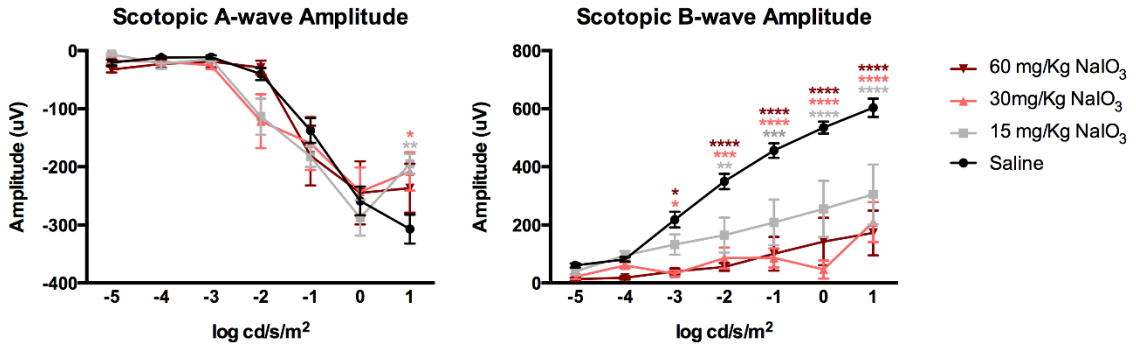

Figure 3.5 Scotopic ERG 3 days after $NaIO_3$ IP dose response.
*The scotopic a-wave is quite robust in $NaIO_3$-treated animals at 3 days. At the highest light intensity there is some significant differences between animals treated with 15 mg/Kg (grey) or 30 mg/Kg (pink) $NaIO_3$ compared to saline-treated animals. Scotopic b-wave amplitudes are decreased in all $NaIO_3$-treated animals and show a dose response where the lower $NaIO_3$ dose of 15 mg/Kg (grey) is less reduced than higher doses of 30 (pink) and 60 mg/Kg (wine). Asterisks indicate significant levels from post hoc tests, colour coded to match dosage groups: *P < 0.05, **P < 0.01, ***P< 0.001, ****P < 0.0001.*

The Photopic b-wave amplitude (Figure 3.6) in $NaIO_3$-treated mice appears to be less affected than the scotopic b-wave amplitude (Figure 3.5). The photopic b-

wave amplitude shows a trend of increasing amplitude with increasing light intensity and $NaIO_3$-treated animals have a lower amplitude than control animals (Table 3).

Table 3 Two-way ANOVA of photopic b-wave amplitude

Two-way RM ANOVA	F (DFn, DFd)	P-value
Dose	F (3, 28) = 5.646	P = 0.0037
Light Intensiy	F (3, 84) = 208.9	P < 0.0001
Interaction	F (9, 84) = 2.508	P = 0.0136
Subjects (matching)	F (28, 84) = 2.298	P = 0.0019

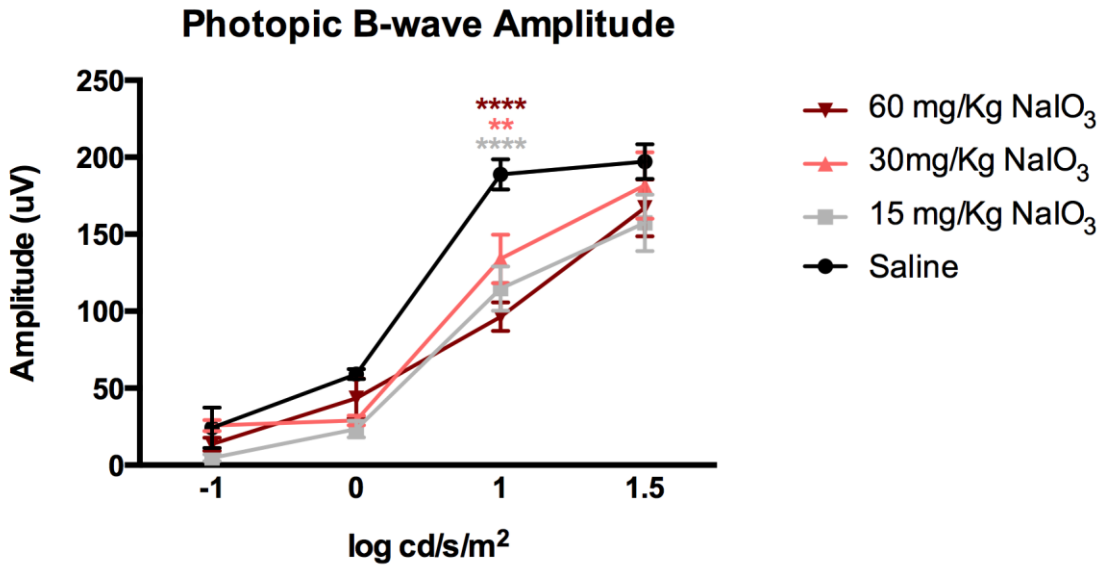

*Figure 3.6 Dose response of $NaIO_3$ on photopic ERG after 3-days. Photopic ERG b-wave amplitudes are reduced in $NaIO_3$-treated animals compared to control animals, although, there is not a clear effect of the different doses of $NaIO_3$ on the photopic b-wave amplitude. Asterisks indicate significance from post-hoc tests: **P < 0.01, ****P < 0.0001.*

While diminishing effects are seen in the ERG of animals treated with $NaIO_3$ on the ERG, there is not an obvious correlation between dose and effect on ERG. This is supported by the variation in traces within groups (Figure 3.7 and Figure 3.8), where the effect of $NaIO_3$ is not entirely consistent even at the highest dose of $NaIO_3$ administered.

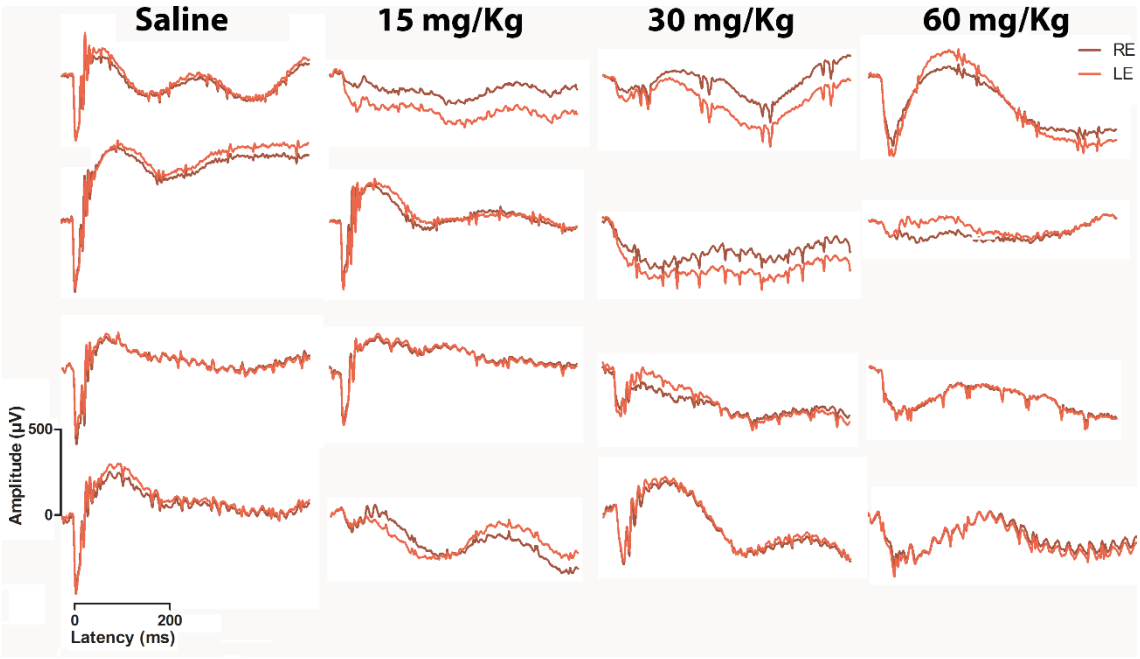

Figure 3.7 Scotopic ERG traces at 1 log cd/s/cm^2 3 days after $NaIO_3$.
This figure displays the average scotopic trace of both eyes for each animal at 1 log cd/s/cm^2. The vertical scale bar indicates 500 μV and the horizontal scale indicates 200 ms. The variability between animals which received the same dose of $NaIO_3$ is clear. RE: right eye; LE: left eye.

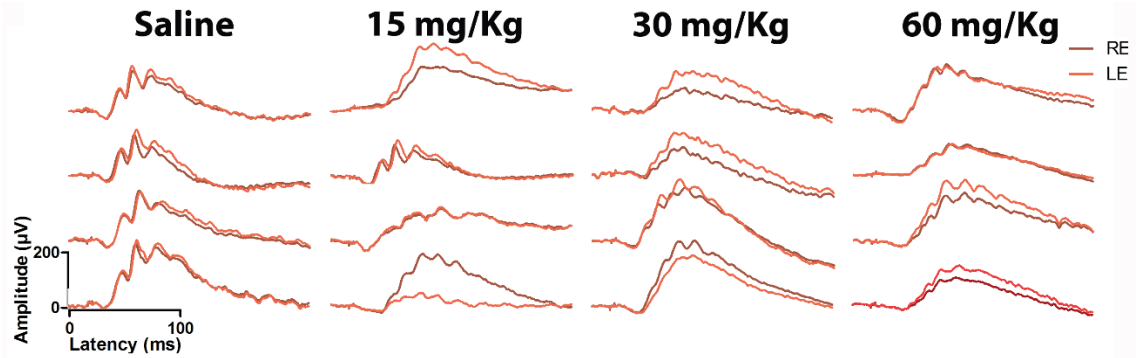

Figure 3.8 Photopic ERG traces at 1.5 log cd/s/cm^2 3 days after $NaIO_3$.
This figure displays average photopic traces of both eyes for each animal at 1.5 log cd/s/cm^2 3 days after $NaIO_3$ administration. The photopic ERG appears to be less affected than the scotopic ERG (Figure 3.7). There is some variation between animals receiving the same dose of $NaIO_3$. RE: right eye; LE: left eye.

Effects of $NaIO_3$ dose response on RPE cell death

The survival of RPE cells in animals from the various dosage groups was analysed qualitatively in RPE flatmount stained with DAPI to show RPE nuclei.

There was a clear degree of variability in RPE cell survival between animals in the same/different dosage groups of $NaIO_3$ (Figure 3.9).

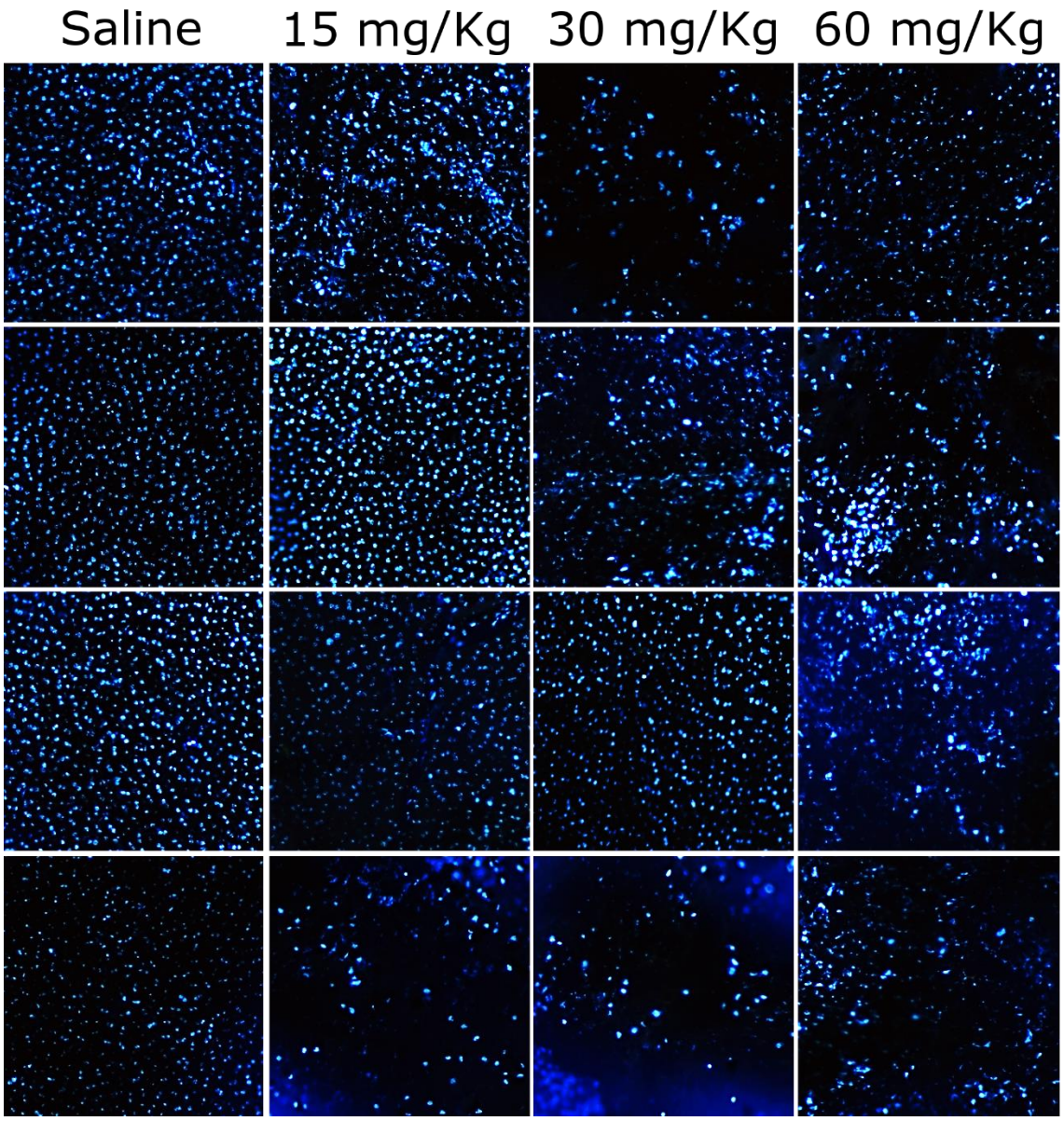

Figure 3.9 Flatmount of RPE Nuclei following $NaIO_3$
This figure displays RPE flatmounts stained with DAPI 3 days after $NaIO_3$ treatment. The images are taken from beside the optic nerve. The results are varied and some flatmounts show greater loss of RPE nuclei than other treated with the same dose of $NaIO_3$. Columns show flatmounts from different animals in the same dosage groups.

3.3.4 Discussion

It is clear that $NaIO_3$ has a diminishing effect on retinal function and this is most pronounced in the scotopic b-wave. Flatmounts illustrate the loss of RPE cells in

the central retina. However, there is much variability between animals receiving the same dose of $NaIO_3$.

3.4 Reversing the functional deficits induced by IP delivery of $NaIO_3$.

3.4.1 Introduction

Having identified $NaIO_3$ induced deficits in the ERG 3 days post-$NaIO_3$ administration, it is important to investigate if this loss of retinal function can be reversed. A key aspect of investigating $NaIO_3$ as a model of AMD with the aim to treat with RPE cell transplantation, is the ability to preserve the retina and its capacity to function. Due to RPE cell loss, the decreased ERG amplitudes may be a direct result of a loss of the visual cycle This possibility will be tested in the current pilot experiment, which examines retinal function following $NaIO_3$ treatment, supplemented with a synthetic chromophore, 9-*cis* retinal.

3.4.2 Methods

NaIO3 administration

Three animals weighing 19-21 g were administered 100 µL 60 mg/Kg $NaIO_3$ in 0.9% NaCl by IP injection. Low numbers were used in this experiment because it used a new untested technique.

9-*cis* retinal administration

9-*cis* retinal was prepared and administered as described in paragraph 2.4.2. Two days after $NaIO_3$-treatment, 2 animals, received 9-*cis* retinal. The remaining

animal received a saline vehicle injection. The animals were then kept in darkness overnight prior to ERG recording the following day.

ERG

Scotopic and photopic ERGs were carried out as described in paragraph 2.2.1.

3.4.3 Results

Effects of 9-*cis* retinal on ERG following 60 mg/Kg $NaIO_3$

These scotopic traces cannot confirm increased ERG with 9-cis, however, this is because $NaIO_3$ did not have a noticeable effect on the ERG (Figure 3.10). Examining the scotopic traces, it is clear that there is too much variability with this $NaIO_3$ method. The $NaIO_3$-treated animal which received saline had a largely unaffected ERG, with an a- and b- wave that falls within the normal range. This suggests that the $NaIO_3$ did significantly affect the ERG in the control animal.

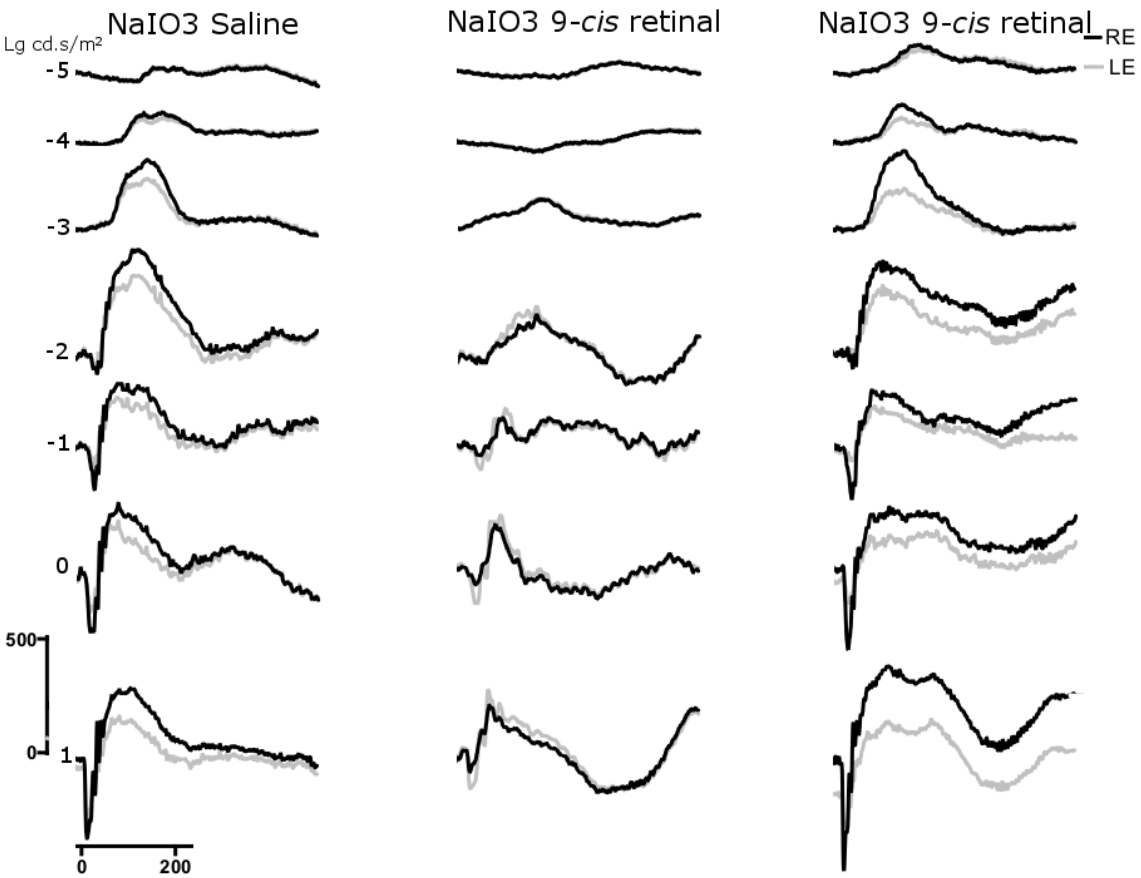

Figure 3.10 Traces of scotopic ERG following 60mg/Kg $NaIO_3$ IP and 9-cis retinal. This figure shows scotopic ERG traces from animals treated with 60mg/Kg $NaIO_3$ and then either given saline or 9-cis retinal. The traces are from increasing light intensities of -5 to 1 log cd/s/cm^2. The vertical scale bar indicates 500 µV and the horizontal scale shows 200 ms. Both left eye (grey) and right eye (black) are shown.

Photopic ERG results (Figure 3.11) tell a similar story to those seen in the scotopic ERG. These results also show strong photopic b-wave in animas treated with $NaIO_3$ and thus no effect of 9-*cis* retinal can be seen.

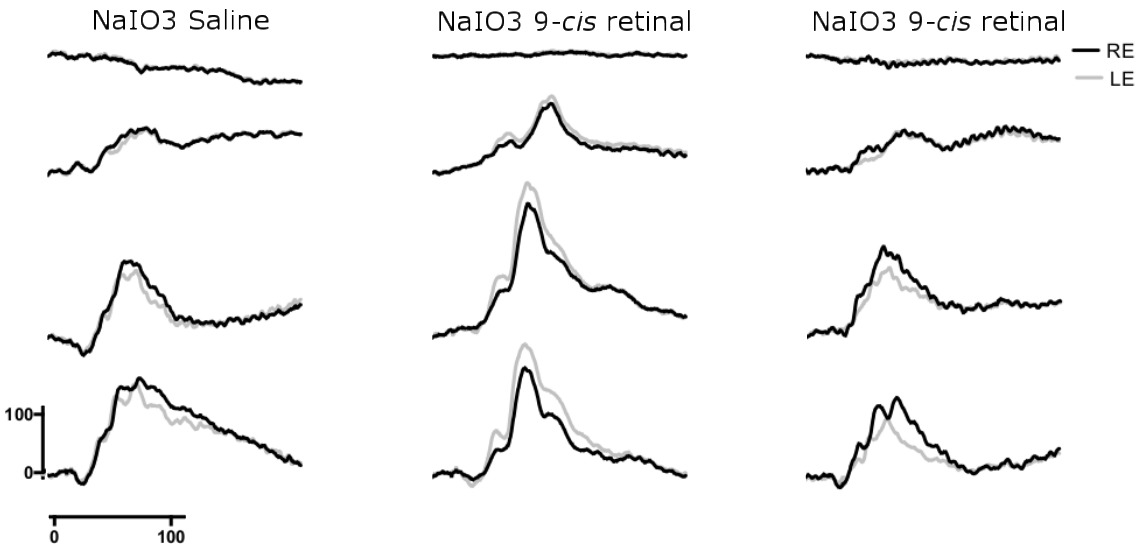

Figure 3.11 Photopic ERG traces following 60mg/Kg $NaIO_3$ IP and 9-cis retinal. This figure displays individual photopic ERG traces from animals treated with 60 mg/Kg $NaIO_3$, who then received either saline or 9-cis retinal. The vertical scale bar indicates 100 µV and the horizontal scale shows 100 ms. Both left eye (grey) and right eye (black) are shown.

3.4.4 Discussion

While this experiment did not show a significant benefit of 9-*cis* retinal, this is likely due to the variability of $NaIO_3$, and the limited number of animals studied. While injecting IP is a simple method of administering $NaIO_3$, it is clear from the data presented above in the experiments 3.3 and 3.4 that this method has a lot of variability. Thus, injecting retro-orbitally, may be more suitable for the purposes of this thesis.

3.5 Retro-orbital injection of $NaIO_3$

3.5.1 Introduction

Given the issue of variability of the effect of $NaIO_3$ using the IP route of administration, it was decided that a retro-orbital approach may help to reduce this variability as the chemical is being delivered to the target site. The literature

shows that a dose of 40 mg/kg delivered retro-orbitally in mice results in the whole RPE being destroyed within 24 hours and a completely diminished the scotopic and photopic ERG by day 3. A lower dose of 20 mg/kg, resulted in the peripheral retina much less severely degenerated, with healthy polygonal cells remaining and a small remaining photopic b-wave observed (Machalinska et al., 2010, Xia et al., 2011). Thus, a dose of 40 mg/Kg $NaIO_3$ was chosen for removing RPE cells. While a range of time points were used for histology assessment, the timepoint of 1 month was chosen for examining functional tests as this was a realistic time point for assessing post-grafting efficacy of RPE cells, the main objective of this chapter.

3.5.2

3.5.3 Methods

Administering $NaIO_3$ retro-orbitally

Female mice aged 11-12 weeks, weighing 19-21 g, were injected retro-orbitally behind the right eye with 40 mg/Kg $NaIO_3$, made up to a concentration of 20 mg/mL, as described in paragraph 2.4.1. Control mice were untreated.

ERG

ERG's were carried out at 1-month post $NaIO_3$ administration as previously described in paragraph 2.2.1. 7 animals which received 40 mg/Kg $NaIO_3$ were examined and 11 control animals. A-wave and b-wave peaks were analysed by repeated measures two-way ANOVA and Holm-sidak multiple comparisons test.

BLA

The presence of BLA 1 month after 40 mg/Kg $NaIO_3$ was investigated as previously described in paragraph 2.2.2. 8 $NaIO_3$-treated mice and 15 control mice were placed in the arena when the front half was illuminated.

PLR

Effects of RPE cell loss on the PLR were tested 1 month after $NaIO_3$ administration. Only right eyes were tested and the PLR was examined as described in paragraph 2.2.3. Light intensities used were from 0.8 – 8000 $\mu W/cm^2/s$, increased in log units. The n numbers used are presented in Table 4. PLRs recorded at 800 and 8000 $\mu W/cm^2/s$ were not analysed statistically due to the low number of controls recorded.

Table 4 numbers of animals examined by pupilometry.

Light Power	8000	800	80	8	0.8
Control	1	1	6	3	2
$NaIO_3$	1	1	8	3	3

Histology

At 3, 7, 30 and 90 days after $NaIO_3$, animals were fixed with 4% PFA by perfusion as described in paragraph 2.3.1 and eyes were cryopreserved, sectioned and stained as described in paragraph 2.3.2. The antibodies used were: anti-RPE65 raised in rabbit (1:500, ab175936; Abcam) or anti-Rhodopsin raised in rabbit (1:1000, Abcam) with the secondary antibody raised in donkey against rabbit tagged with Alexa Fluor 568 (1:2000, ab10042; Abcam), and anti-melanopsin raised in rabbit (1:5000, UF006; Advanced Targeting Systems, San Diego, CA, USA) double labelled with anti-S-opsin raised in goat (1:200, SC-14363, Santa Cruz) with secondary antibodies: anti-rabbit IgG raised in donkey tagged with Alexa Fluor 568 (1:2000, ab10042; Abcam) and anti-goat raised in donkey tagged

with FITC (1:200, Jackson ImmunoResearch, West Grove, PA, USA). Confocal stacks were taken on either a Zeiss LSM 700 microscope and a maximum intensity projection was obtained using Zen software.

3.5.4 Results

Comparison of ERG recordings from right and left eyes 1 month after $NaIO_3$

Following the $NaIO_3$ injection retro-orbitally to the right eye, it was important to determine if $NaIO_3$ had different effects on the left and right eye. ERGs were recorded 1 month after $NaIO_3$ administration and the left eye amplitudes were compared to those of the right eyes (Figure 3.12). No differences were seen between left and right eye A- and B- wave amplitudes in the scotopic or photopic ERG (Table 5). The two-way ANOVAs determined the effect of increasing light intensity on the ERG. Both scotopic a-wave and b-wave amplitudes were quite reduced but increase with increasing light intensity, while photopic b-wave amplitudes did not (Figure 3.12). Given the similar effects of $NaIO_3$ on left and right eyes both eyes are used for assessing the effect of $NaIO_3$ on the ERG.

Table 5 Two-way ANOVA $NaIO_3$ 1 month LE vs RE

Two-way ANOVA	LE Vs RE	Light Intensity	Interaction
Scotopic A-wave Amplitude	F (1, 6) = 0.5546	F (6, 36) = 2.886	F (6, 36) = 0.5176
	P = 0.4846	P = 0.0212	P = 0.7910
Scotopic B-wave Amplitude	F (1, 6) = 0.9725	F (6, 36) = 3.549	F (6, 36) = 0.5857
	P = 0.3621	P = 0.0073	P = 0.7393
Photopic B-wave Amplitude	F (1, 6) = 0.002419	F (3, 18) = 1.375	F (3, 18) = 0.5068
	P = 0.9624	P = 0.2822	P = 0.6825

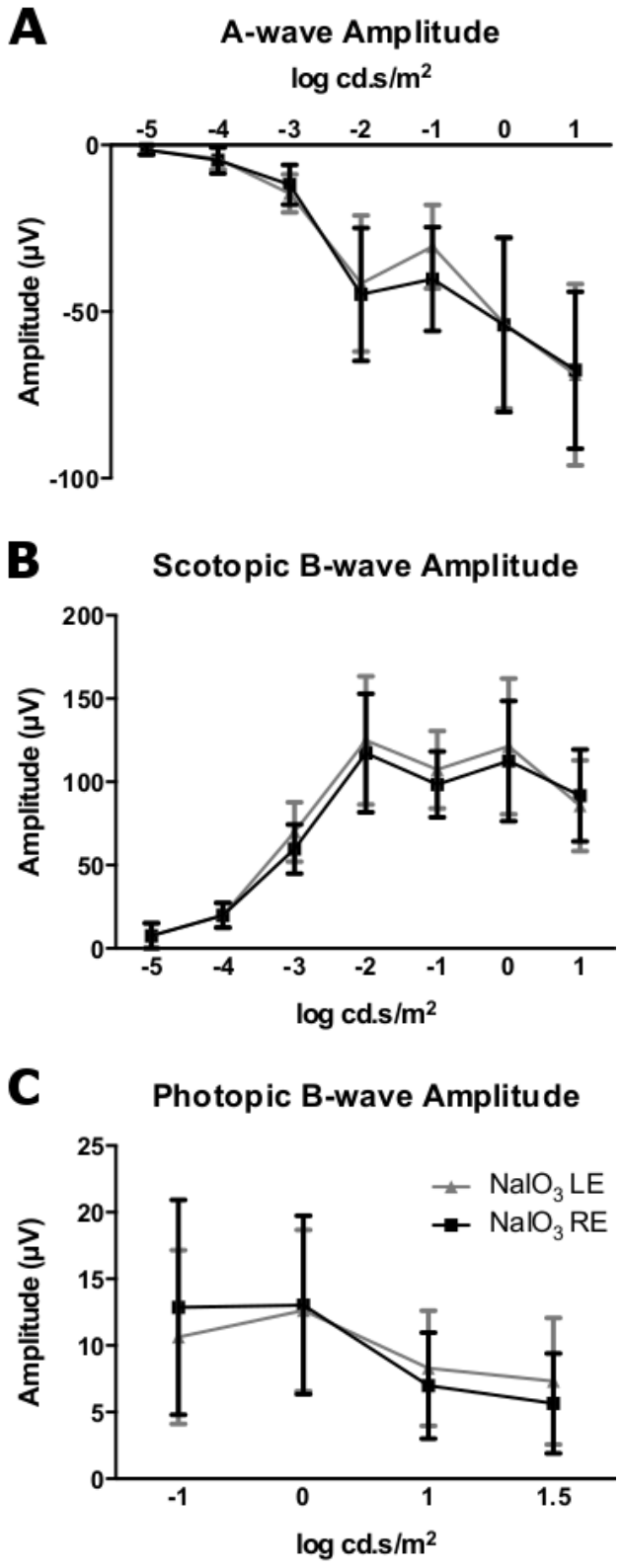

Figure 3.12 ERG amplitudes of left and right eyes following 40 mg/Kg $NaIO_3$. This figure displays graphs of scotopic a-wave (A) and b-wave amplitude (B), and photopic b-wave amplitude (C) from left (LE, grey, n = 7) and right (RE, black, n = 7) eyes. There were no significant differences between ERG responses from left and right eyes.

Effects of 40mg/Kg $NaIO_3$ on the scotopic and photopic ERG

The effects of retro-orbital administration of $NaIO_3$ on the ERG were striking (Figure 3.13, Figure 3.14 and Figure 3.15). The a-wave and b-wave amplitudes were significantly reduced compared to saline treated animals (
Table 6). The average traces illustrate that the a-waves and b-waves were almost

flatlined (Figure 3.14 and Figure 3.15).

Table 6 Two-way ANOVA of ERG 1-month after 40mg/Kg $NaIO_3$

Two-way ANOVA	Scotopic A-wave Amplitude	Scotopic B-wave Amplitude	Photopic B-wave Amplitude
$NaIO_3$	F (1, 34) = 79.62	F (1, 34) = 129.8	F (1, 34) = 163.0
	P < 0.0001	P < 0.0001	P < 0.0001
Light Intensity	F (6, 204) = 99.50	F (6, 204) = 105.5	F (3, 102) = 56.37
	P < 0.0001	P < 0.0001	P < 0.0001
Interaction	F (6, 204) = 42.37	F (6, 204) = 49.77	F (3, 102) = 68.95
	P < 0.0001	P < 0.0001	P < 0.0001
Subjects (matching)	F (34, 204) = 2.339	F (34, 204) = 5.073	F (34, 102) = 2.124
	P = 0.0001	P < 0.0001	P = 0.0020

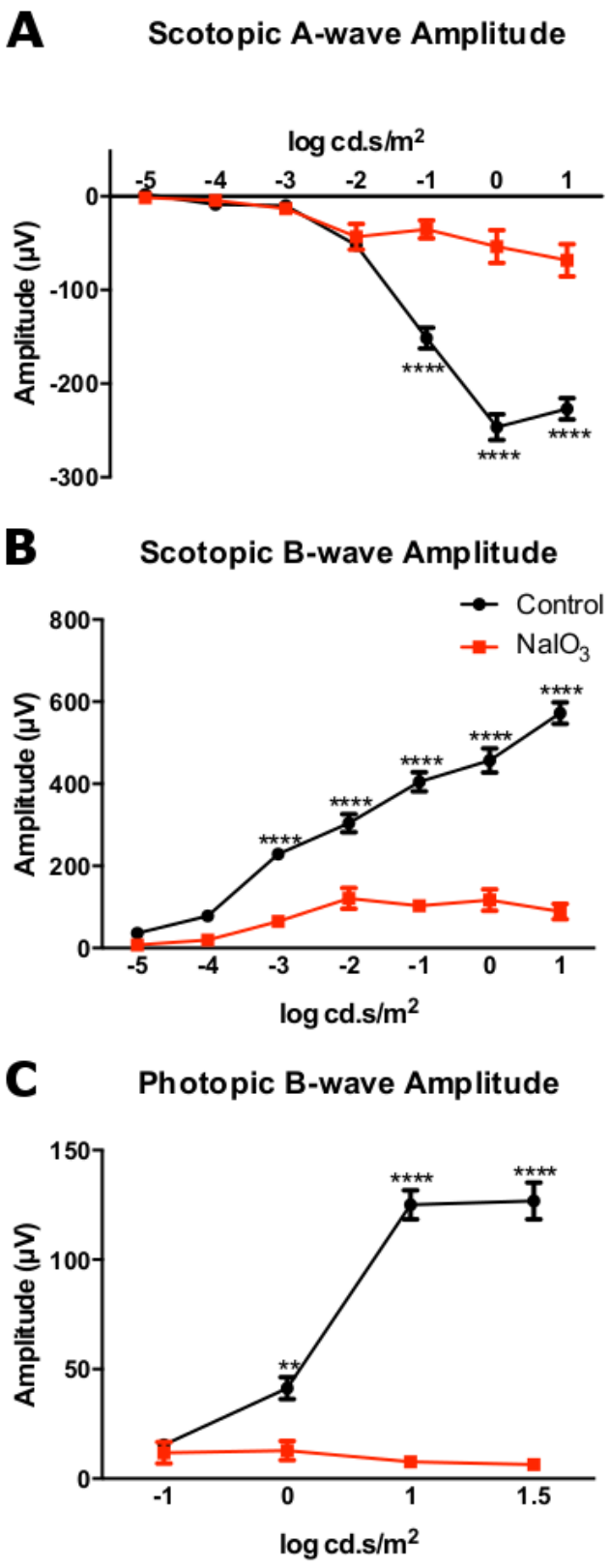

Figure 3.13 Scotopic and Photopic ERG amplitude, latency and implicit time 1 month after 40 mg/Kg $NaIO_3$.
*This figure displays the results of scotopic and photopic a- and b-wave amplitudes from animals treated with 40 mg/Kg $NaIO_3$ (red, N = 14) and control animals (black, N = 22). $NaIO_3$ has a significant dampening effect on scotopic and photopic amplitudes. Asterisks indicate significance of post-hoc tests: **P < 0.01, ****P < 0.0001.*

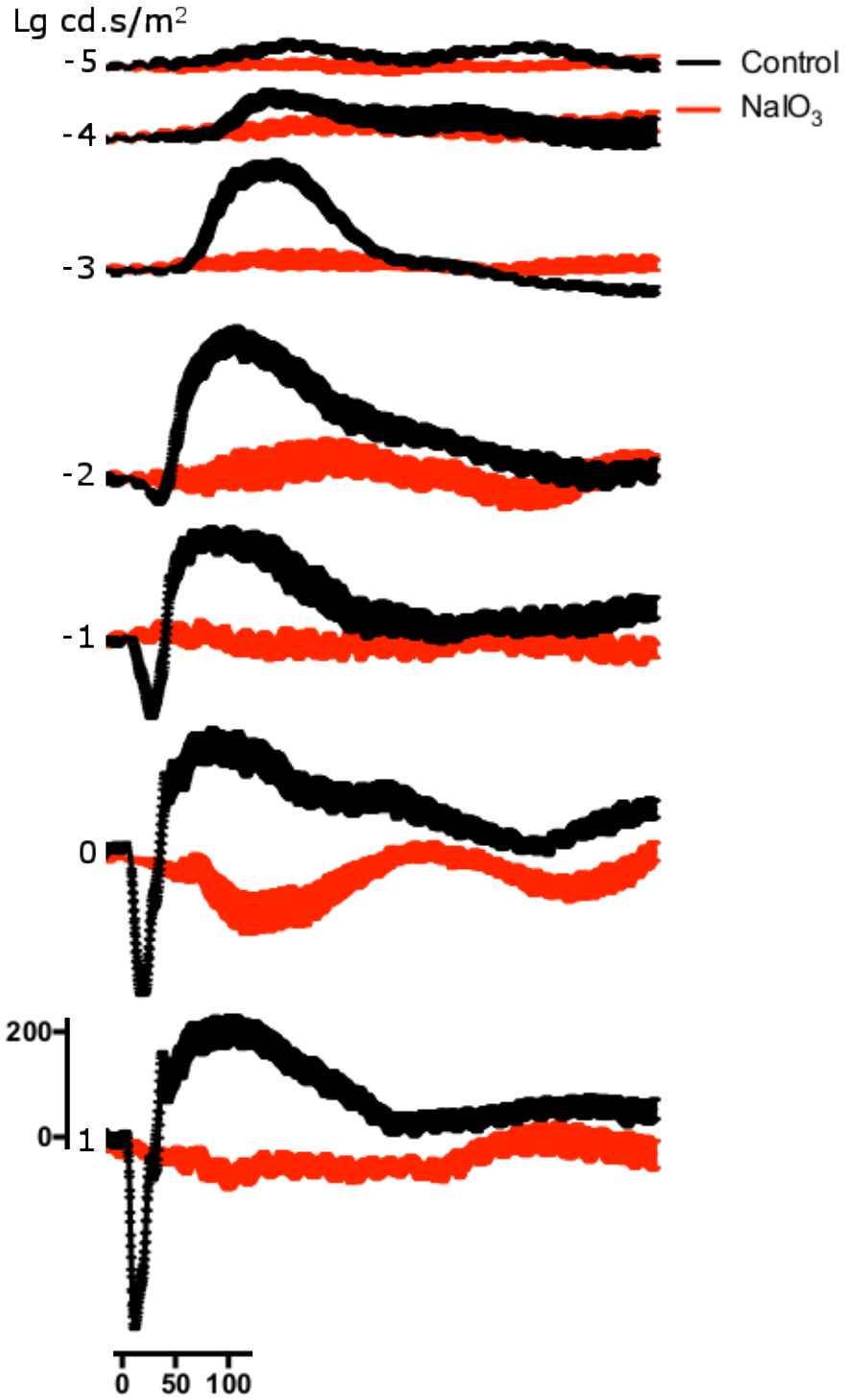

Figure 3.14 Scotopic ERG traces 1 month after 40 mg/Kg $NaIO_3$.
This figure shows average scotopic ERG traces ± SEM of $NaIO_3$-treated animals (red) and controls (black), increasing in log units from -5 to 1 Lg cd.s/m^2. The vertical scale indicated 200 µV and the horizontal scale indicates 100 ms.

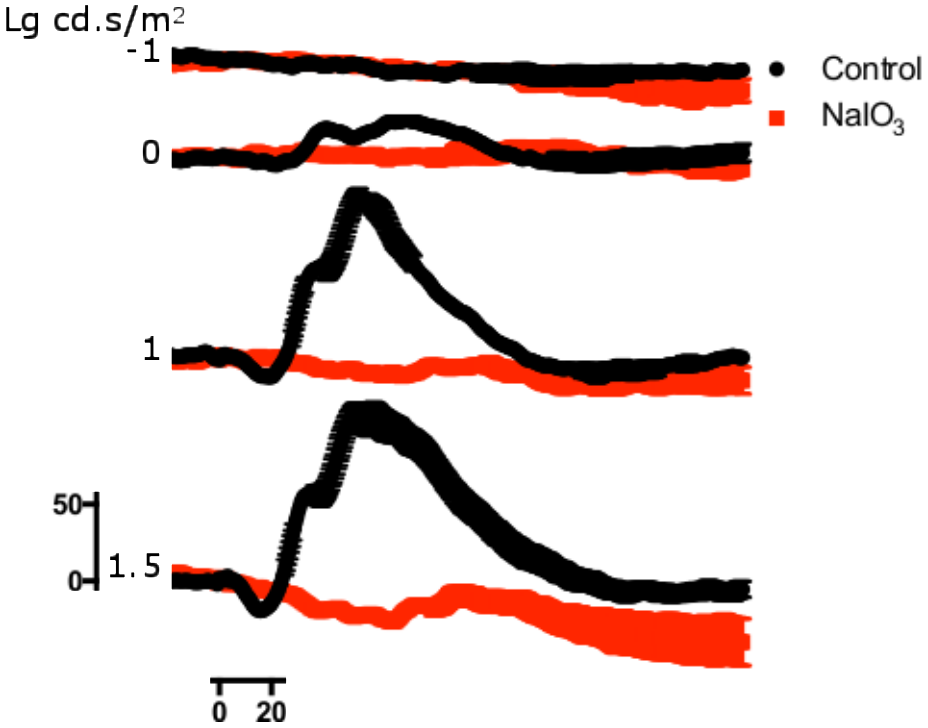

Figure 3.15 Photopic ERG traces 1 month after 40 mg/Kg $NaIO_3$.
This figure shows average ± SEM photopic ERG traces of $NaIO_3$-treated animals (red) and controls (black) in increasing light intensities: -1, 0, 1 and 1.5 lg cd.s/m^2. The vertical scale indicated 50 µV and the horizontal scale indicates 20 ms.

Effects of $NaIO_3$ on BLA

Rodents have a natural aversion to bright lights, but, following treatment with $NaIO_3$, this aversion is significantly reduced (Figure 3.16). Animals treated with $NaIO_3$ spent significantly (P = 0.0052, t-test) less time in the dark (29% ± 5) than control animal (48% ± 4). Analysing the percentage of time, the animals spend in the dark over a 30-minute period neither control nor $NaIO_3$-treated animals significantly increase the percentage of time in the dark with time (Table 7) (P = 0.6, F (1, 134) = 0.2). However, control animals consistently spend around 20% more time in the back half compared to $NaIO_3$-treated animals (P < 0.0001, F (1, 135) = 27.9).

Table 7 Linear Regression of time spent in the dark over 30 minutes

Linear Regression	Control (n = 15)	$NaIO_3$ (n = 8)
Equation of the line	Y = 0.4639*X + 40.32	Y = 0.2595*X + 24.04
Slope	0.4639 ± 0.2759	0.2595 ± 0.3123
R square	0.03113	0.01479
Is the slope significantly non-zero?	F (1, 88) = 2.828	F (1, 46) = 0.6906
	P = 0.0962	P = 0.4102

Table 8 Two-way ANOVA of time spent in the dark over 30 minutes

Two-way RM ANOVA	F (DFn, DFd)	P value
$NaIO_3$	F (1, 21) = 8.264	P = 0.0091
Time	F (5, 105) = 1.724	P = 0.1354
Interaction	F (5, 105) = 0.2758	P = 0.9255
Subjects (matching)	F (21, 105) = 5.837	P < 0.0001

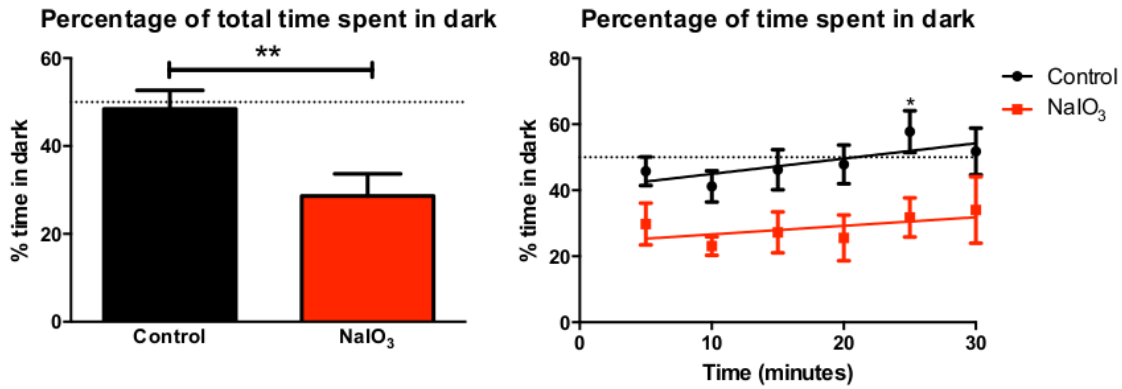

Figure 3.16 BLA is reduced in $NaIO_3$-treated animals
*The first graph shows the percentage of total time animals spent in the dark. $NaIO_3$-treated animals (N = 8) spent significantly less time in the dark compared to control animals (N = 15). The second graph shows the percentage of time spent in the dark in 5-minute bins. Asterisks indicate significance level: *P < 0.05, **P < 0.01.*

Effects of RPE cell death on the PLR

Interestingly the PLR is still quite robust in animals 30 days after $NaIO_3$ treatment (Figure 3.17), although $NaIO_3$ has a significant effect on the PLR at all light intensities (Table 9). $NaIO_3$ appears to have the greatest impact on the lower light powers. A significant constriction is seen in control animals at 0.8 $\mu W/cm^2/s$ light power ($P < 0.0001$), while no constriction is seen in the $NaIO_3$-treated animals (Figure 3.17.A). Maximum constriction was 1 ± 0.22 in $NaIO_3$-treated animals and 0.26 ± 0.02 in controls. At 8 $\mu W/cm^2/s$, a significant constriction is seen in the $NaIO_3$-treated mice ($P = 0.0003$) (Figure 3.17.B), reaching a maximum constriction of 0.62 ± 0.17 and in controls ($P = 0.0002$), reaching 0.52 ± 0.15 in controls. At 80 $\mu W/cm^2/s$, significant constriction is seen in both $NaIO_3$-treated animals ($P < 0.0001$) and controls ($P < 0.0001$). Control animals' constriction became significant 1 second after lights on and stayed significantly constricted during light stimulation and the constriction in $NaIO_3$-treated animals became significant from 4s onwards. Maximum constriction was 0.29 ± 0.04 in $NaIO_3$-treated animals and 0.10 ± 0.008 in controls (Figure 3.17.C). At the two higher light powers, only 1 animal from each group was tested, as these animals were showing clear constriction and because these light levels may be uncomfortable. Maximum constriction in $NaIO_3$-teated mice was 0.038 and 0.057 at 800 and 8000 $\mu W/cm^2/s$ and 0.057 and 0.025 in controls (Figure 3.17.D and E). Two-way ANOVA analysis of the maximum pupil constriction is displayed in Table 10. Post-hoc multiple comparisons test only produced a significant difference at the lowest light power of 0.8 $\mu W/cm^2/s$ ($P < 0.01$) (Figure 3.17.F). Baseline pupil area in control and $NaIO_3$-treated animals were 11.01 ± 1.78 and 9.19 ± 1.026, respectively, which is not significantly different ($P = 0.5$, t-test).

Table 9 Two-way ANOVA on PLR 1 month after $NaIO_3$

Two-way RM ANOVA	0.8 µW/cm^2/s	8 µW/cm^2/s	80 µW/cm^2/s
$NaIO_3$	F (1,) = 23.13	F (1,) = 0.3484	F (1,) = 9.943
	P = 0.0086	P = 0.5867	P = 0.0083
Time	F (5,) = 6.155	F (18,)= 4.492	F (23,) = 75.06
	P = 0.0013	P < 0.0001	P < 0.0001
Interaction	F (5,) = 14.94	F (18,) = 1.003	F (23,) = 9.077
	P < 0.0001	P = 0.4668	P<0.0001
Subjects (matching)	F (4,) = 1.587	F (4,) = 20.11	F (12,) = 29.25
	P = 0.2166	P < 0.0001	P<0.0001

Table 10 Two-way ANOVA of maximum pupil constriction 1 month after $NaIO_3$

Two-way ANOVA	F (DFn, DFd)	P value
$NaIO_3$	F (1, 19) = 5.524	P = 0.0297
Light Power	F (4, 19) = 9.556	P = 0.0002
Interaction	F (4, 19) = 3.037	P = 0.043

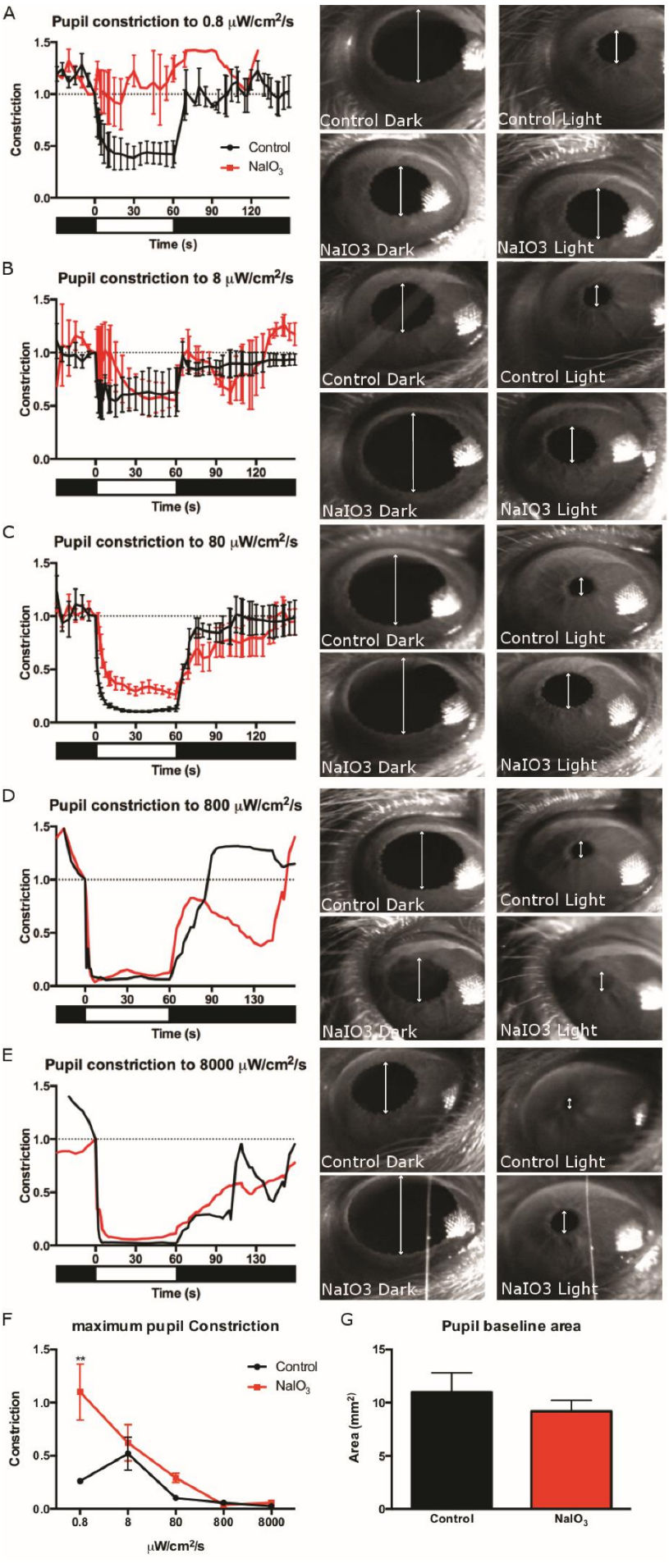

Figure 3.17 PLR constriction 1 month after $NaIO_3$ treatment
*This figure displays PLR constriction at increasing light power and representative video stills before (dark) and after (light) light stimulation. At 0.8 μW/cm²/s, there is no constriction in the $NaIO_3$-treated animals, while a robust constriction is seen in control animals (A). At higher intensities, $NaIO_3$-treated animals have a PLR (B-E). Constriction traces and video stills at each light power show a stronger constriction in control animals compared to $NaIO_3$-treated animals. The maximum pupil constriction mirrors this (F). Asterisks indicate significance level: **P < 0.01. Analysing the effects of $NaIO_3$ on the dilated pupil area shows that $NaIO_3$ does not affect the baseline pupil area (G).*

Effects of RPE cell loss on opsins in the retina

RPE65 expression is a good marker for healthy RPE cells and loss of this maker can indicate RPE cell death. In control retina, RPE65 labelling is specific to the RPE layer, just 3 days after $NaIO_3$ treatment RPE65 labelling is severely diminished, even though there is still pigment in the subretina, although, it is unorganised and not restricted to the RPE layer but found in the POS layer. The RPE layer also does not stain for nuclei. Thus, is can be concluded that the RPE cells are dead but the melanin has yet to be cleared (Figure 3.18).

Studying photoreceptor opsins by immunohistochemistry provides information on the level of opsin expression and the location of opsin expression which can be interpreted to determine the health and functionality of the photoreceptor. Rhodopsin, which is located in the POS, shows disorganisation of the POS 3 days after $NaIO_3$ treatment (Figure 3.19). At 7 days after $NaIO_3$ treatment the pigmented RPE layer becomes patchier as pigment is lost (Figure 3.18) and POS appear shorter (Figure 3.19). 30 days after $NaIO_3$ treatment no RPE65 labelling is identified and much of the RPE pigment is lost. At 90 days pigment is seen spanning the retina (Figure 3.18). It is found in the INL and IPL and appears to be travelling through the retina by Müller glia, which spans the layers of the retina. Similar images to this are reported 3-months after $NaIO_3$ administration (Machalinska et al., 2013). The ONL is reduced to around 7 layers and S-opsin labelling is severely reduced and mislocated to the PIS and ONL. Melanopsin labelling is faint in the GCL, while, melanopsin labelling is still strong in the off sublamina (Figure 3.20). 90 days after administering $NaIO_3$ there is no evidence of RPE cells, except for some pigment mislocated to the inner retina. The ONL is reduced to 1-2 layers and now lie directly on top of the choroid (Figure 3.18). No rhodopsin labelling is detected (Figure 3.19).

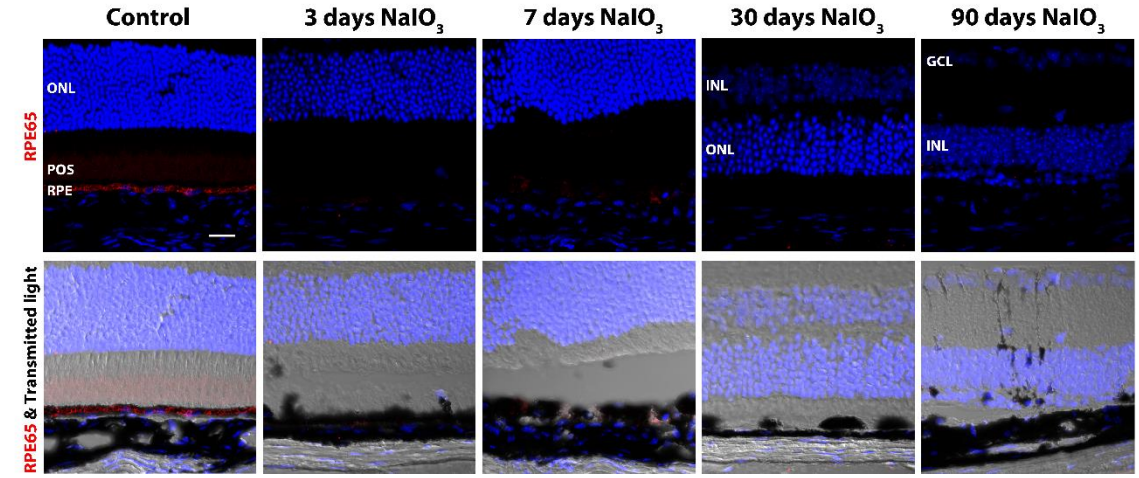

Figure 3.18 RPE65 labelling in $NaIO_3$-treated animals
RPE65-labelling (red) is seen in RPE cells in the control retina. Images with transmitted light show the RPE as a distinct pigmented row of cells. 3 days after $NaIO_3$ administration, RPE65-labelling is greatly diminished and the pigmented row of RPE cells are less organised with pigment in the POS layer and no nuclei stained in the RPE. At 7 days post $NaIO_3$ treatment the pigment is patchy. 30 days after $NaIO_3$ administration no RPE65-labelling is identified and the ONL is reduced to around 7 layers and much of the RPE pigment is lost. 3 months after administering $NaIO_3$ there is no evidence of RPE cells, except for pigment that is mislocated to the inner retina. The ONL is reduced to 1-2 layers and now lie directly on top of the choroid. Scale bar indicates 50 µm.

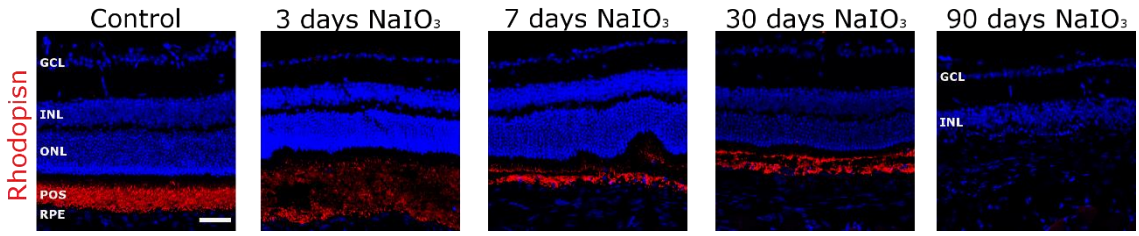

Figure 3.19 Rhodopsin labelling in $NaIO_3$-treated animals.
Rhodopsin labelling (red) is located in POS. 3 days following $NaIO_3$-treatement the POS appear disorganised. At 90 days there is no rhodopsin labelling and the ONL is reduced to one layer. Scale bar indicates 50 µm.

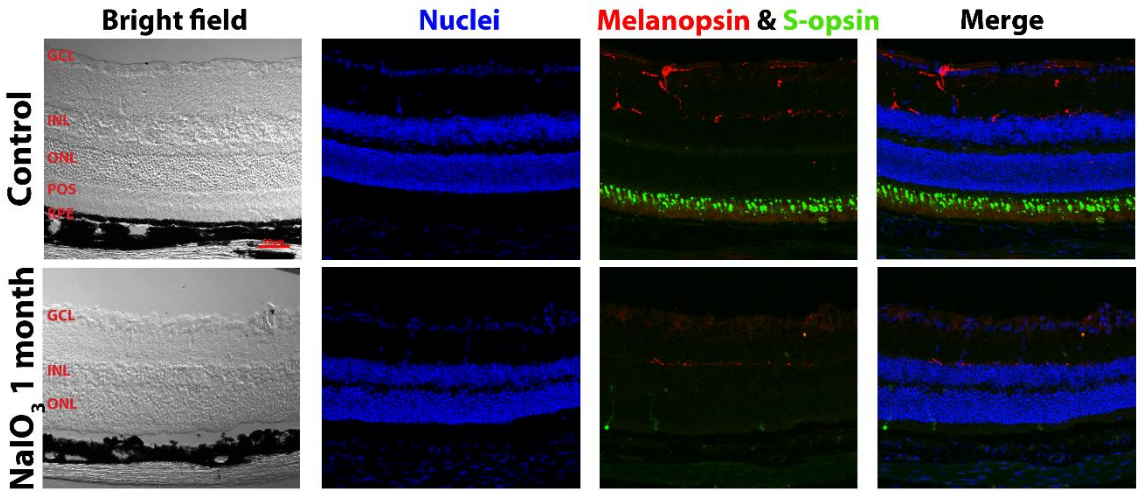

Figure 3.20 Melanopsin and S-opsin labelling 1 month after $NaIO_3$.
At 1 month after $NaIO_3$-treatment S-opsin labelling (green) is severely diminished and mislocated to the PIS. Melanopsin labelling (red) is faint in the GCL, while, melanopsin labelling is still strong in the off sublamina. Scale bar indicates 50 µm.

3.5.5 Discussion

Evaluating the new method of delivering $NaIO_3$, the results show much less variability between animals, compared to the results obtained from administering $NaIO_3$ IP. While $NaIO_3$ is administered retro-orbitally on the right eye, the left eye shows to be equally affected in the ERG. Studies which have used this method in mice, often do not specify whether $NaIO_3$ was administered to both eyes or just one and thus do not specify any differences between eyes in their results (Machalinska et al., 2010, Wang et al., 2014, Xia et al., 2011). But, this has been looked at in papers which have looked at other animals. Rats injected with 40 or 60 mg/Kg $NaIO_3$ via the retro-orbital route also showed a significant loss in the scotopic a- and b-wave amplitude in the contralateral eye, although this effect was significantly milder than that in the ipsilateral eye (Kadkhodaeian et al., 2016). Another study in rabbits given 40 mg/Kg $NaIO_3$ also showed an effect in the contralateral eye. Comparison between contralateral and ipsilateral was not possible in this study as eyes had been treated differently prior to $NaIO_3$

administration (Textorius et al., 1985). A study on primates which were injected into the carotid artery with 10 mg/Kg $NaIO_3$ saw damage in the ipsilateral eye but no affect in the contralateral eye (Nishimura et al., 1990).

The scotopic ERG is significantly diminished. At high light intensities where the scotopic a-wave is pronounced in the control ERG, there is significant differences detected between $NaIO_3$-treated eyes and controls. The scotopic b-wave is also significantly reduced in $NaIO_3$-treated animals again this is more pronounced at higher intensities where the scotopic b-wave is very distinguished in control eyes. This is also true for the photopic b-wave. There is a significant reduction in the photopic b-wave of $NaIO_3$-trreated animals compared to controls, especially at high light intensities where the control photopic b-wave is detected. These results mirror that seen the literature (Machalinska et al., 2011), where both scotopic and photopic b-waves are lost in animals treated with 40 mg/Kg $NaIO_3$ retro-orbitally. At 1 month after $NaIO_3$ administration no RPE65 labelling is identified and S-opsin is strikingly reduced and mislocated to the PIS and ONL justifying results seen in the photopic ERG. This may be due to the loss of chromophore due to RPE cell death. It has been shown in *rpe65*$^{-/-}$ mice that replacing chromophore can restore cone opsin to POS (Rohrer et al., 2005). It is thought that chromophore is required for cone opsin folding and trafficking. The same is not true for rhodopsin, which is located in the POS of $NaIO_3$-treated animals. Although, rhodopsin labelling is still present in the POS, and the ONL, while reduced, has still around 7 layers of cells, the scotopic ERG is almost completely lost. This is most likely because of the lack of chromophore.

Mice have a natural aversion to light and seek out dark environments (Misslin et al., 1989, Semo et al., 2010). Both melanopsin and outer-retinal photoreceptors can drive BLA (Semo et al., 2010). $NaIO_3$ significantly reduces the BLA in mice.

Ideally this experiment would be repeated with mice run in a completely dark arena, to compare. Unfortunately, this was not possible due to restriction in the number of animals available. Thus, it cannot be determined if the BLA is completely lost. However, it is known from immunohistochemistry that melanopsin expression is reduced and thus its function is also likely reduced. Vision is not the only factor that drives the BLA, anxiety also plays a part in this choice (Hascoet et al., 2001, Misslin et al., 1989). C57 mice show less anxious behaviour compared to other mice strains and different behaviours in these light/dark choice tests (Kopp et al., 1999). This may explain differences between these results and experiments run with other mouse strains. The arena is designed so that the animal is placed into the open half of the arena and it is given a choice if it wants to enter the dark closed half or stay in the illuminated or dark open half. This creates a bias for the open half of the arena. This is why it is important to compare the experimental animals to WT controls, as the preference for the front or back half cannot be determined by a 50/50 choice.

The PLR is another functional readout which is driven by both melanopsin and the outer-retinal photoreceptors (Lucas et al., 2003). In $NaIO_3$-treated animals the PLR is still quite robust although the constriction is reduced compared to WT. The greatest deficit in the PLR is seen at low light powers and the maximum constriction graph resembles that seen in an *rd cl* mice (Lucas et al., 2003), where melanopsin drives the PLR at high light irradiances and cannot drive a constriction at lower irradiances of 11 log photons/cm^2/s, comparable to 0.8 μW/cm^2/s used in this study. *Opn4*$^{-/-}$ mice have a PLR at this irradiance and lower irradiances, which is driven by outer-retinal photoreceptors (Lucas et al., 2003). This suggests that any residual function of the outer-retinal photoreceptors in the

$NaIO_3$-treated animals is not enough to drive the PLR. This also supports the results from the ERG.

Thus, it is established that, 1 month following $NaIO_3$ treatment, RPE cells are dead and the pigment is being cleared. Cone photoreceptors are severely diminished and remaining cones have opsin mislocated to the PIS. Rods are still present; however, they are disorganised, there are reductions in the ONL and the function of the outer-retinal photoreceptors is severely diminished. While melanopsin labelling is diminished, it appears that it may still be able to drive the PLR.

3.6 Can retinal function be rescued in $NaIO_3$-treated animals?

3.6.1 Introduction

We know from the last experiment that while outer-retinal photoreceptors have severely diminished responses, rod photoreceptors are still present even 30 days after $NaIO_3$ treatment. Perhaps these rods are not functioning due to the loss of the visual cycle following RPE cell death. It is an important factor to consider as the purpose of investigating this model is for its use in RPE cell transplantation. Carido and colleagues used $NaIO_3$ as a model of RPE degeneration for RPE cell transplantation. They were able to show good RPE cell integration, with grafted RPE cells forming a monolayer in the subretinal space. However, despite the success of RPE cell transplantation, no functional recovery was seen (Carido et al., 2014). There could be a number of factors that resulted in the inability of the grafted RPE cells to restore function. While the grafted RPE cells were able to phagocytose POS, it is unknown if these RPE cells were able to perform the visual cycle (Carido et al., 2014). It is also unknown if function in these remaining

photoreceptors can be rescued. In this experiment, this is examined. 9-*cis* retinal is a synthetic chromophore which can be administered to $NaIO_3$-treated animals. This bypasses the need for a functioning visual cycle and it can be determined if the remaining photoreceptors are functional and if visual responses can be rescued.

3.6.2 Methods

$NaIO_3$ administration

C57 mice were anaesthetised and injected with 40 mg/Kg $NaIO_3$ retro-orbitally on the right eye as described in the methods section of this chapter, page 101. The ability of 9-*cis* retinal to recover visual function was tested 3, 7, and 30 days after $NaIO_3$ treatment by ERG.

Chromophore Replacement

9-*cis* retinal was prepared and administered I.P to mice under dim red light as described in 2.4.2, which were then placed in the dark for 16 hours before the ERG was recorded.

ERG

Animals were anaesthetised and prepared for ERG recordings as described in paragraph 2.2.1. However, as there was a finite amount of chromophore available only scotopic ERGs were recorded and only the brightest intensity flash was used. Flash stimuli of 1 lg cd.s/m^2 were presented three times with 1-minute intervals in a ganzfeld colour dome by LED stimulator and responses were measured using Espion Diagnosis software. Differences between left and right

eyes were first determined and once it was shown that the right and left eye were equally affected by $NaIO_3$ both eyes were used in the analysis and were entered as separate values. Untreated animals were also recorded for comparison. The n numbers were 6 controls, 3 days post $NaIO_3$ had 8 in the saline and 8 in the 9-*cis* retinal group and 7 days post $NaIO_3$ had 8 in the saline and 6 in the 9-*cis* retinal group. The same animal was not used for examining the effects of 9-*cis* reitinal on $NaIO_3$-treated animals in the control and experimental group because of the rapid degeneration that occurs in the retina at 3 and 7 days after $NaIO_3$ administration. At 30 days after $NaIO_3$ administration the retinal degeneration has slowed down and it was decided that he same animals could be used prior to- and after 9-*cis* retinal administration. The 30 days post $NaIO_3$ group used the same 6 animals for $NaIO_3$ and $NaIO_3$ following 9-*cis* retinal ERGs, giving an n of 12 for both groups. Animals were given saline via an IP injection at 26 days after $NaIO_3$ and the ERG was recorded and animals were recovered. On Day 33 after $NaIO_3$ the same animals were given 9-cis retinal and their ERG was recorded. This removed the question of variability in effects of $NaIO_3$.

Statistical Analysis

To determine if there were any differences between left and right eyes in $NaIO_3$ and saline-treated or $NaIO_3$ and 9-*cis* retinal-treated animals a two-way repeated measures ANOVA and post hoc Holm Sidak's multiple comparisons test was used with the different ERG components as the second factor. For analysing the ability of 9-*cis* retinal to recover the ERG, the different ERG components were analysed by non-parametric Kruskal-Wallis test and Dunn's multiple comparisons test.

3.6.3 Results

Restoring the ERG 3 days after $NaIO_3$ treatment

Prior to analysis, both $NaIO_3$ saline and $NaIO_3$ 9-*cis* retinal results were tested for differences between left and right eyes but two-way repeated measures ANOVA and no statistical significance was found, suggesting that both left and right eyes were affected equally by $NaIO_3$.

Similar to the experiment 3.3, which looked 3 days after $NaIO_3$ administration, $NaIO_3$ at 3 days has a greater reduction on the scotopic b-wave than the a-wave. $NaIO_3$ also increased the time to peak amplitude of both and a- and b-wave. 9-*cis* retinal was able to improve these losses to the b-wave amplitude in some but not all animals and it did not improve the latency or implicit time.

A-wave amplitude (Figure 3.21.A) showed no significant differences (P = 0.0958) between untreated (-162.2 ± 10.6 µV), $NaIO_3$ saline (-249.2 ± 26.05 µV) and $NaIO_3$ 9-*cis* retinal (-235.3 ± 53.49 µV). A-wave latency saw a significant difference (P = 0.0005). The average a-wave latency was 13.58 ± 2.396 ms in untreated animals, 80.25 ± 3.255 ms in $NaIO_3$ saline-treated animals and 55.31 ± 12.39 ms in $NaIO_3$ 9-*cis* retinal-treated animals. Animals treated with $NaIO_3$ had a significantly longer a-wave latency compared to untreated animals (Figure 3.21.B). B-wave amplitude (Figure 3.21.C) also was significantly different (P = 0.0408). The average b-wave amplitude was 431.3 ± 40.61 µV in untreated animals, this was significantly reduced to 231.7 ± 43.38 µV in $NaIO_3$ saline-treated animals but was rescued to 408.3 ± 91.41 µV in $NaIO_3$ 9-*cis* retinal-treated animals. B-wave implicit time (Figure 3.21.D) was also significant (P = 0.045). The average b-wave implicit time was 92 ± 9.304 ms in untreated animals, 187.8 ± 30.69 ms in $NaIO_3$ saline-treated animals and 168.3 ± 22.37 ms in $NaIO_3$ 9-*cis*

retinal-treated animals. Similar to the a-wave, the b-wave saw an increase in the implicit time in $NaIO_3$-treated animals.

While no significant differences were seen in $NaIO_3$ saline-treated animals and $NaIO_3$ 9-*cis* retinal-treated animals 3 days after $NaIO_3$ treatment in the different ERG components, there was also no significant difference between $NaIO_3$ 9-*cis* retinal-treated animals and untreated animals. This is likely due to large variation in the $NaIO_3$ 9-*cis* retinal-treated animals. Looking at the individual ERG traces it becomes clear that 3 days after $NaIO_3$ treatment some animals respond to 9-*cis* retinal treatment, while other animals do not (Figure 3.21.E).

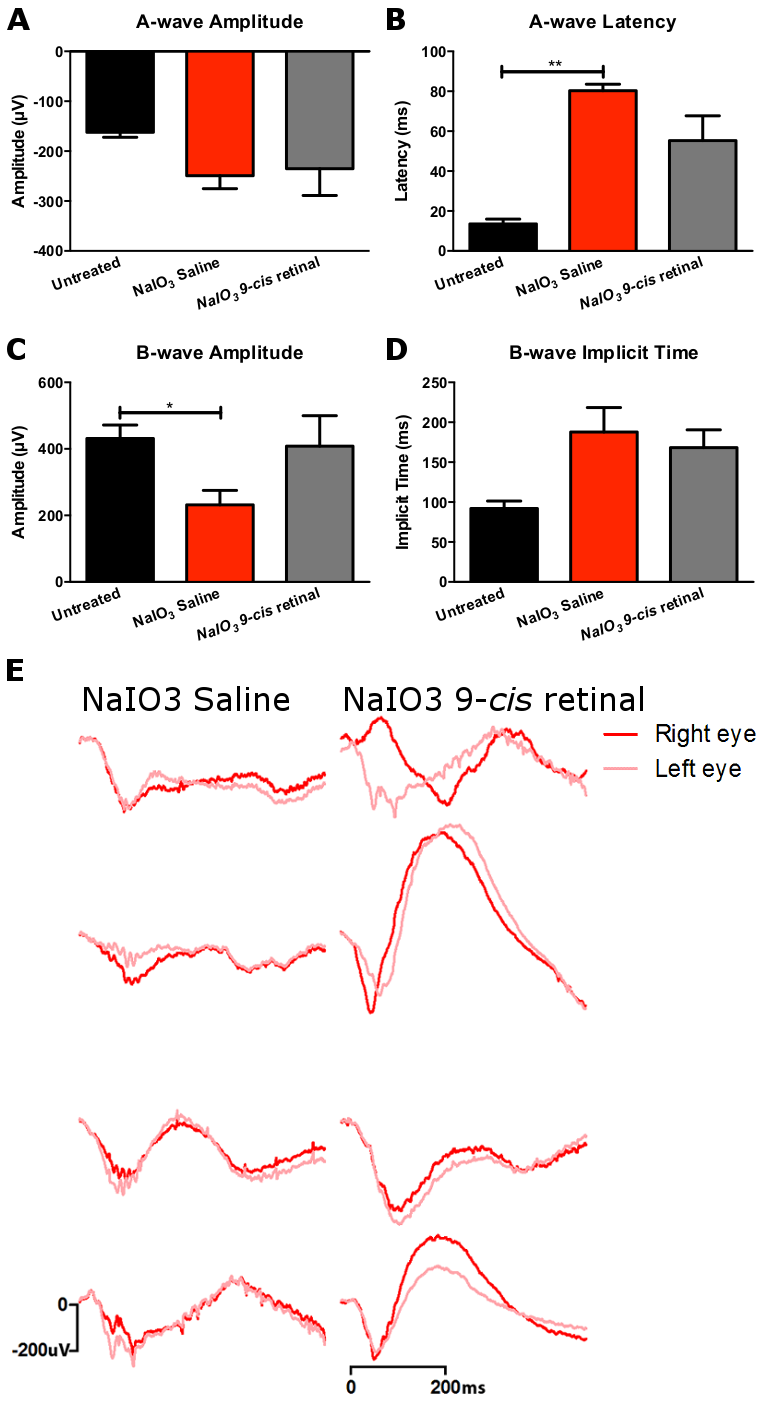

Figure 3.21 ERG 3 days post $NaIO_3$ with 9-cis retinal.
*This figure shows graphs of the scotopic a- and b-wave amplitude, latency and implicit time in animals 3 days after $NaIO_3$-treatment followed by treatment with saline (red, N = 8) or 9-cis retinal (grey, N = 8). Recordings from untreated animals are included for comparison (black, N = 6). The a-wave amplitude is not significantly different between the three groups; however, the latency is increased in $NaIO_3$-treated animals compared to untreated animals. B-wave amplitude is significantly reduced in $NaIO_3$ saline-treated animals compared to untreated animals. Asterisks indicate significance levels revealed in post-hoc tests: *P < 0.05, **P < 0.01. The traces are from individual animals 3 days after $NaIO_3$-treatment which had been treated with saline or 9-cis retinal. The a-wave is still a strong component of the ERG 3 days after $NaIO_3$ treatment. Only half of the animals responded strongly to 9-cis retinal treatment. The vertical scale bar indicates 200 µV and the horizontal scale bar represents 200 ms.*

Can the ERG be restored 7 days after $NaIO_3$ treatment?

At 7 days after $NaIO_3$-treatment, the a-wave is still a strong component of the ERG, albeit with increased latency, but the b-wave is completely lost at this time. At 7 days after $NaIO_3$-treatement, 9-*cis* retinal was unable to restore the b-wave in any animal.

Comparing left and right eyes in both $NaIO_3$ saline- and $NaIO_3$ 9-*cis* retinal-treated animals by two-way repeated measures ANOVA, showed no statistical difference. Thus, both eyes were used in analysis. WT untreated data in this analysis is the same as that used when looking at 3 days post $NaIO_3$ treatment.

There were no significant differences to the a-wave amplitude (Figure 3.22.A between groups ($P = 0.09136$). The average amplitude 7 days after $NaIO_3$ administration was -216.8 ± 52.24 µV and -147.4 ± 15.76 µV in animals treated with saline and 9-*cis* retinal, respectively. There was a significant effect on A-wave latency ($P = 0.0002$). The a-wave latency was significantly longer in $NaIO_3$-treated animals ($P < 0.01$), even with 9-*cis* retinal ($P < 0.05$). No significant difference was found between $NaIO_3$ saline-treated animals and $NaIO_3$ 9-*cis* retinal animals (Figure 3.22.B). The average a-wave latency in $NaIO_3$ saline-treated animals was 63.6 ± 8.5 ms and 46.5 ± 0.6 in $NaIO_3$ 9-*cis* retinal animals. B-wave amplitude also had a significant difference ($P = 0.0003$). The b-wave in the untreated animals was significantly less than animals treated with $NaIO_3$ which received either saline ($P < 0.5$) or 9-*cis* retinal ($P < 0.01$). No significant difference was found between the $NaIO_3$-treated groups (Figure 3.22.C). The average b-wave amplitude 7 days after $NaIO_3$ treatment was 128.6 ± 40.3 µV in animals treated with saline and 54.4 ± 15.9 µV in animals treated with 9-*cis* retinal. These statistics are further supported by the ERG traces (Figure 3.22.D), no improvements on the ERG recordings are seen in the 9-*cis* retinal group.

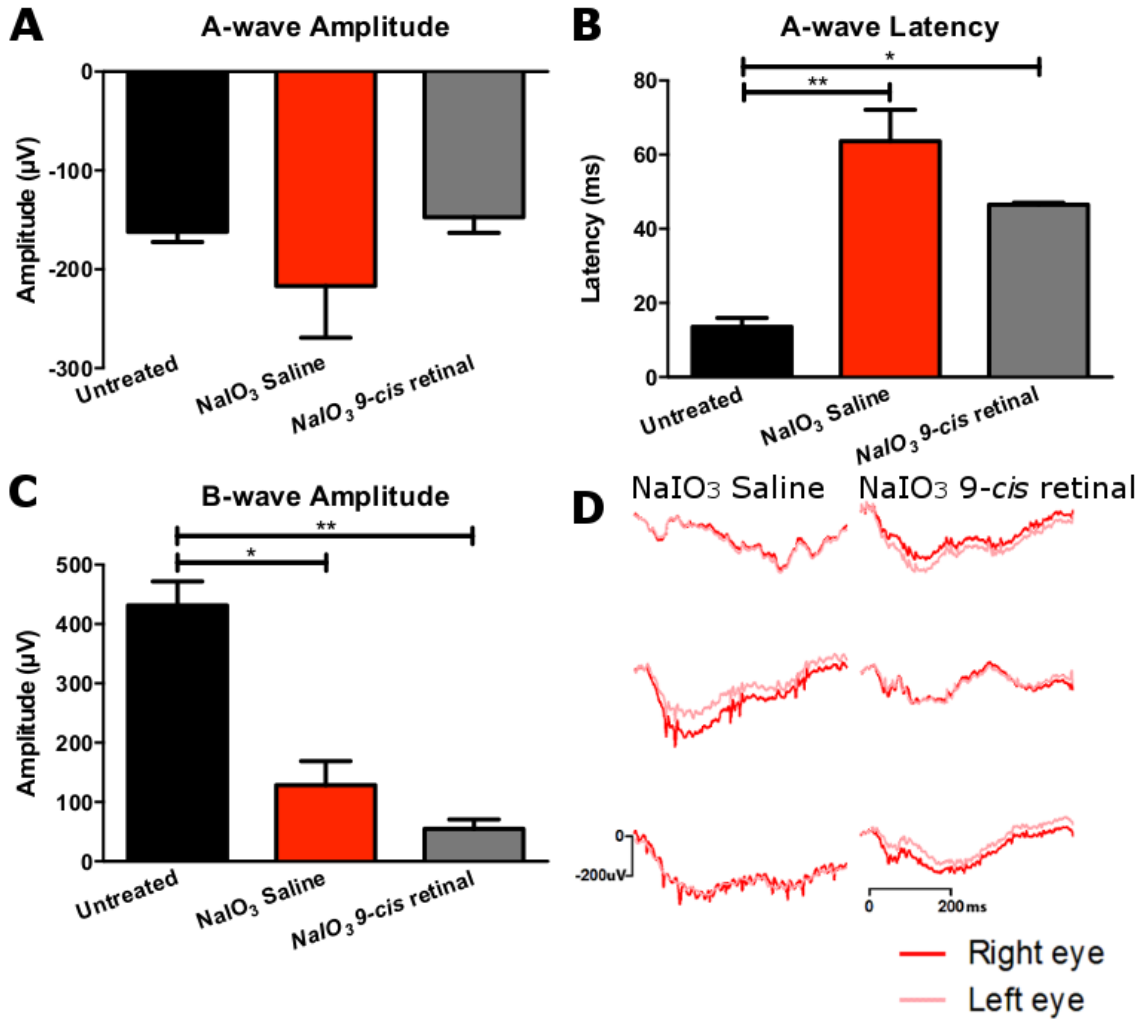

Figure 3.22 ERG 7 days after $NaIO_3$ with 9-cis retinal.
*This figure displays a- (A)and b-wave amplitudes (C), a-wave latency (B) 7 days after $NaIO_3$ treatment followed by treatment with saline (N = 8) or 9-cis retinal (N = 6). Untreated animals are displayed for comparison (N = 6). A-wave amplitude is not significantly different between groups. $NaIO_3$-treated animals with either saline or 9-cis retinal have significantly longer a-wave latency and reduced b-wave amplitude than untreated animals. Asterisks indicate significance level in post-hoc tests: *P < 0.05, **P < 0.01. The traces are from individual animals 7 days after $NaIO_3$-treatement and treated with either saline or 9-cis retinal (D). These $NaIO_3$-treated animals have a negative ERG and no improvements in the ERG are seen in animals which received 9-cis retinal. The vertical scale indicated 200 µV and the horizontal scale bar indicates 200 ms.*

Rescuing visual function 30 days after $NaIO_3$ treatment

Prior to assessing effects of 9-*cis* retinal, two-way ANOVA determined that there was no significant difference between left and right eyes after $NaIO_3$ treatment or after 9-*cis* treatment. Thus, both eyes were used in the analysis.

At 30 days the ERG is flatlined in $NaIO_3$-treated animals. The a-wave which had been present at 3 and 7 days after $NaIO_3$-treatment is lost. Interestingly, 9-*cis* retinal was able to improve both the a- and b-wave amplitudes of $NaIO_3$-treated animals at this time. This was not possible at 7 days after $NaIO_3$-treatment. The a-wave latency and b-wave implicit time are both significantly greater $NaIO_3$- 9-*cis* retinal-treated animals than untreated animals.

There was a significant difference between untreated, $NaIO_3$-treated and $NaIO_3$ 9-*cis* retinal-treated a-wave amplitude ($P < 0.0001$). There is a significant increase in the a-wave amplitude in $NaIO_3$-treated animals after receiving 9-*cis* retinal compared to ERG recording prior to 9-*cis* retinal-treatment ($P < 0.0001$). Average a-wave amplitude reached was -60.2 ± 12.2 µV in $NaIO_3$-treated animals, which improved to -230.2 ± 23.1 µV with 9-*cis* retinal administration, comparable to WT (Figure 3.23.A). A-wave latency was not recorded for $NaIO_3$-treated animals due to the low amplitude. $NaIO_3$-9-*cis* retinal-treated animals have a significantly longer a-wave latency compared to untreated animals (T-test, $P = 0.0006$). Average a-wave latency in $NaIO_3$-treated animal was 95.5 ± 6.4 ms following administration of 9-*cis* retinal and untreated animals' latency was 13.6 ± 2.4 ms (Figure 3.23.B).

B-wave amplitude was also significantly different among groups ($P < 0.0001$). $NaIO_3$ animals had a significantly reduced b-wave amplitude compared to untreated animals ($P < 0.0001$). 9-*cis* retinal significantly increased the b-wave amplitude of $NaIO_3$-treated animals ($P < 0.01$), albeit, lower than WT. The

average b-wave amplitude 30 days after $NaIO_3$ treatment was 74.2 ± 10.1 µV and 245.6 ± 36.7 following 9-*cis* retinal treatment (Figure 3.23.C). B-wave implicit time was not recorded from $NaIO_3$-treated animals prior to 9-*cis* retinal administration as the amplitude was low. The b-wave latency of $NaIO_3$-9-*cis* retinal-treated animals was significantly greater than untreated animals (P = 0.0134). Average b-wave implicit time 30 days after $NaIO_3$ was 249.6 ± 22. ms after receiving 9-*cis* retinal (Figure 3.23.D).

Interestingly, 30 days after $NaIO_3$ treatment, 9-*cis* retinal is able to increase the a- and b-wave amplitudes, having failed to do to at 7 days after $NaIO_3$. However, the latency and implicit time are significantly longer than that in untreated animals. The a-wave amplitude can be rescued to levels comparable to untreated animals, while the b-wave cannot. This loss of the b-wave and increased implicit time reflect retinal damage resulting from the $NaIO_3$. Examining the ERG traces before and after 9-*cis* retinal it is clear to see an increase in the a- and b- wave amplitudes (Figure 3.23.E).

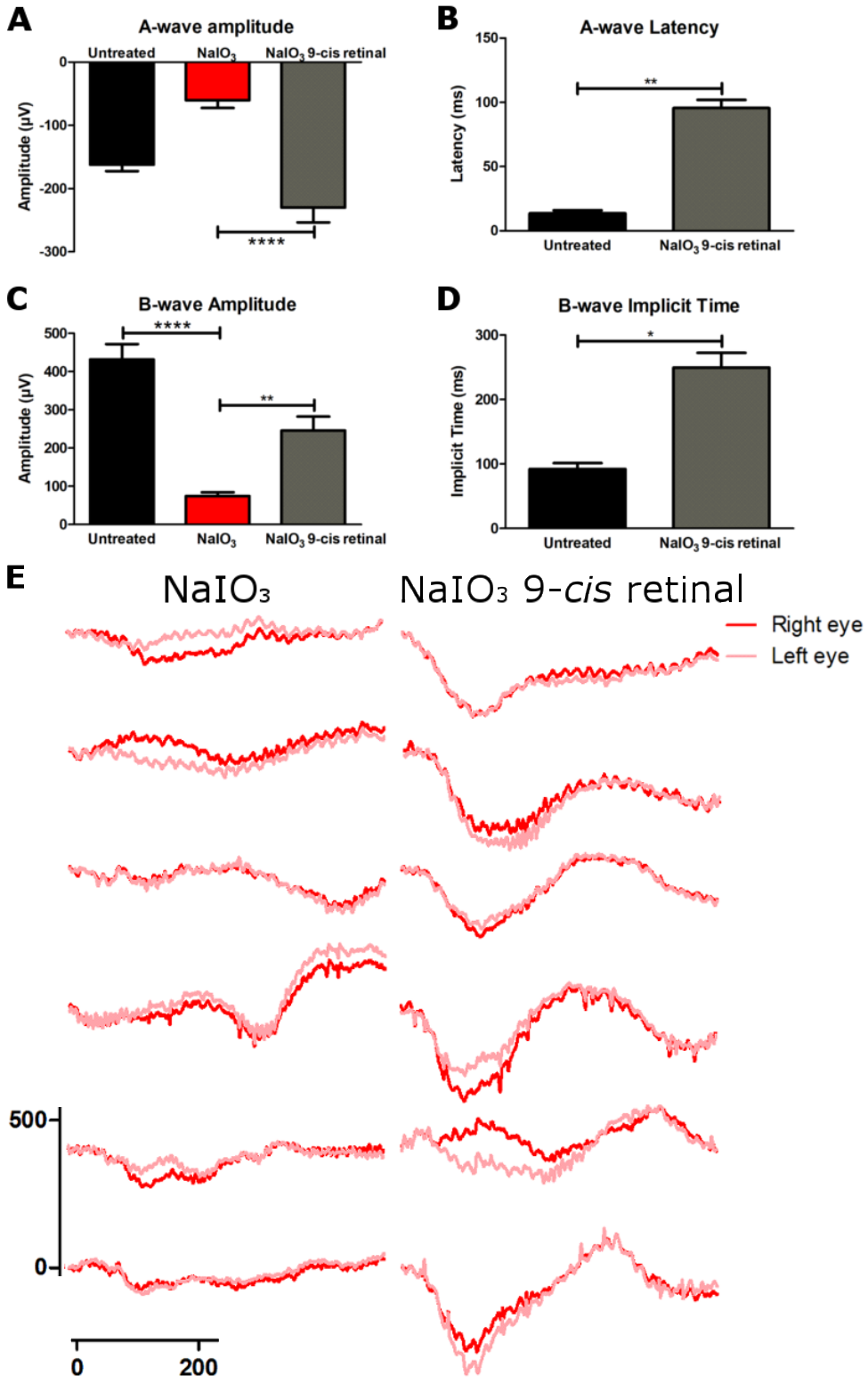

Figure 3.23 ERG 30 days after $NaIO_3$ with 9-cis retinal.
*This figure plots a- (A) and b-wave (C) amplitudes, a-wave latency (B) and b-wave implicit time (D) 30 days after $NaIO_3$ and again following 9-cis retinal-treatment (N = 14). There was a significant difference between groups for each of the ERG components. Asterisks indicate significant results in post-hoc tests: *P < 0.05, **P < 0.01, ***P < 0.001, ****P < 0.0001. E show average traces of animals 1 month after $NaIO_3$ treatment in the left column and a repeated recording following 9-cis retinal-treatment on the right. The vertical scale indicates 500 µV and the horizontal scale indicates 200 ms.*

3.6.4 Discussion

It was shown in the previous experiment that rods are present up to 30 days, thus in this experiment, the functionality of rods is tested. It was shown that despite rods remaining in the retina, the ERG was significantly diminished and the PLR somewhat mirrored that seen in rodless/coneless animals. One theory was that the remaining rods are not able to function due to a lack of chromophore, thus this was tested by administering chromophore supplement in the form of 9-*cis* retinal. 3 days after $NaIO_3$ treatment the a-wave response is still seen although the latency is significantly increased. The b-wave is significantly reduced. At this stage 9-*cis* retinal greatly improves the ERG in around half of the animals. This result was not significant when examining a- and b-waves, it is possible that increasing the number of animals used at this time point may have shown a clearer result. 7 days after $NaIO_3$ treatment the a-wave is still present but the b-wave is lost and unable to be rescued with 9-*cis* retinal. 30 days after $NaIO_3$ treatment the ERG has almost flatlined, however, at this stage 9-*cis* retinal is able to rescue a lot of retinal function and significantly increases the a- and b-wave amplitude. The a- wave is restored to levels comparable to WT. Although, the latency and implicit time are significantly longer than that seen in untreated animals. This experiment shows that retinal recovery is possible 30 days after $NaIO_3$ treatment. It is unknown why retinal recovery was not possible at 7 days but improves by 30 days, this may be due to retinal recovery which has been reported in other studies (Franco et al., 2009, Machalinska et al., 2013, Redfern et al., 2011).

3.7 RPE cell transplant into $NaIO_3$-treated eyes.

3.7.1 Introduction

Carido and colleagues administered 70 mg/Kg $NaIO_3$ to mice via the tail vein. One week later 100,000 – 200,000 hESC-RPE cells were transplanted subretinally. 3 weeks later hESC-RPE cells had formed extensive monolayers in the sub-retinal space, with correct apical-basolateral organisation and attached to Bruch's membrane. There was also evidence of phagocytosis by the grafted HESC-RPE cells, despite this, no functional recovery was seen by ERG (Carido et al., 2014). In this experiment, a similar approach is taken; 40 mg/Kg $NaIO_3$ is administered retro-orbitally, our preferred method of $NaIO_3$ delivery. Also, following the result in the previous experiment, cells will be administered 3 weeks after $NaIO_3$ treatment, with the aim of assessing the capacity for functional recovery by ERG 3 weeks following cell transplantation.

3.7.2 Methods

Administration of $NaIO_3$ retro-orbitally

7 Animals were anaesthetised and 40 mg/Kg $NaIO_3$ was administered retro-orbitally to the right eye as described in paragraph 2.4.1.

hESC-RPE cell preparation and transplantation

3 weeks after $NaIO_3$ was administered, 75,000 hESC-RPE cells were injected subretinally into the left eye of the mice. This was the maximum number of cells that could be delivered on the day. This is determined by the number of dishes of hESC-RPE suitable for transplantation, on the day, and the number of cells on

the dish. These cells then need to be in a workable cell suspension of 50,000 cells per µL and a minimum volume of 20 µL to allow the cell suspension to be drawn up into the needle without air bubbles. This protocol is described in paragraph 2.4.3.

ERG post-transplant

Animal's ERG was recorded 3 weeks after they received the cell transplant. Animals were dark-adapted, anaesthetised and their scotopic and photopic ERG was recorded, as previously described in paragraph 2.2.1.

9-*cis* retinal administration

To test the capacity for rescue in the $NaIO_3$-treated retina, 9-*cis* retinal was administered to the animals the day after their ERG was recorded and the animals were placed back into the dark overnight to be re-assessed by ERG. 9-*cis* retinal was prepared and administered as previously described in paragraph 2.4.2.

ERG after treatment with 9-*cis* retinal

The next day, animals were prepared for ERG recordings as described in paragraph 2.2.1.

Histology

Animals were fixed by perfusion with 4% PFA as described in 2.3.1 and eyes were sectioned and labelled by immunohistochemistry as described in 2.3.2. Eyes were labelled with anti-human mitochondria (1:500, MAB1273, Millipore) and secondary anti-mouse raised in donkey tagged with TRITC (1:200, Jackson

ImmunoResearch, West Grove, PA, USA). Eyes were also labelled with RPE65 raised in rabbit (1:500, ab17936, Abcam) with secondary antibody raised in donkey against rabbit tagged with Alexa Fluor 568 and anti-human nuclei tagged with Alexa Fluor 488 (1:200, MAB1281A4, Milipore). Images were captured with zeiss 700.

3.7.3 Results

Scotopic ERG recordings in $NaIO_3$-treated eyes after RPE cell transplantation

The scotopic a-wave and b-wave amplitudes are notably reduced for all animals as expected following $NaIO_3$-treatment. The scotopic ERG did not see any significant improvements with RPE cell transplant. The a-wave amplitude had a worse a-wave amplitude in eyes which received cells (Figure 3.24.A). The scotopic b-wave amplitude (Figure 3.24.B) shows no difference between eyes which received cells and eyes which did not (Table 11).

Table 11 Two-way ANOVA of ERG amplitude following NaIO3 and hESC-RPE

Two-way ANOVA	a-wave amplitude	b-wave amplitude
Light Intensity	F (6, 36) = 4.1, P = 0.0032	F (6, 36) = 5.8, P = 0.0003
hESC-RPE transplant	F (1, 6) = 11.9, P = 0.0136	F (1, 6) = 1.3, P = 0.2916
Interaction	F (6, 36) = 3.6, P = 0.0070	F (6, 36) = 1.1, P = 0.3921

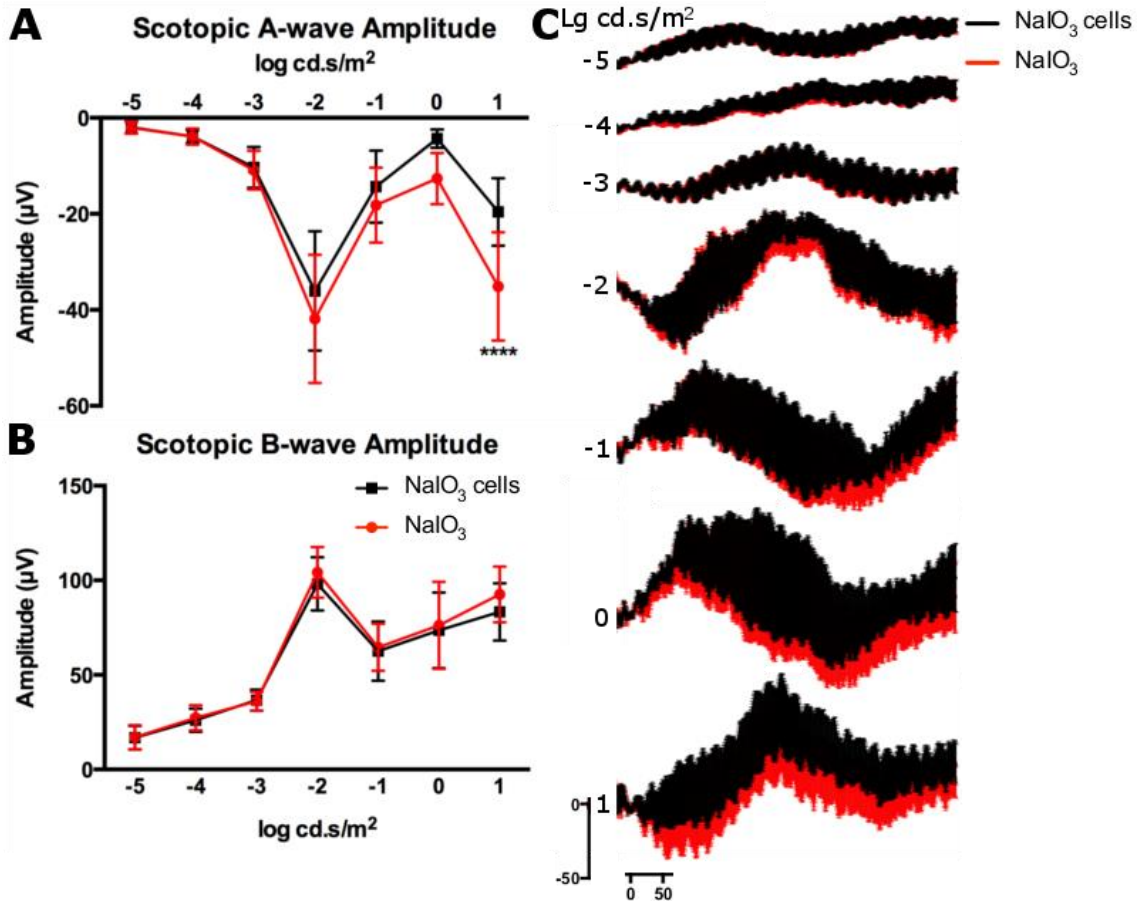

Figure 3.24 Scotopic ERG in $NaIO_3$-treated eyes, which received RPE transplantation.
*This figure displays scotopic a- (A)and b-wave (B) amplitude of $NaIO_3$-treated animals which received cells (black, N = 7) or control eyes (red, N = 7). Eyes that did not receive cells had a greater a-wave amplitude. There was no significant difference between eyes which received cells and eyes which did not in the b-wave. Asterisks indicate significance levels in post-hoc tests: *P < 0.05, ***P< 0.001. C displays average traces ± SEM for increasing light intensities for eyes which received cells (black) and eyes which did not (red). The vertical scale indicates 50 µV and the horizontal scale indicates 50 ms.*

Photopic ERG recordings in $NaIO_3$-treated eyes after RPE cell transplant

In the photopic ERG there is a significant loss in the photopic a-wave in eyes treated with hESC-RPE, similar to that seen under scotopic conditions. Usually under photopic conditions only the b-wave is examined. This is because the a-wave is very small. The a-wave is driven by photoreceptors and under photopic conditions in a WT mouse this is the cones, which are not very numerous, and hence produce a small output. While animals which were treated with $NaIO_3$ have

a strikingly small photopic a- and b-wave, it is clear from the photopic ERG traces that the a-wave is completely lost in animals treated with hESC-RPE (Figure 3.25.C). There is a significant difference between the a-wave amplitude of eyes which received a subretinal injection of hESC-RPE and eyes which did not (Figure 3.25.A, Table 12). There is no significant difference in the photopic b-wave amplitude of eyes which received hESC-RPE cells and the eyes which did not (Figure 3.25.B).

Table 12 Two-way ANOVA of photopic ERG following $NaIO_3$ and hESC-RPE

Two-way ANOVA	a-wave amplitude	b-wave amplitude
Cells	F (1, 6) = 6.58, P = 0.0426	F (1, 6) = 0.421, P = 0.5404
Light Intensity	F (3, 18) = 2.8, P = 0.0698	F (3, 18) = 1.66, P = 0.2120
Interaction	F (3, 18) = 4.82, P = 0.0123	F (3, 18) = 0.868, P = 0.4759

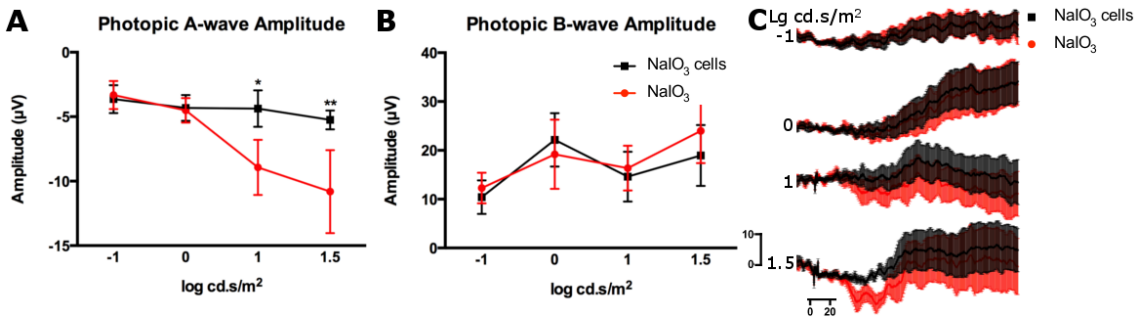

Figure 3.25 Photopic ERG in eyes which received RPE cell transplant following $NaIO_3$ treatment.
*This figure displays the photopic a-wave amplitude (A) and b-wave amplitude (B) in eyes treated with $NaIO_3$ followed by RPE cell transplantation (black, N = 7) or control eyes which did not receive cells (red, N = 7). Asterisks indicate significance level of post-hoc tests: *P < 0.05, **P < 0.01. The traces (C) represent the average trace ± SEM at -1, 0, 1 and 1.5 cd.s/m² in eyes which were treated with cells (black) and eyes which did not receive cells (red).The vertical scale represents 10 µV and the horizontal scale indicates 20 ms.*

Is visual function recoverable by 9-*cis* retinal?

Scotopic ERG recordings following chromophore supplementation

To determine if retinal function could be restored in these $NaIO_3$-animals, they received 9-*cis* retinal and ERGs were recorded again. These results showed a significant increase in scotopic a- and b-wave amplitudes (Table 13). This shows that the eyes treated with $NaIO_3$ could be rescued, but that the subretinal injection of hESC-RPE was unable to rescue retinal function (Figure 3.26).

Table 13 Two-way ANOVA ERG following $NaIO_3$, hESC-RPE and 9-cis retinal

Two-way RM ANOVA	Scotopic a-wave amplitude	Scotopic b-wave amplitude
9-*cis* retinal	F (1, 13) = 16.73, P = 0.0013	F (1, 13) = 19.91, P = 0.0006
Light Intensity	F (6, 78) = 20.53, P < 0.0001	F (6, 78) = 11.50, P < 0.0001
Interaction	F (6, 78) = 9.683, P < 0.0001	F (6, 78) = 1.825, P = 0.1049

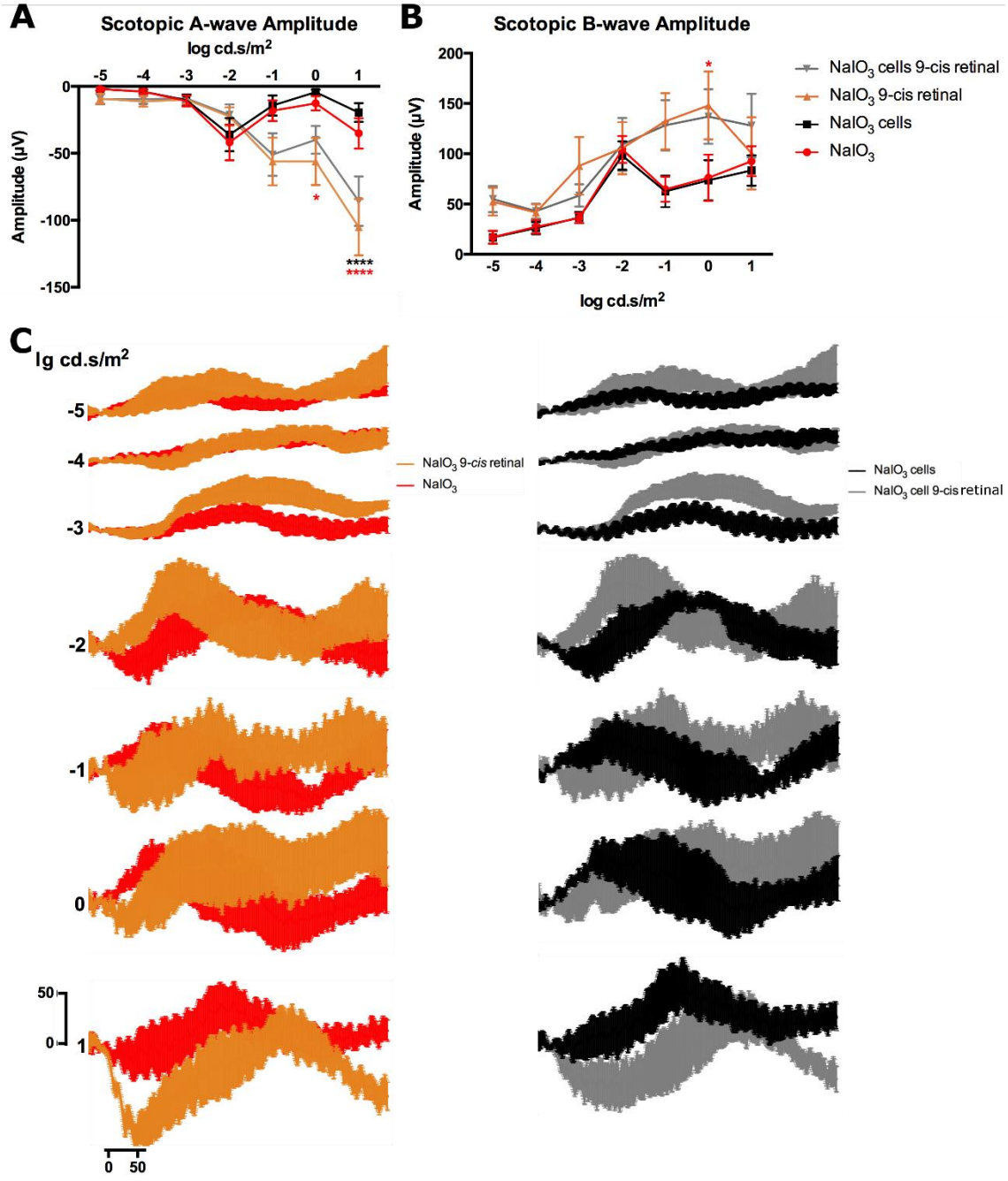

Figure 3.26 Scotopic ERG in eyes treated with $NaIO_3$, hESC-RPE cells and 9-cis retinal.
*A-wave amplitude is significantly increased with supplementary chromophore (A). Asterisks indicate significance level from post-hoc tests: *P < 0.05, ****P < 0.0001. Asterisks in black show a significant difference between eyes which received hESC-RPE cells before and after chromophore supplementation. Asterisks in red show a significant difference between eyes which did not receive cells before and after chromophore supplementation. C shows average traces of eyes which did not receive cell (N=7) on the left before (red) and after (orange) 9-cis supplementation and eyes which receive cells on the right (N = 7) before (black) and after (grey). Vertical scale represents 50 µm and horizontal scale represents 50 ms.*

Effect of chromophore supplementation on photopic ERG

9-*cis* retinal was also able to improve the photopic ERG. This improvement was greatest in eyes which did not receive hESC-RPE transplantation. This suggests that the injection of hESC-RPE impacted negatively on retinal rescue. Perhaps the injection further damaged the already weakened retina. Under these conditions an a-wave was seen in the photopic wave form, as described in (Figure 3.25). 9-*cis* retinal created a significantly greater photopic a-wave amplitude in eyes treated with $NaIO_3$ (Figure 3.27.a). This improvement in the a-wave was not seen in eyes which received a subretinal injection of hESC-RPE. These eyes did not have a photopic a-wave prior to 9-*cis* retinal supplementation. The b-wave is significantly increased with 9-*cis* retinal in eyes which were treated with hESC-RPE and eyes which did not receive cells (Figure 3.27.B). Statistical results are located in Figure 3.27 (Table 14). Average traces (Figure 3.27) illustrate the increased a-wave in $NaIO_3$-treated eyes after receiving 9-*cis* retinal and the greater b-wave with 9-*cis* retinal-treatment.

Table 14 Statistics for photopic ERG of $NaIO_3$-treated mice with RPE-cell grafting and 9-cis retinal.

Two-way RM ANOVA	Photopic a-wave amplitude		Photopic b-wave amplitude	
	F (DFn, DFd)	P value	F (DFn, DFd)	P value
Light Intensity	F (3, 39) = 12	P < 0.0001	F (3, 39) = 14.3	P < 0.0001
9-cis retinal	F (1, 13) = 7.1	P = 0.0193	F (1, 13) = 11.5	P = 0.0048
Interaction	F (3, 39) = 7.2	P = 0.0006	F (3, 39) = 4.88	P = 0.0057

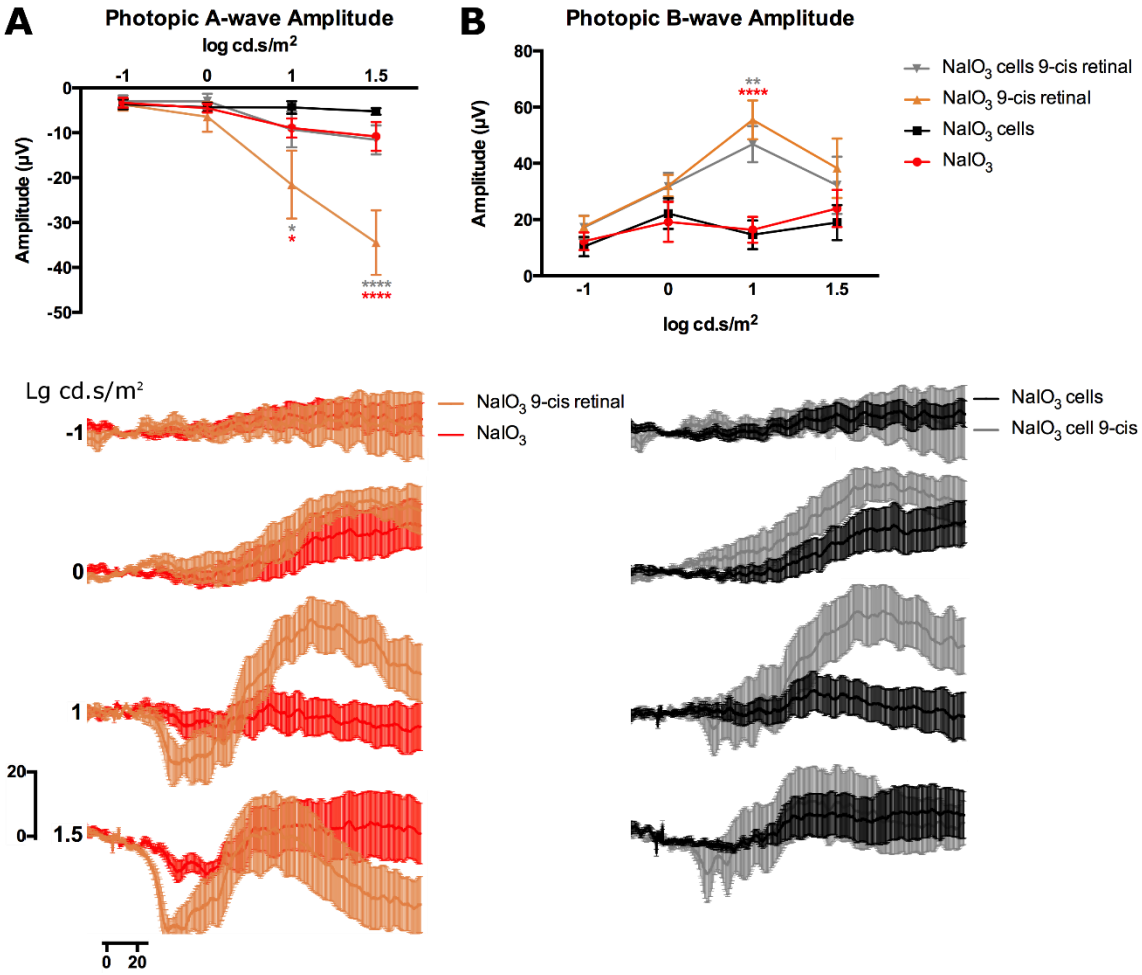

Figure 3.27 Photopic ERG in eyes treated with $NaIO_3$, hESC-RPE cells and 9-cis retinal.
*There is a significant increase in the photopic a-wave in eyes which did not receive RPE cell grafting when given 9-cis retinal (A). Both eyes which received RPE-cell grafting and eyes which did not receive cells had a significantly greater photopic b-wave amplitude (B). Asterisks indicate statistic level from post-hoc tests: *P < 0.05, **P < 0.01, ****P < 0.0001. Average traces of eyes which did not receive cell (N=7) are displayed on the left before (red) and after (orange) 9-cis supplementation. Average traces from eyes which received cells are displayed on the right (N = 7) before (black) and after (grey). Vertical scale represents 20 µm and horizontal scale represents 20 ms.*

Cell transplant histology

No hESC-RPE cells were found in the subretinal space of transplanted eyes. Eyes were labelled for anti-human mitochondria, which was raised in mouse and thus, created a large background stain with the anti-mouse secondary antibody tagged with Alexa Fluor 568 (Figure 3.28.C). While using an antibody raised in mouse to stain mouse tissue is not ideal, this anti-body was helpful in screening for cells. Selected slides were also labelled for RPE65 (Figure 3.29.D) anti-human nuclear antigen (HNA) (Figure 3.29.E), but no cells positive for these markers were detected. hESC-RPE cells were also labelled as a positive control.

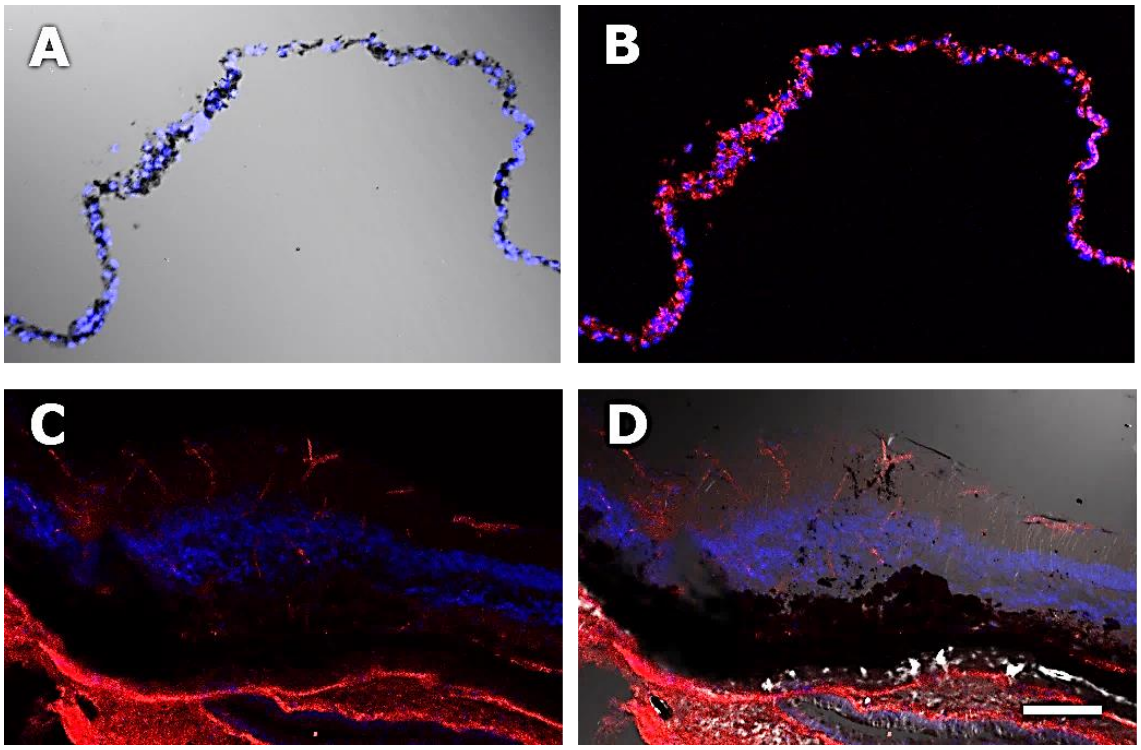

Figure 3.28 labelling of human mitochondria.
A shows nuclei staining (blue) and transmitted light in hESC-RPE cells. B shows human mitochondria (red) and nuclei (blue) labelling in hESC-RPE cells. C is an image of retina which received hESC-RPE cells and labelled for human mitochondria (red) and nuclei (blue). D is the same image as C with transmitted light. This is an image around the site of injections. There is a cluster of pigmented cells subretinally, but these do not stain positively for human mitochondria. No cells positive for human mitochondria were found in transplanted eyes. Scale bar indicates 50 µm.

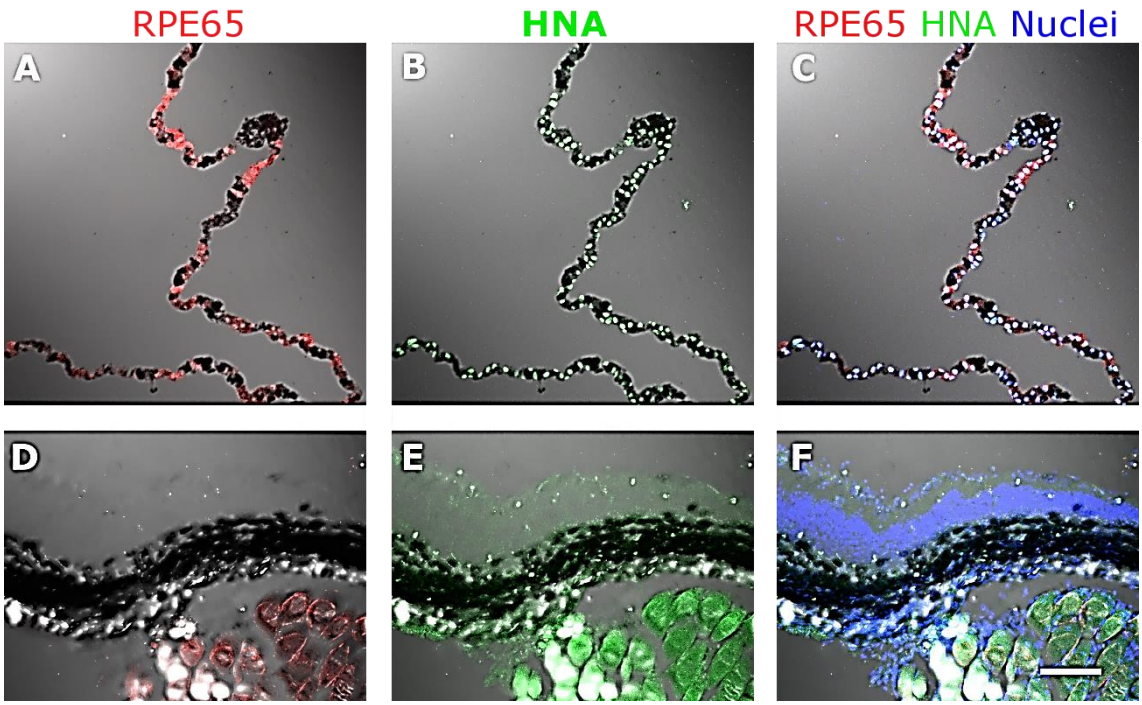

Figure 3.29 labelling of RPE65 and human nuclear antibody.
A, B and C are images of hESC-RPE cells labelled for RPE65 (red), HNA (green) and nuclei (blue) with transmitted light. D, E and F are images of an eye which received a graft of RPE cells. No cells positive for RPE65 or HNA were found in transplanted eyes. The scale bar represents 50 µm.

3.7.4 Discussion

Carido and colleagues administered 70 mg/Kg $NaIO_3$ to mice via the tail vein. One week later 100,000 – 200,000 hESC-RPE cells were transplanted subretinally. 3 weeks later hESC-RPE cells had formed extensive monolayers in the sub-retinal space, with correct apical-basolateral organisation and attached to Bruch's membrane. While, there was evidence of phagocytosis but the grafted cells, no functional recovery was seen by ERG (Carido et al., 2014). Given these results and the results of experiment 3.6, which saw a recovery effect using 9-*cis* retinal at 1 month after $NaIO_3$ treatment, it was decided that grafting hESC-RPE cells 3 weeks after $NaIO_3$ administration may be an optimum for detecting improvements in retinal function. Despite this, no improvements were seen in the scotopic or photopic ERGs. Unfortunately, no hESC-RPE cells were found in the

retina 3 weeks after transplantation. While the subretinal space is an immune privileged space, most studies grafting cells into the subretinal space still have poor survival, possibly due to resident microglia. In the case of $NaIO_3$-treated eyes, had the extra burden of disruption to the BRB, which, reduces graft survival (Xian and Huang, 2015). These were also xenografts, contributing to immune rejection. From these results, it is difficult to gauge how useful this model is for studying RPE transplantation, but rescue of rod retinal function is possible in these eyes, as demonstrated by supplementing the animals with chromophore. The possibility of retinal recovery in $NaIO_3$-treated eyes with grafted hESC-RPE cells, cannot be ruled out, but the model poses many challenges for establishing this as a model for studying RPE transplantation.

3.8 General Conclusions

In this chapter, $NaIO_3$ was used to selectively kill RPE cells to reflect the death of RPE seen in dry AMD, with the aim of assessing potential benefits and discovering the limitations of using this model for studying RPE cell transplantation. In studies where host RPE cells remain, they can be found as clumps in the subretinal space (Carido et al., 2014, Li and Turner, 1991, Seaton and Turner, 1992, Sheedlo et al., 1991, Carr et al., 2009). Thus, the removal of host RPE cells prior to transplantation, may allow grafted RPE cells to attach to Bruch's membrane and survive in the subretinal space.

One of the major difficulties in studying this model, is the variability in the literature in the route of administration, dose of $NaIO_3$ and the time delay following $NaIO_3$ administration. Ideally $NaIO_3$ would kill the RPE in the whole retina, to allow detection of functional improvements following transplantation of hESC-RPE cells.

Comparing the literature there are 3 common methods used for delivering $NaIO_3$: intravenous, IP and retro-orbital. While administering $NaIO_3$ via the caudal tail vein requires a higher dose to achieve similar results to those obtained via the orbital plexus (Enzmann et al., 2006, Machalinska et al., 2010, Redfern et al., 2011), animals require general anaesthesia for retro-orbital injection. Thus, administration of $NaIO_3$ by intravenous injection into the caudal tail vein was the first route explored. However, this is a difficult technique and $NaIO_3$ is a dangerous chemical, and so this route of administration was regarded unsafe. Following this, administration of $NaIO_3$ via the IP route was examined. While this method validated the efficacy of $NaIO_3$, it became clear that this route of administration did not reliably kill RPE cells and some animals had ERG results within normal parameters. There was too much variability to assess potential improvements in retinal function. Thus, retro-orbital administration of $NaIO_3$ was investigated. Given the issue of variability in the effects of $NaIO_3$ using the IP route of administration, it was decided that a retro-orbital approach may help to reduce this variability as the chemical is delivered to the target site.

Studies using this route of administration reported total RPE cell loss within 24 hours and a completely diminished scotopic and photopic ERG by day 3 after a dose of 40 mg/Kg $NaIO_3$ (Machalinska et al., 2010). A lower dose of 20 mg/kg, resulted in the peripheral retina being much less severely degenerated, with healthy polygonal cells remaining and a small residual photopic b-wave observed (Machalinska et al., 2010, Xia et al., 2011). Thus, a dose of 40 mg/Kg $NaIO_3$ was chosen for removing RPE cells.

When evaluating the new method of delivering $NaIO_3$, it was found that the results had much less variability between animals, compared to data obtained from administering $NaIO_3$ IP. Even administering the $NaIO_3$ retro-orbitally to the right

eye gave similar results in the left eye, with no statistical differences found between ERG recordings from left and right eyes. Previous studies which have used this method in mice, often do not specify whether $NaIO_3$ was administered to both eyes or just one and thus do not specify any differences between eyes in their results (Machalinska et al., 2010, Wang et al., 2014, Xia et al., 2011). Thus, this was an important factor to examine in this thesis.

In this thesis, the dose of 40 mg/Kg $NaIO_3$ delivered retro-orbitally to the right eye gave a consistent result of a significantly diminished scotopic and photopic ERG. At 1 month after $NaIO_3$ administration, no RPE65 labelling was identified and S-opsin was strikingly reduced and mislocated to the PIS and ONL, being consistent with results seen in the photopic ERG. Rhodopsin labelling is still present in the POS at 1 month but the ONL is reduced to around 7 layers of cells and the scotopic ERG is almost completely lost. It was believed that this is most likely because of the lack of chromophore, as rods are present but their function is almost completely lost and it has been seen in *rpe65*$^{-/-}$ mice that cones are lost first and their opsin mislocates because cone opsin requires chromophore for correct folding and trafficking (Rohrer et al., 2005).

Analysis of the effects of $NaIO_3$ on the melanopsin system after 1 month saw a significant reduction in BLA, however, this behavioural response to light is driven by both melanopsin and cones (Semo et al., 2010). The PLR is another functional readout which is driven by both melanopsin and the outer-retinal photoreceptors (Lucas et al., 2003). In $NaIO_3$-treated animals the PLR is still quite robust, although, the constriction is reduced compared to WT. The greatest deficit in the PLR is seen at low irradiances and the maximum constriction graph resembled that seen in the rd/rd cl mouse, without rod and cone function (Lucas et al., 2003), where melanopsin drives the PLR at high light irradiances but cannot drive a

constriction at lower irradiances of 11 log photons/cm^2/s, comparable to the 0.8 µW/cm^2/s used in this study. Thus, it is likely that at these low irradiances, where melanopsin cannot drive the PLR, the loss of the PLR in $NaIO_3$-treated animals signifies the loss of outer-retinal photoreceptor function. *Opn4*$^{-/-}$ mice have a PLR at this and lower irradiances, which is driven by outer-retinal photoreceptors (Lucas et al., 2003), suggesting that any residual function of the outer-retinal photoreceptors in the $NaIO_3$-treated animals is not enough to drive the PLR. This supports the results from the ERG. Even though the PLR at high irradiances is still quite robust, the constriction does fall short of that of WT, suggesting that there may also be a small loss in melanopsin function. Consistent with the functional data, immunohistochemical labelling also showed a loss of melanopsin expression in the on sublamina, but robust express in the off sublamina of IPL.

The important question of whether retinal function can be restored in $NaIO_3$-treated mice was initially answered by supplying chromophore. If the remaining rods and the retinal circuitry were still functional, then there was a possibility of functional rescue. At 3 days after $NaIO_3$ treatment, an improvement in the scotopic ERG was seen in half of the animals, by 7 days, 9-*cis* retinal did not show any improvements in the scotopic ERG. Interestingly, by 30 days after $NaIO_3$ administration the ERG had almost flatlined, but 9-*cis* retinal was able to rescue a lot of retinal function and significantly increases the a- and b-wave amplitudes, although, the latency and implicit time were significantly longer than that seen in untreated animals. Thus, this experiment showed that retinal recovery is possible 30 days after $NaIO_3$ treatment.

Many studies have reported improvements in retinal function and retinal histology with time, following $NaIO_3$ administration (Franco et al., 2009, Kiuchi et al., 2002, Redfern et al., 2011, Machalinska et al., 2013). There is evidence of mitosis,

Müller cells proliferation and macrophage migration following $NaIO_3$ administration (Kiuchi et al., 2002, Redfern et al., 2011), which may play a role in the late improvement in $NaIO_3$-treated animals. This may be the reason that retinal function rescue was possible at a later time point, while it was not possible at 7 days after $NaIO_3$ administration.

Carido and colleagues administered 70 mg/Kg $NaIO_3$ to mice via the tail vein. One week later 100,000 – 200,000 hESC-RPE cells were transplanted subretinally. 3 weeks later hESC-RPE cells had formed extensive monolayers in the sub-retinal space, with correct apical-basolateral organisation and attached to Bruch's membrane. There was also evidence of phagocytosis by the grafted hESC-RPE cells, yet, no functional recovery was seen by ERGs recorded at day 0, 3, 7, 14, 21 and 28 after hESC-RPE cell transplantation (Carido et al., 2014). This indicats that either the transplanted hESC-RPE cells were not fully functional, or that the grafted human cells did not survive in sufficient numbers to support a light-driven response. No quantification of surviving hESC-RPE cells was performed in their study and the cells were not shown to express visual cycle markers after transplantation. Thus, given the lack of improvement reported by Carido and colleagues and the lack of improvements in the scotopic ERG seen earlier in this chapter using 9-*cis* retinal at early timepoints, it was decided that a later timepoint for grafting RPE cells may be advantageous for detecting improvements in retinal function. As such, in the final experiment of this chapter, hESC-RPE cells were transplanted subretinally 3 weeks after $NaIO_3$ administration and the ERG was recorded 3 weeks after cell grafting. Unfortunately, no improvements were seen in the scotopic or photopic ERGs after hESC-RPE cell transplantation. This may have been due to the death of transplanted human cells as unfortunately, no viable hESC-RPE cells were found

in the retina 3 weeks after transplantation. These cells were administered into a hostile retinal environment with serve loss of the BRB, which leave the stem cells exposed to the immune system. The possibility of retinal function rescue was validated with chromophore supplementation, which confirmed that retinal function rescue was possible at in these $NaIO_3$-treated eyes.

Chapter 4 Retinal function in the *rd12* mouse

4.1 Introduction

In this thesis, the *rd12* mouse is proposed as an alternative model for studying RPE stem cell replacement. The *rd12* mouse has previously been used in a study to analyse RPE cell transplantation (Li et al., 2012b), but it is an underutilised model. The *rd12* mouse, has a naturally occurring mutation in *rpe65*, disabling the recycling of chromophore needed to preform phototransduction. The *rd12* mouse is also a model of LCA, a rare inherited disease that has an early onset but produces a slow degeneration of the retina. In the *rd12* mouse, cone death is rapid, although, retinal degeneration is slow (Pang et al., 2005). By replacing *rd12* RPE cells with hESC-RPE cells, which do not have the mutation it may be possible to restore visual function. As this model has a relatively slow degeneration and a specific need for chromophore, trophic factors would not be expected to have a huge impact, making any functional results from cell transplantation most likely to be donor RPE specific. Prior to attempting cell transplantation in this model, the course of retinal degeneration and residual retinal function will be assessed. In addition to the outer-retina (rods/cones), this chapter will focus on the anatomical and functional integrity of the inner retinal (melanopsin) system, which has not previously been examined in *rd12* mice and may provide a novel readout of grafted RPE cell function.

4.2 Retinal degeneration in the *rd12* mouse.

4.2.1 Introduction

While the *rd12* mutation results in a slow retinal degeneration, the morphological changes have an early onset. At 3 weeks, lipid-like droplets are found in the RPE (Pang et al., 2005) and the PNA-lectin positive cone count is reduced to 55 % (Li et al., 2011), with cone opsin lost prior to cone cell death. By 3 months, cone counts are further reduced by 16 % and S-opsin expression is lost (Li et al., 2011). By 7 months the POS are distinctively shorter and the ONL is reduced to 6-7 cells thick (Pang et al., 2005, Wright et al., 2014). By 2 years the POS are almost absent and the ONL is reduced to 3-4 layers (Pang et al., 2005).

4.2.2 Methods

Animals

Two breeding pairs of *rd12* mice (B6(A)-*rpe65*^{rd12}/J) were obtained from the Jackson Laboratory, US. The progenies of these mice were used for all subsequent experiment. C57 mice were used as control mice (WT).

Fixation of Tissue

3-month-old adult *Rd12* and WT animals were fixated by perfusion with 4% paraformaldehyde as described in paragraph 2.3.1.

Sectioning and immunostaining

As described in paragraph 2.3.2, eyes were cryopreserving, sectioned and immunolabelled. Anti-RPE65, raised in rabbit (diluted 1:200), provided by Dr T.

Michael Redmond, National Eye Institute, Bethesda, Maryland, US (Ma et al., 2001, Pang et al., 2005), anti-RGR raised in rabbit (1:800 dilution, kind gift from Henry Fong, UCLA), anti-rhodopsin raised in rabbit (1:1000, Abcam) and anti-M/L opsin raised in rabbit (1:15000, Milipore) were used as a primary antibody with a secondary antibody raised in donkey against rabbit IgG tagged with Alexa Fluor 568 (ab10042; Abcam) diluted at 1:2000. Anti-M/L opsin was double labelled with anti-S-opsin raised in goat (SC-14363, Santa Cruz), diluted to 1:200 with secondary antibody anti-goat raised in donkey tagged with FITC diluted to 1:200 (Jackson ImmunoResearch, West Grove, PA, USA).

Imaging sections

Labelled sections were imaged in a z-stack using the Zeiss 700 microscope. These z-stacks were then flattened to extract a maximum intensity projection using zen software.

4.2.3 Results

Validation of the model

To validate the absence of RPE65 in our *rd12* mice, retinal sections from *rd12* and WT mice were labelled for RPE65. In the WT retina, RPE65 labelling is specific to the RPE layer. No RPE65 labelling is seen in the *rd12* retina (Figure 4.1). RGR was also labelled, to investigate if expression of other isomerase enzymes in the visual cycle were disrupted due to the *rd12* mutation. RGR is an opsin expressed in the RPE and Müller glia (Jiang et al., 1993). In the dark, RGR contains all-*trans*-retinal (Hao and Fong, 1999) and controls the visual cycle

production of 11-*cis* retinol until illumination (Radu et al., 2008). RGR labelling is seen in the RPE of both WT and *rd12* mice (Figure 4.2).

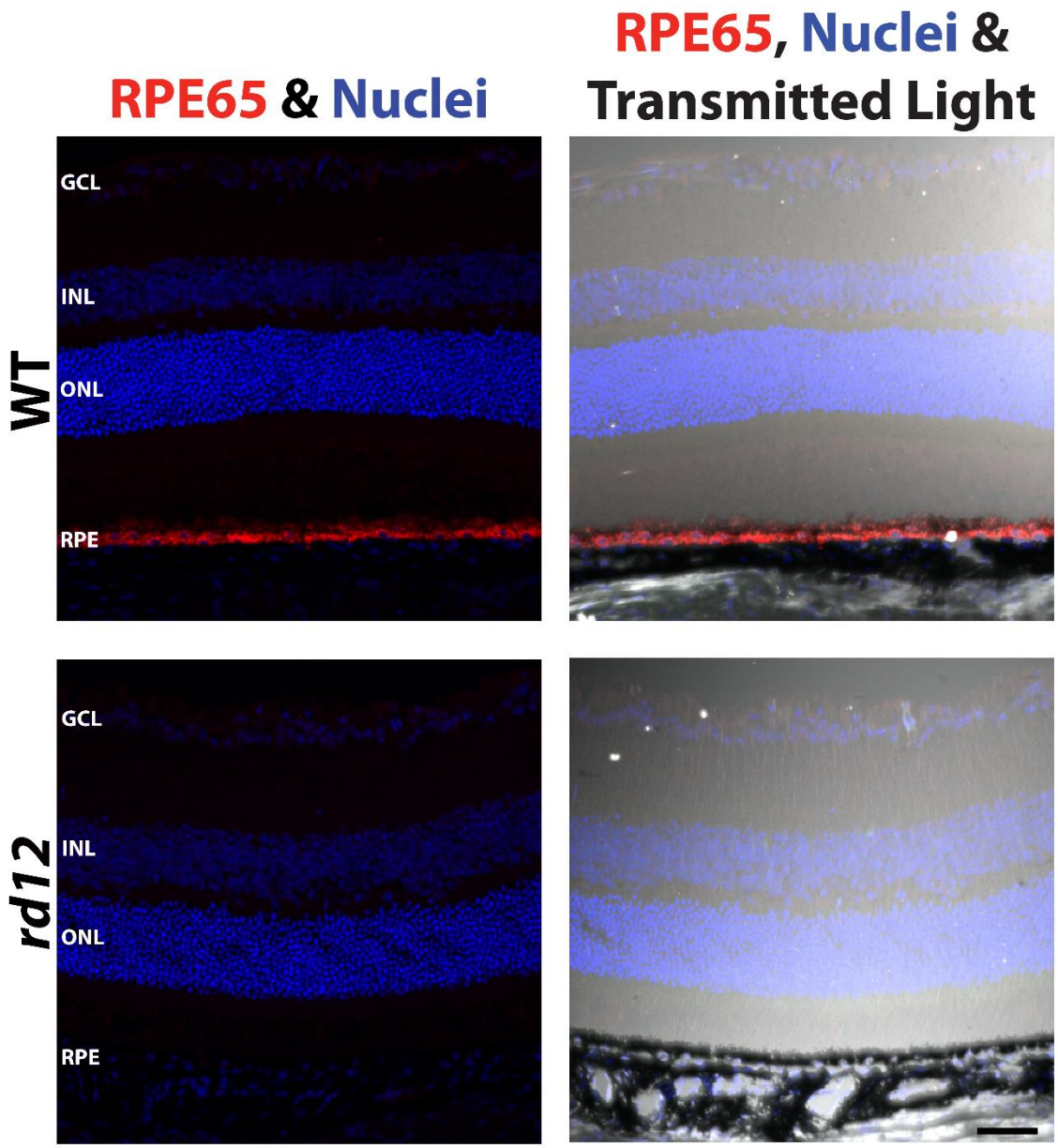

Figure 4.1 Absence of RPE65 labelling in the rd12 retina.
This figure displays RPE65 labelling (red) and transmitted light in WT and rd12 retina. *RPE65 (red) is seen in the RPE in WT retina. No RPE65 labelling is seen in the rd12 retina. Scale bar indicates 50 µm.*

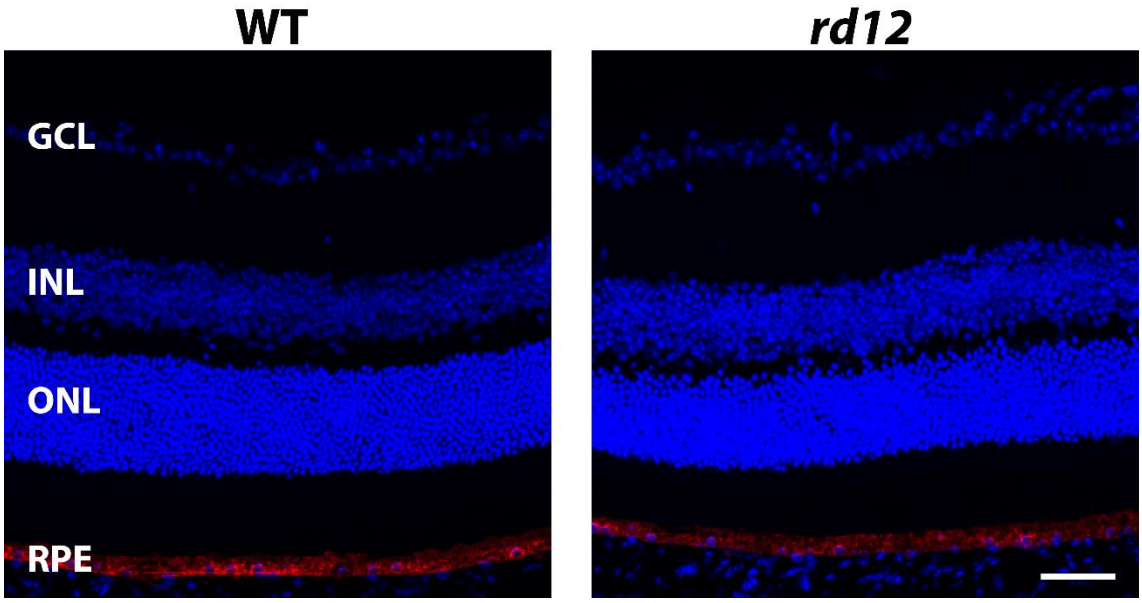

Figure 4.2 RGR labelling in rd12 retina.
RGR labelling (red) is seen in the RPE in both WT and rd12 retina. Scale bar indicates 50 µm.

Loss of rods and cones in the *rd12* retina

At 3 months, rhodopsin levels are still comparable to WT levels (Figure 4.3). Cones are more notably affected by the *rd12* mutation. No M/L-opsin was detected (Figure 4.4). S-opsin can still be seen, although, the number of cones expressing S-opsin was notably reduced and S-opsin is seen mislocated to the PIS, ONL and outer plexiform layer (OPL). S-opsin expression is stronger in the ventral retina, and, it is known that S-cones are more abundant in the ventral retina (Ortin-Martinez et al., 2014).

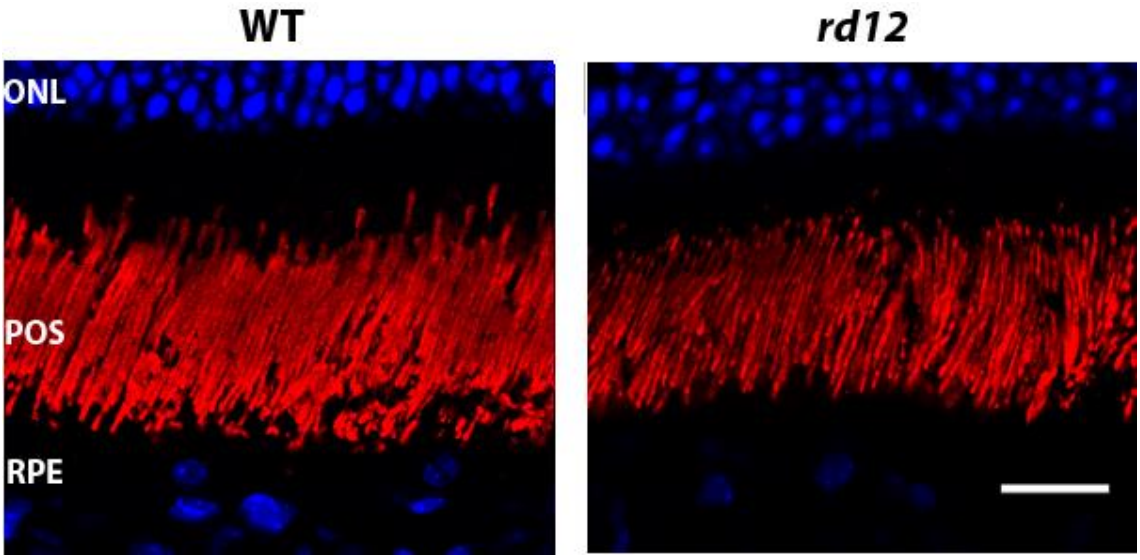

Figure 4.3 Rhodopsin labelling in rd12 retina.
Rhodopsin labelling (red) is seen in the POS in both 3 month WT and rd12 retina. Scale bar represents 20 µm.

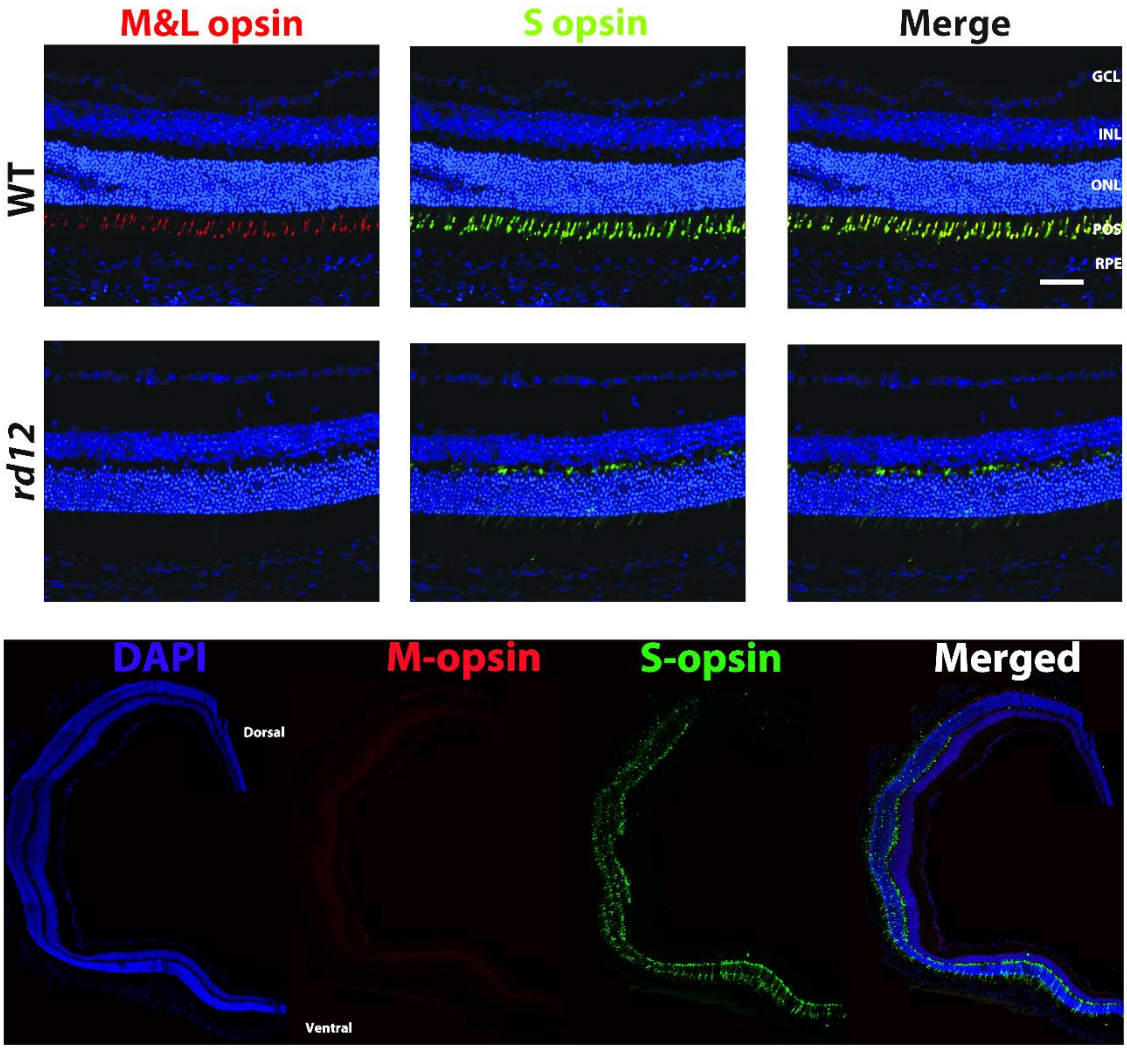

Figure 4.4 Cone opsin labelling in 3-month rd12 retina.
Top images display nuclei staining (blue) with M/ L- (red) and S-opsin (green) labelling in 3-month WT and rd12 retinas. M/L-opsin labelling is not detected in 3-month rd12 retina. The number of cones expressing S-opsin is reduced and S-opsin is mislocated to the PIS and the outer plexiform layer. Scale bar indicates 50 µm. Sagittal section of rd12 retina shows loss of M/L-opsin and S-opsin mislocation.

4.2.4 Discussion

The *rd12* mouse was validated by immunohistochemistry. No RPE65 was identified in the *rd12* RPE. This antibody was kindly provided by Dr T. Michael Redmond, National Eye Institute, Bethesda, Maryland, US (Ma et al., 2001) and was also used by Pang and colleagues to validate the *rd12* mouse (Pang et al., 2005).

RGR was also labelled to investigate other visual cycle protein levels and was seen in the RPE layer in *rd12* mice. Since this experiment, Zheng and colleagues have found 7 visual cycle-associated proteins which have altered proteomics, including: CRALBP, retinol-binding protein 1 (RBP-1), IRBP, RDH-2, RDH-5, LRAT, and ezrin-radixin-moesin-binding phosphoprotein 50 (EBP-50) (Zheng et al., 2015).

The loss of the visual cycle has a destructive effect on outer-retinal photoreceptors. At 3 months, M/L-opsin is lost. Li and colleagues showed that the number of cones is significantly reduced by P21 in the *rd12* retina (Li et al., 2011). In WT rat development *rpe65* reaches its peak and steady state expression around P10-P12, which coincides with peak opsin expression in rat and mouse (Bowes et al., 1988, Manes et al., 1998, Hamel et al., 1993). Li and colleagues showed that P14 PNA-positive cone counts are similar to WT, but, after this, cone loss is rapid. A slower degeneration of S-cones in the *rd12* retina was observed. However, the opsin was mislocated to the PIS, ONL and OPL. This mislocation of cone opsins is also seen in the *rpe65*$^{-/-}$ mouse and can be appropriately localised with the treatment of chromophore (Rohrer et al., 2005). Chromophore has been shown to be required for cone opsin trafficking to outer-segments (Bandyopadhyay et al., 2013). This slower loss of S-opsin, seen in these results, is contradicting results reported by Li and colleagues, who found no S-opsin at 2 months (Li et al., 2011), however, their study looked in flatmounts, which may not detect S-opsin that has been mislocated to the ONL and OPL. Also, a different antibody was used, which may not detect a mis-folded protein. Pang and colleagues described how *rpe65* gene therapy at P35 protected M/L-cone loss but S-cones could only be saved with earlier treatment at P14 (Pang et al., 2010).

However, treatment with chromophore was more successful in correcting the localisation of M/L-opsin than S-opsin (Rohrer et al., 2005).

Rods on the other hand, are lost at a slower rate. Rhodopsin staining intensity in the POS appeared similar in *rd12* compared to WT. This is supported by results showing no significant alterations in rhodopsin mRNA levels in the *rpe65*$^{-/-}$ up to 8 weeks (Znoiko et al., 2005). Unlike cones, chromophore is not required for rhodopsin trafficking. While rhodopsin protein levels are strong, rhodopsin spectral absorbance is not detectable (Pang et al., 2005), presumable due to the absence of chromophore.

4.3 Is Melanopsin expression affected by the loss of RPE65 in *rd12* mice?

4.3.1 Introduction

Melanopsin is the opsin used by the ipRGCs in the inner retina. It's action spectrum indicates that it uses a vitamin A-based photopigment (Berson et al., 2002), converting 11-*cis* retinal to all-*trans* retinal upon the capture of light. It is not clear where this chromophore is generated as ipRGCs are separated by several retinal layers from the RPE. Melanopsin has many characteristics that resemble rhabdomeric photoreceptors, such as depolarisation upon illumination (Hartwick et al., 2007) and more importantly, its ability to work as a bi-stable pigment with photoisomerase capacity to generate 11-*cis* retinaldehyde from all-*trans* retinaldehyde upon exposure to long wavelength light (Melyan et al., 2005, Fu et al., 2005). However, this bi-stable property may not be enough for normal melanopsin function, as *rpe65*$^{-/-}$ mice have attenuated melanopsin functions (Doyle et al., 2006).

To date no studies have assessed the melanopsin system in *rd12* mice. As such, in this experiment, melanopsin in the *rd12* retina is labelled by immunohistochemistry and analysed to determine if the *rd12* mutation influences melanopsin expression. As a control, the influence of this mutation on general ganglion cell health is also assessed using the RGC specific marker Brn3a.

4.3.2 Methods

Retinal preparation and immunohistochemistry

1-, 3- and 8-month animals were sacrificed and the tissue fixed by perfusion as described in paragraph 2.3.1. Retinas from the left eye were stained as described in paragraph 2.3.3. Retinas were double labelled with primary antibodies raised in rabbit against melanopsin (1:5000, UF006; Advanced Targeting Systems, San Diego, CA, USA) and a goat antibody raised against Brn3a (1:200, sc-31987; Santa Cruz Biotechnology, Dallas, TX, USA). Secondary antibodies used were antibodies raised in donkey against rabbit FITC-labelled and against goat TRITC-labelled (1:200, Jackson ImmunoResearch, West Grove, PA, USA).

Imaging and analysis

Using the Zeiss 700 confocal microscope, images were taken of the SN, ST, IN and IT regions of the retina and SN rim and IN rim. Analysis of images is described in paragraph 2.3.4. Thresholds used for dendrite analysis were 0.1, 0.05 and 0.02, where 0.1 is the highest threshold to detect strongly stained neurites.

Entire retinal images of melanopsin labelling were taken using the Zeiss 710 confocal microscope, where multiple z-stacks were captured and stitched using the Zen software.

Statistical Analysis

For this experiment a range of ages were examined: 1 month (WT n = 4, *rd12* n=4), 3 months (WT n = 4, *rd12* n = 4) and 8 months (WT n = 3, *rd12* n = 3). Regional analysis includes all ages and is analysed by two-way repeated measures ANOVA with post-hoc Holm-Sidak's multiple comparisons tests. Nasal Vs Temporal melanopsin^{+}-cell counts were analysed by Mann Whitney one-tailed t-test for both WT and *rd12.* Age analysis used average data from the four regions of each animal and was analysed by two-way ANOVA and post-hoc Holm-Sidak's multiple comparisons tests. Dendrite analysis used two-way repeated measures ANOVA and post-hoc Holm-Sidak's multiple comparisons tests.

4.3.3 Results

As shown in Figure 4.5 below, the *rd12* retina had a striking reduction in melanopsin labelling.

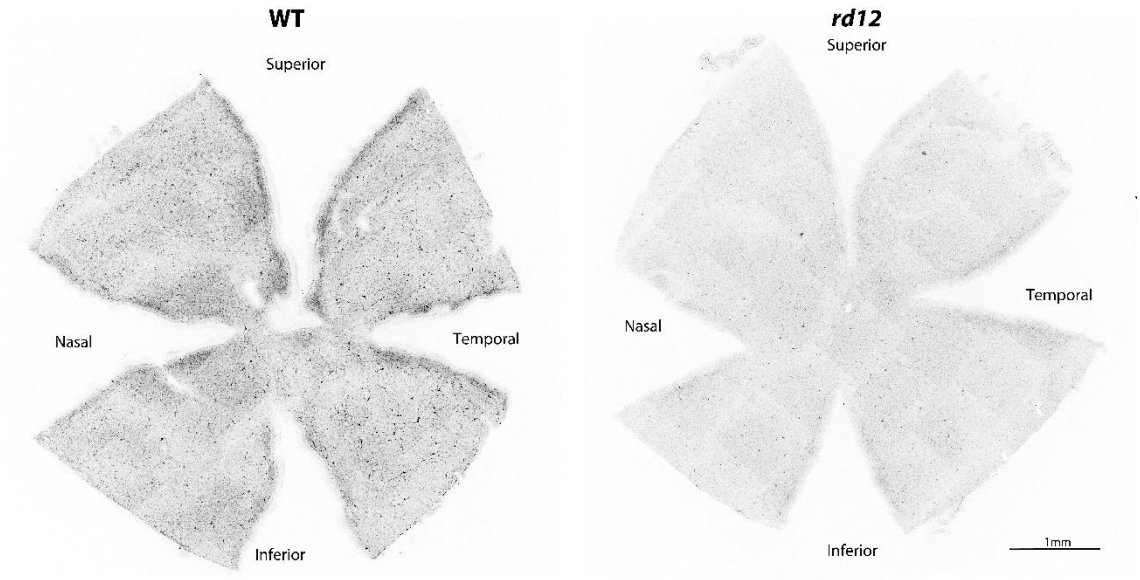

Figure 4.5 Melanopsin labelling in rd12 retinal flatmount.
Melanopsin staining at 3 months of age in retinal flatmounts. Strong melanopsin labelling is seen in the WT retina (left), compared to a very weak signal in the rd12 (right). Scale bar indicates 1 mm.

Regional analysis of melanopsin

In the *rd12* retina there is a striking reduction in melanopsin labelling compared to WT. The number of melanopsin$^+$-cells was reduced by 46% in *rd12* mice (Figure 4.6), with WT retina having an average of 106 ± 4 melanopsin$^+$-cells per mm^2, while the *rd12* retina has an average of 71 ± 4 melanopsin$^+$-cells per mm^2. Retinas were divided into four quadrants: superior-temporal (ST), superior-nasal (SN), inferior-nasal (IN) and inferior-temporal (IT). Two-way ANOVA showed a significant difference between *rd12* and WT ($P < 0.0001$, $F(1, 20) = 39.46$), also, a significant difference among regions ($P = 0.0004$, $F(3, 60) = 7.071$). This regional difference was similar in both WT and *rd12* ($P = 0.9$, $F(3, 60) = 0.2$). This differential regional distribution suggests that the different quadrants may contain different populations of melanopsin$^+$-cells. Although, the reduction in melanopsin$^+$-cell density in *rd12* retinas occurs across the retina. Post-hoc analysis shows significant reduction in melanopsin$^+$-cells in all quadrants in the *rd12* retina (Figure 4.6). Examining the populations of melanopsin$^+$-cells in the

different retinal regions revealed an increase in melanopsin$^+$-cells in the temporal retina in both WT (t-test, P = 0.0017) and *rd12* (t-test, P = 0.0089). WT retina have 26% more melanopsin$^+$-cells in the temporal retina (118 ± 5 per mm^2) compared to nasal (93 ± 5 per mm^2). Similarly, the *rd12* retina has a 28% increase in melanopsin$^+$-cells in the temporal retina (79 ± 4 per mm^2) compared to nasal (62 ± 5 per mm^2).

Melanopsin-labelling in ipRGC somas is also reduced by 30% in *rd12* retinas compared to WT (Figure 4.6). Average greylevel of *rd12* melanopsin$^+$-cells is reduced to 56 ± 2.6 compared to 80.2 ± 3.1 seen in WT. Two-way repeated measures ANOVA shows that this difference between WT and *rd12* is significant (P = 0.0016, F (1, 20) = 13.37). Melanopsin-labelling in ipRGC is also significantly different among different regions in the retina (P < 0.0001, F (3, 60) = 11.32), with the strongest labelling seen in the IN region in both WT and *rd12* retinas. The regional differences of melanopsin expression in melanopsin$^+$-cells, while significantly reduced in *rd12*, is similar to WT regional paterns (P = 0.4, F (3, 60) = 1.1). Post-hoc tests show a significant difference between staining intensity in WT and *rd12* mice in each region of the retina.

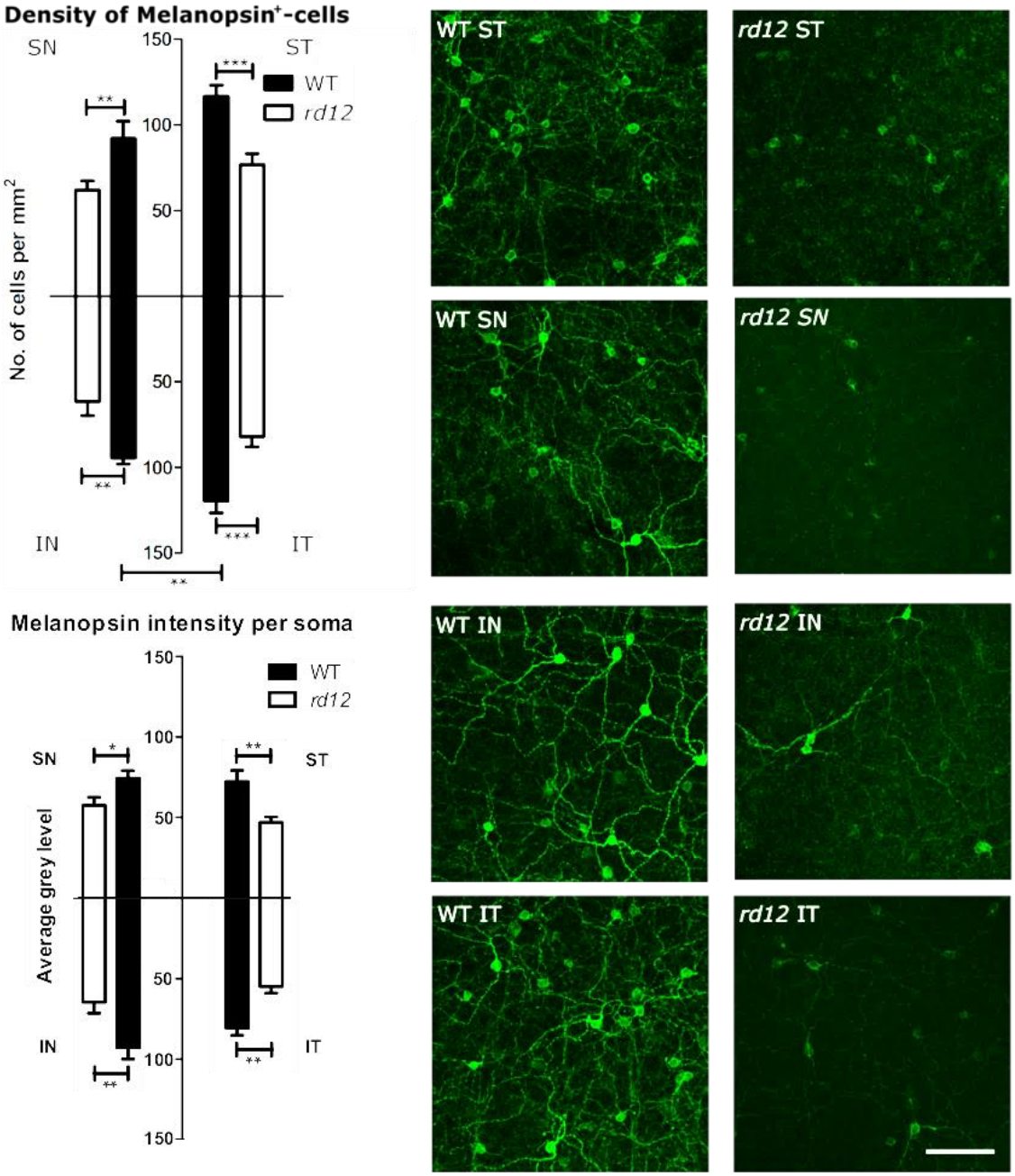

Figure 4.6 ipRGC regional soma analysis in WT and rd12 retina.
*This figure displays graphs of the density of melanopsin$^+$-cells and the intensity of this labelling in melanopsin$^+$-somas in the different retinal regions in WT (black, n = 11) and rd12 (white, n = 11). The density of melanopsin$^+$-cells is significantly reduced in the rd12 retina in each quadrant. There is a significantly higher density of melanopsin$^+$-cells in the temporal retina compared to nasal in both WT and rd12. Melanopsin intensity in somas is significantly reduced in rd12 ipRGCs in each retinal quadrant. The brightest melanopsin$^+$-somas are in the inferior nasal quadrant in both WT and rd12 retinas. Asterisks indicate statistical power *P < 0.05, **P < 0.01, ***P < 0.001. Representative images of each quadrant in 3--month WT and rd12 retinas are shown on the right, where the reduction in melanopsin$^+$-cell density and melanopsin-labelling in rd12 retina is clear. Scale bar indicates 100 µm.*

The ipRGC dendrites are also less visible in the *rd12* retina (Figure 4.6). Melanopsin expression in dendrites was quantified using a thresholding method as demonstrated in Figure 4.7. Here, a low threshold of 0.02, recognises dendrites with low levels of melanopsin expression as well as brightly stained dendrites. Higher thresholds do not recognise axons with low levels of melanopsin, and he highest threshold, 0.1, recognises only dendrites labelling strongly for melanopsin. A threshold of 0.1 recognises all pixels above greylevel 255 x 0.1. This method also filters out cell bodies and so only axons are analysed. Two-way ANOVA determined a significant difference in dendrites between WT and *rd12* mice ($P < 0.0001$, $F(1, 20) = 40.72$). The different thresholds created a significant difference in dendritic coverage ($P < 0.0001$, $F(2, 40) = 177.3$), showing the difference of the different populations of weak- and strong-expressing melanopsin^{+}-dendrites. These different populations were significantly different between WT and *rd12* ($P < 0.0001$, $F(2, 40) = 24.69$), with greater loss in *rd12* at the higher threshold. Post-hoc tests determined a significant difference in dendritic coverage between WT and *rd12* at all thresholds tested. There was a 60% reduction in the area covered by dendrites above threshold 0.02 in *rd12* retinas compared to WT retinas ($P < 0.0001$). Above a threshold of 0.05, there was a 73% reduction in area covered by dendrites in *rd12* compared to that in WT ($P < 0.0001$). At the high threshold of 0.1, only very bright dendrites were recognised, most likely the M1 dendrites (Schmidt et al., 2011). At this threshold, dendritic coverage is reduced by 70% in *rd12* retinas compared to WT ($P < 0.01$). Dendritic coverage of the different retinal regions was analysed by two-way ANOVA; which, did not show regional differences as significant.

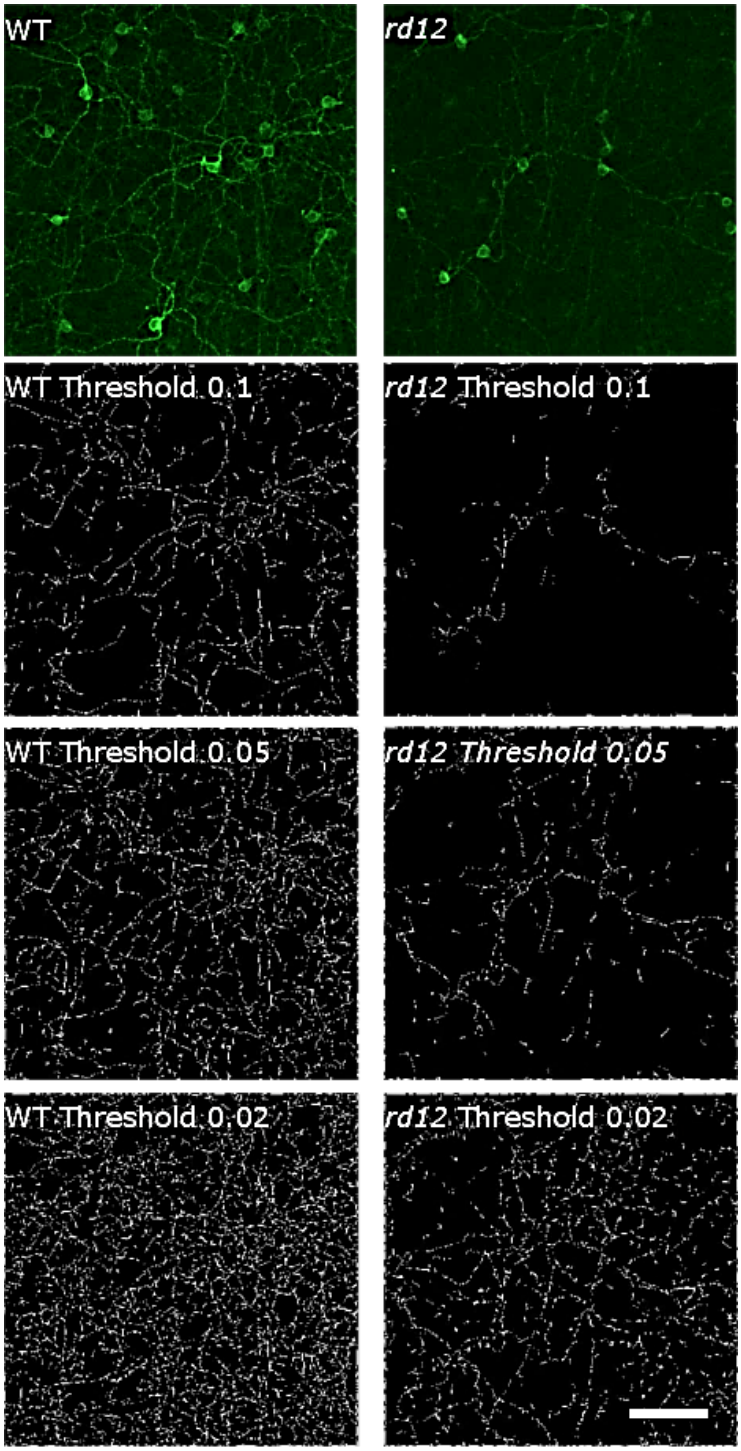

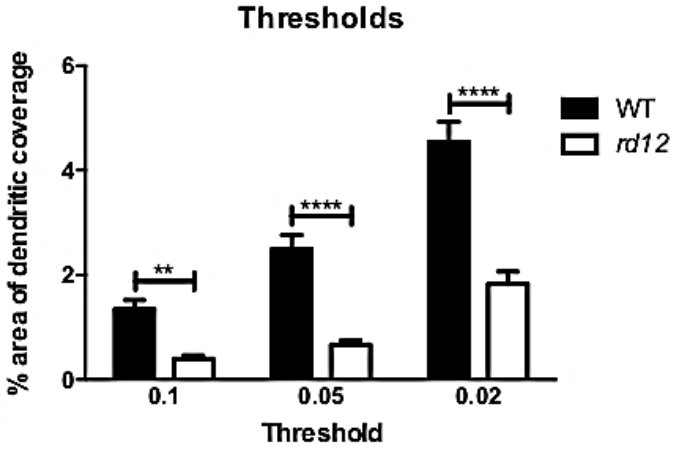

Figure 4.7 ipRGC dendrite analysis in WT and rd12 mice.
*This figure displays a representative image of WT and rd12 melanopsin labelling taken from the IT region in 3-month mice. Beneath are representations of these images filtered at the different thresholds. Scale bar represents 100 µm. The graph presents the percentage of area covered by dendrites at different thresholds in WT (n = 11) and rd12 (n = 11). Regional analysis was averaged per retina. Asterisks indicate significance levels: **P < 0.01, ****P < 0.0001.*

As shown in Figure 4.8, melanopsin labelling was analysed in mice of 1, 3 and 8 months of age. Density of melanopsin^{+}-cells, intensity of melanopsin labelling and dendritic coverage were analysed by two-way ANOVA, including age as a factor, and showed that age was not a significant factor for any of these measures. Analysis of each measure was consistent in showing that there was a significant difference between WT and *rd12* mice but age did not affect these results.

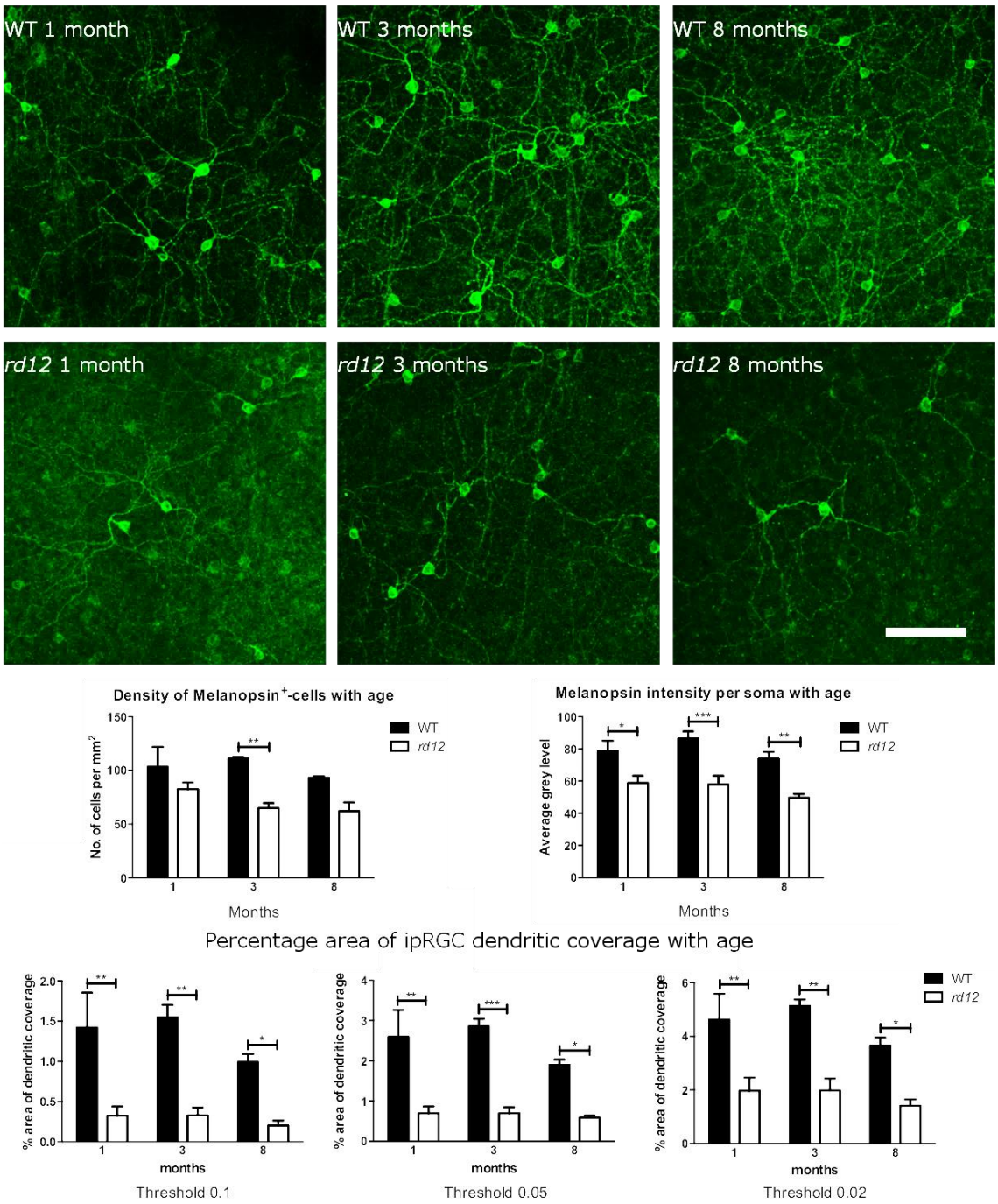

*Figure 4.8 Melanopsin labelling at different ages in WT and rd12 mice. Melanopsin labelling does not change significantly between 1 and 8 months in either WT or rd12 retinas. Representative images of WT and rd12 retina at different ages are taken from the IT region. Scale bar indicates 100 µm. Graphs display density of melanopsin$^+$-cells, labelling intensity per soma and the percentage of area covered by melanopsin$^+$-dendrites. None of these measurements were significantly altered with age in WT or rd12. Asterisks indicate significant differences between WT and rd12 from post-hoc analysis: *P < 0.05, **P < 0.01, ***P < 0.001. At 1 month n = 4, at 3 months n = 4 and at 8 months n = 3 for both WT and rd12.*

A rim of melanopsin previously reported at the retinal edge, with the strongest labelling in the nasal retina (Semo et al., 2014, Vugler et al., 2008b) was examined in the *rd12* mouse. Images of melanopsin labelling in the SN and IN were analysed in both WT and *rd12* (Figure 4.9). The density of melanopsin^{+}-cells was similar in the *rd12* retina and WT, with similar cell numbers in SN and IN regions of both animal strains. Differences were seen in the melanopsin-labelling in somas (melanopsin intensity) which is significantly reduced in *rd12* retinas (P = 0.0148, F (1, 20) = 7.113). Average pixel greylevel was 62.9 ± 4.9 in *rd12* while WT greylevel was 87.7 ± 7.5. Similar to data reported in Figure 4.6, the melanopsin soma intensity in the IN region is greater than in the SN region (P = 0.0003, F (1, 20) = 18.89), seen in both WT and *rd12* (P = 0.1, F (1, 20) = 3).

Dendritic coverage was significantly reduced in the *rd12* at both the SN and IN marginal zone (Table 15Figure 4.9). There are different populations of weak and strong-expression of melanopsin in these dendrites, identified by the significance of the different thresholds. Post-hoc tests show a significant reduction in dendritic coverage in *rd12* in both SN and IN at each threshold tested. No significant changes in melanopsin labelling at the CMZ were seen between 1 and 8 months in either WT or *rd12.* Melanopsin^{+}-processes were seen projecting into the ciliary body in WT retinas (Figure 4.10), which have been previously reported (Semo et al., 2014).

Table 15 Two-way ANOVA of melanopsin dendrites at rd12 retinal rim

Two-way ANOVA	SN	IN
Rd12 Vs WT	P = 0.0014, F (1, 20) = 13.7	P < 0.0001, F (1, 20) = 25.7
Threshold effect	P < 0.0001, F (2, 40) = 309	P < 0.0001, F (2, 40) = 451
Interaction	P = 0.0104, F (2, 40) = 5.1	P = 0.2, F (2, 40) = 1.8

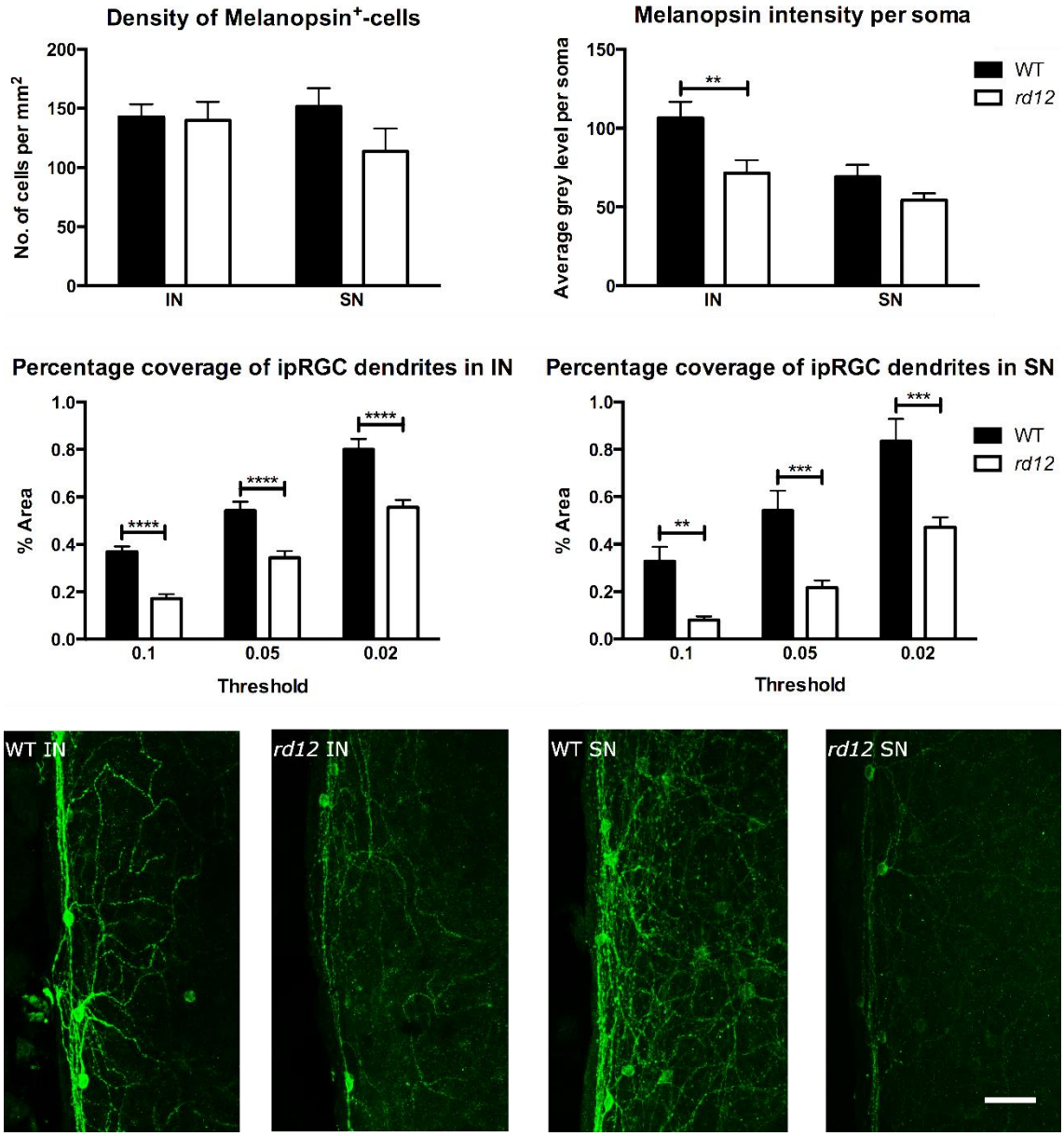

Figure 4.9 Analysis of melanopsin labelling at the retinal marginal zone.
A rim of melanopsin is seen along the nasal retinal edge. The density of melanopsin⁺-cells along this rim is similar in rd12 (white, n = 11) and WT (black, n = 11) but the strength of melanopsin labelling is reduced in rd12 compared to WT and in the SN rim compared to the IN rim. Percentage area of dendritic coverage is also reduced in rd12 compared to WT. Representative images of melanopsin labelling in WT and rd12 at the SN and IN rim show this reduction in melanopsin labelling in the rd12 retina. The scale bar indicates 50 µm.

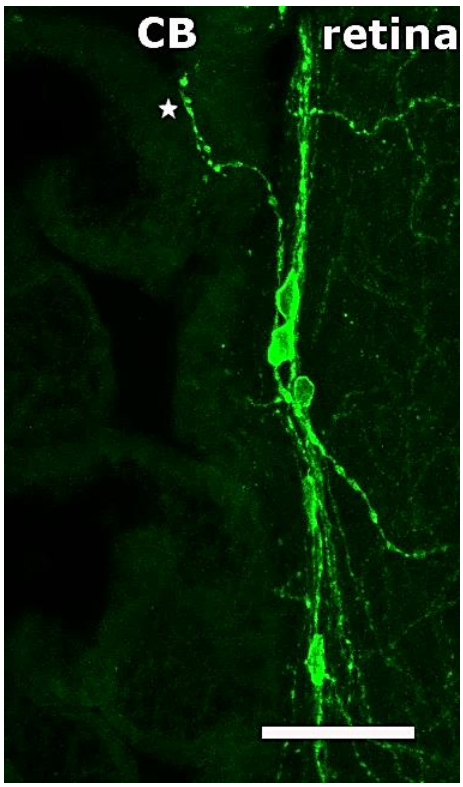

Figure 4.10 Melanopsin^{+}-dendrite projecting into ciliary body.
A melanopsin^{+}-dendrite is seen projecting into the ciliary body (CB), indicated by the star, in an 8-month-old WT retina in the IN melanopsin rim. The scale bar represents 50 µm.

To investigate if the loss of melanopsin cells is a result of an overall decrease in the number of ganglion cells rather than ipRGCs specifically, retinas were labelled for Brn3a, which is expressed by the majority (~90%) of RGCs (Mead et al., 2014, Nadal-Nicolas et al., 2009) and only about 2% of ipRGCs in WT mouse retinas (Valiente-Soriano et al., 2014).

No differences in the number of $Brn3a^+$-cells nor in the strength of Brn3a labelling were detected between WT and *rd12* (Figure 4.11). $Brn3a^+$-cells counts in *rd12* retinas were 2628 ± 132 cells per mm^2, similar to 2707 ± 75.2, seen in WT ($P = 0.6$, $F(1, 20) = 0.3$), suggesting that the reduction of $melanopsin^+$-cells is not due to an overall reduction in the RGC population of *rd12* mice. There are significant differences in the $Brn3a^+$-cell populations in the different regions of the retina ($P < 0.0001$, $F(3, 60) = 17.46$). The ST region has fewer RGCs than other regions in both WT and *rd12* (Figure 4.11) and similar results are seen in the literature (Valiente-Soriano et al., 2014). The average density of $Brn3a^+$-cells in the ST region in WT is 2029.545 ± 251.5 per mm^2 and 1622.156 ± 105.261 per mm^2 in *rd12*, which is considerably less than the retinal average mentioned above. The regional differences in RGC populations is similar in both WT and *rd12* ($P = 0.6$, $F(3, 60) = 0.7$). There was no significant loss of $Brn3a^+$-cells over time (1 – 8 months) in either WT or *rd12* retinas.

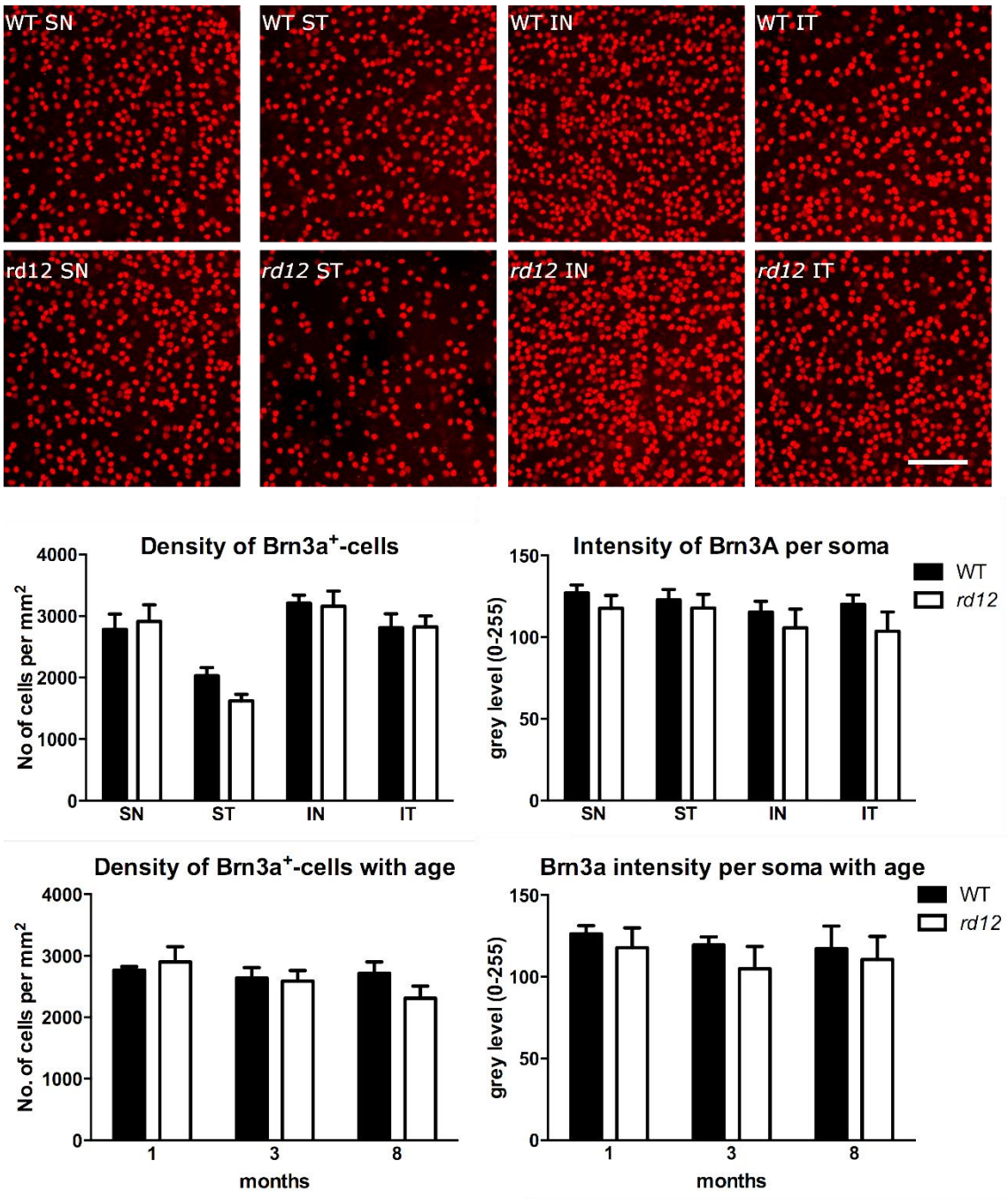

Figure 4.11 RGC analysis in WT and rd12 retina.
Representative images of Brn3a labelling are taken from 3-month WT and rd12 retina. Scale bar indicates 100 µm. There are no significant differences between WT (black, n = 11) and rd12 (white, n = 11) in regional analysis of Brn3a$^+$-cell density or labelling strength. Significant differences in Brn3a$^+$-cell density are seen between regions of the retina, with less Brn3a$^+$-cells in the ST region. There were no significant changes in RGC population between 1 (WT n = 4, rd12 n = 4), 3 (WT n = 4, rd12 n = 4) and 8 (WT n = 3, rd12 n = 3) months.

4.3.4 Discussion

It has been shown by the action spectrum of melanopsin that it requires a vitamin A-based photopigment (Berson et al., 2002). While melanopsin uses chromophore for phototransduction, the source of this chromophore is only just beginning to be elucidated (Zhao et al., 2016). While the RPE is the classic site of 11-*cis* isomerisation, it is separated by several layers from the ipRGCs, on the inner retina. In this experiment, the effects of the *rd12* mutation on melanopsin expression was examined. It was discovered that the density of melanopsin$^+$-cells was significantly reduced in the *rd12* retina and this density did not significantly change between 1 and 8 months. The density of RGCs was not reduced in the *rd12* retina, thus, the reduction in melanopsin$^+$-cells was not due to an overall loss of RGC but specific loss of ipRGCs. The loss of melanopsin$^+$-cells was accompanied by a reduction of melanopsin in these cells, with melanopsin labelling intensity reduced by 30% in *rd12* melanopsin$^+$-somas. Melanopsin$^+$-dendrites were also significantly reduced in the *rd12* retina.

Interestingly, the number of melanopsin$^+$-cells along the nasal CMZ were not reduced in the *rd12* retina, while, melanopsin labelling intensity in melanopsin$^+$-somas was significantly reduced similarly to melanopsin$^+$-somas in the central retina. Melanopsin$^+$-dendrites were also reduced in *rd12* CMZ.

All these metrics were examined at 1, 3 and 8 months and no significant changes were see over this time period in WT or *rd12.*

Melanopsin expression has been shown to be affected by other RPE mutations. The RCS dystrophic rat retina has a significant (>90%) reduction of melanopsin mRNA and protein levels (Sakamoto et al., 2004). The rat can still produce chromophore, raising the question if the effects on melanopsin expression are due to the loss of outer-retinal photoreceptor function. Contradicting this is the

ability for phototransduction in ipRGCs in new born mice, prior to rod and cone function which occurs after P10 (Hannibal and Fahrenkrug, 2004, Sekaran et al., 2005). Also, the influence of the *Mertk* mutation on the visual cycle cannot be ruled out. Without phagocytosis of shed POS there is a lack of chromophore being recycled and shed POS in the debris zone may absorb any chromophore produced by the RPE.

These results support those reported in the *rpe65*$^{-/-}$ mouse, showing a reduction in melanopsin and attenuated melanopsin functions (Doyle et al., 2006) and add to the growing body of evidence that the RPE visual cycle is important for melanopsin expression. It is known that the loss of the visual cycle reduces the sensitivity of the PLR more so than the loss of the outer-retinal photoreceptors (Tu et al., 2006), highlighting the importance of the visual cycle for melanopsin function.

While the loss of the visual cycle in *rd12* mice causes a significant reduction in melanopsin expression, it is not clear if this, like cone opsin, is directly due to loss of chromophore produced in the RPE. The melanopsin system is often not considered when assessing retinal degeneration, yet, it has the clear potential to provide additional readouts on RPE function. Thus, in the next experiment, the effect of the *rd12* mutation on retinal function is examined, with recordings of both outer-retinal photoreceptor function and ipRGC function.

4.4 Visual function in the *rd12* mouse

4.4.1 Introduction

Without RPE65, rhodopsin is undetectable by spectral absorbance in the *rd12* retina (Nusinowitz et al., 2006, Pang et al., 2005), despite this, there is still visual function. *Rd12* mice respond to photopic ERG (Pang et al., 2005, Pang et al., 2006) and despite the absence of detectable rhodopsin by spectral absorbance, it is thought that these photopic responses are rod driven, from studies in *rpe65*$^{-/-}$ *mice* (Cachafeiro et al., 2010, Dai et al., 2015, Seeliger et al., 2001). The lack of chromophore in *rd12* mice allows rods to function at brighter light intensities without bleaching. In this experiment, the residual visual function in *rd12* mice driven by both outer-retinal photoreceptors and ipRGCs is recorded.

4.4.2 Methods

ERG

ERGs were recorded as described in paragraph 2.2.1 from 3-month WT (n = 14) and *rd12* (n = 10). To investigate the rod response at high intensities some animals were also recorded from a high light intensity scotopic protocol with flash intensity from -4.5 to 3.5 lg cd.s/m^2. To reach these light intensities a xenon light source was used, unfortunately, this xenon light required long periods of rest between uses and so only 2 WT (n = 4) and 1 *rd12* (n = 2) mice were recorded using this protocol. After light adaption for 15 minutes, photopic responses were recorded in WT (n = 14) and *rd12* (n = 10).

Assessment of retinal function using light-driven Fos induction

Fos is a transcription factor that is found in the cytosol in dark adapted DA-ACs. Upon exposure to bright light, Fos is localised to the nucleus in DA-ACs. The presence of nuclear Fos after light exposure can therefore be used as a method of determining inner retinal circuitry function. This method has been published previously (Cameron et al., 2009). In brief, mice were dark adapted overnight and then exposed to 190 uW/cm^2 (~380 Lux) white light for 120 minutes and then euthanised and perfused for tissue collection as described in paragraph 2.3.1. Control animals remained in the dark and were euthanised and perfused in the dark. Retinas were isolated from the left eye of 3 WT and 3 *rd12* and labelled for Fos and tyrosine hydroxylase (TH), as described in paragraph 2.3.3. TH, is used to identify DA-ACs and is the rate-limiting enzyme in catecholamine biosynthesis, which results in dopamine production and release. Anti-Fos was raised in rabbit and used at a dilution of 1:5000 (Cell Signal). Anti-TH was raised in sheep and diluted 1:5000 (Milipore). Secondary antibodies used were FITC-labelled anti-rabbit and TRITC-labelled anti-sheep, both raised in donkey diluted 1:200 (Jackson ImmunoResearch, West Grove, PA, USA). Images from the different retinal quadrants in *rd12* and WT were captured as described in paragraph 2.3.4 and analysed by counting DA-ACs with and without nuclear Fos. A nuclear fos signal was considered as a positive result, whereas a cytoplasmic or absent Fos signal was considered as a negative result. Regional results were analysed in eyes which were exposed to light by two-way repeated measures ANOVA. Fos activation between WT and *rd12*, dark adapted and light exposed were analysed by averaging the regional data per animal and applying a two-way ANOVA. Both tests were followed by Holm-Sidak's multiple comparisons tests.

BLA

The presence of light aversion was tested at 1 month and 3 months as described in paragraph 2.2.2. Animals were either placed into an area which had the front half illuminated (light) or in an area that was completely in the dark (dark). Numbers of WT and *rd12* assessed in the BLA arena are shown in Table 16.

Table 16 Numbers of WT and rd12 assessed in BLA arena

Numbers	1-month WT	1-month *rd12*	3-month WT	3-month *rd12*
Light	5	9	16	11
Dark	7	9	7	10

PLR

The PLR was recorded and analysed as described in paragraph 2.2.3. The light powers tested were 80 (WT n = 6, *rd12* n = 6), 800 (WT n = 1, *rd12* n = 8) and 8000 (WT n = 1, *rd12* n = 8) $\mu W/cm^2/s$.

iPLR

The iPLR was recorded as described in paragraph 2.2.4. 3-month *rd12* (n = 4) constriction was compared to WT (n = 10). Aged *rd12 (n = 6)* was compared to 3-month *rd12* the same way.

4.4.3 Results

ERG recordings from the *rd12* retina

At three months, the *rd12* mouse has no evidence of a scotopic a-wave (Figure 4.12.B). The scotopic b-wave is identifiable at 1 lg cd.s/m^2, albeit reduced by 82% compared to WT (Figure 4.12.B). This difference between rd12 and WT scotopic b-wave amplitude is significant (Table 17).

Table 17 Two-way ANOVA of scotopic b-wave amplitude in 3-month rd12

Two-way ANOVA	F (DFn, DFd)	P value
Rd12	F (1, 126) = 154.94	P < 0.0001
Light intensity	F (6, 126) = 113	P < 0.0001
interaction	F (6, 126) = 54.02	P < 0.0001
Subjects (matching)	F (21,126) = 4.749	P < 0.0001

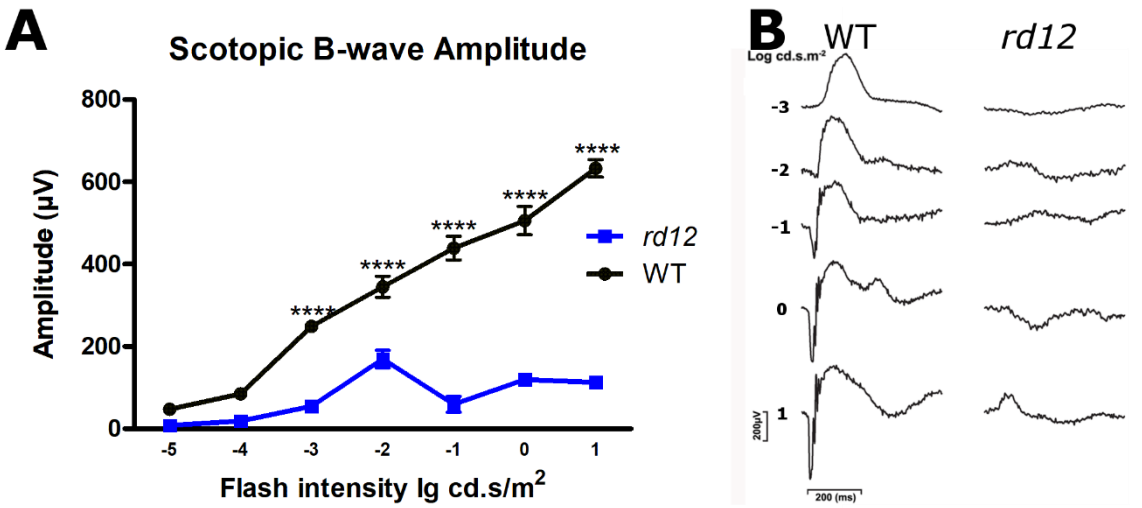

Figure 4.12 Scotopic ERG in 3-month-old WT and rd12 mice.
*At three months, the scotopic b-wave amplitude is severely diminished in the rd12 mouse (blue, n=10), compared to WT (black, n = 14) (A). There is no evidence of an a-wave and only a very small b-wave can be seen at high intensities in some rd12 animals. Asterisks indicate significance: **** P<0.0001. Representative traces for 3-month WT and rd12 are displayed (B). Vertical scale indicates 200 µV and horizontal scale indicates 200 ms.*

Another scotopic protocol was also used to determine if the *rd12* mouse could respond similarly to the WT with very high intensities up to 3.5 log cd/m^2 under scotopic conditions. Unfortunately, due to the temperamental nature of the xenon bulb used in this protocol, it was not possible to run large numbers of animals with this protocol, thus these results are assessed from a small population of samples. This protocol revealed that even at high intensities there is still no evidence of an a-wave for any intensity in the *rd12* mouse (Figure 4.13.B). At 0.5 lg cd.s/m^2 the WT rod a-wave saturates and the a-wave amplitude starts to reduce. Scotopic b-wave can be seen at high light intensities in the *rd12*, however, it does not increase with light intensity (Figure 4.13.A) and remains significantly smaller than WT (Table 18). WT b-wave amplitude starts to saturate at 2 lg cd.s/m^2, and the b-wave amplitude starts to reduce and WT b-wave implicit time reduce steadily with increasing light intensity (Figure 4.13.B). This protocol shows that under scotopic conditions, even at very high intensities the *rd12* mouse cannot produce an a-wave and its b-wave is severely diminished.

Table 18 Two-way ANOVA rd12 b-wave amplitude at high light intensities

Two-way RM ANOVA	F (DFn, DFd)	P value
Rd12	F (1, 64) = 1047	P < 0.0001
Light Intensity	F (16, 64) = 36.45	P < 0.0001
Interaction	F (16, 64) = 15.66	P < 0.0001
Subjects (matching)	F (4, 64) = 1.23	P = 0.3

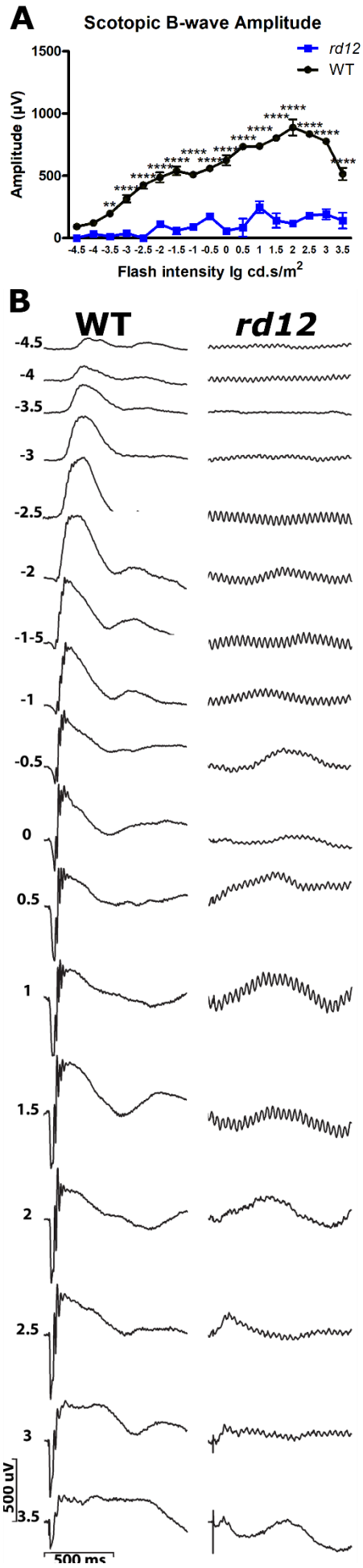

Figure 4.13 Scotopic ERG at higher light intensities in WT and rd12 mouse.
*Using a scotopic protocol that reached high levels of intensity the rd12 (blue, n = 2) still have a significantly reduced b-wave which plateaus and does not grow with increased intensity (A). Asterisks indicate significance level from post-hoc tests: **P<0.01; **** P<0.0001. Representative traces at each light intensity are displayed (B). rd12 do not have an obvious a-wave. The vertical scale bar represents 500 µV and the horizontal scale bar represents 500 ms.*

The photopic b-wave in the *rd12* mouse is much more robust (Figure 4.14). Although, it is still significantly reduced compared to WT (Table 19). At 1.5 lg cd.s/m^2 the *rd12* amplitude is reduced by 45% (Figure 4.14). Both WT and *rd12* amplitude increases with light intensity (Table 19). Photopic b-wave implicit time is not significantly different between *rd12* and WT (Figure 4.14).

Table 19 Two-way ANOVA of rd12 photopic ERG at 3 months

Two-way ANOVA	Photopic B-wave Amplitude	Photopic B-wave Implicit Time
Rd12	F(1, 21) = 25.1, P < 0.0001	F(1, 21) = 1.8, P = 0.1976
Light Intensity	F(3, 63) = 67.9, P < 0.0001	F(3, 63) = 12.5, P < 0.0001
Interaction	F(3, 63) = 13.9, P < 0.0001	F(3, 63) = 0.9, P = 0.4605
Subjects (matching)	F(21, 63) = 2.8, P = 0.001	F(21, 63) = 1.9, P = 0.0303

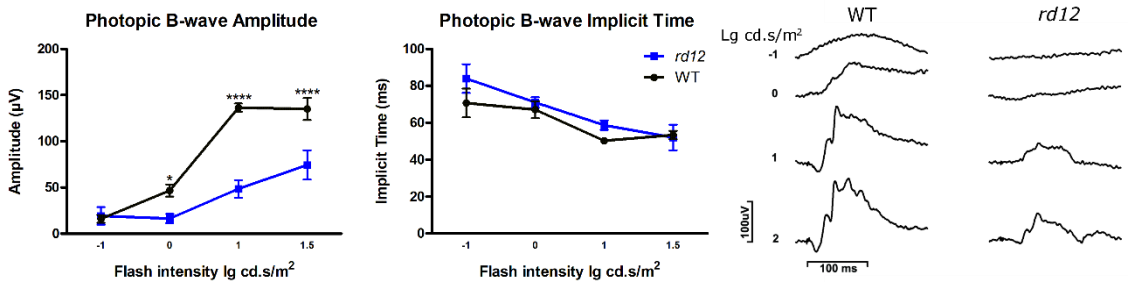

Figure 4.14 Photopic ERG in 3-month-old WT and rd12 mice.
*The photopic b-wave amplitude is significantly reduced in rd12 mice (blue, n = 10) compared to WT (black, n = 14). Photopic latency is similar between rd12 and WT. Asterisks indicate significance levels from post-hoc test: * P<0.05; **** P<0.0001. Representative traces from 3-month-old WT and rd12 mice are displayed on the right. The vertical scale bar represents 100 µV and the horizontal scale bar represents 100 ms.*

Fos induction in DA-ACs of *rd12* mice.

The retinal dopamine system provides another useful measure of photoreceptor function (Nir et al., 2000), observed by the induction of Fos activation in DA-ACs. Fos is a transcription factor, which is found in the cytosol of DA-ACs in dark-adapted retinas. After exposure to light, Fos is located in the nucleus. It is unknown if it is caused by translocation of Fos, *de novo* synthesis of Fos, or a combination of both. Following light exposure, *rd12* and WT retina were stained

for Fos and TH (DA-AC marker) and sample images from each retinal quadrant were blinded and analysed. Fos activation is also found in the GCL, and can be found in the INL in TH negative cells, and so the TH labelling allows the isolation of DA-ACs in the analysis (Hanzlicek et al., 2004). WT mice had a significantly greater increase in nuclear fos in TH^+-cells than *rd12* mice (Table 20). While adult WT mice had a 31-fold increase in nuclear Fos following 2 hours of light exposure, 3-month *rd12* mice showed no significant increase in Fos activation (Figure 4.15). Dark-adapted WT had nuclear Fos in 3 ± 2.2 % of DA-ACs, which following light exposure increased to 95.5 ± 3.5 %. *Rd12* had 4.3 ± 2.5 % TH cells with nuclear Fos after dark adaptation which increases to 8.8 ± 4.5 % following light exposure. Two-way ANOVA analysis shows that light exposure has a significant effect on nuclear fos, but this effect is significantly different between WT and *rd12* (Table 20). Post-hoc analysis revealed significantly greater fos activation in WT exposed to light compared to WT kept in the dark ($P < 0.0001$) and, also compared to *rd12* exposed to light ($P < 0.0001$). Fos activation in the different retinal regions were analysed and showed no significant regional differences (Table 20). This was similar in both animal strains. Thus, DA-ACs are activated similarly among the different retinal regions in both WT and *rd12* (Figure 4.15). Post-hoc tests showed that each region had significantly greater fos activation in WT compared to *rd12.*

Table 20 Two-way ANOVA fos expression in rd12

Two-way ANOVA	F (DFn, DFd)	P value
WT Vs *rd12*	F (1, 8) = 166.9	P < 0.0001
Light Exposure	F (1, 8) = 214.8	P < 0.0001
Light exposure*strain	F (1, 8) = 176.8	P < 0.0001
Retinal region	F (3, 12) = 2	P = 0.2
Retinal region*strain	F (3, 12) = 3	P = 0.1

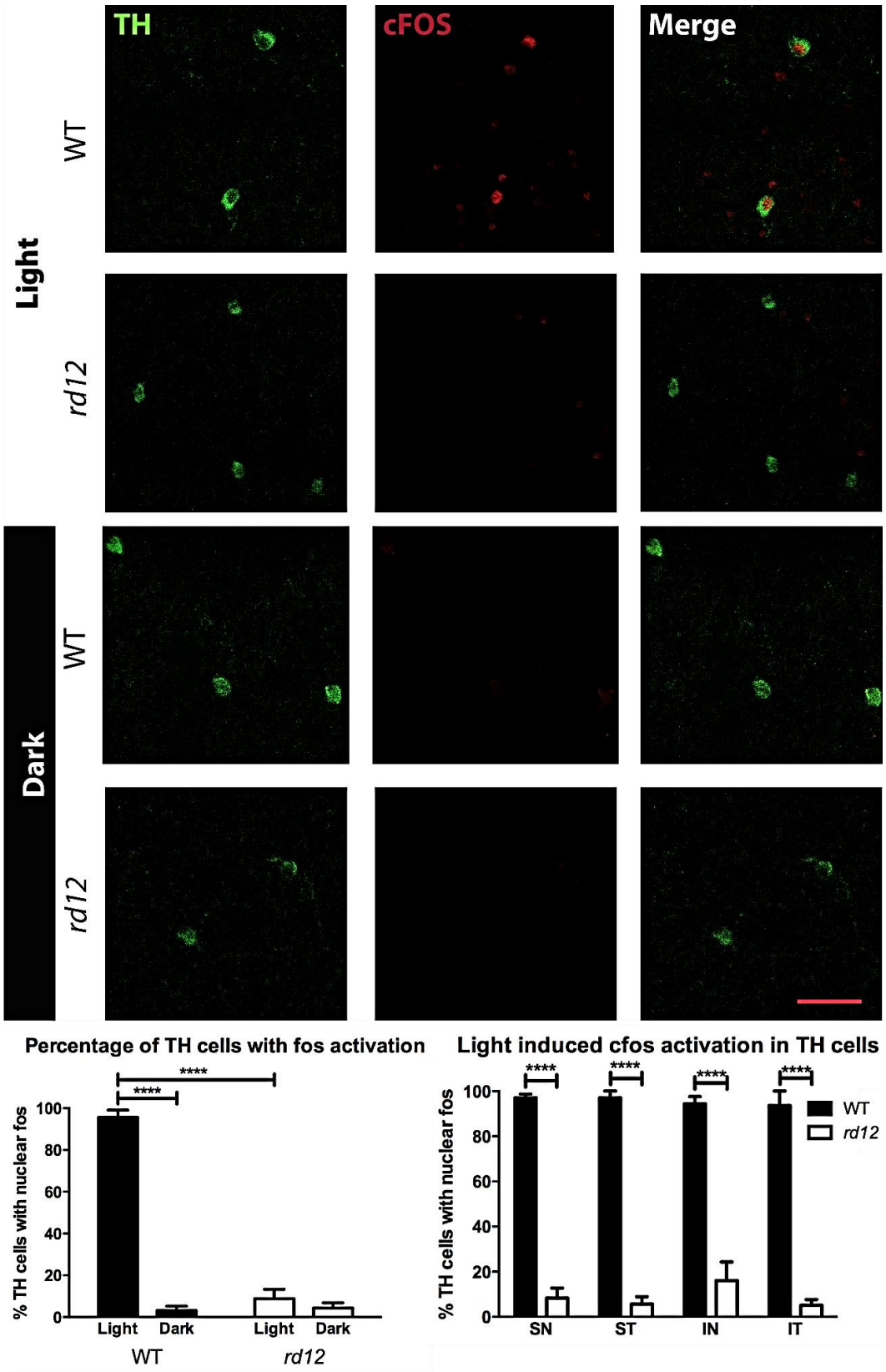

Figure 4.15 Fos activation in DA-ACs of WT and rd12 mice.
*FOS activation peaks ~2 h after light exposure. WT retinal images show fos labelling in nuclei of 95.5 ± 3.5 % TH-expressing DA-ACs. This is significantly greater than animals kept in the dark or rd12 exposed to light. No regional differences of fos activation were seen in WT or rd12. The scale bar represents 50 µm. **** indicates a significance level of P < 0.0001. N = 3 for all group.*

BLA response in *rd12* mice

WT mice have an aversion to light, and prefer to seek out an area of darkness when placed in an illuminated area (Figure 4.16). 1-month-old WT mice spend twice as much time in the dark back half of the arena when the front half is illuminated (light) than when the front half is also dark ($P < 0.05$). WT mice spent 21 ± 2 % of their time in the back half when the front half of the arena is also dark. This is increased to 42 ± 9 % when the front half is illuminated. This is not significantly different in 1-month *rd12* mice ($P = 0.7$, $F(1, 26) = 0.2$), which spend 26 ± 3 % of their time in the back half when the whole arena is in darkness and 34 ± 4 % when the front half is illuminated. Illumination of the front half of the arena has a significant effect on the amount of time spent in the dark back half ($P = 0.0022$, $F(1, 26) = 11.53$) and this effect is not significantly different between WT and *rd12* ($P = 0.2$, $F(1, 26) = 2$).

WT mice behave differently when in a completely dark arena compared to when the front half is illuminated ($P = 0.0359$, $F(1, 74) = 4.56526$). When the arena is completely dark WT mice spend significantly less and less time in the back half (Table 21). They show a preference for the dark open front half and spend significantly increasing amounts of time there. This behaviour is likely driven by neophobia and a desire to return to their cage, thus returning to the side of the arena into which the mouse was initially placed (Semo et al., 2010). This effect of light on the BLA of WT mice is only seen when examined over the 30 minutes (Table 22). During the last 5 minutes WT mice spend 3 times as much time in the dark back half when the front half is illuminated (Figure 4.16).

One-month *rd12* do not adjust their preference for the front or back half of the arena over the 30 minutes (Table 21), and continually spend more time in the

back half of the arena over the 30 minutes, when the front half is illuminated (P= 0.0111, F (1, 105) = 6.7).

Table 21 Linear Regression of time 1-month rd12 spent in back half of BLA arena

Linear Regression	Slope	r^2	Is slope significantly non-zero?
WT Dark	-0.4 ± 0.2	0.1098	F (1, 40) = 4.9, P = 0.032
WT Light	0.7 ± 0.5	0.05115	F (1, 34) = 1.8, P = 0.1847
Rd12 Dark	-0.02 ± 0.2	0.00009	F (1, 52) = 0.005, P = 0.9449
Rd12 Light	-0.4 ± 0.3	0.02881	F (1, 52) = 1.5, P = 0.2198

Table 22 Two-way ANOVA effects of light and time on the BLA in 1 month rd12

Two-way ANOVA	WT	*Rd12*
Light	F (1, 11) = 2.2, P = 0.1664	F (1, 16) = 3, P = 0.1028
Time	F (5, 55) = 1, P = 0.4286	F (5, 80) = 1.9, P = 0.107
Light effect over time	F (5, 55) = 3, P = 0.0169	F (5, 80) = 0.3, P = 0.8905
Subjects (matching)	F (11, 55) = 12.4, P < 0.0001	F (16, 80) = 2.9, P = 0.0009

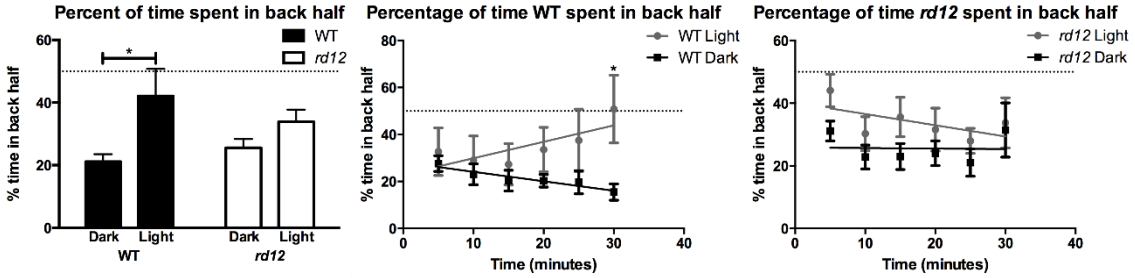

Figure 4.16 BLA in WT and rd12 mice at 1 month.
At 1 month, rd12 mice have some BLA. The total amount of time spent in the back half is not significantly different from WT, which spend significantly more time in the dark back half when the front half of the arena is illuminated compared to a completely dark arena. WT mice spend significantly less and less time in the dark back half when the front half is also dark (n = 7) compared to WT in an arena with the front half illuminated (n = 5). By the end of the 30 minutes the WT mice in an arena with the front half illuminated spend 3 times as much time in the dark back half compared to WT in a dark arena. The effect of light exposure on the BLA does not increase over time in 1-month rd12, but rd12 spend more time in the dark back half when the front half is illuminated (n = 9) compared to when the arena is fully dark (n = 9). Asterisk indicates a significance level of P < 0.05.

At 3 months, the BLA is strengthened in the WT and lost in the *rd12* mouse (Figure 4.17). There is a significant difference between WT and *rd12* in the total amount of time spent in the back half (P = 0.0295, F (1, 31) = 5.2). Both WT and *rd12* spend more time in the back half of the arena when the front half is illuminated (P = 0.0002, F (1, 31) = 17.9). Though, this effect of time is

significantly greater in WT than *rd12* (P = 0.0053, F (1, 31) = 9). 3-month-old WT spend significantly more time in the back half when the front half is illuminated compared to WT placed in a dark arena (P < 0.001) and compared to *rd12* placed in an arena with the front half illuminated (P < 0.01). WT mice will spend 26.3 ± 3.5 % of their time in the back half when the whole arena is in darkness. This doubles to 54.7 ± 5.2 % when the front half is illuminated (Figure 4.17). 3- month *rd12* spend 29.1 ± 2.8 % of their time in the back half when the whole arena is in darkness. This only increases to 33.9 ± 3.9 % when the front half is illuminated (Figure 4.17).

3-month WT spend significantly decreasing amounts of time in the dark back half when the whole arena is in darkness (Table 23), similar to what was seen at 1-month. This behaviour is significantly different to the behaviour of WT mice in an arena with the front half illuminated (P = 0.0379, F (1, 128) = 4.40231). At 3-months, significant differences in the time spent in the back half are seen earlier than they were in 1-month WT mice. While at 1-month a significant difference between light and dark was seen only in the last 5 minutes with post-hoc tests, at 3-months, significant differences are seen in the last 15 minutes (Figure 4.17). During the last 15 minutes, WT mice spend twice as much time in the back half than the front half when it is illuminated.

By 3 months *rd12* mice have greatly lost their BLA (Figure 4.17). There are no significant differences in how they behave over the 30 minutes (P = 0.8, F (1, 122) = 0.05) and no preference for the back half under illumination or total darkness (P = 0.07, F (1, 123) = 3), calculated by linear regression. 3-month *rd12* do not increase or decrease the preference for the front half in darkness or illumination (Table 23). These results are reiterated by those found by two-way ANOVA (Table 24).

Table 23 Linear Regression of time 3-month rd12 spend in BLA arena back half

Linear Regression	Slope	r^2	Is slope significantly non-zero?
WT Dark	-0.4 ± 0.2	0.1	P = 0.0374, F (1, 40) = 4.6
WT Light	0.5 ± 0.3	0.03	P = 0.0962, F (1, 88) = 2.8
Rd12 Dark	-0.1 ± 0.2	0.005	P = 0.578, F (1, 58) = 0.3
Rd12 Light	-0.05 ± 0.2	0.0006	P = 0.8409, F (1, 64) = 0.04

Table 24 Two-way ANOVA of time and light influence on the BLA in 3-month rd12

Two-way ANOVA	WT	*Rd12*
Light	P = 0.0036, F (1, 20) = 10.9	P = 0.34, F (1, 19) = 1
Time	P = 0.64, F (5, 100) = 0.7	P = 0.44, F (5, 95) = 1
Light effect over time	P = 0.098, F (5, 100) = 1.9	P = 0.997, F (5, 95) = 0.07
Subjects (matching)	P < 0.0001, F (20, 100) = 6	P < 0.0001, F (19, 95) = 6

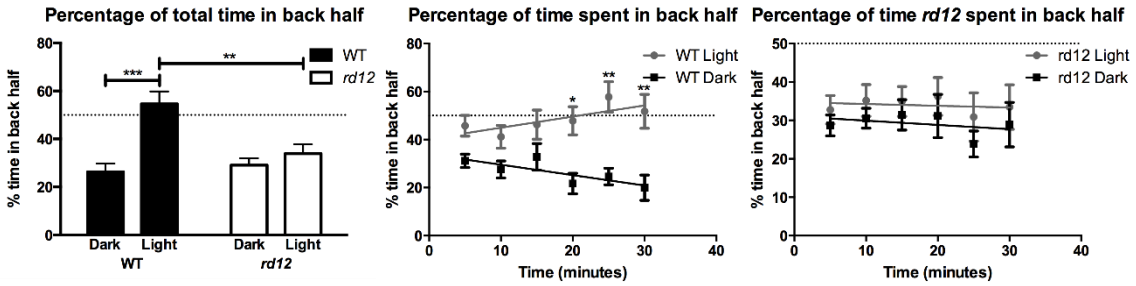

Figure 4.17 BLA in 3-month-old WT and rd12 mice.
*3-month WT mice spend twice as much time in the back-half when the front-half of the arena is illuminated (n = 16), compared to when the arena is in darkness (n = 7). No difference is seen for 3-month rd12 mice when the front half is lit (n=11) or in total darkness (n=10). The effect of arena illumination on percentage of time WT mice spend in the back-half increases with time. There are no significant changes in the amount of time rd12 spend in the back half over the 30 minutes, regardless of illumination in the arena. Asterisks indicate significant level from post-hoc tests: *P < 0.5; **P < 0.01; ***P < 0.001.*

The PLR in *rd12* mice

Both RPE65 (Fu et al., 2005, Tu et al., 2006) and melanopsin (Hattar et al., 2003, Lucas et al., 2003, Lucas et al., 2001) have been reported to affect the PLR. The PLR is reduced in *rd12* mice (Figure 4.18). Analysis at each irradiance level examined showed a reduced constriction in *rd12* mice compared to WT and *rd12*. There is no significant difference between baseline pupil area of WT and *rd12* (P = 0.18). Statistical analysis is restricted to 80 μW/cm^2/s as WT are reduced to N=1 at higher irradiances.

At 80 µW/cm^2/s there is a significant difference in the PLR between WT and *rd12* (Table 25). Time had a significant effect on the constriction and this was also significantly different between strains. At 80 µW/cm^2/s, significant differences are seen between *rd12* and WT from 1 s post-light onset until the end of the light stimulus. WT mice have a significant constriction ($P < 0.0001$), and this is significant at all time points during light stimulation. *rd12* mice do not have a significant constriction to 80 µW/cm^2/s ($P = 0.08$), and this is true at all time points during light stimulation. Peak constriction in WT reached 0.1 ± 0.008 normalized pupil area after light exposure, while *rd12* maximum pupil constriction only reached 0.89 ± 0.04.

At 800 µW/cm^2/s, both WT ($P < 0.0001$) and *rd12* ($P < 0.0001$) had a significant constriction, although, no particular timepoint is significant in the *rd12* constriction. Peak constriction reached 0.8 ± 0.07 in *rd12*, and reached 0.057 in WT. At 8000 µW/cm^2/s, both WT ($P < 0.0001$) and *rd12* ($P < 0.0001$) had a significant constriction. The *rd12* constriction is significant from 3s after light onset and significant for the remainder of the light stimulation. The *rd12* constriction reached 0.34 ± 0.07 and WT reached 0.025. Analysis of peak constriction showed a significant different in peak constriction between WT and *rd12* at 80 µW/cm^2/s ($P < 0.0001$).

Table 25 Two-way ANOVA PLR in rd12

Two-way ANOVA	WT Vs *rd12*	Time	Interaction
80 µW/cm^2/s	F (1, 416) = 196.1	F (51, 413) = 7.4	F (51, 413) = 8.2
	P < 0.0001	P < 0.0001	P < 0.0001

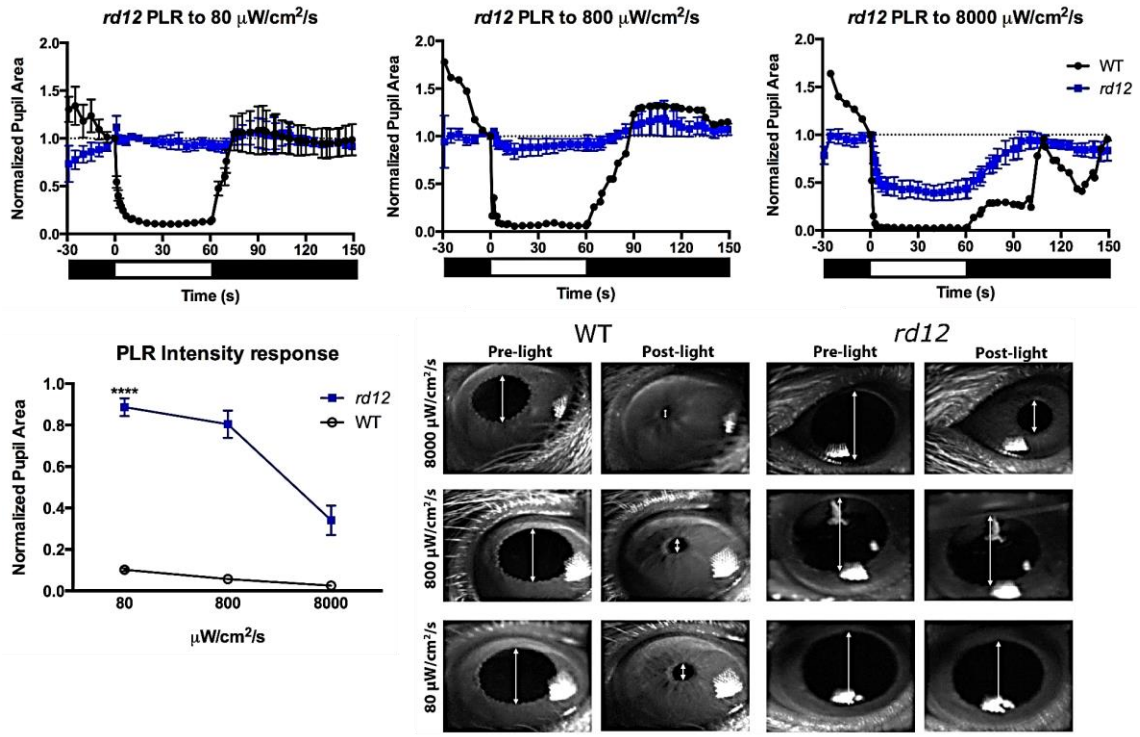

Figure 4.18 PLR in 3-month rd12 mice.
*No PLR is seen in 3-month-old rd12 mice at 80 μW/cm²/s (n = 6), while WT have a peak constriction of 0.1 ± 0.043 (n = 6). A small response is seen in rd12 at 800 μW/cm²/s (n = 8) and a 50 % constriction is seen in rd12 at 8000 μW/cm²/s (n = 8). At 800 and 8000 μW/cm²/s WT pupils are almost fully constricted, with peak constriction reaching 0.057 (n = 1) and 0.025 (n = 1), respectively. Black and white bars under constriction graphs indicate light stimulus off and light stimulus on, respectively. Asterisks indicate significance levels of post-hoc test: ***P < 0.001; ****P < 0.0001. Video stills were taken before light stimulus and around 30 s after light stimulus onset. Arrows highlight pupil diameter.*

The intrinsic Pupillary Light Reflex is deficient in *rd12* mice

While, the mechanism of the iPLR is not fully understood, constriction to light appears to involve both melanopsin signalling in the iris/ciliary body and ipRGCs in the retina (Semo et al., 2014, Vugler et al., 2015). In the *rd12* mouse there is a very small constriction, only detectable when pupil area is measured (Figure 4.19), and is significant (P < 0.001). Although, this constriction is not significant at any specific time point. WT mice also have a significant constriction (P < 0.0001), which is significant from 2s after light onset and remained significantly constricted throughout the recording. WT mice have a constriction which starts to

dilate after the end of light stimulation, while *rd12* do not re-dilate, although, their eyes are significantly less constricted. There is a significant difference between the iPLR of WT and *rd12* ($P < 0.0001$, $F(1, 712) = 807.5$). Light had a significant effect on the constriction ($P < 0.0001$, $F(50, 712) = 10.6$). Though, WT and *rd12* reacted differently over time ($P < 0.0001$, $F(50, 712) = 5.312$). Post-hoc tests show a significant difference between WT and *rd12* from 7s post light onset until the end of the recording. There is a significant difference in the maximum constriction ($P < 0.001$). WT mice have a constriction which reaches 0.43 ± 0.05 and *rd12* only reaches 0.81 ± 0.07. WT mice reach 90% constriction at 37.7 ± 6 s, and *rd12* mice reach 90% constriction at 81.3 ± 33.6 s. The *rd12* mutation did not affect baseline pupil area ($P = 0.4$).

Aged mice (12 months) were also assessed for the iPLR, as it has been shown that the iPLR can improve with age in retinal degenerate mice (Vugler et al., 2015). Interestingly, the iPLR is significantly reduced in *rd12* mice by 12 months (Figure 4.19), with maximum constriction only reaching 0.92 ± 0.04. The *rd12* mice do have a significant constriction ($P = 0.0002$) at 12 months, and similarly to the young *rd12* this is not significant at any isolate time point. Some 12-month *rd12* do not have a constriction. Comparing the iPLR at 3-months and 12-months, there is a significant difference ($P < 0.0001$, $F(1, 408) = 78.46$). Time is no-longer significant ($P = 0.1$, $F(50, 408) = 1$) and the interaction of these different ages over time is not significant ($P = 0.9999$, $F(50, 408) = 0.4$). No time points were significantly different between *rd12* at 3 months and 12 months in post-hoc tests. Latency in the 12-month *rd12* iPLR is 42 ± 22.2 s.

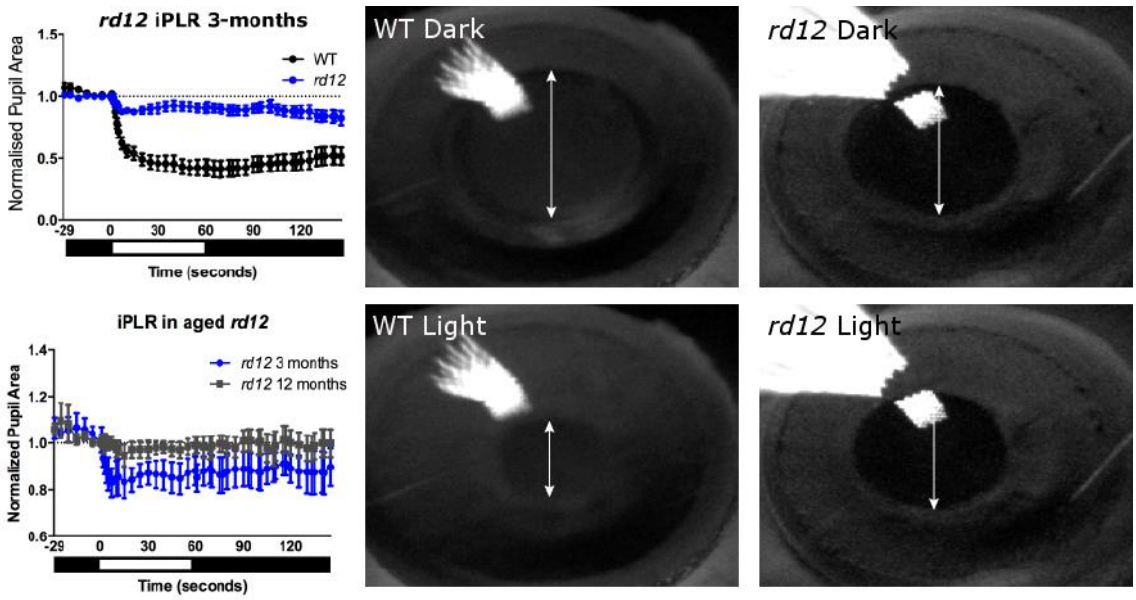

Figure 4.19 iPLR in rd12 mice.
The top graph shows 3-month rd12 (blue, n = 4) pupil constriction compared to WT (black, n = 10) in the isolated eye. Rd12 mice have a small pupil constriction which is maintained, while WT reached 50% pupil constriction. Images are representative video stills from 3-month WT and rd12 before light stimulus and around 30s after light onset. Arrows highlight the pupil diameter. The bottom graph shows that the iPLR constriction is diminished in 12-month rd12 (n = 6). Bars under graphs indicate light stimulus off (black) and on (white).

4.4.4 Discussion

Before attempting to treat with RPE cell transplantation, it is important to understand baseline retinal function in the *rd12* mouse. While the previous experiment showed that rods are largely intact at 3 months, the scotopic ERG is significantly reduced. The scotopic ERG response appears only as a small b-wave response at very high light intensities. There is no evidence of an a-wave response at any intensity. The photopic ERG is much more robust but still significantly reduced from that of WT. It has been reported that these amplitudes diminish with age (Pang et al., 2005, Pang et al., 2006). Usually, cones are responsible for the photopic response due to bleaching of rods, despite this, it is known that without RPE65, the photopic response is rod driven (Cachafeiro et al., 2010, Dai et al., 2015, Seeliger et al., 2001). Perhaps the lack of chromophore

prevents rods from bleaching and thus allows rods to respond under bright light. It has also been reported that P18 *rd12* mice have visually evoked potentials to low spatial and temporal frequencies but this response is lost at high spatial and temporal frequencies (Nusinowitz et al., 2006), suggesting rod and a lack of cone function at P18. Under scotopic conditions when high intensities are reached *rd12* mice still have a significantly reduced b-wave compared to WT mice even after saturation in WT b-wave. Under normal conditions the scotopic b-wave can reach much higher amplitudes than under photopic conditions, when cones are responsible for this response. What is interesting is that under the same flash intensities the scotopic response in the *rd12* is higher than that of the photopic, which has an additional background light, thus there may be some bleaching in the *rd12* rods or perhaps there is more chromophore available under scotopic conditions. The source of the chromophore is unknown; although, it has been shown that rods can use isorhodopsin, which contains 9-*cis* retinal as an alternative chromophore, in the absence of a functioning visual cycle. Although, the level of this is only detectable after a long period of dark-rearing (Fan et al., 2003).Interestingly, these results are similar to those seen in the $NaIO_3$-treated animals of the previous chapter, which also saw a reduced scotopic ERG with a robust photopic ERG.

FOS activation in DA-ACs is seen after exposure to two hours of light in wild-type animals. However, in the *rd12* mouse, even though there is still a small ERG response at three months, this is insufficient to drive FOS activation. Thus, it raises the question of how useful the remaining ERG response is to the *rd12* vision. Although DA-ACs and ipRGC dendrites have a close physical association (Vugler et al., 2007b) and there is evidence of melanopsin driving sustained depolarisation of DA-ACs (Zhang et al., 2012), the evidence that Fos activation

in DA-ACs can be melanopsin driven is unclear as it was shown that melanopsin was neither necessary nor sufficient to drive this photoresponse (Cameron et al., 2009), and yet, after blocking ON-bipolar cells, Fos induction was still observed (Zhang et al., 2008). However, the loss of activation of DA-ACs may have an effect on melanopsin cells. As, under normal conditions, dopamine would modulate the sensitivity of ganglion cells in response to light (Jensen and Daw, 1986), via increased dopamine release.

The *rd12* shows a behavioural light aversion at 1 month. BLA is driven by both outer-retinal photoreceptors and ipRGCs (Semo et al., 2010). However, at 3 months this behavioural light aversion is lost in the *rd12* mouse. There is an obvious preference for the front half, when the experiment is run with the arena in complete darkness. This may be due to neophobia and as the animal is placed in the open front half at the beginning on the experiment, it will return there looking for a route home.

The PLR in 3-month *rd12* is significantly reduced. A response is only seen at high light levels, where the WT have an almost total pupil constriction. It is known that *rpe65*$^{-/-}$ and *lrat*$^{-/-}$ mice have a less sensitive PLR than WT, but also have a less sensitive PLR than *rdta or rd1* mice (Tu et al., 2006). The PLR in *rd12* mice is more severely affected than that seen in $NaIO_3$-treated mice. This lower baseline observed in *rd12* mice is therefore potentially useful for assessing transplanted RPE cell function.

There is evidence to suggest that the iPLR is melanopsin driven (Xue et al., 2011) and at three months *rd12* mice only produce a small constriction, which is lost with age. This result does not necessarily mean that the melanopsin system is reliant on the chromophore produced in the RPE, as it has been shown in two papers that melanopsin function is significantly restored in mice with both outer-

retinal photoreceptor and visual cycle loss compared to loss of visual cycle alone (Doyle et al., 2006, Tu et al., 2006). In *rpe65*$^{-/-}$ and *lrat*$^{-/-}$ mice ipRGC have electrophysiological responses to light at P8, an age that precedes the onset of outer-retinal photoreceptor function (Tu et al., 2006). Another theory could be that melanopsin function is lost as the photoreceptors start to compete for chromophore.

In conclusion, at 3 months the *rd12* mouse has a residual ERG response, however, this does not translate to DA-AC activation or BLA. The PLR is significantly less sensitive and the iPLR can only produce a small response. It is clear that outer-retinal photoreceptor function and ipRGC function are both significantly reduced in the *rd12* mouse, but not absent and hopefully function can be restored by RPE cell transplantation.

4.5 Can retinal function be rescued in the *rd12* mouse?

4.5.1 Introduction

In this chapter, the retinal function in the *rd12* mouse is shown to be severely diminished, yet, retinal degeneration is slow and it is anticipated that the diminished rod and melanopsin function can be rescued. In this experiment, chromophore is administered in the form of 9-*cis* retinal, and outer-retinal photoreceptor function and ipRGC function are assessed by ERG and the iPLR, respectively. The iPLR is used to assess melanopsin function as it is solely driven by melanopsin (Semo et al., 2014, Xue et al., 2011).

9-*cis* retinal has not been previously shown to rescue the *rd12* phenotype, however, there is evidence showing phenotypic improvements in *rpe65*$^{-/-}$ mice. Oral delivery of 9-*cis* retinal has been shown to rescue ERG recordings, PLR and retinal histology in *rpe65*$^{-/-}$ mice (Maeda et al., 2009a, Van Hooser et al., 2000, Aleman et al., 2004). 9-*cis* retinal was able to fully restore ipRGC function in single cell recordings (Fu et al., 2005). It is also thought that isorhodopsin, which uses 9-*cis* retinal, rather than rhodopsin mediates the residual rod function in *rpe65*$^{-/-}$ mice (Fan et al., 2003).

This is an important experiment to determine if functional recovery can be detected in *rd12* mice treated with 9-*cis* retinal, prior to RPE cell transplantation.

4.5.2 Methods

Preparation and administration of 9-*cis* retinal

9-*cis* retinal was prepared and administered to *rd12* mice as described in paragraph 2.4.2.

Scotopic ERG

Following 9-*cis* retinal administration, 3-month animals were placed in the dark overnight and prepared for scotopic ERG as described in paragraph 2.2.1. Only the brightest scotopic intensity of 1 Lg cd.s/m^2 was used. Responses from three repeats of this flash intensity were recorded with intervals of 60 seconds. Amplitudes, latency and implicit time were analysed by one-way ANOVA and Holm-Sidaks multiple comparisons tests. Both eyes were analysed. WT: n = 6; *rd12* Saline: n = 6; *rd12* 9-*cis* retinal: n = 5.

iPLR

Following 9-*cis* retinal administration, animals were placed in the dark overnight. Animals were sacrificed and their eyes prepared and recorded as described in paragraph 2.2.4, using a white light at 8000 µW/cm^2/s. Maximum constriction in WT (n = 10) and 3-month *rd12* with either saline (n = 4) or *9-cis* retinal (n = 6) were analysed by one-way ANOVA. Aged *rd12* (12 months) maximum constriction with saline (n = 6) or 9-*cis* retinal (n = 6) treatment was compared to young *rd12* by two-way ANOVA.

Melanopsin Labelling and analysis

16 hours after 9-*cis* retinal was administrated to 3-month *rd12*, animals were sacrificed and the tissue fixed by perfusion with 4% paraformaldehyde, as described in paragraph 2.3.1. Improvements in the *rd12* iPLR with 9-*cis* retinal were seen 16 hours after administration of the chromophore. Thus, it was important to keep this incubation time constant for his experiment to determine if an increase in melanopsin was driving the improved iPLR. Retinas were removed and stained as described in paragraph 2.3.3. Retinas were labelled with primary

antibodies raised in rabbit against melanopsin (1:5000, UF006; Advanced Targeting Systems, San Diego, CA, USA) and secondary antibody used was raised in donkey against rabbit FITC-labelled (1:200, Jackson ImmunoResearch, West Grove, PA, USA). Confocal images were taken on Zeiss 700 of SN, ST, IN and IT regions of the retina and superior-nasal rim and inferior-nasal rim which covered 399.72 µm x 399.72 µm. Analysis of images is described in paragraph 2.3.4. Thresholds used for dendrite analysis were 0.1, 0.05 and 0.02. There were 6 saline-treated *rd12* retinas and 7 9-*cis* retinal-treated retinas. Results were analysed using one-tailed Mann Whitney tests.

4.5.3 Results

Rd12 Scotopic ERG responses with 9-*cis* retinal treatment

9-*cis* retinal was administered as a replacement for 11-*cis* retinal, which due to the mutation in *rpe65* is not produced in the *rd12* mouse. 9-*cis* retinal significantly improved the scotopic ERG in *rd12* mice (Figure 4.20.E). Although, comparing these improved ERG results to that of WT, this was not a full recovery.

9-*cis* retinal significantly improved both the a-wave amplitude (P = 0.0411, t-test) = 30.45) and the b-wave amplitude (P = 0.026, t-test) of *rd12* mice. This improvement in amplitude was seen with an increase in latency and implicit time, much greater than that of *rd12* or WT mice (Figure 4.20.B and D).

There are significant differences in the a-wave amplitudes of the WT, *rd12* with saline and *rd12* with 9-*cis* retinal (F (2, 14) = 30, P < 0.0001). The a-wave amplitude is reduced by 76% in *rd12*, reaching -39 ± 8 µV after exposure to 1 Lg cd.s/m^2 (Figure 4.20.A), compared to WT amplitudes of -162 ± 10 µV. 9-*cis*-retinal significantly restored scotopic a-wave amplitude in the *rd12* mouse to 49% that

of WT, reaching -80 ± 17 µV. Though, this was still significantly reduced compared to WT a-wave amplitude ($P < 0.001$).

The a-wave latency of 9-*cis* retinal-treated *rd12,* 76 ± 17 ms, is 5 times longer than that of WT mice, 14 ± 2 ms. The a-wave latency of the saline-treated *rd12* mice was not recorded due to the difficulty detecting the a-wave (Figure 4.20.E). There are also significant differences between b-wave amplitudes ($F (2, 14) = 32$, $P < 0.0001$). B-wave amplitudes are reduced in 3-month *rd12* mice (Figure 4.20.C), with peak amplitude of 97 ± 25 µV which is 22% that of WT b-wave amplitudes of 431 ± 41 µV. 9-*cis* retinal, could provide partial recovery of the b-wave to 195.5 ± 21.10 µV increasing the b-wave to 45% of WT, still significantly less than WT.

Significant differences are also seen in the b-wave implicit time ($P < 0.0001$, $F (2, 14) = 90.49$). The *rd12* b-wave implicit time of 93 ± 3 ms was not significantly different from WT implicit time, 92 ± 9 ms (Figure 4.20.D). However, the b-wave implicit time of *rd12* mice treated with 9-*cis* retinal increased to 221 ± 9 ms, which is significantly longer than both saline-treated animals and WT.

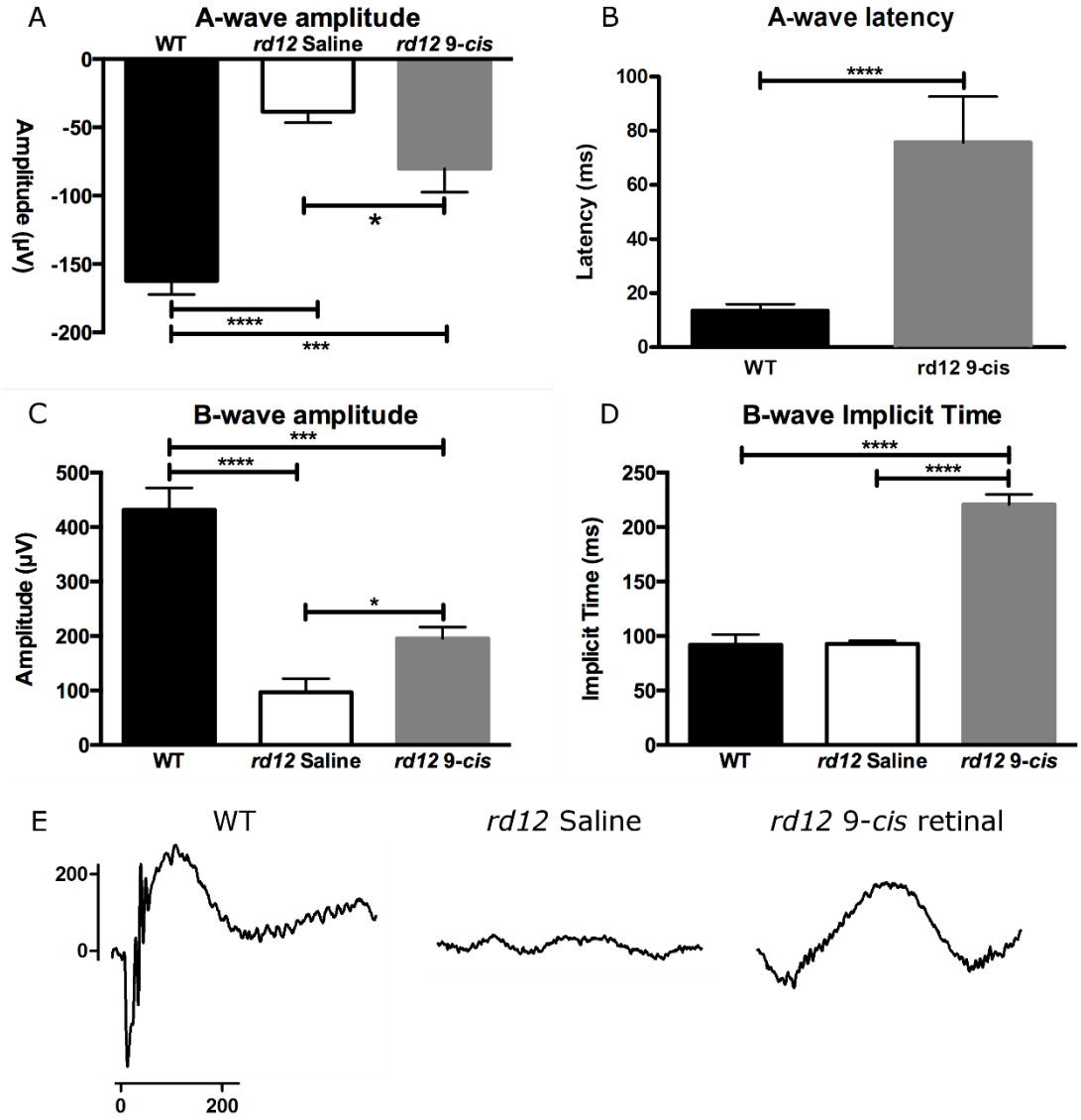

Figure 4.20 Scotopic ERG from rd12 mice treated with 9-cis retinal.
*9-cis retinal can significantly increase the a-wave by 108% (A) and the b-wave amplitude by 102% (C) in the 3-month rd12 mouse. Interestingly, the latency is increased. The a-wave latency of 9-cis retinal-treated rd12 is 5 times longer than that of WT (B) and the b-wave implicit time has increased by 138% in rd12 when treated with 9-cis retinal (D). Asterisks indicate significance level from post-hoc tests: *P< 0.05; ***P< 0.001; ****P< 0.0001. Both eyes were analysed; WT n = 6, rd12 saline n = 6 and rd12 9-cis retinal n = 5. E shows representative traces from a WT, rd12 with saline and rd12 with 9-cis retinal, respectively. Amplitude is indicated by the vertical scale bar, representing 200 µV and latency is indicated by the horizontal scale representing 200 mS.*

Improvements in the *rd12* iPLR with 9-*cis* retinal

The iPLR was examined as it is a means of isolating melanopsin function (Semo et al., 2014, Xue et al., 2011) and nothing is known about chromophore dependence in the iPLR. While 9-*cis* retinal only partially recovered the *rd12*

ERG, the synthetic chromophore produced an extra constricted iPLR (Figure 4.21). Maximum constriction was significantly different among WT, *rd12* saline and *rd12* 9-*cis* reitnal ($P < 0.0001$, $F(2, 17) = 36.57$). The *rd12* mouse has a diminished iPLR with peak constriction of 0.81 ± 0.07 normalised pupil area, and the addition of 9-*cis* retinal not only increases the iPLR maximum constriction to 0.08 ± 0.01 ($P < 0.0001$), but this even surpasses that of WT ($P < 0.001$), which have a peak constriction of 0.43 ± 0.05 (Figure 4.21.B). From 2s post-light-onset *rd12* animals treated with 9-*cis* retinal had a significantly greater constriction than both *rd12* treated with saline and WT mice, which remained significantly greater until the end of the recording.

Latency was analysed by time to 90% peak constriction and was significant between groups ($P = 0.0005$). There was a significant difference between WT and *rd12* 9-*cis* retinal ($P < 0.05$), where 90% peak constriction is reached at 37.7 ± 6 s for WT and 9.7 ± 2.1 s for *rd12* 9-*cis*. *rd12* 9-*cis* retinal also have a significantly faster constriction compared to *rd12* saline ($P < 0.001$), which reach 90% peak constriction at 81.3 ± 33.6.

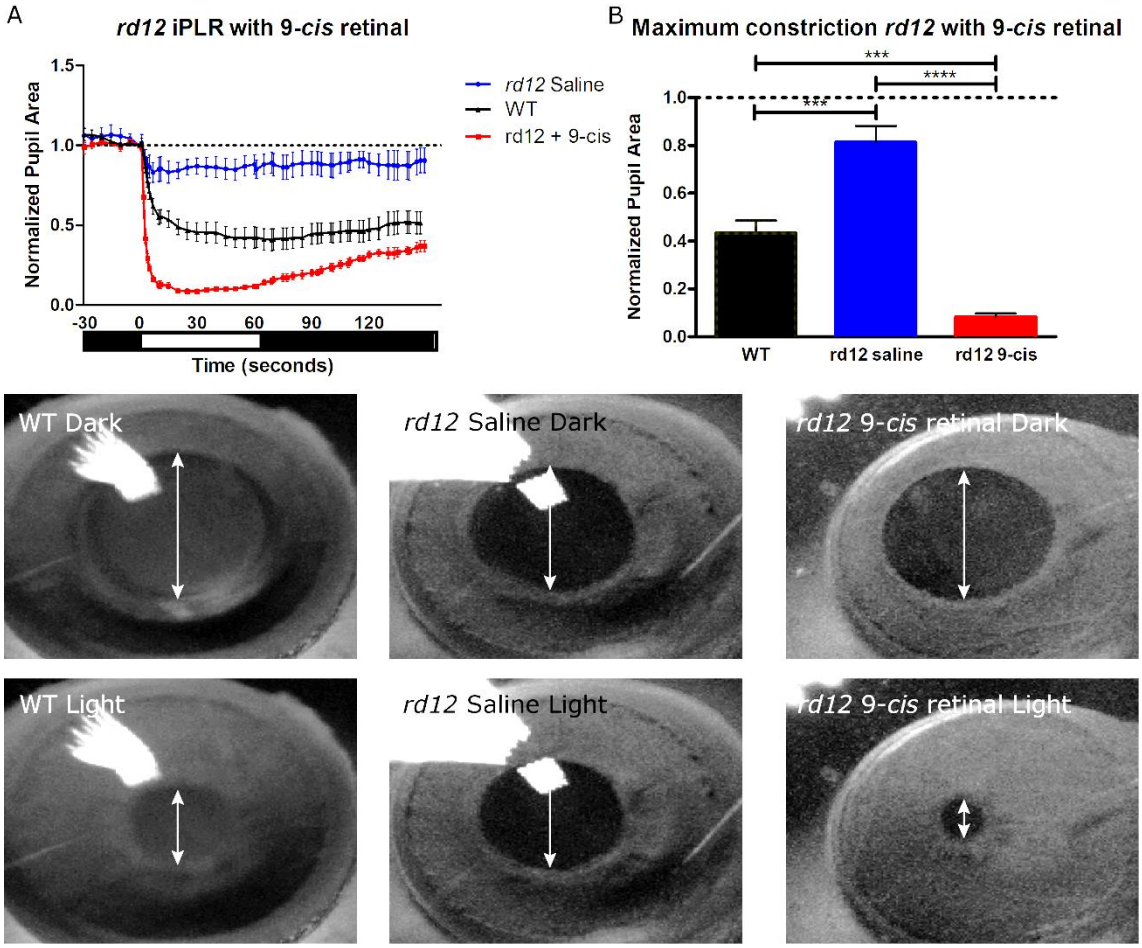

Figure 4.21 iPLR in rd12 mice with 9-cis retinal.
*A shows a graph of the average constriction ± SEM normalised to baseline pupil area in isolated eyes of 3-month rd12 mice with saline (n = 4) or 9-cis-retinal (rd12 + 9-cis, n = 6) and WT (n = 10) to 8000 µW/cm^2/s white light. B plots the maximum constriction. 9-cis retinal can not only restore the intrinsic pupil light reflex, it resulted in a constriction of 91%, which is beyond that of WT at 58% and rd12 saline at 19%. Asterisks indicate significance level from post-hoc tests: ***P < 0.001; ****P < 0.0001. Video stills underneath the graphs show a representative image of the iPLR in WT, rd12 treated with saline and rd12 treated with 9-cis retinal, prior to light exposure and after 30 seconds of light exposure. Arrows highlight pupil diameter.*

iPLR recovery in aged *rd12* mice

This significant increase in the iPLR in *rd12* with 9-*cis* retinal was still seen in 12-month old *rd12* mice (Figure 4.22.*A*). There is a significant effect of 9-*cis* retinal on the iPLR in both 3-month and 12-month *rd12* (Table 26). Maximum constriction (Figure 4.22.B) was significantly greater in animals treated with 9-*cis* retinal compared animals treated with saline ($P < 0.0001$, $F(1, 18) = 428.2$). Although,

younger animals had a greater constriction compared to the older *rd12*, whether treated with saline or 9-*cis* retinal (P = 0.0086, F (1, 18) = 8.697). 9-*cis* retinal increased the maximum constriction from 0.92 ± 0.04 to 0.19 ± 0.01 in 12-month *rd12*.

9-*cis* retinal accelerates the constriction (P = 0.00186, F (1, 17) = 6.77). Latency to 90% maximum constriction is not affected by age (P = 0.5, F (1, 17) = 0.4). 9-*cis* retinal has the same effect on both ages (P = 0.1, F (1, 17) = 3). 12-month saline-treated *rd12* took 42 ± 22.2s to reach 90% maximum constriction and 12-month *rd12* mice treated with 9-*cis* retinal took 27.5 ± 2.8s. The effect of age is also seen when comparing the point at which the iPLR from animals treated with 9-*cis* retinal become significantly more constricted than saline-treated animals. At 3-months *rd12* treated with 9-*cis* retinal have a significantly greater constriction from 2s post light onset. At 12-months, this is increased to 3s.

12-month 9-*cis* retinal-treated *rd12* continued their constriction following light off, while younger mice had greater pupil dilation when the light stimulation end. Thus, while younger mice had a constriction that surpassed the aged mice, after light stimulation, the constriction of the young mice became significantly less than that of aged mice, due to dilation. The constriction is of 3-month 9-*cis* retinal-treated *rd12* is significantly greater than 12-month 9-*cis* retinal-treated *rd12* from 2 s after light onset until 30 s, where the aged mice's constriction starts to reach maximum. Then when light stimulation ends, the young 9-*cis* retinal-treated *rd12* have pupil dilation and from 55 s after the light stimulation ended until the end of the recording the constriction of aged aged *rd12* becomes significantly greater than the young *rd12*. Age also had an effect on the baseline pupil area (P = 0.0104, F (1, 18) = 8.171), significantly increasing the baseline pupil area. 9-*cis* retinal had no effect on the baseline pupil area (P = 0.4, F (1, 18) = 0.6). 9-*cis*

retinal treated 12-month *rd12* had a significantly larger baseline pupil area compared to 9-*cis* retinal-treated 3-month *rd12* ($P < 0.05$).

Table 26 Two-way ANOVA of effects of 9-cis retinal on the rd12 iPLR

Two-way ANOVA	3 months	12 months
9-*cis* retinal	F (1, 408) = 156, P < 0.0001	F (1, 512) = 9036, P < 0.0001
Time	F (51, 408) = 86, P < 0.0001	F (51, 512) = 52, P < 0.0001
Interaction	F (51, 408) = 38, P < 0.0001	F (51, 512) = 43, P < 0.0001

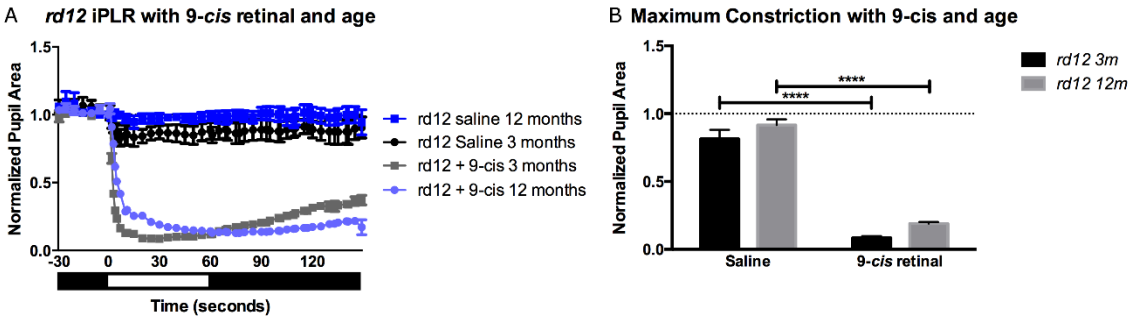

Figure 4.22 iPLR in aged rd12 with 9-cis retinal.
*12-month rd12 mice also produce a constriction which surpasses that of WT, when given 9-cis retinal, albeit less constricted than 3-month rd12 mice (A). Aged rd12 have a slower latency when treated with either saline (n = 6) or 9-cis retinal (n = 6) compared to 3-month rd12 saline (n = 4) and 9-cis retinal (n = 6). B shows the maximum constriction and asterisks indicate significance levels determined by post-hoc tests: ****P < 0.0001.*

Effects of 9-*cis* retinal on melanopsin expression

This increase in iPLR by 9-*cis* retinal is not accompanied by an increase in melanopsin labelling in the *rd12* retina, 16 hours after 9-*cis* retinal administration (Figure 4.23). Density of ipRGCs in saline-treated *rd12* is 83.5 ± 6.07 cells per mm^2 and 81.43 ± 5.2 in 9-*cis* retinal-treated *rd12* (t-test, P = 0.5). Average greylevel per soma in saline-treated rd12 is 51.95 ± 4.5 and 60.33 ± 5.5 in rd12 treated with 9-*cis* retinal (t-test, P = 0.2). Dendritic coverage is also similar in saline-treated and 9-*cis* retinal-treated *rd12* covering 0.41 ± 0.04 % and 0.49 ± 0.07 % of total area, respectively, when threshold at 0.1 (t-test, P = 0.3). Other thresholds of 0.05 (t-test, P = 0.2) and 0.02 (t-test, P = 0.2) also showed no significant differences between saline-treated and 9-*cis* retinal-treated *rd12* (data

not shown). Regional analysis also showed no significant differences between saline-treated and 9-*cis* retinal-treated *rd12* (data not shown).

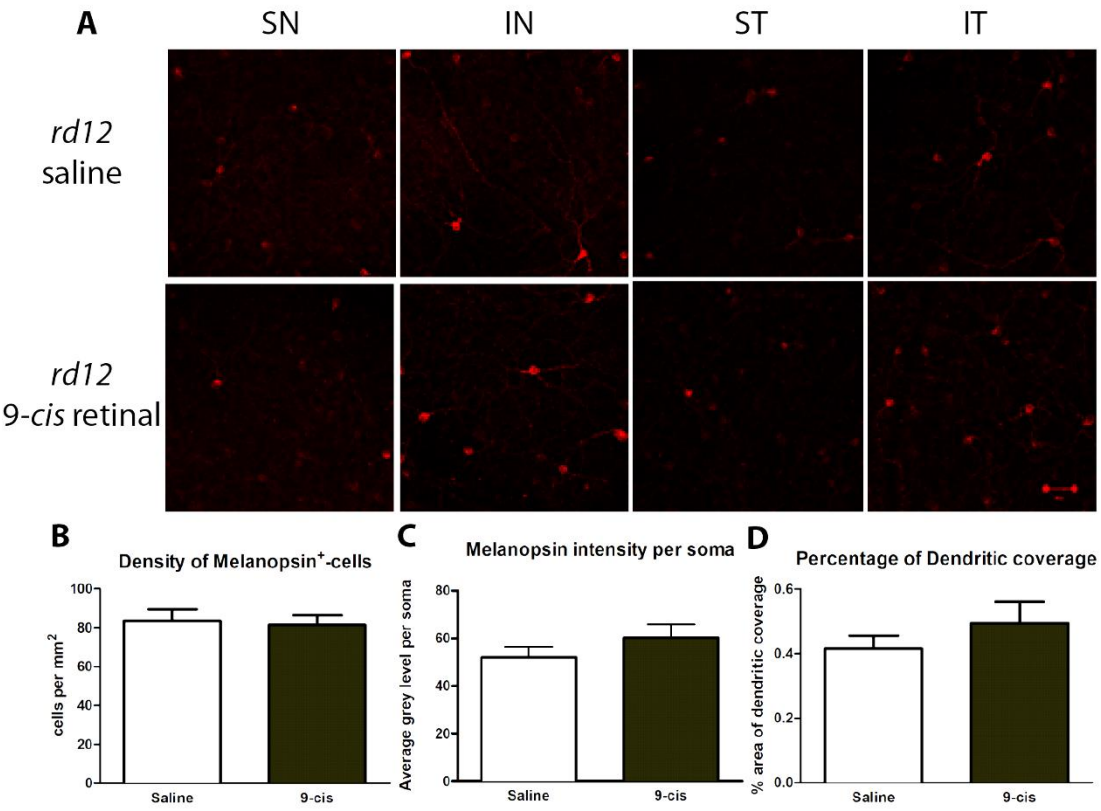

Figure 4.23 Melanopsin labelling in rd12 mice 16 hours following 9-cis retinal. A shows representative images from the different retinal quadrants from both saline-treated and 9-cis retinal-treated rd12 mice. There was no change in the number of melanopsin$^+$-cells (B), nor melanopsin-labelling in somas (C). The dendritic coverage of melanopsin cells also remained unchanged. D is the graph of dendritic coverage at threshold 0.1, showing that the percentage area covered by rd12 with 9-cis retinal (grey, n = 7) was not significantly different from rd12 with saline (white, n = 6). This graph is similar to that seen at other thresholds.

4.5.4 Discussion

This experiment is important to determine if functional recovery is possible, prior to attempting retinal rescue with RPE cell transplantation. In this experiment rod function is investigated by scotopic ERG and ipRGC function is investigated by examining the iPLR. Cone function was not investigated by ERG because a finite amount of chromophore was administered, and this may be bleached in the light-

adaption process, also, as these photoreceptors suffer the most degeneration in the *rd12* mouse, they would likely be the most difficult to recover function.

Replacing the chromophore significantly restored the amplitude of the scotopic a- and b-wave. This functional restoration was still significantly smaller than that seen in the WT retina, indicating retinal degeneration in the 3-month *rd12* retina. However, this increase in amplitude comes at a cost of increased latency and implicit time. This could indicate problems with remaining photoreceptor function and synaptic connections in the retina. These ERG results are similar to those seen in $NaIO_3$-treated mice which received 9-*cis* retinal; there is an increase in amplitude but also an increase in latency and implicit time. While 9-*cis* retinal has been used to improve the ERG of many animal with visual cycle defects, none have reported on changes to the latency (Gao et al., 2012, Maeda et al., 2006, Maeda et al., 2009b, Parker and Crouch, 2010, Parker et al., 2009, Tang et al., 2010).

While 9-*cis* retinal only partially recovered the *rd12* ERG, the synthetic chromophore produced a super constricted iPLR. Normal *rd12* mice have a significantly diminished iPLR, while, 9-*cis* retinal drives this constriction to surpass that of WT. This is unexpected as the melanopsin expression is very low in the retina and the response from the rods in the scotopic ERG was not as strong as WT. This suggests that the iPLR function is only diminished due to the lack of chromophore and an increase in chromophore results in an increased constriction. Along with significantly increased constriction, *rd12* treated with 9-*cis* retinal had a significantly shorter latency of constriction compared to WT. At 12 months, this striking increase in the iPLR is still seen. Age increased the latency in *rd12* treated with 9-*cis* retinal. Age also sustained pupil constriction following light-off in *rd12* treated with 9-*cis* retinal. This effect of age was not

reported in WT or *rd* mice (Vugler et al., 2015). This loss of re-dilation in aged *rd12* may be a loss of cholinergic transmission as the constriction pattern resembles that of WT treated with atropine (Vugler et al., 2015).

This super iPLR is surprising given the significant reduction in melanopsin labelling and loss of melanopsin^{+}-cells seen in experiment 4.3. One possible theory was that melanopsin, being similar to a rhabdomeric opsin, may need chromophore to fold properly (Ozaki et al., 1993). This hypothesis was tested by replacing the chromophore with 9-*cis* retinal supplementation. Results showed that 9-*cis* retinal had no effect on melanopsin expression levels nor on the density of melanopsin^{+}-cells. While this expression was examined only 16 hours after 9-*cis* retinal administration, this is the same time between 9-*cis* retinal administration and the increased iPLR is recorded.

Other uses of 9-*cis* retinal in the literature show that 9-*cis* retinal is able to improve both rod and cone function in *rpe65*$^{-/-}$ mice. Cone function and opsin levels were increased in *rpe65*$^{-/-}$ mice following 9-*cis* retinal administration (Tang et al., 2010, Znoiko et al., 2005). Currently, 9-cis retinyl acetate is being trialled for treatment of patients with mutation in *rpe65* or *lrat* (Koenekoop et al., 2014, Scholl et al., 2015).

This is an important experiment to determine if retinal functional in *rd12* mice can be improved with 9-*cis* retinal treatment, prior to RPE cell transplantation. From this experiment, it is determined that while the *rd12* mouse has severely diminished retinal function, it is possible to recover a significant level of retinal function by providing chromophore. In the next experiment, the possibility of achieving functional recovery by RPE cell transplantation is examined.

4.6 Can RPE transplantation improve *rd12* retinal function?

4.6.1 Introduction

Very few studies have been reported using the *rd12* mouse as a cell therapy recipient. ESC-derived neuroprogenitors were injected into the vitreous and appeared to integrate into the neural retina (Chaudhry et al., 2009).

Li et al injected 1,000 iPSC-RPE cells into 2-day old albino *rd12* mice and saw pigmented RPE cells at 5 months. They also injected 1,000 iPSC-RPE cells into P2 *rd12* crossed with *Prkdc*^{scid}/*Prkdc*^{scid} mice for a double homozygous SCID/*rpe65* mutation. While increased b-wave amplitude was seen, the a-wave was still absent (Li et al., 2012b).

Despite the small number of studies using the *rd12* mouse as cell therapy recipient, previous experiments in this chapter have shown that the *rd12* has a slow retinal degeneration and retinal function is severely reduced, both of which are ideal factors for studying the effects of RPE cell transplantation. In this experiment, hESC-derived RPE cells were transplanted subretinally into *rd12* mice to determine the utility of this model for studying RPE cell transplantation. This is determined by the ability of RPE cell transplantation to improve retinal function and the survival of the graft in the subretinal space in the *rd12* mouse.

4.6.2 Methods

hESC-RPE cell preparation and injection

Cells were prepared and injected subretinally into both eyes as described in paragraph 2.4.3. 8 *rd12* animals received 75,000 hESC-derived RPE cells in 1.5 µL DRS suspension and 5 *rd12* mice received 1.5 µL DRS only. A range of ages

were treated from 1.5 months – 11 months balanced by age and sex between groups.

ERG

Scotopic and photopic ERG recordings were carried out on both eyes as previously described in paragraph 2.2.1.

PLR

PLR was recorded in left eyes as described in paragraph 2.2.3. The light powers examined were 80, 800 and 8000 µW/cm^2/s. The number of animals tested at each light power is displayed in Table 27.

Table 27 Number of rd12 which received hESC-RPE assessed by PLR

Light Power	8000 µW/cm^2/s	800 µW/cm^2/s	80 µW/cm^2/s
hESC-RPE	6	6	8
Control	4	3	3

Immunohistochemistry

Animals were perfused with 4% PFA as described in paragraph 2.3.1 and immunohistochemically stained as described in paragraph 2.3.2. Eyes were labelled with anti-human mitochondria (1:500, MAB1273, Millipore) and secondary anti-mouse raised in donkey tagged with FITC (1:200, Jackson ImmunoResearch, West Grove, PA, USA).

4.6.3 Results

Changes in the scotopic and photopic ERG in eyes with hESC-RPE cell grafts.

Differences in the scotopic and photopic ERG are seen between eyes which received cells and eyes which received the vehicle only (Figure 4.24). There are

small increases in the scotopic a-wave and b-wave amplitude and a significant decrease in the photopic b-wave amplitude in eyes which received the cell graft. Scotopic a-wave analysis does not show a significant difference between animals which received cells and animals which received vehicle (Table 28), albeit at -2 Lg cd.s/m^2, where post-hoc tests show that animals which received cells have a significantly greater a-wave compared to vehicle ($P < 0.01$) (Figure 4.24.A). Traces, at -2 Lg cd.s/m^2, have a distinguishable a-wave in eyes which received hESC-RPE cells (Figure 4.24.E), which is lost at higher light intensities.

Analysis of the scotopic b-wave amplitude reveals that there is not a significant difference between eyes which received hESC-RPE cells and those which received vehicle (Table 28), although, post-hoc tests show a significant difference between these eyes at Lg 0 cd.s/m^2 ($P < 0.01$) (Figure 4.24.B).

The Photopic b-wave amplitude is significantly higher in vehicle-treated eyes compared to eyes which received hESC-RPE (Table 28). Post-hoc tests revel that amplitude at the highest light intensity is significantly greater in eyes treated with vehicle ($P < 0.001$), reaching 75 ± 8 µV, compared to eyes treated with hESC-RPE cells which reached 37 ± 8 µV (Figure 4.24.C).

Table 28 Two-way ANOVA of ERG in rd12 following hESC-RPE graft

Two-way ANOVA	Scotopic A-wave	Scotopic B-wave	Photopic B-wave
hESC-RPE	F (1, 144) = 3.84, P = 0.0617	F (1, 144) = 1.35, P = 0.2563	F (1, 95) = 10.66, P = 0.0015
Light Intensity	F (6, 144) = 8.08, P < 0.001	F (6, 144) = 14.2, P < 0.0001	F (3, 95) = 18.79, P < 0.0001
Interaction	F (6, 144) = 1.71, P = 0.1221	F (6, 144) = 2.15, P = 0.0516	F (3, 95) = 5.04, P = 0.0028

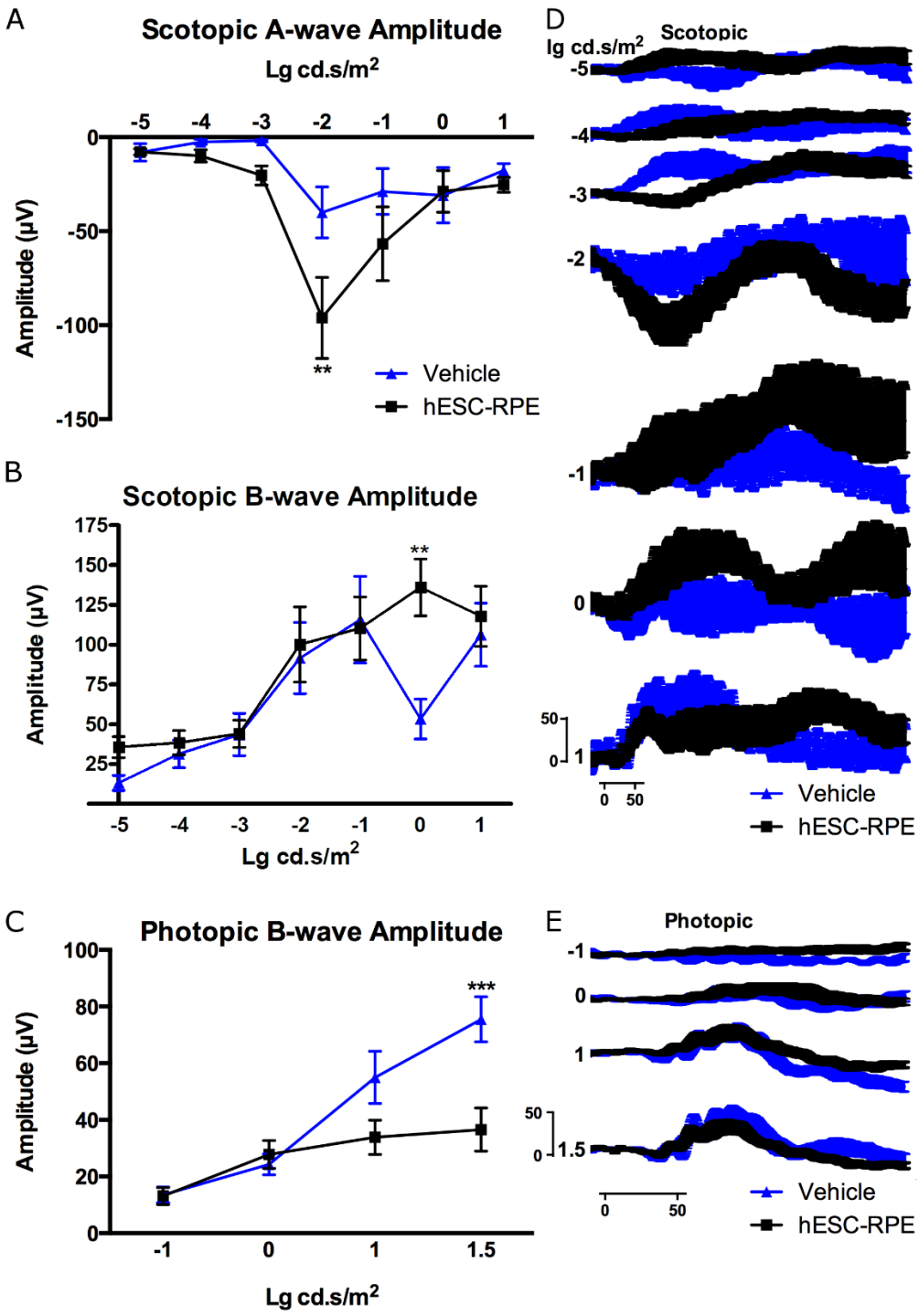

Figure 4.24 Scotopic and photopic ERG recordings following hESC-RPE cell grafting into rd12 mice.
*Eyes which received hESC-RPE cell grafts have a scotopic wave that changes with inceasing light intensities. Eyes which received hESC-RPE cell grafts had a significantly greater a-wave amplitude at -2 Lg cd.s/m^2 only (A). Scotopic b-wave amplitude is significantly greater in eyes which received hESC-RPE cells at 0 Lg cd.s/m^2 only (B). Photopic b-wave amplitude is reduced in hESC-RPE-treated eyes (C). Asterisks indicate post-hoc significant differences between hESC-RPE-treated eyes (n = 16) and vehicle treated eyes (n = 10): **P < 0.01, ***P < 0.001. Traces show the average scotopic (D) and photopic (E) trace ± SEM of eyes treated with hESC-RPE cells (black) and vehicle (blue). The vertical scale bar in D and E represent 50 µm and the horizontal scale bars indicate 50 ms.*

PLR recordings in *rd12* mice following hESC-RPE cell grafting

The PLR has significantly greater constriction in eyes treated with hESC-RPE cells at 80 µW/s/cm^2 (Figure 4.25.A), but not at the higher light intensities (Table 29). The presence of a significant constriction is determined by the average normalised pupil area during light stimulation (0-60s), being significantly lower than 1 (baseline area). At 80 µW/s/cm^2 eyes treated with vehicle do not have a significant constriction (P = 0.6). The maximum constriction reached was 0.92 ± 0.05. The Average pupil area is significantly less than 1 in eyes treated with hESC-RPE at 80 µW/s/cm^2 (P = 0.0071). These pupils reached a peak constriction of 0.81 ± 0.04. This is greater than untreated *rd12*, which had a peak constriction of 0.89 ± 0.04. The normalised pupil area between 0-60s in significantly lower than 1 in both animals treated with hESC-RPE cells and vehicle at both 800 and 8000 µW/s/cm^2 (Figure 4.25.B and C). Peak constrictions reached 0.66 ± 0.14 in eyes that received vehicle at 800 µW/s/cm^2 and 0.24 ± 0.03 at 8000 µW/s/cm^2. Eyes that received hESC-RPE had a peak constriction of 0.67 ± 0.1 at 800 µW/s/cm^2 and 0.22 ± 0.04 at 8000 µW/s/cm^2. Untreated *rd12* had a peak constriction of 0.34 ± 0.07 at 800 µW/s/cm^2, which is greater than both treatment groups. This is possibly due to the average age increase of around 1.5 months of these *rd12* and the untreated *rd12* assessed in 4.4.3. No significant differences were found between hESC-RPE- and vehicle-treated eyes at these light powers. Maximum pupil constriction within the first 30s after light onset was not significantly different between animals treated with hESC-RPE cells and animals treated with vehicle (P = 0.5, F (1, 24) = 0.4) (Figure 4.25.D). Constrictions became greater with increased light power (P < 0.001, F (2, 24) = 40.4). This increased constriction with increased light power was not different between eyes treated with hESC-RPE and vehicle (P = 0.7, F (2, 24) = 0.3).

Table 29 Statistics from PLR of rd12 treated with hESC-RPE

Two-way ANOVA	8000 µW/s/cm^2	800 µW/s/cm^2	80 µW/s/cm^2
Interaction	P = 0.9993 F (12, 92) = 0.17	P = 0.9758 F (13, 76) = 0.37	P = 0.0506 F (13, 109) = 1.81
Time	P < 0.0001 F (12, 92) = 30.24	P = 0.0746 F (13, 76) = 1.99	P = 0.0085 F (13, 109) = 2.34
Group	P = 0.7671 F (1, 92) = 0.09	P = 0.0746 F (1, 76) = 3.27	P = 0.0015 F (1, 109) = 10.59

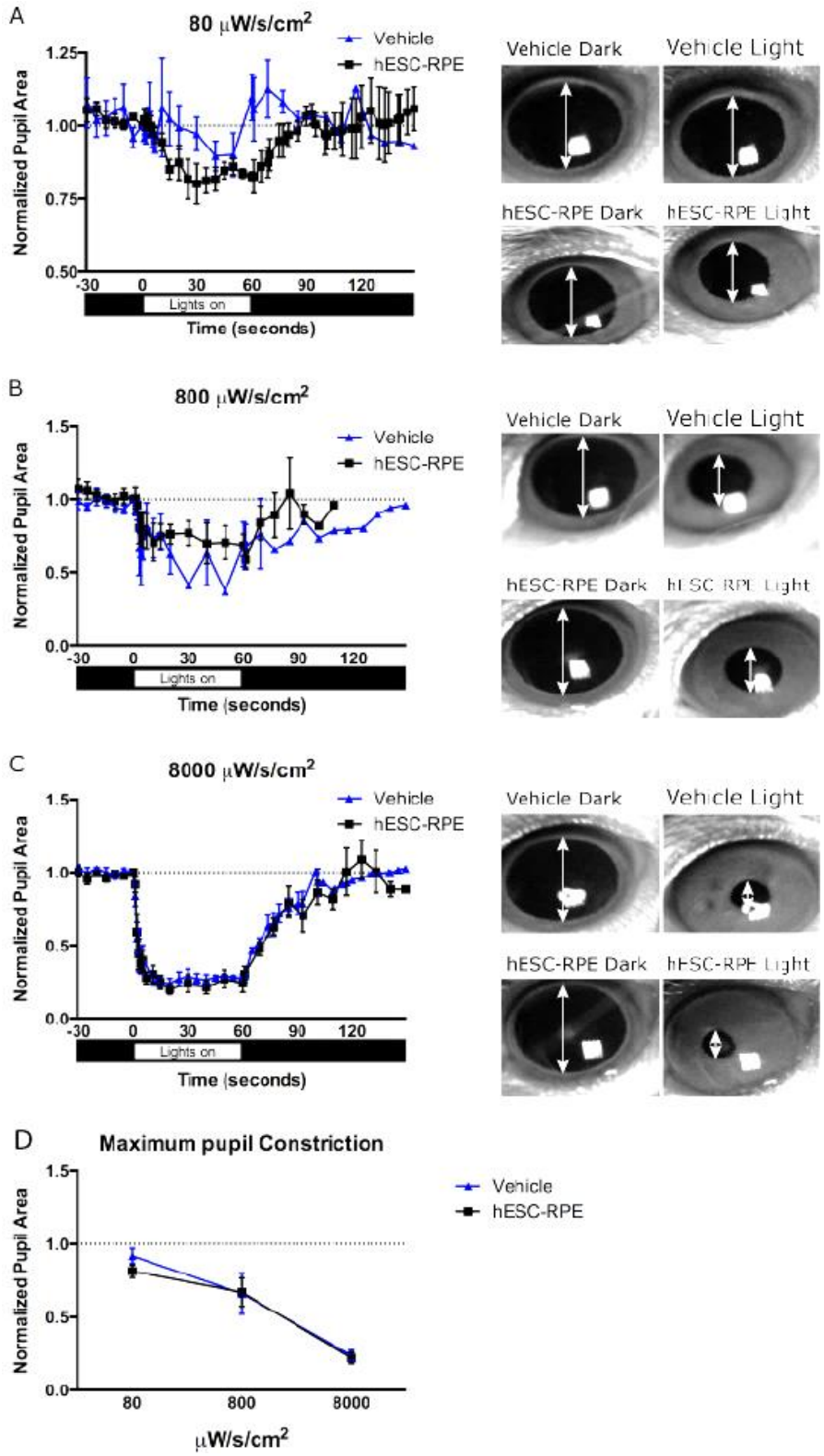

Figure 4.25 PLR in rd12 treated with hESC-RPE cells.
At 80 μW/s/cm² (A), hESC-RPE-treated eyes (n = 8) have a significantly greater constriction than vehicle-treated eyes (n = 3), which did not have a significant constriction. At 800 μW/s/cm² (B), there is no significant different between hESC-RPE- (n = 6) and vehicle-treated (n = 3) animals. At 8000 μW/s/cm² (C), there is no significant difference between hESC-RPE- (n = 6) and vehicle-treated (n = 4) animals. Representative images before (dark) and around 30s after (light) light onset are seen to the right of each graph of corresponding light powers.

Cell transplant histology

No viable hESC-RPE cells were found in the subretinal space of transplanted eyes. Eyes were labelled for anti-human mitochondria, which was raised in mouse and thus, created a large background stain with the anti-mouse secondary antibody, as can be seen in Figure 4.26.C. While using an antibody raised in mouse to stain mouse tissue is not ideal, this anti-body was helpful in screening for cells. hESC-RPE cells were also labelled as a positive control. The site of injection was located by a mass of pigmented cells in the subretinal space. However, these cells did not show stain positive for human mitochondria (Figure 4.26)

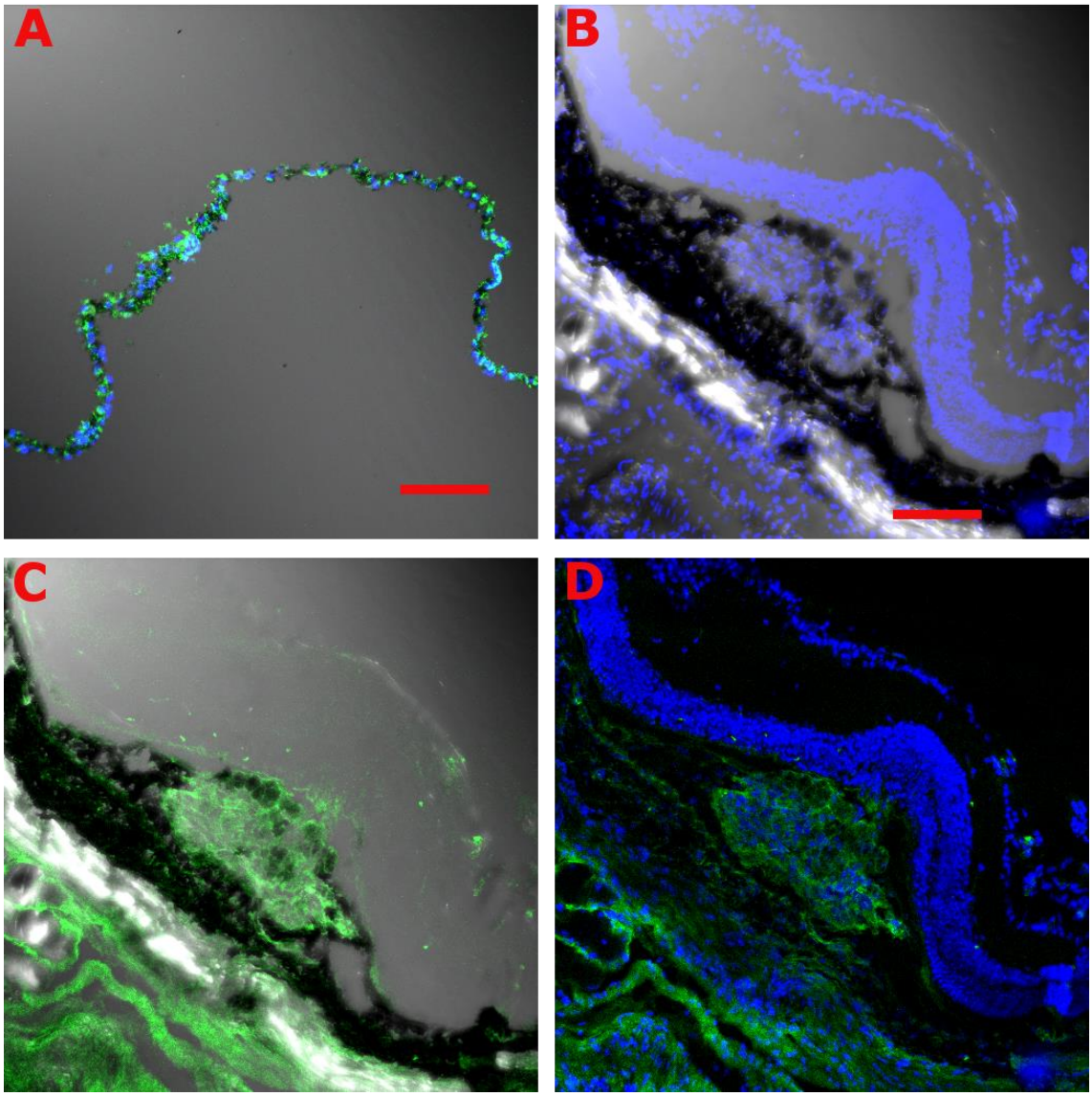

Figure 4.26 Absence of labelling of human mitochondria in injection site in rd12 *mice.*
The image A shows nuclei staining (blue), human mitochondria (green) and transmitted light in hESC-RPE cells. The image B shows a cluster of cells in the subretinal space with pigmented cells and nuclei. C shows the same image with transmitted light and human mitochondria labelled. D show the image with nuclei staining and human mitochondria. The cells do not label positive for human mitochondria as the green fluorescence is seen outside the cell bodies. Scale bars indicates 50 µm.

4.6.4 Discussion

This was an important experiment to determine if the *rd12* is a useful model for studying RPE transplantation, i.e. can retinal function be rescued with hESC-RPE cells and can hESC-RPE cells survive in the *rd12* retina? In this experiment, it was found that eyes which received hESC-RPE cells had some improvements on the scotopic a- and b-wave amplitude but reductions in the photopic b-wave amplitude. While under normal conditions a reduction in photopic b-wave amplitude would be an obvious loss of function, in the *rd12* mouse it is known that this photopic ERG response is rod driven (Dai et al., 2015), thus, a loss of photopic function could mean a loss of rods or could indicate an increase in chromophore preventing rods from functioning under photopic conditions. When also considering the scotopic amplitudes in the hESC-RPE-treated eyes, the former theory is less likely.

The PLR had a small improvement at 80 µW/s/cm^2, but not at higher irradiances. It is unknown if this improvement is from outer-retinal photoreceptors or ipRGCs or both. Unfortunately, the iPLR which can isolate melanopsin function was not examined as animals were perfused to preserve retinal histology.

While the site of injection was hound in *rd12* eyes, cells did not stain positive for human mitochondria, suggesting that the cells were no-longer viable. Studies reporting similar results have previously been reported in eyes where no viable cell grafts were found. Improvements in head tracking and fos activation, along with preservation of photoreceptors, were recorded in RCS rats 13 weeks after receiving iPS-RPE cells, while no viable cell grafts were found (Carr et al., 2009). These animals received oral cyclosporin immunosuppressant, although, xenografts can be compromised even after triple immunosuppression (Del Priore et al., 2003). It is possible that macrophage/microglia infiltration and activation

play a role in the improvement of retinal histology and function. Improvements have been reported where grafted cells are no longer viable but many large pigmented cells positive for macrophage markers are found near the graft site (Carr et al., 2009, Del Priore et al., 2003).

4.7 General Conclusions

The mutation in *rpe65* in the *rd12* mouse results in the absence of RPE65 protein formation, which was validated here by immunohistochemistry. RPE65 is necessary for the recycling of chromophore. This loss of chromophore leads to retinal degeneration. At 3 months, no M/L-opsin was detected and S-opsin is mislocated to PIS, ONL and IPL. This mislocation of cone opsin and cone loss may be due to the requirement of chromophore for correct opsin folding and trafficking (Bandyopadhyay et al., 2013) and timeline of cone loss observed in the literature (Li et al., 2011, Pang et al., 2010) coincides with WT development of peak expression of RPE65 (Bowes et al., 1988, Manes et al., 1998, Hamel et al., 1993). Rods have a slower rate of degeneration, and rhodopsin is found located in the POS in *rd12* at 3 months. It has been published that rhodopsin spectral absorbance is not detected in the *rd12* mouse (Pang et al., 2005), however, rhodopsin protein presence and location have not been previously reported in *rd12* by immunohistochemistry. ERG recordings under scotopic conditions have a small b-wave response only at high light intensities in 3-month *rd12.* There is a more robust photopic b-wave, however, it is known that this is rod driven (Dai et al., 2015). Thus, rods in the *rd12* mouse can function albeit at much lower sensitivity. Patients with mutations in *rpe65* have similar ERG patterns (Lorenz et al., 2000). This rod response is insufficient to activate Fos in DA-ACs.

IpRGCs make up a third type of photoreceptor. Often these photoreceptors are overlooked because they do not play a strong role in image forming vision. It is unknown to what extent these cells require the RPE for normal function, however, it is clear in the *rd12* mouse that the mutation in *rpe65* has resulted in loss of these cells and reduction in melanopsin from 1 month. This loss of melanopsin and loss of ipRGC did not significantly reduce further up to 8 months. This reduction may be developmental. This loss of ipRGCs is also specific to this subtype of RGC as no significant reduction is seen in the RGC population in *rd12* mice. Melanopsin expression has been shown to be affected by other RPE mutations, such as mutation in *mertk* (Li et al., 2012a, Sakamoto et al., 2004, Vugler et al., 2007b, Vugler et al., 2008b).

The deficit in melanopsin function is evident in the *rd12* mouse. The BLA which is driven by both outer-retinal photoreceptors and ipRGCs is present at 1 month, but is lost by 3 months. This behaviour is seen in mice without rods or cones and so melanopsin alone can drive the response (Semo et al., 2010), despite this, melanopsin is not able to drive this behaviour in 3-month *rd12* mice. The PLR is also driven by outer-retinal photoreceptors and melanopsin (Lucas et al., 2003) and is significantly reduced in the *rd12* mouse. A response is only seen at high light levels, where the WT have an almost total pupil constriction. Comparing these results to those published by Lucas et al, it suggests that both outer-retinal photoreceptors and ipRGC have reduced function in the *rd12*. The iPLR is a functional readout selective for melanopsin function (Semo et al., 2014, Xue et al., 2011). At three months *rd12* mice only produce a small constriction, which is lost with age.

The *rd12* mouse was chosen to be studied because it appears to be an ideal model for investigating RPE therapies. Cone, rod and ipRGC function is

significantly reduced in the *rd12* mouse, even though, the retinal degeneration is slow for rods and ipRGCs. Functional recovery was tested, prior to RPE cell transplantation, by providing chromophore in the form of 9-*cis* retinal, to determine if the remaining photoreceptors were functional. Rod function was examined by scotopic ERG and ipRGC function was assessed by analysing the iPLR, this allowed separation from cone function, which is likely to be the most difficult function to restore, as they undergo a faster degeneration. 9-*cis* retinal provided a significant increase in both scotopic a- and b-wave amplitudes, although this was at the cost of longer latency and implicit time. The amplitudes were significantly lower than WT. The loss of a-wave amplitude signifies the level of rod degeneration at 3 months in the *rd12* retina. The longer latencies could indicate problems with remaining photoreceptor function and synaptic connections in the retina.

While 9-*cis* retinal only partially recovered the *rd12* scotopic ERG, the synthetic chromophore produced a super constricted iPLR. Normal *rd12* mice have a significantly diminished iPLR, still, 9-*cis* retinal drives this constriction to surpass that of WT and at a significantly faster latency. This is unexpected as the melanopsin expression is significantly lower in the *rd12* retina and the response from the rods in the scotopic ERG was not as strong as WT. This suggests that the iPLR function is only diminished due to the lack of chromophore and an increase in chromophore results in an increased constriction. This ability of 9-*cis* retinal to recover the iPLR was still seen at 12 months, suggesting a strong preservation of this functional pathway. Latency is lost in the *rd12* mouse with age and pupil re-dilation was lost in aged mice, as the mechanism of the iPLR is largely unknown. It is difficult to speculate why this effect of age is seen, especially when this was not reported in aged WT or *rd* mice (Vugler et al., 2015).

Though, these mice were only 9-months and this may account for a difference, when comparing them to mice used in this study, which were 12 months.

The super iPLR, created by 9-*cis* retinal is surprising given the significant reduction in melanopsin labelling and loss of melanopsin^{+}-cells in the *rd12* mouse. One possible theory was that melanopsin, may require chromophore to fold properly, similar to cone photoreceptors. Contrasting this, no significant changes to melanopsin expression levels nor on the density of melanopsin^{+}-cells were seen in *rd12* mice treated with 9-*cis* retinal. This demonstrates that the enhanced iPLR seen in *rd12* mice treated with 9-*cis* retinal was achieved with significantly lower melanopsin expression and melanopsin^{+}-cell density.

The *rd12* mouse was chosen to be studied because it appears to be an ideal model for investigating RPE therapies. Cone, rod and ipRGC function is significantly reduced, even though, the retinal degeneration is slow. It is also shown that retinal function can be significantly improved by supplementing chromophore. It was then determined if hESC-RPE cell grafting could improve retinal function and following the grafting of hESC-RPE cells into the subretinal space some functional improvements were seen in the scotopic ERG and the PLR. It is difficult to determine if the PLR improvements seen were from outer-retinal photoreceptors or ipRGCs. Unfortunately, no viable hESC-RPE cells were found in the *rd12* retina. Cells were discovered at the site of injection and did not integrate into the *rd12* retina. It is difficult to attribute the visual function improvements to the hESC-RPE cells grafted, perhaps they released trophic factors, or if the improvements should be attributed to an increased immune response, which has been reported in many studies (Lawrence et al., 2000, Carr et al., 2009, Del Priore, 2005).

Chapter 5 Investigating if the RPE supplies chromophore for ipRGC function and the iPLR.

5.1 Introduction

It is not known if ipRGCs require the RPE for chromophore production. Rods and cones have many physical connections with the RPE aiding chromophore transportation, however, ipRGCs are situated in the inner retina and separated from the RPE by many layers of cells. While melanopsin has been reported to work as a bi-stable pigment (Melyan et al., 2005, Fu et al., 2005), my experiment in chapter 4 suggest that this bistability is insufficient to drive a normal iPLR in the *rd12* mouse. However, it was shown in experiment 4.5 that supplementing the *rd12* mouse with systemically administered 9-*cis* retinal not only restores the iPLR but actually causes a super iPLR constriction which significantly exceeds that seen in the WT mice. This phenomenon occurred without an increase in melanopsin^{+}-cells or an increase in melanopsin expression, a finding which raises the question of whether this supplementary chromophore was acting on ipRGCs in the retina or was it driving the function of an opsin in the iris/ciliary body?

As such, leading on from these interesting observations in this last experimental chapter, the important question of whether the RPE supplies chromophore for ipRGCs and if these retinal cells drive the iPLR is addressed.

5.2 Is the iPLR driven by chromophore acting in the retina?

5.2.1 Introduction

The super iPLR, created by 9-*cis* retinal in *rd12* mice, seen in experiment 4.5 is surprising given the significant reduction in melanopsin labelling and loss of melanopsin^{+}-cells in the *rd12* mouse, which was not enhanced by 9-*cis* retinal. One possible explanation is that the supplemental chromophore was acting directly on the iris/ciliary body. It is unknown if the iPLR is initiated in the retina or is solely a result of light acting directly on the iris (Semo et al., 2014, Wang et al., 2017, Xue et al., 2011). As such, in this experiment, it is determined if the 9-*cis* retinal driving the iPLR in *rd12* mice is acting on the retina or on the iris/ciliary body directly. This is done using intrinsic pupillometry on isolated anterior chambers together with immunohistochemical staining for RPE65, to confirm the presence or absence of this key enzyme in WT mouse iris.

5.2.2 Methods

Histology

To determine where RPE65 is expressed in the iris, WT (n = 1) retina and iris was labelled for RPE65. The animal was perfused as described in paragraph 2.3.1. The eyes were fixed overnight in 4% PFA, embedded, sectioned and stained as described in paragraph 2.3.2. The antibodies used were: anti-RPE65 raised in rabbit (1:500, ab173596; Abcam) with the secondary antibody raised in donkey against rabbit tagged with FITC (1:200, Jackson ImmunoResearch, West Grove, PA, USA). Images were taken on a Zeiss 700 microscope.

9-*cis* retinal preparation and administration

9-*cis* retinal was prepared and administered to 16 *rd12* mice as described in paragraph 2.4.2, with 6 additional *rd12* mice receiving a control injection. Animals were kept in darkness overnight 16 – 18 hours prior to recording iPLR function.

iPLR

Following 9-*cis* retinal administration and dark-adaptation, animals were culled by cervical dislocation under dim red light. Each animal had one eye cut along the CMZ to remove the retina (- retina) and isolate the anterior chamber and ciliary body. The other eye was cut 1mm below the CMZ in order to retain a ring of retina attached to the anterior chamber (+ retina). This technique was previously published and described by this lab (Semo et al., 2014). Anterior chambers +/- retinas were then examined for an iPLR using methods described in paragraph 2.2.4. Animals treated with 9-*cis* retinal and animals treated with saline were alternated for iPLR recordings. The first and second eye were also counterbalanced between receiving a + or – retina cut.

5.2.3 Results

RPE65 labelling in the WT retina

RPE65 labelling is only seen in the RPE of the WT mouse (Figure 5.1). No RPE65 labelling was seen in the iris of this animal.

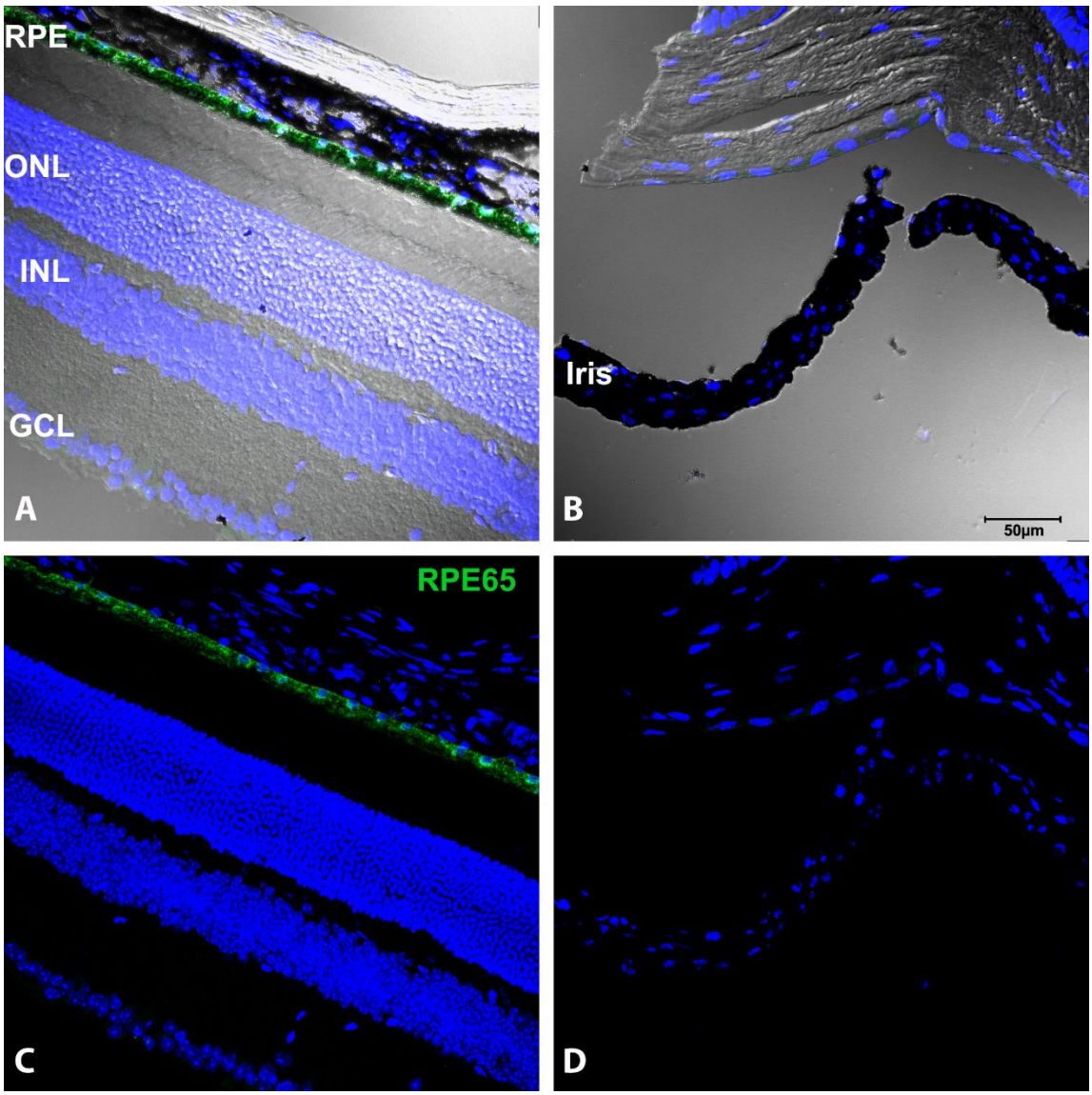

Figure 5.1 RPE65 labelling in WT retina and iris.
RPE65 (green) is seen in the RPE in the wild-type retina (A and C), however, there is no evidence of RPE65 in the iris (B and D). Images B and D display pigmented iris and clear cornea. Images A and B were taken with transmitted light to identify the pigmented tissue in the RPE and iris. Scale bar represents 50 µm.

Chromophore acting in the retina drives the iPLR

To determine if 9-*cis* retinal is acting on the retina or ciliary body/iris to produce the iPLR in *rd12* mice, the iPLR was examined in *rd12* treated with 9-*cis* retinal when the retina was removed. To do this, eyes were prepared by either cutting along the CMZ to remove retina but keep the ciliary body intact (- retina) or eyes were cut ~1 mm below the CMZ to include a rim of retina (+ retina). When testing

the iPLR animals were alternated between saline-treated and 9-*cis* retinal-treated. One eye was prepared + retina and the other prepared - retina. This was also alternated to remove a bias of testing one eye first. Neither retinal attachment ($P = 0.3$) nor order of examination had an effect on the baseline pupil area ($P = 0.2$).

All groups have an average pupil area, during light stimulation (0-60s), that is significantly smaller than baseline pupil area: saline + retina ($P = 0.0004$), saline – retina ($P = 0.0287$), 9-*cis* retinal + retina ($P < 0.0001$) and 9-*cis* retinal – retina ($P < 0.0001$). *Rd12* mice treated with 9-*cis* retinal that have a rim of retina attached to the anterior chamber have a significantly constricted pupil from 2s after light onset onwards. While *rd12* mice treated with 9-*cis* retinal without retina have a significant constriction at 20s and 60s only. *Rd12* mice treated with saline with retina attached to the anterior chamber only show a significantly reduced pupil area at 60s post-light onset. *Rd12* mice treated with saline without retina attached to the anterior chamber do not have a significantly smaller pupil area at any specific time point during light stimulation. So, while saline-treated *rd12* pupil - retina have a pupil area during light stimulation that is significantly less than 1, this is not apparent at any specific time point.

It has already been shown that 9-*cis* retinal increases the constriction *rd12* whole eye preparations (Figure 4.21). This is shown to be the case when only a 1 mm rim of retina is attached to the anterior chamber (Figure 5.2.A). *Rd12* mice with a rim of retina attached to the anterior chamber have a significantly greater iPLR when treated with 9-*cis* retinal, compared to *rd12* mice treated with saline. A significant difference is seen from 7s to 117s after light onset.

Comparing this to isolated anterior chambers (-retina), there is no longer an obvious constriction (Figure 5.2.B). Without retina attached there is no longer an

effect of 9-*cis* retinal (P = 0.6, F (1, 949) = 0.3). Interestingly, no significant changes in pupil area were detected throughout the recording (P = 0.9997, F (51, 949) = 0.5), reiterating the loss of an obvious constriction. Even though, isolated anterior chambers from both saline-treated and 9-*cis* retinal-treated *rd12* mice have an average pupil area that is significantly less than baseline during light stimulation.

Retinal attachment significantly increases the effect of 9-*cis* retinal on the iPLR. *Rd12* mice treated with 9-*cis* retinal that have a rim of retina attached to the anterior chamber have a significantly greater iPLR than *rd12* mice treated with 9-*cis* retinal without retina (P < 0.001, F (1, 1512) = 842). A significant difference between pupil area is seen from 7s after light onset until the end of the recording (Figure 5.2.C).

Comparing these results to those obtained from whole eye preparations, there is no significant difference at any time point between saline-treated *rd12* whole eye pupil area and that of 9-*cis* retinal-treated *rd12* without retina, saline-treated *rd12* without retina or saline-treated with retina.

Calculating the maximum constriction showed that treatment with 9-*cis* retinal provided a greater constriction (P = 0.0016, F (1, 39) = 11.53) (Figure 5.2.D). Retinal attachment also improved the constriction (P = 0.001, F (1, 39) = 12.73) and the greatest constriction was seen in pupils with retina attached from mice treated with 9-*cis* retinal-treatment (P = 0.026, F (1, 39) = 5.354). Maximum constriction in *rd12* treated with 9-*cis* retinal and retina attached is 0.35 ± 0.05. Without retina attached, constriction is reduced to 0.76 ± 0.05 (Figure 5.2.D). Maximum constriction in *rd12* pupils with retina attached from animals treated with saline only reached 0.75 ± 0.05. Without retinal attachment maximum constriction reached 0.84 ± 0.09, from saline-treated animals.

Neither retina attached to the anterior chamber (P = 0.9, F (1, 38) = 0.4) nor 9-*cis* retinal supplementation (P = 0.07, F (1, 38) = 3) had a significant effect on the latency.

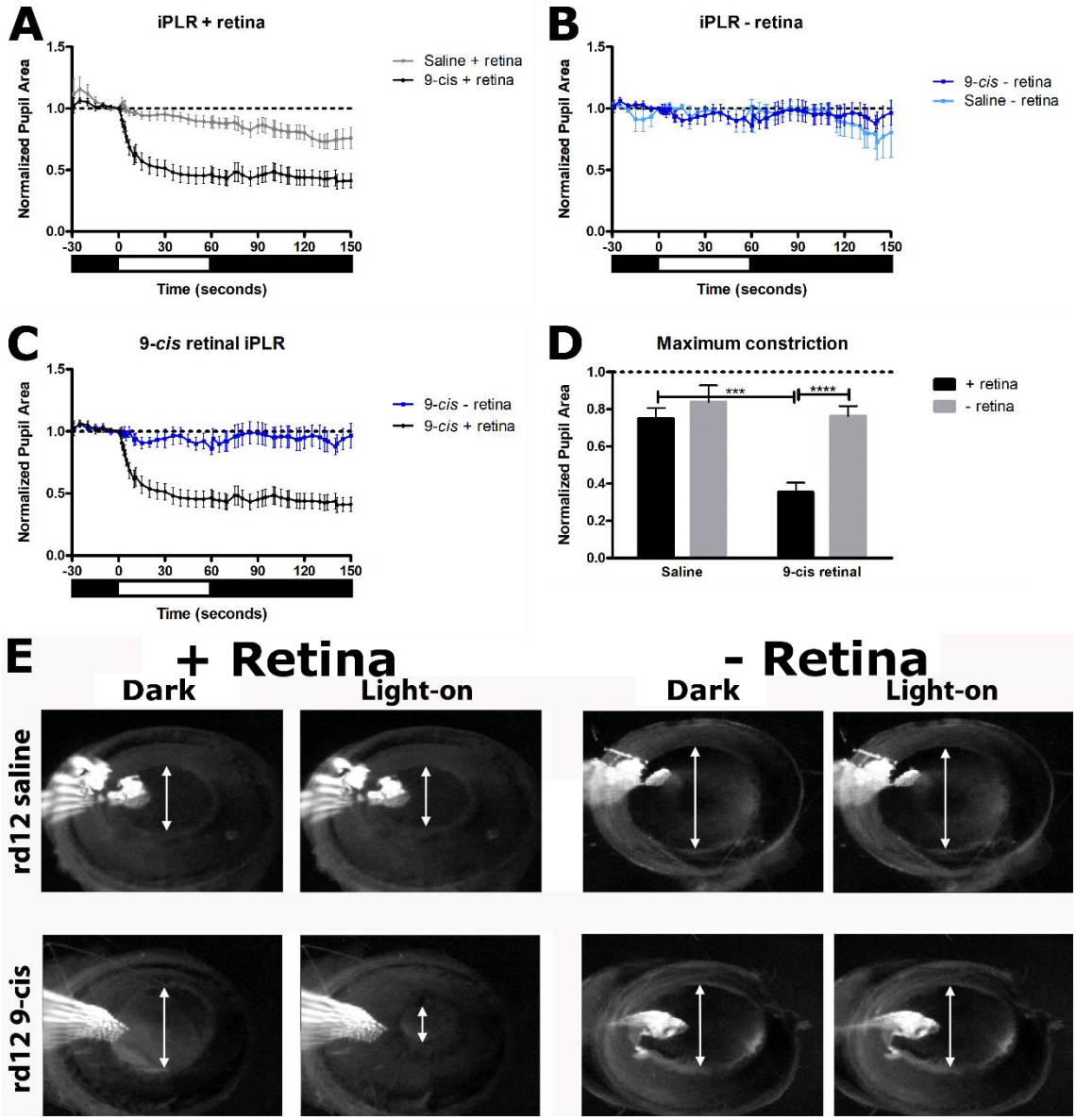

*Figure 5.2 iPLR in isolated anterior chambers of rd12 mice with 9-cis retinal. Pupil constriction of anterior chambers with a rim of retina attached (+ retina) is greater when the animal was treated with 9-cis retinal (n = 16), compared to saline-treated animals (n = 6) (A). No difference is seen in the iPLR between animals treated with 9-cis retinal (n = 16) or saline (n = 5) when the retina is removed from the anterior chamber (- retina) (B). The constriction in rd12 mice treated with 9-cis retinal is significantly greater + retina compared – retina (C). Black (lights off) and white (lights on) bars below graphs indicate light stimulation. D plots peak pupil constrictions. Asterisks indicate post-hoc test significance: ***P < 0.001; ****P < 0.0001. E shows representative images of the pupil area at baseline (dark) and at 30s post-light onset (light-on). Arrows highlight pupil area.*

5.2.4 Discussion

This experiment examined the question of whether the iPLR was driven by chromophore working in the retina. What is evident from the iPLR data presented here, is that 9-*cis* retinal is acting in the retina. In Figure 4.21, treatment with 9-*cis* retinal produced an iPLR in *rd12* mice, which surpassed that of WT. It was unknown if this chromophore was acting directly on the iris/ciliary body. In contrast to this, 9-*cis* retinal does not improve the iPLR when the iris/ciliary body is isolated from the retina. This functional data is consistent with RPE65 labelling in WT eye, which shows RPE65 expression restricted to the RPE and being absent from the iris.

When the current results are compared to those in Figure 4.21, no difference is apparent at any time point when comparing saline-treated *rd12* intact eye with saline-treated *rd12* with only a 1mm rim of retina, saline-treated *rd12* with no retina or 9-*cis* retinal-treated *rd12* with no retina. Interestingly, when 9-*cis* retinal-treated *rd12* have only 1 mm retina the constriction is significantly less than that of 9-*cis* retinal-treated *rd12* with an intact eye.

It has previously been shown that melanopsin and an intact CMZ are necessary for a complete iPLR response (Semo et al., 2014, Xue et al., 2011). In this experiment, functional evidence that chromophore may be acting in the retina to drive the iPLR is provided. It has also been shown that melanopsin can work as a bistable pigment (Fu et al., 2005), still, it is clear that this capability is insufficient in the *rd12* mouse to drive normal melanopsin function and, that 9-*cis* retinal can improve melanopsin function significantly, suggests that ipRGCs require another source of chromophore.

While this experiment provides compelling evidence that chromophore may act on the retina to produce the iPLR, it is unknown if RPE65 in the RPE would

normally supply chromophore to drive any retinal component of the iPLR. In the next experiment, addressing this question is attempted using a more targeted approach.

5.3 Is the iPLR driven by chromophore from the RPE?

5.3.1 Introduction

Previous work has shown the presence of RPE65 in human M/L-cones (Tang et al., 2011), which has so far not been detected in mice. While it was shown in the previous experiment of this chapter, that RPE65 labelling appeared restricted to the RPE, the possibility cannot be excluded that this is not the only location of RPE65 expression in the mouse retina. In this experiment *rpe65* expression will be restored in the *rd12* mouse by gene therapy. The gene will be delivered in a viral vector placed into the subretinal space in one eye and into the vitreous of the other eye. The aim here is to see if RPE65 is expressed in cells of the inner retina using the intravitreal delivery route and if so, to determine how RPE65 expressed at this location influences, the iPLR relative to the predominantly RPE based expression of RPE65 expected by the subretinal delivery route.

5.3.2 Methods

Delivery of virus

3-month *rd12* mice received pAAV5-CAG-RPE65-Venus subretinally into the left eye (RPE65 SBR) and intravitreally in the right eye (RPE65 IVT) (n = 11) as described in paragraph 2.4.4. A separate group of 3-month old *rd12* mice received a control virus (n = 9), which did not contain the *rpe65* gene (pAAV5-

CAG-Venus). This was also placed subretinally into the left eye (Control SBR) and intravitreally into the right eye (Control IVT) of each mouse. The viral construct included Venus, a fluorescent reporter protein, to aid visualisation of transfected retinal cell types. The virus was constructed by our collaborator Dr Eriko Sugano, University of Iwate, Japan. Visual function (ERG, BLA and PLR) was used to assess the success of this gene therapy approach 7 – 8 weeks after viral administration, prior to examination of the iPLR.

Scotopic and Photopic ERG

7 weeks after virus administration, scotopic and photopic ERGs were recorded from all animals, as described in paragraph 2.2.1.

BLA

7 weeks after virus administration BLA was assessed as described in paragraph 2.2.2. 5 *rpe65* and 5 control animals were placed in an arena with the front half illuminated. 2 *rpe65* and 4 control animals were placed in a dark arena.

PLR

8 weeks after virus administration PLR was recorded from left and right eyes of animals as described in paragraph 2.2.3. The number of animals assessed are presented in
Table 30.

Table 30 Number of rd12 treated with virus assessed by PLR

µW/cm^2/s	800	80	8	0.8	0.08
Control SBR	5	5	8	0	0
Control IVT	5	4	0	0	0
Rpe65 SBR	9	5	4	4	9
Rpe65 IVT	11	4	11	3	0

iPLR

8 weeks after the delivery of the virus, animals were culled and the iPLR was recorded from all eyes as described in paragraph 2.2.4. Following iPLR recordings, the cornea was pierced and the eye placed in 4% PFA overnight.

RPE65 labelling

In order to keep the iris intact, eyes did not have their lens removed prior to embedding. Whole eyes were embedded, sectioned and labelled for RPE65 using immunohistochemistry as described in paragraph 2.3.2. The antibodies used were anti-RPE65 raised in rabbit (1:500, ab173596; Abcam) with the secondary antibody raised in donkey against rabbit tagged with Alexa Fluor 568 (1:2000, ab10042; Abcam). Images were captured on a Zeiss 700 microscope. Venus (green) was also imaged to show the extent of viral expression within the retina.

5.3.3 Results

Scotopic ERG following virus administration

A trend of increased scotopic a- and b-wave amplitude was seen in eyes which received a virus encoding *rpe65* subretinally (Figure 5.3). There was no significant effect on the scotopic a-wave of having *rpe65* encoded in the virus or where the virus was inserted (Table 31). There was a greater effect on the scotopic b-wave amplitude. While the encoding of *rpe65* on its own was not significant (Table 31), it had a significant effect over the different light intensities ($F(6, 60) = 2.887$, $P = 0.0154$) and post-hoc tests shows significant differences between eyes receiving a subretinal injection of a virus encoding *rpe65* and the

control virus at -1 ($P < 0.05$) and 0 Lg cd.s/m^2 ($P < 0.01$). Also, where the virus encoding *rpe65* was placed had a significant effect on the scotopic b-wave.

Table 31 Two-way ANOVA of virus and site of injection on scotopic ERG in rd12

Two-way ANOVA	Scotopic A-wave	Scotopic B-wave
RPE65 Vs Control	F (1, 10) = 1.2, P = 0.2998	F (1, 10) = 3.05, P = 0.1111
SBR Vs IVT	F (1, 18) = 2.55, P = 0.1274	F (1, 18) = 4.91, P = 0.0398

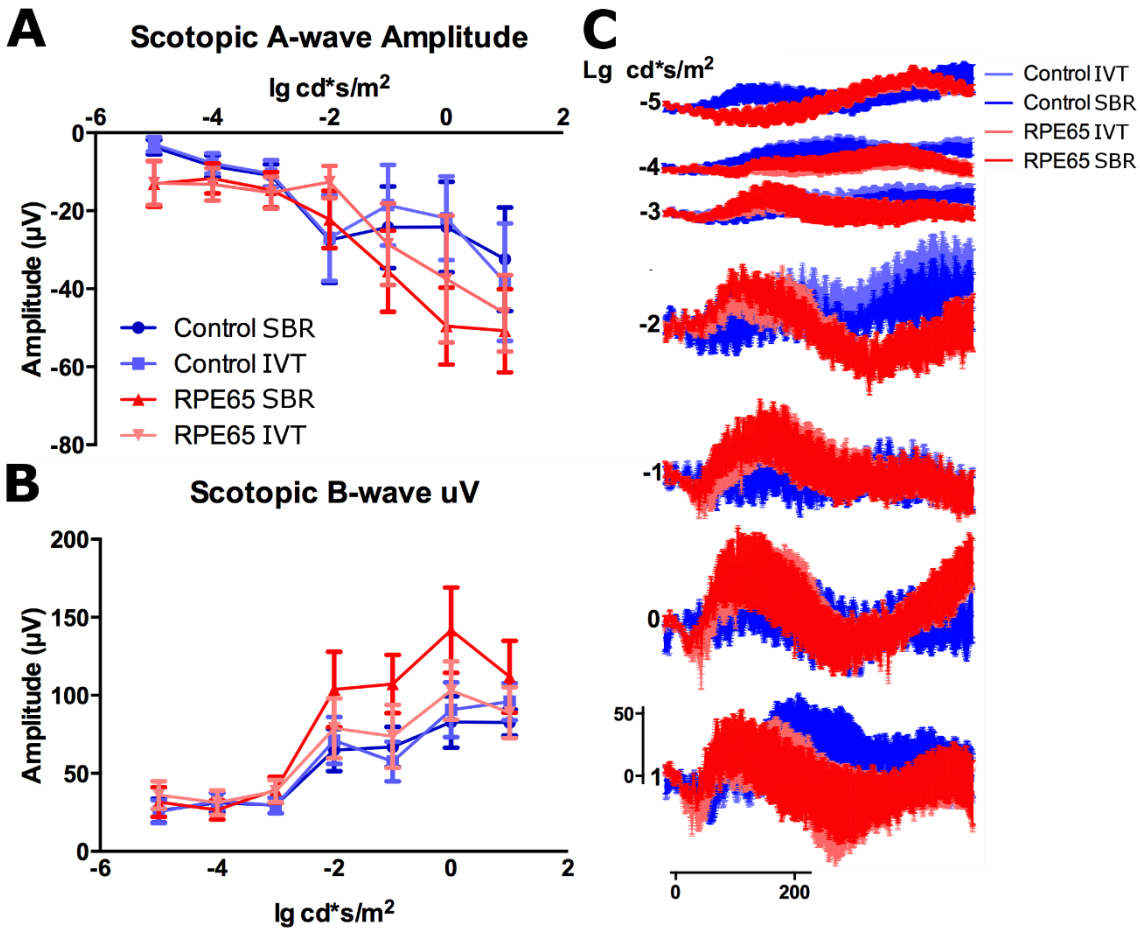

Figure 5.3 Scotopic ERG results in rd12 mice which received gene therapy. Graphs plot scotopic a-wave amplitude (A) and b-wave amplitude (B) for eyes which received virus encoding rpe65 subretinally (RPE65 SBR, n = 11), virus encoding rpe65 intravitreally (RPE65 IVT, n = 11), control virus subretinally (n = 9) and contrl virus intravitreally (n = 9). C displays the average trace ± SEM for each group at each light intensity. Vertical scale represents 50 µV and the horizontal scale indicates 200 ms.

Photopic ERG in *rd12* mice which received virus treatment

There is a trend of increased b-wave amplitude in eyes which received virus encoding *rpe65*, but this is not a significant effect (Figure 5.4). There was not a

significant effect of the virus encoding *rpe65* or the site of injection on the photopic b-wave amplitude (Table 32).

Table 32 Two-way ANOVA of effects of virus encoding rpe65 on Photopic ERG

Two-way ANOVA	F (DFn, DFd)	P value
Rpe65 Vs Control	F (1, 18) = 1.766	P = 0.2005
SBR Vs IVT	F (1, 20) = 2.136	P = 0.1594

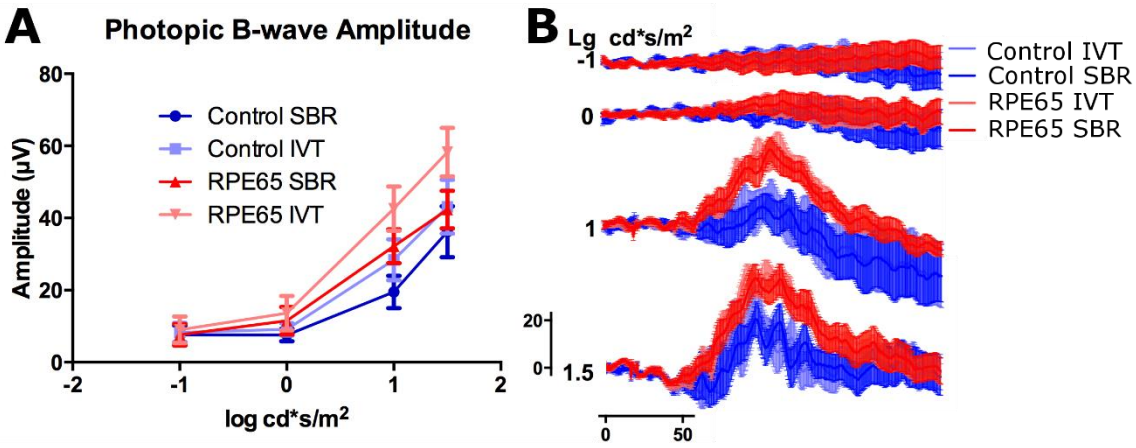

Figure 5.4 Photopic ERG in rd12 mice treated with virus.
A displays the photopic b-wave amplitude which increases with increased light intensity in eyes which received rpe65 gene subretinally (RPE65 SBR, n = 11), rpe65 gene intravitreally (RPE65 IVT, n = 11) and eyes which received a control virus subretinally (Control SBR, n = 9) or intravitreally (Control IVT, n = 9). B shows average traces ± SEM at the different light intensities. The vertical scale indicates 20 μV and the horizontal scale represents 50 ms.

BLA in *rd12* mice treated with virus

Both control-treated mice and mice receiving the *rpe65* gene spent more time in the back half when the front half was illuminated compared to when the whole arena was in darkness (P = 0.0136, F (1, 12) = 8.354). This indicates the presence of BLA. *Rd12* which received the virus with *rpe65* spent 11.3 ± 9.4 % of their total time in the back half when the arena was in darkness, this was increased to 39.6 ± 8.1 % when the front half was illuminated (Figure 5.5.A). Control mice spent 19.7 ± 1.9 % of total time in the back half when the arena was in darkness and this increased to 31.5 ± 4.9 % when the front half is illuminated. The virus encoding *rpe65* did not increase BLA. There was no significant

difference between animals receiving the virus which contained *rpe65* and the control virus (P = 0.98, F (1, 12) = 0.0008). Comparing this to untreated *rd12*, which spent 34 ± 4 % of their time in the back half when the front half was illuminated, *rd12* receiving virus encoding *rpe65* spend more time avoiding the light.

Rd12 receiving the control virus spend significantly more time in the back half off the arena when the front half is illuminated compared to when the front half is dark (P = 0.0061, F (1, 51) = 8). The preference for the back half, of mice placed in an illuminated or dark arena, does not significantly change over the 30 minutes (P = 0.3, F (1, 50) = 0.9). Although, preferences diverge enough that, in the last 5 minutes, *rd12* receiving the control virus spent 3 times more time in the back half of the arena when the front is illuminated, than when the front half is also dark (Figure 5.5.B).

The behavior of *rd12* receiving virus encoding *rpe65* have significantly different behavior when placed in the arena under an illuminated front half compared to being placed in a dark arena (P = 0.0355, F (1, 8) = 6). *Rd12* receiving virus encoding *rpe65* have a growing preference for the back half when placed in an arena with the front half illuminated, while if they are placed in a dark arena, they have a growing preference for the front half (Table 33). This is likely driven by the desire to return home. *Rd12* receiving virus encoding *rpe65* spend significantly more time in the back half when the front half is illuminated (Table 34). This was not seen in untreated 3-month *rd12* (Figure 4.17).

Table 33 Linear regression of BLA in rd12 receiving virus encoding rpe65

Linear Regression	Slope	r^2	Is the slope significantly non-zero?	Equation
Control Dark	-0.3 ± 0.3	0.03	P = 0.422, F (1, 22) = 0.6696	Y = -0.3x + 25
Control Light	0.2 ± 0.3	0.01	P = 0.5823, F (1, 28) = 0.31	Y = 0.2x + 28
Rpe65 Dark	-0.5 ± 0.4	0.1	P = 0.2557, F (1, 10) = 1.454	Y = -0.5x + 19
Rpe65 Light	0.2 ± 0.4	0.01	P = 0.6068, F (1, 27) = 0.271	Y = 0.2x + 35

Table 34 Two-way ANOVA of effects of virus on BLA over 30 minutes

Two-way ANOVA	Control Virus	Virus encoding *rpe65*
Light	P = 0.826, F (1, 7) = 4.099	P = 0.0004, F (1, 29) = 15.92
Time	P = 0.9092, F (5, 35) = 0.30	P = 0.9919, F (5, 29) = 0.097
Light over time	P = 0.3952, F (5, 35) = 1.07	P = 0.9345, F (5, 29) = 0.254

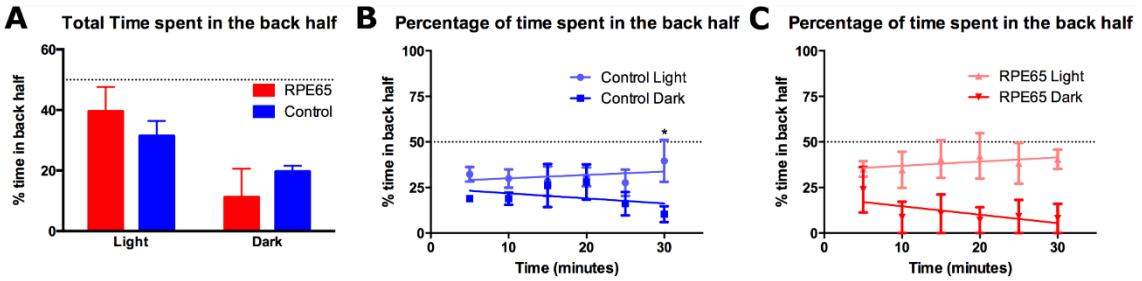

Figure 5.5 BLA in rd12 mice treated with virus.
A shows the total time spent in the dark back half of the arena when the front half was illuminated (light) or in darkness (dark). Both rd12 which received virus with rpe65 (red) and rd12 mice receiving control virus (blue) spent more time in the back half when the front half was illuminated. B illustrates the amount of time spent in the back half by rd12 mice receiving control virus over the 30 minutes. During the last time bin of 25 – 30 minutes, control mice spent significantly more time in the back half when placed in an illuminated arena (n = 5) compared to a dark arena (n = 4) (P < 0.05). C illustrates the amount of time rd12 mice receiving the rpe65 gene spent in the back when the front half was illuminated (n = 5) and when the arena was in darkness (n = 2).

PLR of *rd12* mice treated with virus

Improvements are seen in the PLR in eyes that received virus encoding *rpe65* subretinally. At 800 µW/s/cm^2, all treatment groups had a significant constriction (Figure 5.6.E). During light stimulation (0 – 60s) the average pupil area was significantly different to 1, the normalised baseline (P < 0.0001 for each treatment group). Analysis of each time point showed that eyes which received *rpe65* subretinally were significantly constricted throughout the light stimulation (0-60s), with a peak constriction of 0.21 ± 0.06. Eyes receiving *rpe65* intravitreally were significant from 2 – 60s and had a peak constriction of 0.41 ± 0.05. Eyes that received the control virus subretinally had significant constriction from 4 – 60s and a peak constriction of 0.42 ± 0.07. Eyes that received the control virus intravitreally were significantly constricted from 3 – 60s and had a peak

constriction of 0.4 ± 0.04. Comparing these results to untreated *rd12,* which had a peak constriction of 0.34 ± 0.07 at this light power, only eyes which received virus encoding *rpe65* subretinally appear to have an improved constriction. Untreated *rd12* also did not have a significant constriction at this light power. Their maximum constriction reached 0.89 ± 0.04. At 800 µW/s/cm^2, there was a significant difference between virus treatment groups and how they constricted to light stimulation (Table 35). Eyes receiving *rpe65* subretinally had a better constriction than other virus treatments (Figure 5.6.E). They were significantly more constricted than eyes receiving the control virus subretinally and eyes receiving *rpe65* intravitreally from 2 – 69s. There were no significantly different time points between *rd12* which received the control virus subretinally and those that received it intravitreally, and no significant difference between animals that received intravitreal injections of control virus or the virus encoding *rpe65*. These improvements to the constriction do not have a significant effect on the latency to 90% maximum constriction.

At the lower irradiances of 80 µW/s/cm^2 (Figure 5.6.D), the average pupil area is significantly less than 1 during light on for eyes receiving the *rpe65* virus subretinally ($P < 0.0001$) or intravitreally ($P < 0.0001$). Eyes receiving the control virus either subretinally or intravitreally did not have an average pupil area significantly less than 1. Analysis of each time point showed that eyes receiving *rpe65* subretinally were significantly constricted from 1 – 60s and had a peak constriction of 0.26 ± 0.06. Eyes that received *rpe65* intravitreally, although, they had an average pupil area significantly less than 1 during lights on, were only significantly less than 1 at 20s, and other time points were not individually significant. Their peak constriction reached 0.83 ± 0.03. Eyes which received the control virus subretinally had a peak constriction of 0.99 ± 0.04, also not

significantly less than 1 (P = 0.8). Eyes treated with control virus intravitreally had a peak constriction of 0.86 ± 0.05, also not significantly different from 1 (P = 0.06). Thus, it is clear that eyes which received the control virus did not have a constriction at this light power. At 80 µW/s/cm^2, there was a significant difference between virus treatment groups and how they constricted to light stimulation (Table 35). Eyes receiving *rpe65* subretinally had a better constriction than other virus treatments (Figure 5.6.D). They were significantly more constricted than eyes receiving the control virus subretinally and eyes receiving *rpe65* intravitreally from 2 – 69s. There were no significantly different time points between *rd12* which received the control virus subretinally and those that received it intravitreally, and no significant difference between animals that received intravitreal injections of control virus or the virus encoding *rpe65*.

At 8 µW/s/cm^2, the average normalised pupil area was significantly less than 1 during lights on in eyes receiving *rpe65* subretinally (P < 0.0001) and intravitreally (P = 0.0031). Eyes receiving the control virus subretinally did not have an average pupil size significantly less than 1. Eyes receiving the *rpe65* virus subretinally had a significantly constricted pupil during light stimulation, 1 – 60s (Figure 5.6.C). Their peak constriction was 0.51 ± 0.06. Eyes receiving the *rpe65* virus intravitreally had significant pupil constriction from 3 – 20s and a peak constriction of 0.74 ± 0.05. Eyes receiving the control virus subretinally did not have a significant constriction at any time point and their maximum constriction reached 0.93 ± 0.02. At 8 µW/s/cm^2, there was a significant difference between virus treatment groups and how they constricted to light stimulation (Table 35). Eyes receiving *rpe65* subretinally had a better constriction than other virus treatments (Figure 5.6.C). They were significantly more constricted than eyes receiving the

control virus subretinally from 1 – 69s and significantly greater than eyes receiving *rpe65* intravitreally from 7 – 77s.

At 0.8 μW/s/cm^2, only eyes which received the virus encoding *rpe65* were examined (Figure 5.6.B). Both subretinally and intravitreally injected eyes had an average normalised pupil area that was significantly less than 1 during lights on (SBR: P < 0.0001, IVT: P = 0.0104). Subretinally injected eyes had significant constriction at 1 - 4s, 7 – 11s and at 40s, though, 5s, 15-30s and 50 -60s were not significant (Figure 5.6.B). Their peak constriction reached 0.51 ± 0.11. There were no timepoints in eyes treated with an intravitreal injection that were significantly less than 1. Their peak constriction reached 0.86 ± 0.08, but was not significantly less than 1 (P = 0.2). At 0.8 μW/s/cm^2, there was a significant effect of the site of injection and the constricted to light stimulation (

Table 35). Eyes receiving *rpe65* subretinally had a better constriction than eyes receiving *rpe65* intravitreally (Figure 5.6.B). They were significantly more constricted than eyes receiving *rpe65* intravitreally at 3s and 11-15s (P < 0.05).

Eyes receiving *rpe65* subretinally were also examined at 0.08 μW/s/cm^2. Average normalised pupil area was significantly less than 1 from 0-60s (Figure 5.6.A). Analysis of individual time points only showed a significant constriction at 4s post light onset (P = 0.0043). Their peak constriction reached 0.76 ± 0.06.

Table 35 Two-way ANOVA of PLR in rd12 receiving virus encoding rpe65

Two-way ANOVA	Virus treatment	Light	Interaction
800 μW/s/cm^2	P < 0.0001, F (3, 1063) = 89.8	P < 0.0001, F (51, 1063) = 33	P < 0.0001, F (153, 1063) = 2
80 μW/s/cm^2	P < 0.0001, F (3, 460) = 195.7	P < 0.0001, F (46, 460) = 4.75	P < 0.0001, F (138, 460) = 2.63
8 μW/s/cm^2	P < 0.0001, F (2, 580) = 234.6	P < 0.0001, F (30, 580) = 5.73	P < 0.0001, F (60, 580) = 5.42
0.8 μW/s/cm^2	P = 0.0063, F (1, 112) = 25.76	P = 0.0388, F (32, 112) = 1.6	P = 0.0063, F (32, 112) = 1.931

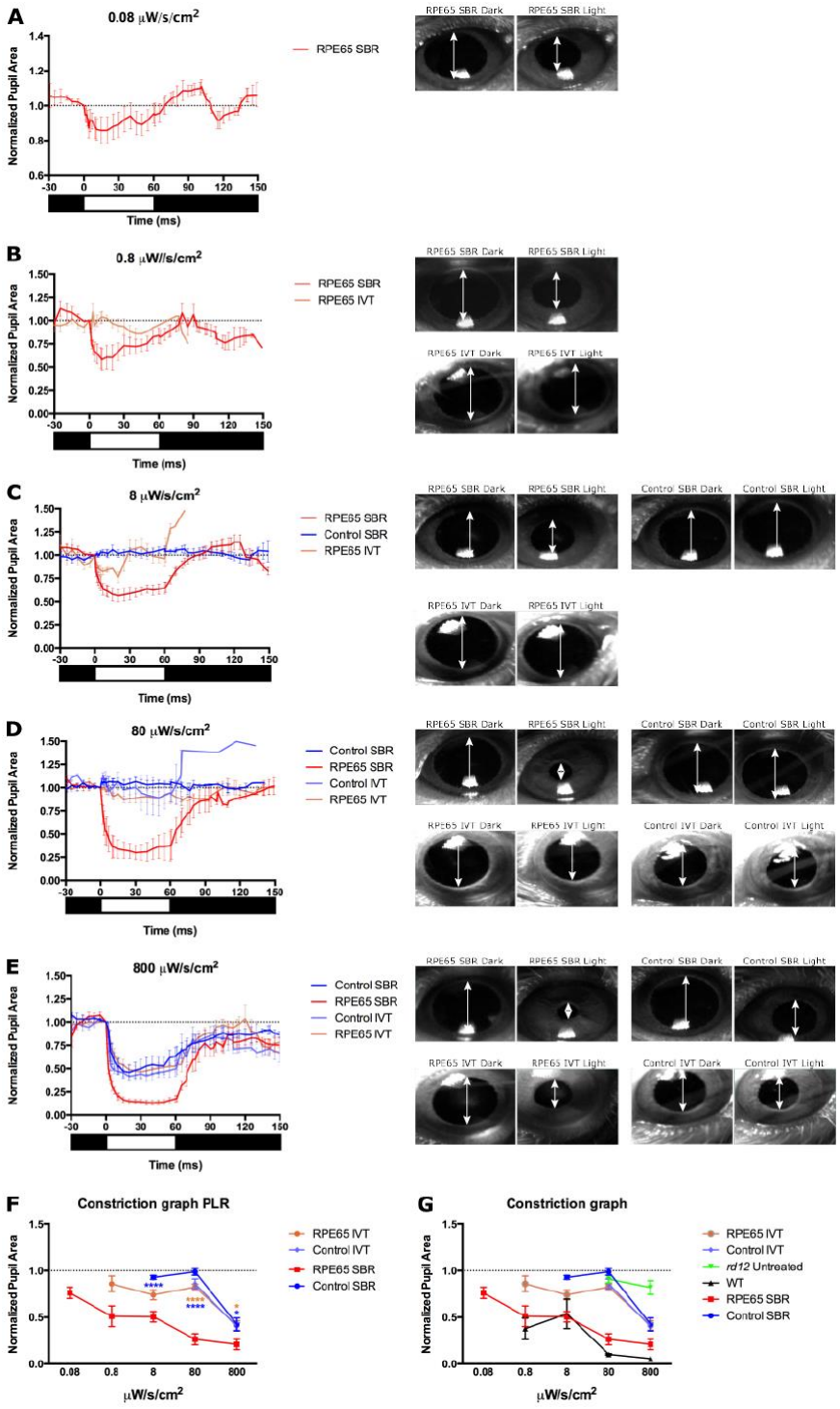

*Figure 5.6 PLR in rd12 mice treated with virus. A-E display graphs of the pupil area normalised to baseline at time 0. Video stills show representative images of pupil area before (dark) and ~30s after (light) light-onset. Arrows highlight the pupil diameter. Eyes treated with virus containing rpe65 subretinally (RPE65 SBR) had a PLR at 0.08 µW/s/cm² (A, n = 9). At 0.8 µW/s/cm² (B), both RPE65 SBR (n = 4) and eyes which received the rpe65 virus intravitreally (RPE65 IVT, n = 3) had significant constrictions during lights on, with RPE65 SBR PLR significantly greater. At 8 µW/s/cm² (C), RPE65 SBR (n = 11) had significant pupil constrictions and RPE65 IVT (n = 4) less restricted and no response in eyes receiving the control virus subretinally (Control SBR n = 8). At 80 µW/s/cm² (D), RPE65 SBR (n = 5), RPE65 IVT (n = 4) and Control SBR (n = 4) had significant pupil constrictions. At 800 µW/s/cm² (E), RPE65 SBR (n = 9), RPE65 IVT (n = 11) and Control SBR (n = 5) and Control IVT (n = 5) all had significant pupil constrictions, with the strongest response in the RPE65 SBR group for both D and E. There was no difference between Control IVT and Control SBR, or Control IVT and RPE65 IVT in E. F displays a graph of peak pupil constrictions Asterisks indicate significance levels between RPE65 SBR and RPE65 IVT (orange asterisks) or Control SBR (blue asterisks): ****P < 0.0001, *P < 0.05. G displays the same peak constrictions as F but also has WT and rd12 untreated results included for comparison.*

iPLR of *rd12* mice treated with virus

Finally, mice were culled and the iPLR was recorded from isolated eyes (Figure 5.7). The virus treatment received had a significant effect on the constriction ($P = 0.0248$, $F(3, 1762) = 3.13$). All treatment groups have a significant constriction ($P < 0.0001$, for all groups), but the greatest constriction was seen in eyes which received virus encoding *rpe65* subretinally.

Assessing the effects of *rpe65* the site of injection on the maximum constriction, neither the encoding of *rpe65* ($P = 0.8$, $F(1, 34) = 0.09$) in the virus ($P = 0.8$, $F(1, 34) = 0.09$) nor the site of injections alone significantly increased the constriction. A combination of *rpe65* encoded in the virus and subretinal administration produced a significantly greater constriction ($P = 0.021$, $F(1, 34) = 5.311$). Peak constriction reached 0.55 ± 0.05 in eyes treated with virus encoding *rpe65* subretinally and 0.71 ± 0.04 in eyes receiving *rpe65* virus intravitreally. Eyes that received the control virus subretinally had a peak constriction of 0.68 ± 0.05 and eyes receiving the control virus intravitreally had a peak constriction of 0.6 ± 0.06. Thus, while eyes which received the virus encoding *rpe65* subretinally had the greatest constriction, this was not considerably greater than the other treatment groups. There were no significant changes in the latency of the constriction between treatment groups (Figure 5.7.E).

What becomes apparent when the results are compared to untreated *rd12* (Figure 5.7.C) is that all treatment groups have a greater constriction than untreated *rd12,* which has a maximum constriction of 0.81 ± 0.07. This may be an effect of the surgery, as it has been shown previously that improvements in visual function are seen which are unspecific to the treatment (see sections 3.7.3 & 4.6.3). Although, a key factor for regard in this experiment is that the virus

produced the expression of venus, which emits a green wavelength, capable of activating melanopsin. This is an important consideration as such a confounding factor could also dilute the effect of re-introducing *rpe65*.

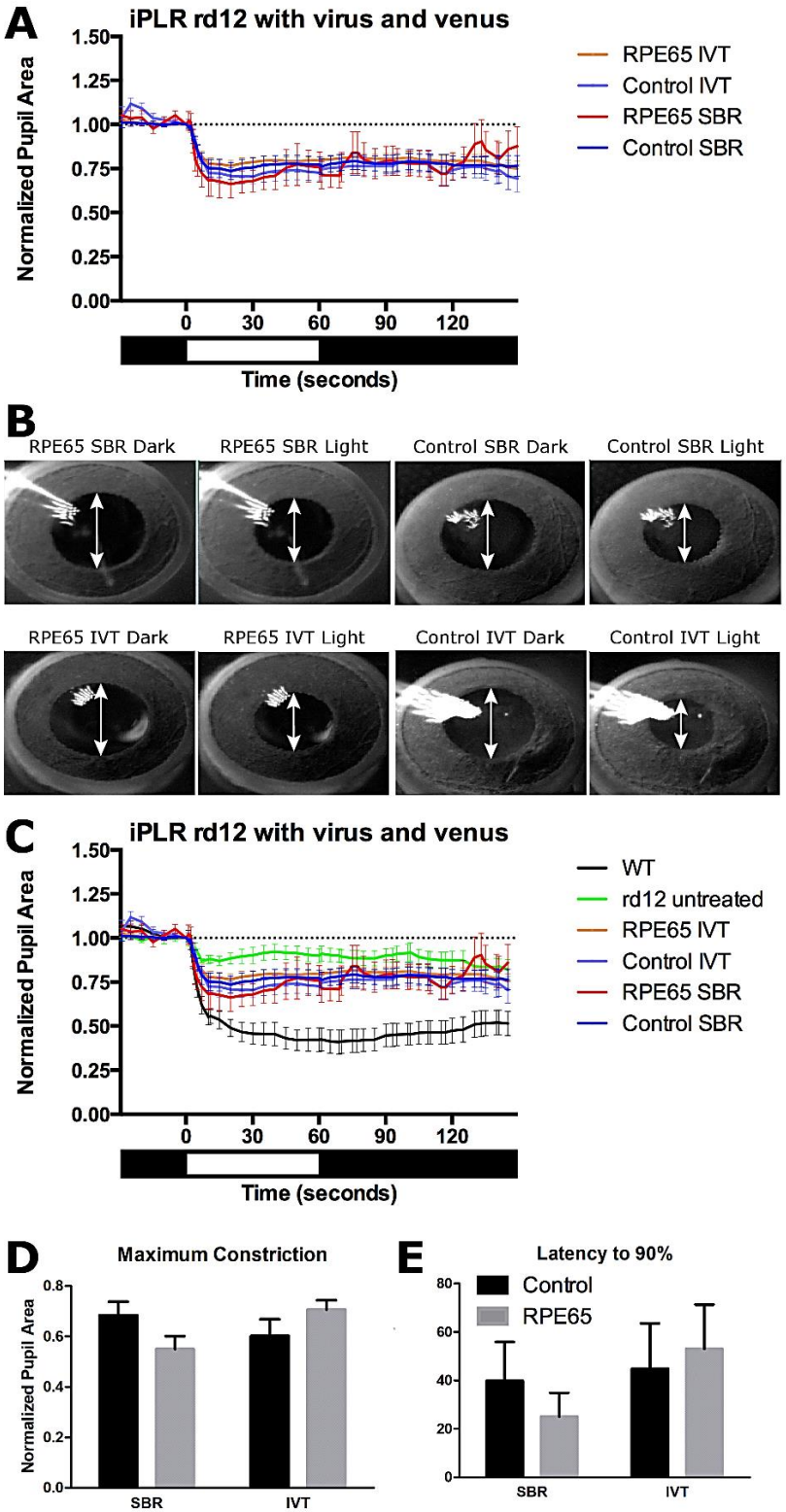

Figure 5.7 iPLR in rd12 mice treated with virus.
A displays a graph of the iPLR constriction of rd12 treated with virus. Eyes received the rpe65 virus subretinally (RPE65 SBR, N = 9), rpe65 virus intravitreally (RPE65 IVT, n = 11), control virus subretinally (Control SBR n = 9) or Control virus intravitreally (Control IVT n = 9). The black and white bars below the graph represent lights off (black) and lights on (white). B displays representative video stills from before (Dark) and 30s after (Light) light onset. C shows data from A with WT and untreated rd12 data for comparison. E displays the peak constriction. E displays the time taken to reach 90% peak constriction.

RPE65 labelling with venus

RPE65 was identified by both immunohistochemical staining for RPE65 and venus reporter fluorescence. Immunostaining for RPE65 was restricted to the RPE of eyes which received virus encoding the *rpe65* gene delivered subretinally (Figure 5.8). However, eyes which received the virus encoding the *rpe65* gene delivered intravitreally did not label for RPE65 by immunohistochemistry. RPE65 was not detected by immunohistochemistry outside of the RPE in any eye examined. While the venus reporter (green) was seen in all cells expressing the virus in various retinal layers, including, the RPE of eyes receiving virus subretinally. However, eyes that received virus intravitreally had venus expression throughout the retina, with the exception of the RPE. Venus expression was also found in the iris and the endothelial layer of the cornea, in eyes which received virus subretinally and intravitreally but RPE65 expression was absent from these structures by immunostaining.

One noticeable trend observed was that the eyes which received the control virus had greater expression of venus compared to eyes which received the virus which also encoded *rpe65*. This difference was not quantified. It is unknown why this is the case, but this may be brought about by the size of the genetic material in the vector. AAV vectors are limited to carrying ~4.5 Kb of exogenous genetic materal. This is much more limited compared to retroviruses, adenoviruses or herpes simplex viruses. The viral vector encoding *rpe65* is 1.6 Kb larger than the control virus. This is a considerable amount and may affect the infection and expression of the viral vector.

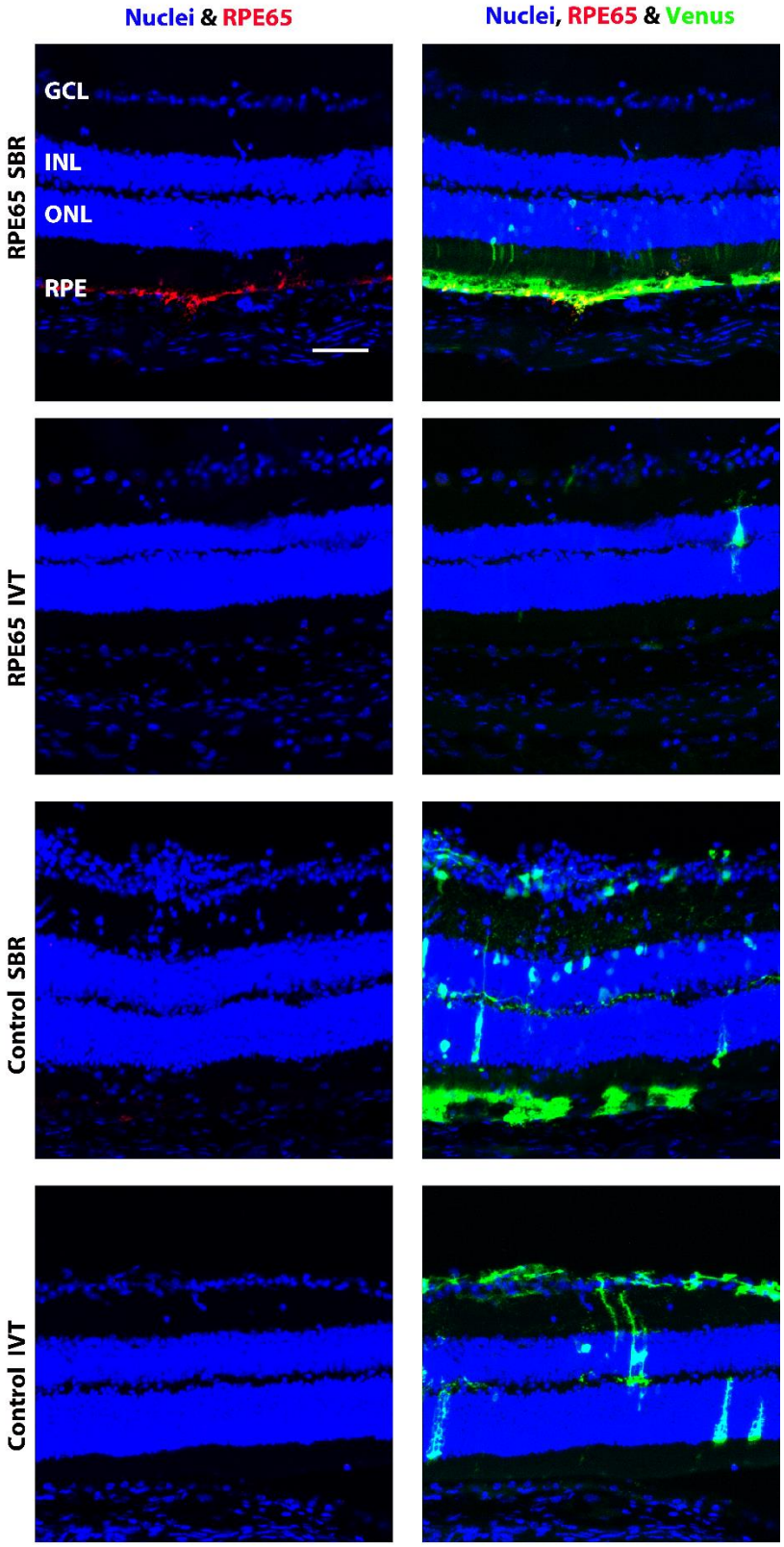

Figure 5.8 RPE65 labelling and venus expression in rd12 eyes treated with virus. RPE65 labelling (red) is only found in the RPE of eyes receiving virus encoding rpe65, delivered subretinally. Venus (green) shows where the virus is expressed. It is found in all eyes. Eyes receiving the virus subretinally show venus expression in the RPE as well as other retinal layers. Eyes receiving the virus intravitreally express venus in many retinal layers but not the RPE. Scale bar indicates 50 um.

5.3.4 Discussion

This experiment was carried out to determine if *rpe65* could be expressed outside the RPE and drive the iPLR. In the last experiment, it was seen that in WT retina RPE65 labelling was only detected in the RPE, however, this did not necessarily mean that it was not expressed in low levels elsewhere. By placing the *rpe65* gene intravitreally and comparing the results to placing the gene subretinally it was hoped that the origin of chromophore required for the iPLR could be determined. RPE65 was only seen in eyes which received the virus containing *rpe65* subretinally and its expression was restricted to the RPE.

ERGs were recorded to determine if the gene therapy improved outer-retinal photoreceptor function. While positive trends were seen, the *rpe65* virus was not able to significantly improve the scotopic a-wave amplitude, however, at 0 Lg cd.s/m^2 eyes treated with *rpe65* subretinally had a significantly greater b-wave amplitude than eyes which received the control virus subretinally. The photopic ERG also showed a positive trend of improved b-wave amplitude in eyes treated with *rpe65*, however, this was not significant.

BLA is a functional read out of both outer retinal photoreceptor function and melanopsin function. While animals that received the virus showed a BLA response, there was no significant difference between animals which received the virus encoding *rpe65* and animals that received the control virus. Although, there is a trend of increase light aversion in animals which received *rpe65*. This may become statistically significant with a greater n-number as there is large deviation from the mean with this test. There is also a lack of literature using this test for investigating restoration of visual function. Thus, there could be many factors unknown about restoring this behavioural function including restoration of vision in only one eye.

The PLR can also be used as a functional readout of both outer-retinal photoreceptors and ipRGCs. However, this readout showed a greater difference between eyes treated with the control virus and eyes treated with *rpe65*. All treatment groups had a significant constriction only at 800 μW/s/cm^2. At 80 μW/s/cm^2, only eyes treated with *rpe65* had a significant constriction. Eyes receiving the control virus did not have a significant constriction. At 8 and 0.8 μW/s/cm^2 both eyes with *rpe65* subretinally and intravitreally had significant pupil constrictions. Only eyes which received *rpe65* subretinally were examined at 0.08 μW/s/cm^2, and they had a significant pupil constriction to this irradiance. Eyes receiving *rpe65* subretinally had a significantly greater constriction than eyes receiving the control virus subretinally or eyes which received *rpe65* intravitreally at every irradiance examined. No significant differences were seen between eyes receiving the control virus intravitreally and eyes receiving the *rpe65* virus intravitreally and any irradiance, nor were there any significant differences seen between control eyes receiving the virus subretinally and control eyes which received the virus intravitreally at any irradiance.

Subretinal placement of *rpe65* significantly improved the constriction and also the sensitivity of the PLR. Placement of *rpe65* intravitreally had a significant effect on the sensitivity of the PLR, as there was a significant constriction at 0.8 μW/s/cm^2, however the constriction was not significantly greater than eyes which received the control virus intravitreally at either 800 or 80 μW/s/cm^2. Comparing these results to untreated *rd12* mice, the sensitivity was increased in all treated eyes as *rd12* peak constriction only reached 0.82 ± 0.07, at 800 μW/s/cm^2, but was not significantly less than 1. While the effects of sham injections on retinal preservation and improved function is well known (Woch et al., 2001, Keegan et al., 2003, Del Priore, 2005), there is a concern that this improved PLR could be

due to the presence of venus, which emits green light, and is possibly able to stimulate melanopsin in ipRGCs.

The iPLR has the greatest constriction in eyes receiving the *rpe65* virus subretinally and the effect of treatment was significant. However, there were no significant differences in post-hoc tests. Given the widespread expression of venus it is difficult to separate any sham effect from the possible effect of venus on the iPLR. Venus is a very useful tool for evaluating viral delivery and expression, however, the presence of this flurorescent protein may well influence functional assessments. As such, this experiment is replicated without venus.

5.4 Re-assessing the question “Is the iPLR driven by chromophore from the RPE?” using a virus without venus.

5.4.1 Introduction

Given the improved PLR and iPLR of the control groups in the last experiment it was decided that the experiment needed to be repeated without venus encoded in the virus.

5.4.2 Methods

Delivery of virus

12, 2-month old *rd12* received pAAV5-CAG-RPE65 subretinally into the left eye and intravitreally into the right eye as described in paragraph 2.4.4. 10 2-month old *rd12* mice received a control virus, which did not contain the *rpe65* gene, pAAV5-CAG. Visual function was analysed 7 – 8 weeks after viral administration.

BLA

6 weeks after virus administration BLA was assessed as described in paragraph 2.2.2. 4 *rpe65* and 5 control animals were placed in an arena with the front half illuminated. 3 *rpe65* and 5 control animals were placed in a dark arena.

PLR

7 weeks after virus administration PLR was recorded from left and right eyes of animals as described in paragraph 2.2.3. The number of animals assessed are shown in Table 36.

Table 36 Numbers rd12 treated with virus without venus assessed by PLR

µW/s/cm^2	Control SBR	Control IVT	*Rpe65* SBR	*Rpe65* IVT
800	10	7	12	11
80	4	7	12	11
0.08	4	0	11	0

iPLR

7 weeks after the delivery of the virus, iPLR was recorded from all eyes as described in paragraph 2.2.4. Following iPLR recordings, the cornea was pierced and the eye placed in 4% PFA overnight to fix prior to immunohistochemically labelling retinas.

RPE65 and melanopsin labelling

Eyes did not have their lens removed prior to embedding, to keep the iris intact. Whole eyes were embedded, sectioned and labelled for RPE65 and some sections were then also labelled for melanopsin using immunohistochemistry as described in paragraph 2.3.2. The antibodies used were anti-RPE65 raised in rabbit (1:500, ab173596; Abcam) with the secondary antibody raised in donkey against rabbit tagged with Alexa Fluor 568 (1:2000, ab10042; Abcam). Then anti-

melanopsin (1:5000, UF006; Advanced Targeting Systems, San Diego, CA, USA) was used with the secondary antibody used was raised in donkey against rabbit FITC-labelled (1:200, Jackson ImmunoResearch, West Grove, PA, USA). Because both anti-RPE65 and anti-melanopsin are raised in rabbit, this FITC labelled secondary will adhere to both primary antibodies. This will create a yellow label for RPE65 (green and red) and a green label for melanopsin. Images were captured on a Zeiss 700 confocal microscope. Analysis of melanopsin in the On and Off sublamina of the IPL was conducted in imageJ by thresholding above a greylevel of 20. Images were cropped to 67.4 µm x 404.4 µm and pixel intensity was measured on remaining pixels. N-numbers: (AAV5 RPE65 SR, n = 9, AAV5 RPE65 IVT, n = 6, AAV5 Control SR, n =6, AAV5 Control IVT, n =6).

5.4.3 Results

BLA in *rd12* mice with virus lacking venus

Both control-treated mice and mice which received the *rpe65* gene spent more time in the back half when the front half was illuminated compared to when the whole arena was in darkness ($P = 0.011$, $F(1, 13) = 8.77$). This indicates the presence of BLA. *Rd12* which received the virus with *rpe65* spent 28.9 ± 3.7 % of their total time in the back half when the arena was in darkness, this was increased to 37 ± 4.8 % when the front half was illuminated (Figure 5.9.A). Control mice spent 22.7 ± 3.2 % of total time in the back half when the arena was in darkness and this increased to 37.9 ± 3.5 % when the front half is illuminated. There was no significant difference in the total time spent in the front half between animals which received the virus encoding *rpe65* and the control virus ($P = 0.5$, $F(1, 13) = 0.5$). The effect of light was not significantly different between *rpe65* and control animals ($P = 0.4$, $F(1, 13) = 0.8$), and, these results are not

substantially greater than untreated *rd12* with spend 34 ± 4 % of their time in the back half when the front half is illuminated.

Rd12 which received the control virus exhibit BLA (Figure 5.9.B). When placed in an arena with the front half illuminated spend more time in the back half than then placed in a dark arena ($P<0.0001$, $F(1, 57) = 30.5$). Although, with time, control animals placed in an arena with the front half illuminated, spend less time in the dark back half (Table 37).

Unfortunately, *Rd12* which received virus encoding *rpe65* do not exhibit a BLA (Figure 5.9.C). While, overall, these mice spend more time in the back half when the front half is illuminated, this is not significant (Table 38). The preference for the back half does not change over the 30 minutes (Table 37).

Table 37 Linear Regression of BLA over time in rd12 with virus without venus

Linear Regression	Slope	r^2	Is the slope significantly non-zero?	Equation
Control Dark	-0.3 ± 0.2	0.07	P = 0.1475 F (1, 28) = 2.2	Y = -0.3x + 28
Control Light	-0.6 ± 0.3	0.16	P = 0.0277 F (1, 28) = 5.4	Y = -0.6x + 48
Rpe65 Dark	-0.005 ± 0.3	0.00001	P = 0.9885 F (1, 16) = 0.0002	Y = -0.005x + 29
Rpe65 Light	-0.3 ± 0.3	0.05	P = 0.2267 F (1, 28) = 1.5	Y = -0.3x + 41

Table 38 Two-way ANOVA of BLA of rd12 with virus encoding rpe65

Two-way ANOVA	Control virus	Virus encoding *rpe65*
Light	P < 0.0001, F (1, 48) = 28	P = 0.4348, F (1, 36) = 2.09
Time	P = 0.2432, F (5, 48) = 1.4	P = 0.4348, F (5, 36) = 1
Change in BLA over time	P = 0.5865, F (5, 48) = 0.8	P = 0.8765, F (5, 36) = 0.35

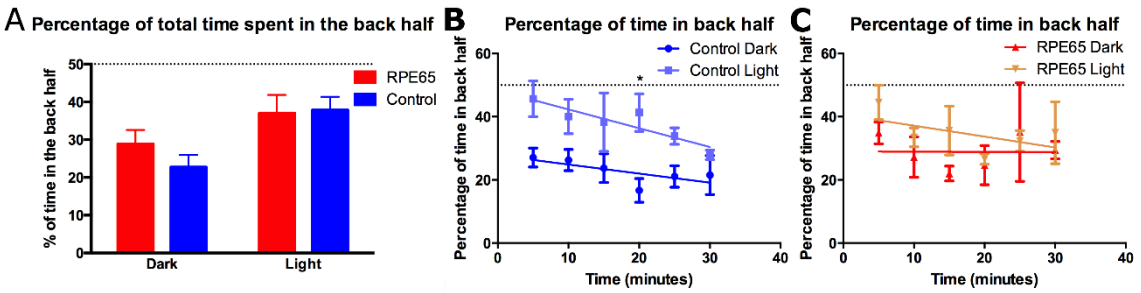

Figure 5.9 BLA in rd12 mice with virus lacking the venus reporter.
A shows the percentage of total time spent in the back half by animals treated with virus containing rpe65 (red) or control virus (blue) placed in an arena that is in darkness (dark) or an arena which has the front half was illuminated (light). B plots the percentage of time control animals spent in the back half when the front half of the arena was illuminated (Control Light, n = 5) and when the whole arena was in darkness (Control Dark, n = 5). The asterisk indicates a significance between Control light and control dark (P < 0.05). C plots the percentage of time animals treated with virus containing rpe65 spent in the back half when the front half of the arena was illuminated (RPE65 Light, n = 4) and when the whole arena was in darkness (RPE65 Dark, n = 3).

PLR of *rd12* treated with virus lacking venus.

Again, the results show that *rpe65* gene replacement improves the PLR in *rd12* mice when delivered subretinally (Figure 5.10). At 800 µW/s/cm^2, all treatment groups did have a significant constriction (Figure 5.10.C); during lights on (0 – 60s) the average pupil size was significantly different to 1, the normalised baseline ($P < 0.0001$ for each treatment group). Analysis of each time point showed that eyes receiving *rpe65* subretinally were significant during light stimulation 1 – 60s, with a peak constriction of 0.18 ± 0.04. Eyes receiving *rpe65* intravitreally were significantly constricted from 2 – 60s and had a peak constriction of 0.58 ± 0.05. Eyes receiving the control virus subretinally had significant constriction from 2 – 60s and a peak constriction of 0.58 ± 0.05. Eyes which received the control virus intravitreally were significant from 5 – 30 s and at 60 s, but not from 40 – 50 s, and had a peak constriction of 0.67 ± 0.02. Only eyes which received virus encoding *rpe65* subretinally had a greater constriction than untreated *rd12,* which had a maximum constriction of 0.34 ± 0.7 at this light

power. Eyes receiving *rpe65* subretinally had a better constriction than other virus treatments (Figure 5.10.C). Eyes which received a subretinal injection of virus encoding *rpe65* had a significantly greater constriction than eyes which received a subretinal injection of the control virus from 1 – 101s post light-onset. Constriction in eyes receiving *rpe65* subretinally was also significantly greater than eyes receiving *rpe65* intravitreally from 2 – 77s post light-onset. Eyes that received the virus encoding *rpe65* intravitreally had a significantly greater constriction than eyes that received the control virus intravitreally at 30s ($P < 0.05$). There were no significantly different time points between *rd12* which received the control virus subretinally and intravitreally. There was no significant effect of the virus treatment on the latency.

At 80 $\mu W/s/cm^2$ (Figure 5.10.B), the average pupil area is significantly less than 1 during light on for eyes receiving *rpe65* subretinally ($P < 0.0001$) and eyes receiving the control virus subretinally ($P < 0.001$) or intravitreally ($P < 0.0001$). Eyes which received the *rpe65* virus intravitreally did not have an average pupil area significantly less than 1 ($P = 0.2$). Analysis of each time point showed that eyes receiving *rpe65* subretinally were significantly constricted during light stimulation 1 – 60s and had a peak constriction of 0.47 ± 0.07. Eyes which received virus encoding *rpe65* intravitreally did not have a pupil area significantly less than 1 at any individual time point. Their peak constriction reached 0.89 ± 0.04. Eyes which received the control virus subretinally were also not significantly less than 1 at any individual time point, although their average pupil area was significantly less than 1. Their peak constriction was 0.83 ± 0.1. Eyes treated with control virus intravitreally were significantly less than 1 at 5s, 15 - 20s and 40 – 50s. At 7 – 11s and 30s the pupil constriction was not significantly less than 1.

Their peak constriction was 0.87 ± 0.07. Untreated *rd12* did not have a significant constriction at this light power. Their maximum constriction reached 0.89 ± 0.04. There was a significant difference in the constriction at this light power between the treatment groups (Table 39). Eyes receiving *rpe65* subretinally were significantly more constricted than eyes receiving the control virus subretinally from 2 – 61s. Eyes receiving *rpe65* subretinally were also significantly more constricted than eyes receiving the *rpe65* intravitreally from 2 – 69s. There were no significantly different time points between *rd12* which received the control virus subretinally and intravitreally, and no significant difference between animals receiving the intravitreal injections of the control virus or the virus with *rpe65*.

At 0.08 μW/s/cm^2 (Figure 5.10.A), only eyes that received subretinal injections of either *rpe65* or control virus were examined. At this irradiance, eyes receiving *rpe65* ($P < 0.0001$) and eyes injected with control virus ($P = 0.0386$) had an average pupil area that was significantly less than 1. Analysis of individual time points showed a significant constriction at 7s and 20 – 30s in eyes which received *rpe65* subretinally. At 11-15s the constriction was not significant. These eyes had a peak constriction of 0.79 ± 0.05. Eyes which received the control virus subretinally only had a significant constriction at 1s. Their peak constriction reached 0.91 ± 0.003. There was a significant difference between these two groups (Table 39).

Table 39 Two-way ANOVA of rd12 PLR with virus encoding rpe65 without venus

Two-way ANOVA	Virus treatment	Light	Interaction
800 μW/s/cm^2	$P < 0.0001$, $F (3, 1269) = 177$	$P < 0.0001$, $F (50, 1269) = 28$	$P < 0.0001$, $F (150, 1269) = 3$
80 μW/s/cm^2	$P < 0.0001$, $F (3, 638) = 98.93$	$P < 0.0001$, $F (23, 638) = 3.79$	$P < 0.0001$, $F (69, 638) = 3.67$
0.08 μW/s/cm^2	$P < 0.0299$, $F (1, 297) = 4.762$	$P = 0.3$, $F (30, 297) = 1$	$P = 0.98$, $F (30, 297) = 0.5$

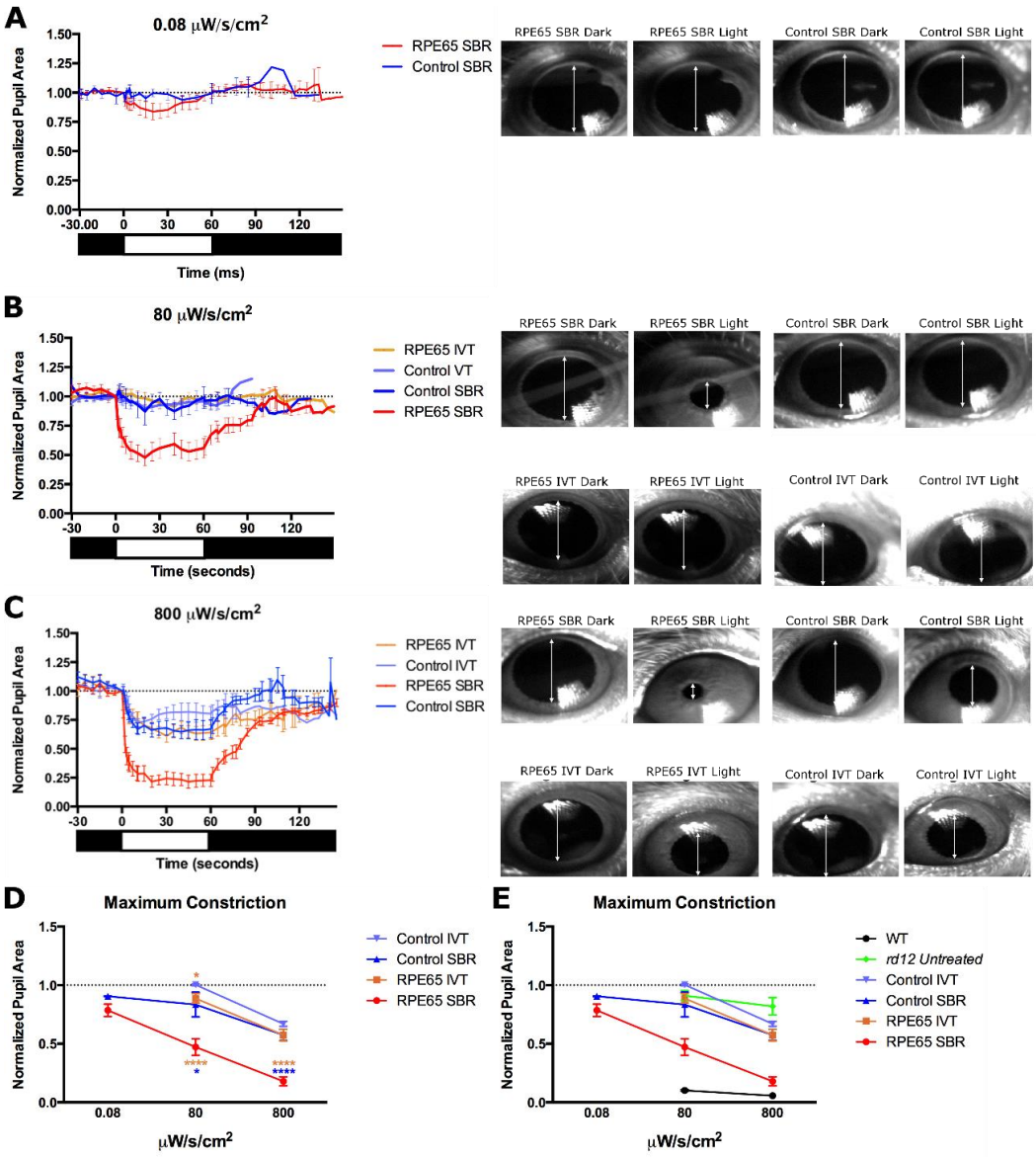

Figure 5.10 PLR in rd12 mice treated with virus lacking the venus reporter.
A displays the PLR at 0.08 μW/s/cm² of eyes which received control virus subretinally (Control SBR, n = 4) and eyes which received virus encoding rpe65 subretinally (RPE65 SBR, n = 11). Note the small RPE65 SBR response. Bars beneath the graph indicate lights off (black) and lights on (white). video stills are representative of animals before (dark) and ~30s after (light) lights on. B displays the PLR at 80 μW/s/cm², where there is a robust constriction in RPE65 SBR (n = 12), and is not apparent in Control SBR (n = 4) or Control IVT (n = 7). Eyes receiving the rpe65 *virus intravitreally (RPE65 IVT, n = 11) did not have constriction. At 800 μW/s/cm², all treatment groups had a significant constriction (C). RPE65 SBR (n = 12) had a significantly greater constriction than Control SBR (n = 10) and REP65 IVT (n = 11). RPE65 IVT had a significantly greater constriction than Control IVT (n = 7). There was no significant difference between Control SBR and Control IVT. D displays the peak constriction within the first 30s after lights on. Orange asterisk above the graph represents a significant difference between RPE65 IVT and control IVT (P < 0.05). The other orange asterisks indicate significance levels between RPE65 SBR and RPE65 IVT (P < 0.0001) and the blue asterisks represent a significance between RPE65 SBR and Control SBR (*P < 0.05, ****P < 0.0001). E shows data from D, plus untreated rd12 (green) and WT (black) data for comparison.*

iPLR of *rd12* mice with virus treatment lacking venus.

Replacement of rpe65 in rd12 mice increases the iPLR, with all treatment groups showing significant constrictions and the largest constriction found when virus encoding *rpe65* is delivered subretinally (Figure 5.11.A). Eyes which received the virus with rpe65 subretinally had a significant constriction from 3s until the end of the recording. Eyes which received the virus encoding *rpe65* intravitreally had a significant constriction from 5s until 40s after light-onset. Eyes receiving the control virus subretinally had a significant constriction at 5s, 20s, 40s and 69s – 150s. Eyes that received the control virus intravitreally had a significant constriction from 3 – 30s and from 50s – 150s. There was a significant effect of different virus treatments on the iPLR (Table 40).

Eyes which received virus encoding *rpe65* subretinally had a significantly greater constriction compared to eyes which received the control virus subretinally from 7 – 30s and eyes which received the *rpe65* virus intravitreally from 7s until the end of the recording (Figure 5.11.A). There was no significant difference between eyes which received the control virus subretinally and intravitreally. Also, there was no significant difference between eyes which received intravitreal injections of control virus and virus encoding *rpe65 (*Figure 5.11*.A and B)*.

Rpe65 encoded in the virus did not have a significant effect on the maximum constriction on its own (Table 41). When this virus is administered subretinally this has a significant effect on the iPLR maximum constriction. The subretinal injection by itself saw an improvement on the iPLR maximum constriction. This site of injection may allow greater number of macrophage to infiltrate the retina, which can improve visual function. Despite this, eyes that received the virus containing *rpe65* subretinally had the greatest constriction, that reached a peak constriction of 0.7 ± 0.04 (Figure 5.11.C). Eyes that received the control virus

subretinally peaked at 0.83 ± 0.04. Placement of the virus encoding *rpe65* into the vitreous had a peak constriction of 0.93 ± 0.008 and this was significantly less than eyes which received virus encoding *rpe65* subretinally. Eyes which received the control virus intravitreally had a peak constriction of 0.87 ± 0.02 which is not significantly different from eyes which received the control virus subretinally. There were no significant changes to the latency of the iPLR response. Eyes which received virus encoding *rpe65* are the only group which had an iPLR that was greater than those recoded in untreated *rd12*, which had a maximum constriction of 0.81 ± 0.07.

When comparing these results to those received with a virus that also encoded venus, it is clear to see the effects of the venus on the iPLR (Figure 5.7). Venus allowed the pupil to constrict around 15% more, and the greatest effects were seen in eyes which received the virus encoding venus intravitreally, positioning the venus in the inner retina, close to the ipRGCs.

Table 40 Two-way ANOVA of rd12 iPLR with virus encoding rpe65 without venus

Two-way ANOVA	P-value	F (DFn, DFd)
Virus treatment	P = 0.0006	F (3, 38) = 7.148
Light	P < 0.0001	F (51, 1938) = 19.05
Interaction	P < 0.0001	F (153, 1938) = 2.747

Table 41 Two-way ANOVA of maximum iPLR constriction in rd12 with virus encoding rpe65 without venus

Two-way ANOVA	P-value	F (DFn, DFd)
Site of Injection	P < 0.0001	F (1, 38) = 19.15
Rpe65	P = 0.2	F (1, 38) = 2
Interaction	P = 0.0039	F (1, 38) = 9.425

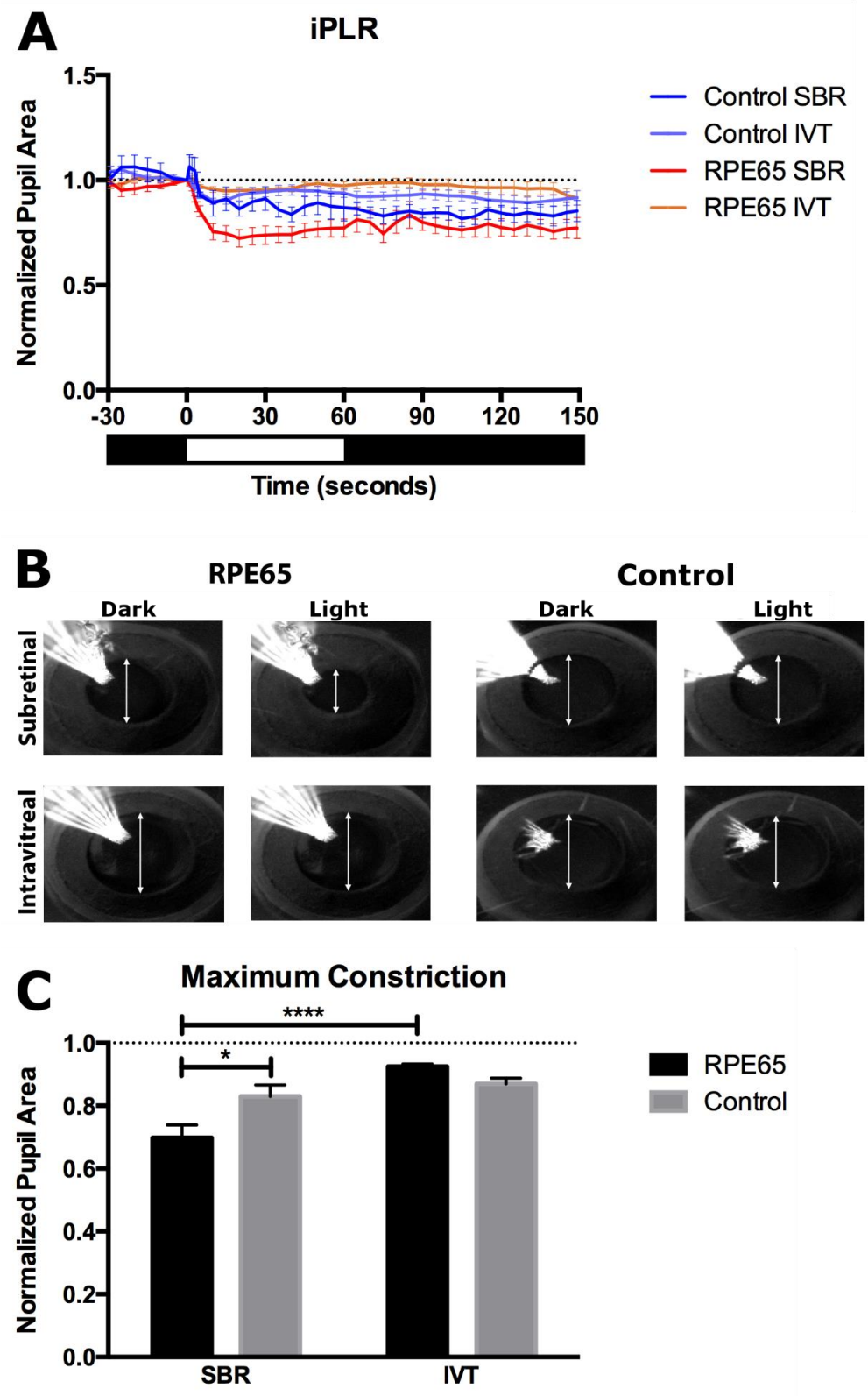

*Figure 5.11 iPLR rd12 mice with rpe65 gene therapy lacking venus reporter. A displays the iPLR of rd12 mice treated subretinally with virus encoding rpe65 (RPE65 SBR, N = 12), virus encoding rpe65 intravitreally (RPE65 IVT, N = 10). Control virus delivered subretinally (Control SBR, N = 10) or control virus delivered intravitreally (Control IVT, N = 10). The bars beneath indicate lights off (Black) and lights on (white). B displays video stills from T = 0 (dark) and T = 30 (light). Arrows highlight pupil diameter. C plots peak constriction. Asterisks indicate significance level from post-hoc tests: *P < 0.05, ****P < 0.0001.*

RPE65 labelling in *rd12* mice treated with virus lacking venus.

RPE65-labelling is only found in the RPE of eyes that received virus containing the *rpe65* gene subretinally (Figure 5.12 and Figure 5.13). In these eyes RPE65 labelling can be seen to extend to the retinal rim, but it was not found in the ciliary body/iris. Eyes that received the virus containing *rpe65* injected into the vitreous did not label positively for RPE65 in any location.

Autofluorescent cells are seen on the apical side of RPE cells in eyes receiving subretinal injections of both *rpe65* (Figure 5.14) or the control virus (Figure 5.15). These cells are most likely macrophage. Interestingly, these macrophage-like cells were not found in eyes receiving intravitreal injections. It is possible that these played a role in improving the peak constriction in the iPLR, as it was found that eyes which received a subretinal injection had a greater maximum constriction.

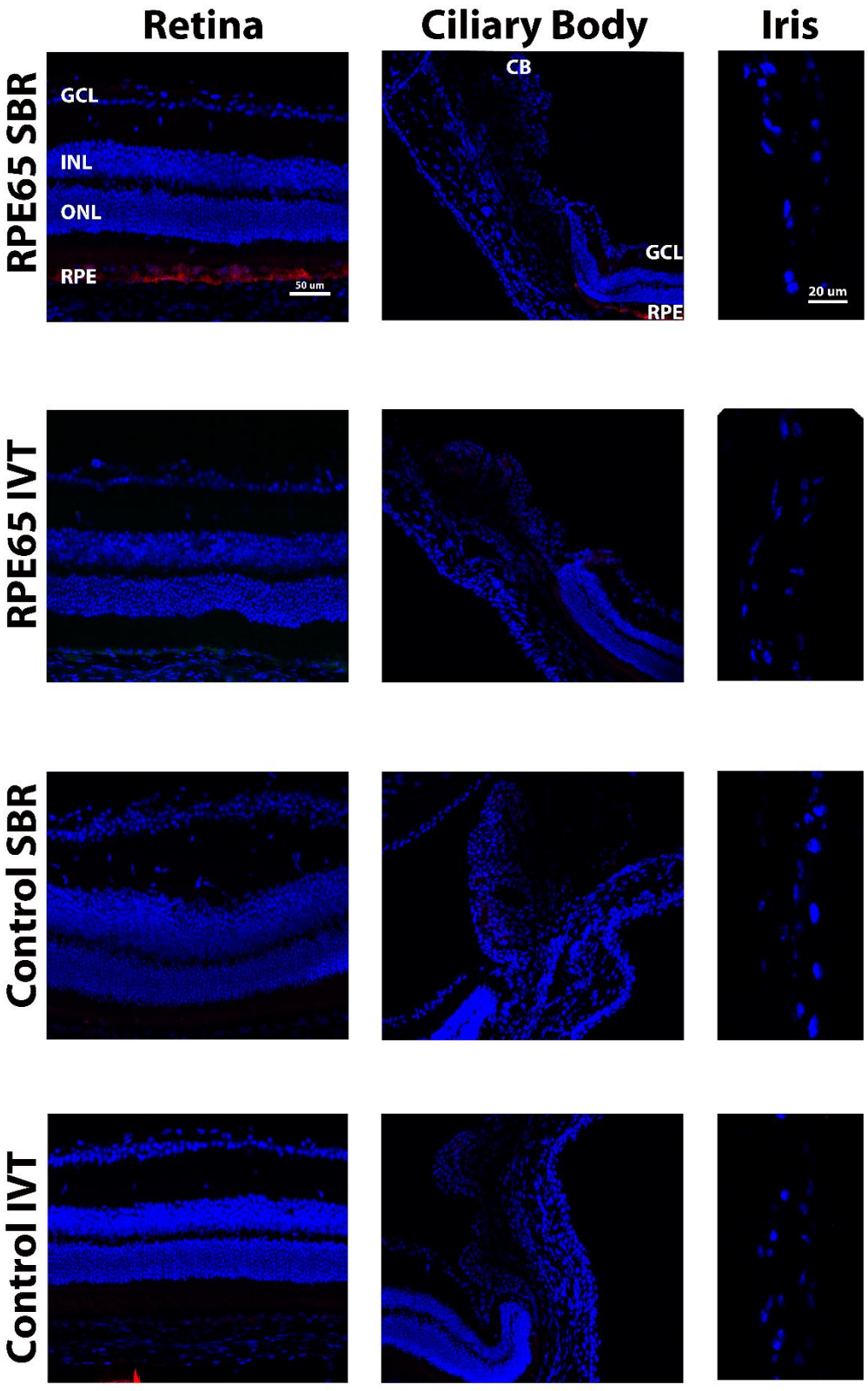

Figure 5.12 RPE65 labelling in rd12 mice treated with virus lacking venus. Representative images of RPE65 labelling (red) are displayed. RPE65 labelling is found only in the RPE of eyes that received virus encoding rpe65 subretinally. Retina and ciliary body images are taken at the same magnification and the scale bar represents 50 µm. The iris is imaged at a higher magnification and the scale bar indicates 20 µm.

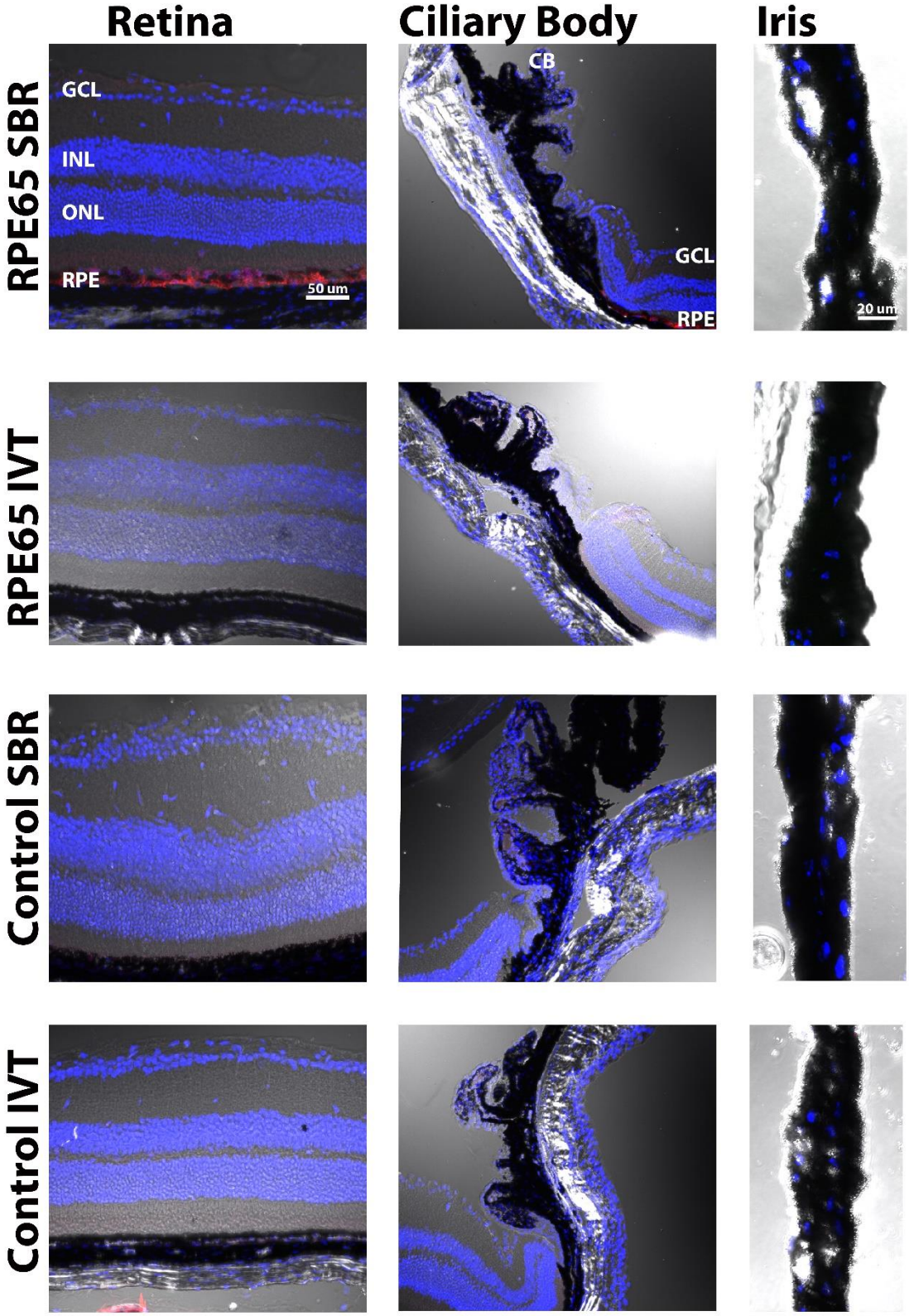

Figure 5.13 RPE65 labelling with transmitted light in rd12 mice treated with virus lacking venus.
This figure displays the same images from Figure 5.12, with the transmitted light channel included. This helps identify the pigmented RPE, ciliary body and iris. Images of the retina and ciliary body are taken at the same magnification and the scale bar represents 50 µm. The iris is imaged at a higher magnification and the scale bar indicates 20 µm.

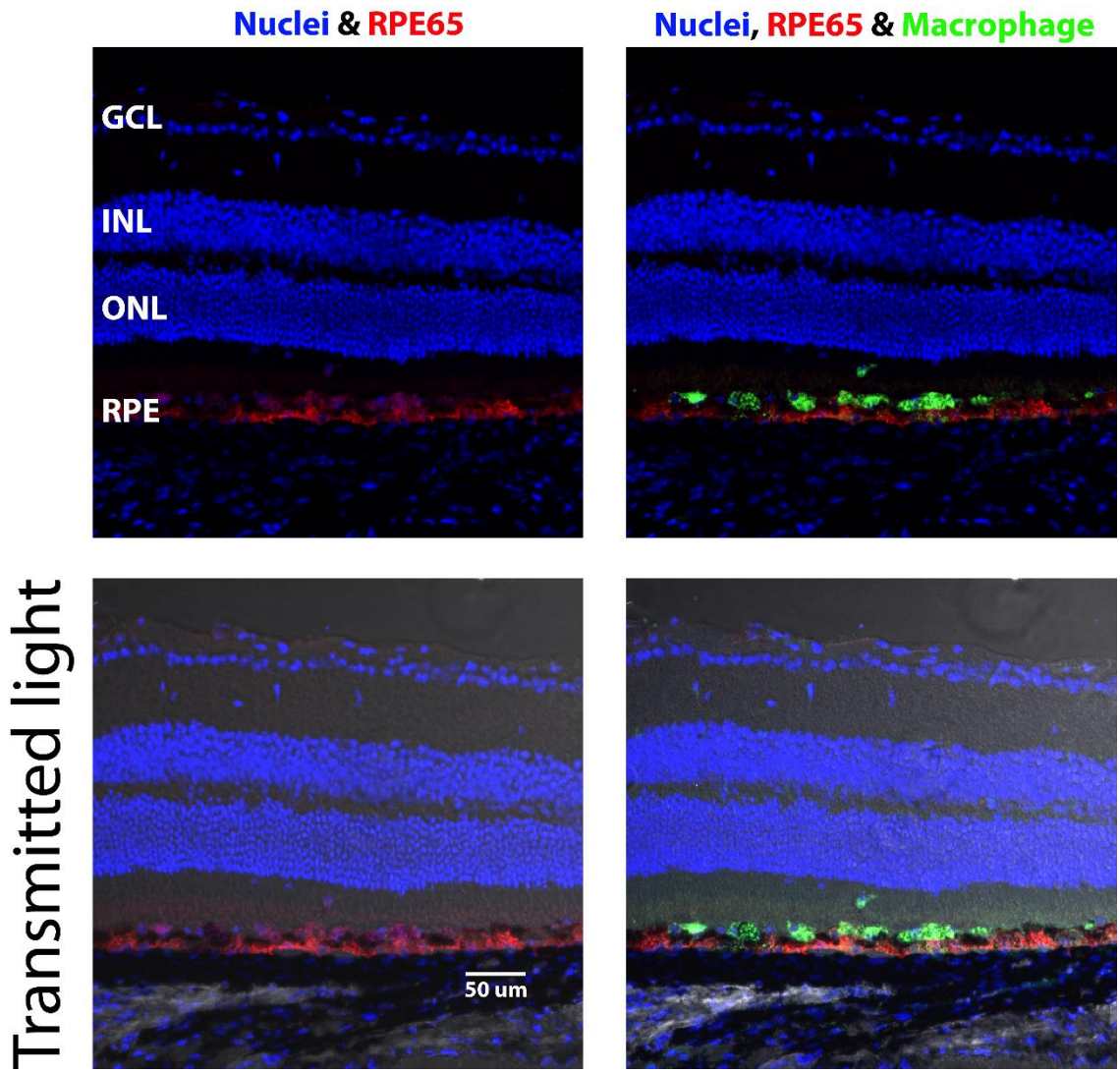

Figure 5.14 Macrophage in rd12 mice treated with virus encoding rpe65 without venus.
This figure displays the same retinal image of RPE65 SBR as above in Figure 5.12 and Figure 5.13, with the green channel turned on, which reveals auto-fluorescent macrophage that appear in both the red and green channel. They sit on top of the RPE. The scale bar indicates 50 µm.

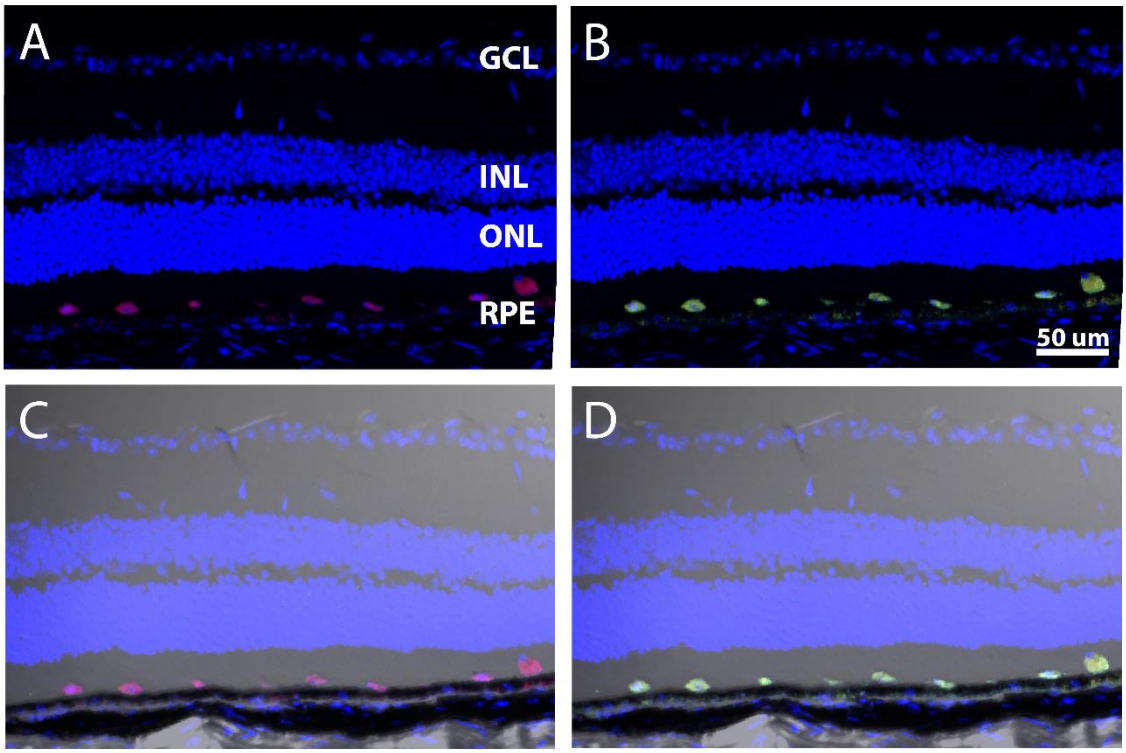

Figure 5.15 Macrophage in rd12 mice treated with control virus subretinally. This figure displays images from eyes that received a subretinal injection of control virus. Red cells appear in the subretinal space (A); however, the transmitted light helps to show that these cells lie on top of the RPE and do not co-localise to the RPE layer (C). The cells also appear under the green channel (B and D), suggesting that it is autofluorescence, rather than specific antibody binding. The scale bar indicates 50 µm.

Melanopsin labelling in *rd12* mice treated with virus lacking venus.

Melanopsin labelling was examined in retinal section. No significant differences were found in either the density of melanopsin^{+}-cells or the intensity of melanopsin labelling in the cell somas. Examining melanopsin expression in retinal sections provided a different perspective on the relationship between RPE65 and melanopsin staining. This sectional view revealed a significant increase in the melanopsin labelling of the off sublamina in eyes that received subretinal injections of the virus encoding *rpe65*.

Both the on and off sublamina of IPL were analysed for dendritic coverage and the average melanopsin labelling intensity (Table 42). The on sublamina did not show a significant effect of virus treatment on the area of melanopsin^{+}-dendritic

coverage (Figure 5.16.A) nor the intensity of melanopsin labelling (Figure 5.16.B). The off sublamina also did not show a significant effect of the virus or site of injection on the area of melanopsin^{+}-dendritic coverage (Figure 5.16.C). The virus treatment did significant effect the intensity of melanopsin labelling in the off sublamina (Table 42). Melanopsin expressed in the off sublamina of eyes which received virus encoding *rpe65* subretinally was stronger than eyes which received virus encoding *rpe65* intravitreally ($P < 0.05$) and eyes which received the control virus subretinally ($P < 0.05$) (Figure 5.16.D).

This effect is seen in eyes that received the *rpe65* virus subretinally, where *rpe65* expression was only partially restored in the RPE. In areas of the retina where RPE65 labelling is seen in the RPE, melanopsin-labelling in the off sublamina directly above this RPE has increased melanopsin labelling intensity (Figure 5.16.E), whereas, areas of the same retinal section which do not show RPE65 labelling, do not show a corresponding increase in melanopsin staining intensity, in the overlying off sublamina.

Table 42 Two-way ANOVA of effects of rpe65 on melanopsin in IPL

Two-way ANOVA		*Rep65*	Site of injection	Interaction
On	% area	P = 0.4, F (1, 21) = 0.8	P = 0.2 F (1, 21) = 2	P = 0.8 F (1, 21) = 0.05
	intensity	P = 0.7 F (1, 21) = 0.3	P = 0.6 F (1, 21) = 3	P = 0.4 F (1, 21) = 0.7
Off	% area	P = 0.1, F (1, 23) = 3	P = 0.8, F (1, 23) = 0.05	P = 0.5, F (1, 23) = 0.5
	intensity	P = 0.08, F (1, 23) = 3	P = 0.0178, F (1, 23) = 6.51	P = 0.054, F (1, 23) = 4

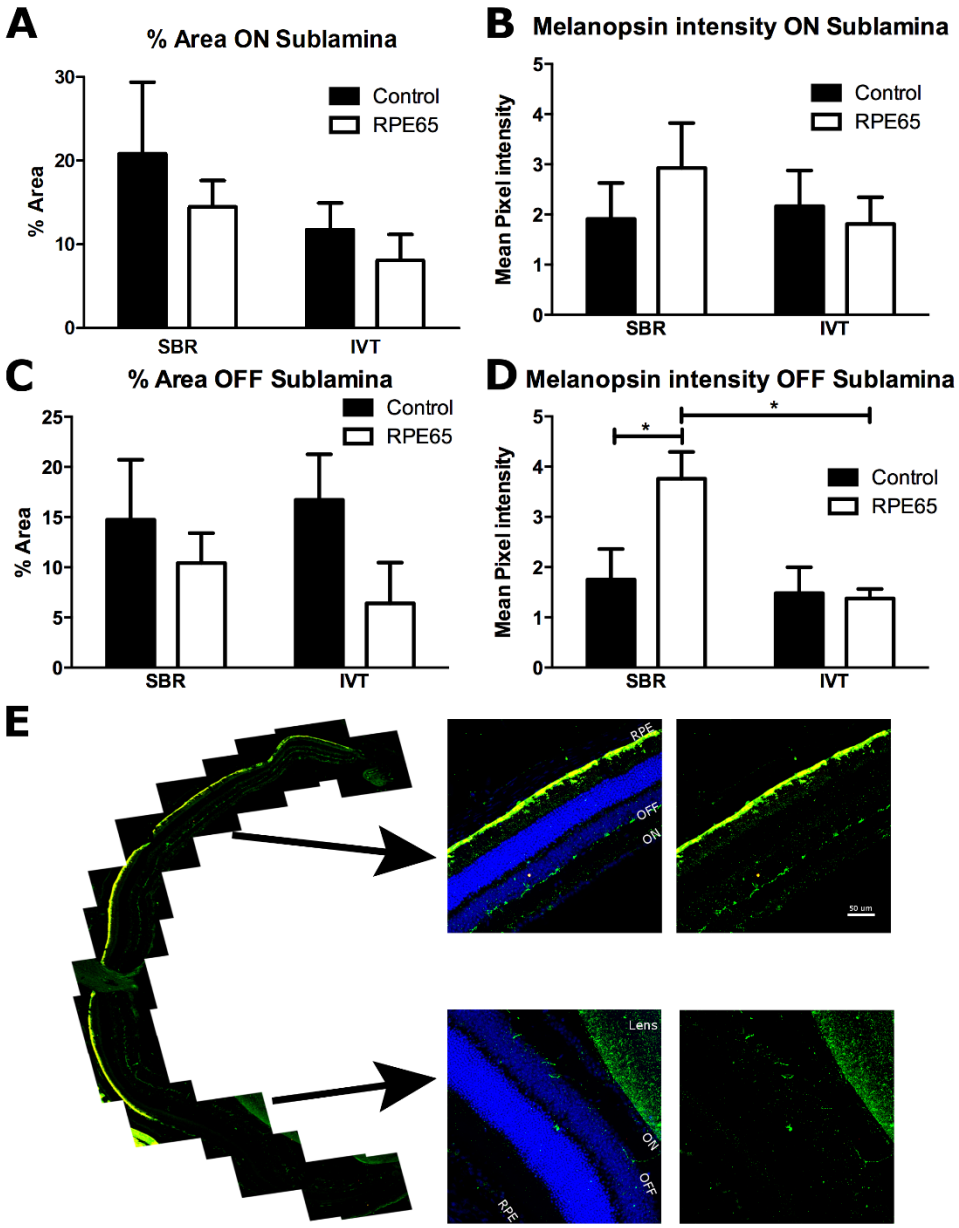

Figure 5.16 Melanopsin labelling in the on and off sublamina of iPL in rd12 mice treated with virus lacking venus.
A shows the percentage area covered by melanopsin^{+}-dendrites in the on sublamina in eyes receiving control virus (black) subretinally (SBR, n = 7) or intravitreally (IVT, n = 6) and eyes receiving virus encoding rpe65 (white) SBR (n = 8) or IVT (n = 4). B shows the average pixel intensity (above a pixel threshold of 20) in the on-sublamina. C shows the percentage area covered by melanopsin^{+}-dendrites in the off sublamina in eyes which received control virus SBR (n = 6) or IVT (n = 6) and eyes which received virus encoding rpe65 SBR (n = 6) or IVT (n = 6). D shows the average pixel intensity greater than 20 in the off sublamina. Asterisks indicate a significance level of $P < 0.05$, determined by post-hoc tests. E displays a sagittal section of the retina labelled for RPE65 (yellow) and melanopsin (green). Enlarged Images show an area of the retina with RPE65 labelling in the RPE and increased melanopsin labelling in the off sublamina (above) and an area where RPE labelling is absent, and reduced melanopsin labelling in the off sublamina (below). These higher magnification images are shown with nuclear marker, DAPI (blue, left, to illustrate retinal layers and without DAPI (right) to highlight melanopsin labelling. The scale bar indicates 50 µm.

5.4.4 Discussion

This experiment was a repeat of the last experiment without the venus gene. Venus is a fluorescent protein that emits green light at 530 nm (Nagai et al., 2002), which is within the spectral sensitivity of melanopsin (Berson et al., 2002). Thus, it was decided that the experiment should be repeated without the influencing factor of venus.

The BLA results were similar to those from the experiment 5.3. Both control-treated mice and mice which received the *rpe65* gene spent more time in the back half when the front half was illuminated compared to when the whole arena was in darkness, indicating the presence of BLA. However, there was no effect of the virus, as there was no significant difference between animals which received the virus encoding *rpe65* and the control virus. The BLA response provides a functional readout of both outer-retinal photoreceptors and ipRGCs, however, no improvements from receiving *rpe65* were detected with this method. There is also a lack of literature using this test for investigating restoration of visual function. Thus, there could be many factors unknown about restoring this behavioural function including restoration of vision in only one eye, or whether this behaviour can be restored, as it is confounded by many other factors such as anxiety and learned behaviour.

The PLR is another functional readout of outer-retinal photoreceptors and ipRGCs. A significant PLR in all treatment groups was seen at 800 µW/s/cm^2. At 80 µW/s/cm^2, eyes receiving the *rpe65* virus intravitreally no longer had a significant constriction, while other treatment groups did. Eyes receiving virus with *rpe65* subretinally had a significantly greater constriction than eyes which received virus with *rpe65* intravitreally and eyes receiving the control virus subretinally at both 80 and 800 µW/s/cm^2. There was no significant difference

between eyes receiving the control virus subretinally and those receiving the control virus intravitreally at either 80 or 800 μW/s/cm^2. At 800 μW/s/cm^2, eyes which received the virus with *rpe65* intravitreally had a significantly greater constriction than eyes receiving the control virus intravitreally at 30s post light onset, however, at 80 μW/s/cm^2, eyes which received the virus with *rpe65* intravitreally no longer had a significant constriction, while eyes which received the control virus intravitreally did. However, at this irradiance there was no significant difference between eyes receiving intravitreal injection of the control virus and those receiving the virus with *rpe65.* At 0.08 μW/s/cm^2, only eyes receiving subretinal injections of control virus or virus containing *rpe65* were examined. At this light power, both treatments had a significant constriction. Two-way ANOVA showed a significant difference between treatments, however, there was no significant difference in post-hoc tests. These results show a definite increase in the PLR in eyes which received *rpe65* subretinally. They had a significantly greater constriction at each light power examined.

The iPLR is a readout of melanopsin function and showed that while all treatment groups had a significant constriction, only eyes which received *rpe65* subretinally had a constant constriction that was maintained. They also had a significantly greater constriction compared to eyes receiving the control virus subretinally and eyes that received the virus with *rpe65* intravitreally. There was no significant difference between eyes which received the control virus subretinally and eyes which received the control virus intravitreally and no significant difference between eyes which received intravitreal injections of control virus and virus containing rpe65. These results are the same for the peak constriction. These results are more definitive than those from experiment 5.3, highlighting the effect of venus on melanopsin function and the importance of repeating this experiment.

Histology confirmed that RPE65-labelling is only found in the RPE of eyes which received virus containing the *rpe65* gene subretinally. In these eyes RPE65 labelling was seen to extend to the retinal rim, but was not found in the ciliary body/iris. In contrast, eyes which received the virus containing *rpe65* in the vitreous did not label positively for RPE65. These results along with the functional data show that RPE65 is only found in the RPE and that placing virus containing *rpe65* into the vitreous cavity cannot restore ipRGC function. Thus, the iPLR must require chromophore from the RPE.

Autofluorescent cells were found in the subretinal space on the apical side of RPE in eyes that received subretinal injections of *rpe65* or control virus. These cells are most likely macrophage but were not found in eyes which received intravitreal injections. The potential functional effects of these autofluorescent cells was examined by comparing eyes receiving the control virus subretinally to eyes receiving the control virus intravitreally. There was a trend towards greater constrictions in eyes which received the subretinal injection of control virus in both the PLR and the iPLR.

An interesting observation found in the melanopsin expression pattern was an increase in the intensity of melanopsin in the off sublamina of eyes that received *rpe65* subretinally. Topographically, within retinal sections, it was clear this increase in the melanopsin labelling intensity occurred potentially in areas where the RPE labelled positively for RPE65. There was no effect on the dendrites in the on sublamina of IPL and no significant differences were found in either the density of melanopsin^{+}-cells or in the intensity of melanopsin labelling in the cell somas.

M1 ipRGCs are the only sub-type of ipRGC to stratify exclusively in the off sublamina. While M3 ipRGCs can also stratify in the off sublamina, they are rare

and do not label strongly for melanopsin (Schmidt and Kofuji, 2011). M1 ipRGCs rely on intrinsic responses more than extrinsic (Schmidt and Kofuji, 2010), suggesting that they rely more heavily on chromophore than other subtypes and this perhaps is why the increase in chromophore in *rd12* eyes receiving subretinal *rpe65* gene therapy had a selective improvement on the dendrites of M1 ipRGCs. Brn3b-negative M1 ipRGCs have functions in the entrainment of the circadian clock (Berson et al., 2002, Provencio et al., 2000, Lucas et al., 2003, Lupi et al., 1999), and project into the suprachiasmatic nucleus of the hypothalamus, the primary pacemaker in mammals (Baver et al., 2008, Chen et al., 2011). Brn3b-negative ipRGCs also have projections from the retina into the ciliary body in mice (Semo et al., 2014), which may mediate the iPLR.

Thus, it can be concluded from this experiment that the iPLR is driven by chromophore from the RPE and that M1 ipRGCs may mediate this response, as they appear to respond to RPE-driven chromophore with enhanced melanopsin expression.

5.5 General Conclusions

This chapter was constructed to determine if ipRGCs require chromophore from the RPE to initiate the iPLR. Rods and cones have many physical connections with the RPE aiding chromophore transportation, however, ipRGCs are situated in the inner retina and separated from the RPE by many layers of cells. While melanopsin has been reported to work as a bi-stable pigment (Melyan et al., 2005, Fu et al., 2005), this is insufficient to drive a normal iPLR in the *rd12* mouse, as reported in chapter 4. In experiment 4.5, it was shown that by supplementing the *rd12* mouse with 9-*cis* retinal the iPLR can not only be fully restored but the pupil constricts significantly more than that of the WT. This raised the question of

whether this supplementary chromophore was acting on ipRGCs in the retina or more directly on an opsin in the iris/ciliary body. This question was addressed in the first experiment of this chapter. Supplementary chromophore was only able to improve the iPLR when retina was attached to the anterior chamber and was unable to drive the iPLR in an isolated anterior chamber. Interestingly, the iPLR with anterior chamber with 1mm retina was much smaller than whole eye preparations from *rd12* treated with 9-*cis* retinal, this may suggest that the iPLR is driven by the whole retina and not just the melanopsin rim, however this would have to be investigated further. While this experiment strongly suggests that chromophore acts on the retina to produce the iPLR, it did not prove that the RPE is the source of this chromophore. However, there was no evidence of RPE65 labelling in the iris in WT retina, an observation that strongly implicated the RPE as being the site of chromophore production under normal circumstances.

In chapter 4 it was shown that chromophore supplementation significantly improved the iPLR in *rd12* mice, which suggested that melanopsin requires a source of chromophore to drive the iPLR and that the bi-stable property of melanopsin (Melyan et al., 2005, Fu et al., 2005) is insufficient to drive a normal iPLR. The source of this chromophore was investigated in this chapter. As ipRGCs lie on the vitreous side of the retina, and the RPE is located in the outer retina, by placing a virus encoding the *rpe65* gene in the vitreous in *rd12* mice and comparing melanopsin function with *rd12* mice receiving the *rpe65* gene subretinally (beside the RPE), it was determined that *rpe65* in the RPE caused a significant improvement in melanopsin function. This was not the case when *rpe65* was delivered in the vitreous, closer to ipRGCs, with no difference in melanopsin function compared to that seen following injection of a control virus. Anatomically, this was explained by the fact that labelling for RPE65 was only

seen in eyes receiving a subretinal injection of virus encoding *rpe65* with expression of this protein restricted to the RPE layer.

The expression of venus revealed the extent of retinal cells infected by the virus. This illustrated that intravitreal injections, while able to infect the neural retina, did not infect the RPE. Also, while many cell types expressed the venus reporter, only the RPE labelled for RPE65. Both venus and *rpe65* used the same constitutive CAG promoter, with the *rpe65* gene coming before the venus gene. As such, in eyes receiving the virus containing *rpe65*, wherever venus is expressed*, rpe65* would have been expected to be transcribed in the same cells. However, RPE65 labelling was not detected in all cells expressing venus suggesting that not all cells can produce RPE65 from the mRNA.

ERGs provide a functional readout of outer-retinal photoreceptors. While positive trends were seen in both scotopic and photopic ERGs, this was not-significant, except at 0 Lg cd.s/m^2, where, the scotopic b-wave amplitude was significantly greater in eyes treated with *rpe65* subretinally. This is possibly due to the age that the *rd12* mice were treated, as it has been reported that the earlier the treatment, the greater the ERG rescue and that gene therapy at 3 months was not able to rescue the ERG (Pang et al., 2010, Li et al., 2011, Nusinowitz et al., 2006). At 3 months, it was shown in chapter 4 that there are still many rod photoreceptors present and while rescue of scotopic ERG was not significant using gene therapy, it was significantly improved with supplemented chromophore.

BLA provides a functional read out of outer retinal photoreceptor function and melanopsin function. While animals that received the virus exhibited a BLA response, there was no significant difference found between animals receiving the virus containing *rpe65* and animals receiving the control virus. These results

were similar whether the virus contained venus or not. As each animal received an injection of virus subretinally into the left eye and an intravitreal injection into the right eye, this readout could not determine an effect of the site of injection.

The PLR provides another functional readout of outer-retinal photoreceptors and ipRGCs, however, this readout did allow for comparisons between intravitreal and subretinal injections. The results of experiment 5.3 (with venus) and 5.4 (without venus) both showed that eyes which received *rpe65* delivered subretinally had a significantly greater constriction compared to eyes which received the control virus and eyes which received virus with *rpe65* delivered intravitreally at each irradiance. However, there was also a strong effect of the venus reporter, which is seen at 800 µW/s/cm^2, the brightest light power examined. At 800 µW/s/cm^2, eyes receiving the control virus subretinally or intravitreally and eyes which received virus with *rpe65* intravitreally had an average peak constriction of 0.4 – 0.42 with venus, this was reduced to 0.58 – 0.67 without venus.

The iPLR is a readout of melanopsin function (Xue et al., 2011, Semo et al., 2014). While both experiments 5.3 (with venus) and 5.4 (without venus) show that eyes receiving *rpe65* subretinally had the greatest constriction, this failed to reach statistical significance in experiment 5.3 where venus is expressed. The effect of venus on the iPLR is strong; treatment groups had a 13 – 23% greater constriction when the virus contained venus. Experiment 5.4, which used virus without venus showed that while all treatment groups had a significant constriction, only eyes which received *rpe65* subretinally had a robust constriction that was maintained. They also had a significantly greater constriction compared to eyes which received the control virus subretinally and eyes which received the virus with *rpe65* intravitreally. There was no significant difference between eyes receiving the control virus subretinally and eyes receiving the control virus

intravitreally and no significant difference between eyes receiving intravitreal injections of control virus and virus containing rpe65. These results were the same for the peak constriction and collectively were much more definitive than experiment 5.3, highlighting the effect of venus on melanopsin function and the importance of repeating this experiment. It is clear from experiment 5.4 that the iPLR is driven by chromophore from the RPE.

The expression of *rpe65* in host RPE cells increased the melanopsin labelling intensity in M1 ipRGCs. M1 ipRGCs contain the most melanopsin under normal conditions and are thought to rely on their intrinsic responses more than extrinsic inputs from rods and cones (Schmidt and Kofuji, 2010). This suggests that M1 ipRGCs rely more heavily on chromophore than other subtypes of ipRGC and perhaps this is why the increase in chromophore in *rd12* mice receiving *rpe65* gene therapy subretinally had particular effect on M1 ipRGCs.

Thus, it can be concluded from this experiment that the iPLR is driven by chromophore from the RPE and that M1 ipRGCs also receive chromophore from the RPE.

Chapter 6 Discussion

6.1 The importance of the RPE

The RPE lies in the outer-retina adjacent to POS and acts as a support cell for outer-retinal photoreceptors. The RPE separates the retina from the blood supply (Tornquist et al., 1990). The RPE cells have tight junctions on their lateral side, making diffusion between cells difficult. This acts as part of the BRB preventing blood leaking and the infiltration of immune cells, selectively supplying rods and cones with oxygen, glucose, ions, metabolites and vitamin A from the blood.

RPE cells have an apical and basal polarisation. The basal membrane is a component of Bruch's membrane and interacts with the choroid. The apical membrane has large microvilli, which extend to surround the POS. This is important to facilitate close communication between RPE and photoreceptors to optimise RPE functions that enhance photoreceptor performance, including the secretion of pigment endothelium-derived factor (PEDF), which inhibits the growth of blood vessels and prevents apoptosis (Cayouette et al., 1999). Photoreceptors have a very high metabolic rate and accumulate toxic photo-oxidative compounds due to the high light exposure, so they shed the tips of the POS every day and constantly renew the POS to maintain photoreceptor health. The long RPE apical processes phagocytose the shed POS and recycle useful components such as 11-cis-retinal, while, waste is excreted to the choroid.

The RPE also absorbs toxins to prevent neurotoxicity of photoreceptors. Upon activation by light, extracellular glutamate is taken up by the RPE to prevent non-specific stimulation during the light phase. Excess light is absorbed by the RPE for visual clarity by preventing light from reflecting into the retina. The RPE

contains a pigment called melanin, which absorbs the excess light and gives the RPE a dark colour. Water is pumped out of the retina by the RPE to maintain the retina in a proper state of hydration for visual clarity. These supporting roles of the RPE help to keep a healthy environment for photoreceptor survival.

The RPE also plays a crucial role in vision by recycling vitamin A (all-*trans*-retinol) into 11-*cis* retinal, which forms the visual pigment with the opsin in photoreceptors, allowing for the detection of light. All-*trans*-retinol is sourced from the diet transported to the RPE via the choroid. It is esterfied by LRAT to all-*trans*-retinyl ester and then hydrolysed and isomerised by RPE65 to form 11-*cis*-retinol (Redmond et al., 1998). This is oxidised by 11-*cis*-retinal dehydrogenase to form 11-*cis*-retinal and subsequently transported to photoreceptors. In the photoreceptor 11-*cis*-retinal sits in the opsin to form the visual pigment. Upon illumination, 11-*cis*-retinal changes to all-*trans*-retinal and is then reduced by RDH to form all-*trans*-retinol, at which point it is transported back to the RPE for recycling. Mutations in *lrat* or *rpe65* can result in many retinal degenerative diseases, such as retinitis pigmentosa and Leber's congenital amaurosis (Morimura et al., 1998, Marlhens et al., 1997, Sweeney et al., 2007, Fan et al., 2008, Senechal et al., 2006).

With such a strong dependence on the RPE for photoreceptor function it is unsurprising that many diseases resulting in photoreceptor degeneration are primarily diseases of the RPE and many genes involved in the visual cycle can result in blindness. AMD is the leading cause of blindness in the developed world and is recognised as a disease of the RPE. The exact pathology and causes of AMD are not fully understood. There are many genes associated with the disease but no single gene accounts for all cases of the disease. There are also many environmental factors, such as smoking, diet and age, which contribute to the risk

and severity of the disease. This makes treating the source of the disease difficult. Replacement of RPE cells using stem cells is currently being validated as a suitable treatment for AMD (Schwartz et al., 2012, Carr et al., 2013, Nommiste et al., 2017, Kamao et al., 2014, Reardon and Cyranoski, 2014, da Cruz et al., 2018). Stem cells provide a means of regenerative medicine by replacing damaged or lost tissue. Human embryonic stem cells (hESC) are stem cells derived from the inner cell mass of a blastocyst, an early-stage embryo (5 days post fertilisation). These cells are pluripotent and as such, can develop into any cell type in the body (Thomson et al., 1998) baring gametes. They are also renewable, such that stem cells derived from one blastocyst can produce cells to treat many patients. HESC-RPE cell shape, organisation and phenotype are almost identical to that of human macular RPE cells, which makes these cells prime candidates for cell therapy in AMD (Vugler et al., 2008a).

To date, the majority of RPE cell transplant studies have been carried out on the RCS rat, a model of retinal dystrophy with progressive and early photoreceptor loss (Dowling and Sidman, 1962). The RCS rat has a mutation in *mertk,* a gene responsible for the phagocytosis of POS. This results in accumulation of shed POS, creating a debris zone and consequent separation of photoreceptors and RPE, resulting in fast photoreceptor degeneration (D'Cruz et al., 2000). This model of retinal degeneration was discovered almost 80 years ago, and it is a well-studied model. However, the RCS rat is a less than ideal model for studying the effects of RPE cell transplantation due to the early onset and fast rod and cone degeneration, making full visual restoration difficult. The death of RGCs in the RCS rat is also quite extensive and to date transplantation has failed to prevent RGC pathology (Klassen et al., 2001). Photoreceptor preservation and improved visual function in RCS rats has been improved by cell transplantation.

However, improvements can be achieved by an array of cells, including hESC-RPE cells (Idelson et al., 2009, Zhu et al., 2013), iPS-RPE cells (Carr et al., 2009, Krohne et al., 2012), human RPE cells (Little et al., 1996), rat RPE cells (Jiang and Hamasaki, 1994), ARPE-19 cells (Coffey et al., 2002), but also, neural progenitors (Wang et al., 2008) and Schwann cells (Lawrence et al., 2000). Thus, identifying RPE-specific therapeutic effects is complicated as many studies show that photoreceptor survival is most likely due to trophic effects. This is supported by areas of photoreceptor rescue larger than the graft of human RPE cells and Schwann cells (Wang et al., 2005), suggesting the diffusion of trophic factors is responsible for cell survival. In this thesis two mouse models, $NaIO_3$ and *rd12* are examined as alternative models for studying RPE cell transplantation.

6.2 Is sodium iodate a suitable model for studying RPE cell transplantation?

A major issue with RPE cell transplantation is achieving cell integration. Many animal models do not mirror the RPE cell loss seen in dry AMD, in which photoreceptors die subsequent to RPE cell death. In many studies involving sub-retinal transplantation into rodent models where host RPE cells remain, the grafted RPE cells clump together to form a bolus of cells and do not sit down in a monolayer (Carido et al., 2014, Li and Turner, 1991, Seaton and Turner, 1992, Sheedlo et al., 1991, Carr et al., 2009). Studies have shown that RPE cells undergo apoptosis in the absence of a suitable substrate to attach to (Tezel and Del Priore, 1997, Tezel et al., 2004). This is known as anoikis. In human, it is possible to surgically remove RPE and this occurs with AMD progression in the form of geographic atrophy. However, due to the small size of a rodent eye, physical removal of the host RPE prior to grafting is unfeasible, but chemical

removal of the RPE is feasible. However, the loss of RPE cells prior to transplantation will damage the BRB (Wenkel and Streilein, 1998) which can complicate donor cell survival.

Sodium iodate ($NaIO_3$) is a drug, which is selectively toxic to the RPE and causes RPE cell necrosis. Benefits of using $NaIO_3$ to create a model of retinal degeneration include it's selective effects on the RPE after a single administration and the rapid onset of RPE cell death, with oedema observed 1 hour after administration via the tail vein (Hariri et al., 2013). This selective death of the RPE is followed by photoreceptor cell apoptosis.

It was determined in this thesis that the route of administration of $NaIO_3$ had a large effect on the efficacy of $NaIO_3$. Administering $NaIO_3$ IP created varied results. Animals that received the same dose of $NaIO_3$ could have either flatline ERG recordings or an ERG that fell within normal parameters. Thus, this route of administration was deemed unsuitable for this study. Administering $NaIO_3$ retro-orbitally to the right eye, gave a consistent result of a significantly diminished scotopic and photopic ERG. While $NaIO_3$ was only administered to the right eye, no statistical difference in ERG recordings was seen between right and left eyes. At 1 month after $NaIO_3$ administration no RPE65 labelling was identified and S-opsin was strikingly reduced and mislocated to the PIS and ONL. However, rhodopsin labelling was still present in the POS at 1 month and ~ 7 layers of cells in the ONL remained. These results may be attributed, at least in part, to the loss of chromophore, as rods are present but their function is almost completely lost. It has been seen in *rpe65*$^{-/-}$ mice that cones are lost first and their opsin mislocates because cone opsin requires chromophore for correct folding and trafficking (Rohrer et al., 2005).

The ability to restore retinal function in $NaIO_3$-treated mice was tested by scotopic ERG recordings following chromophore supplementation. This will only bypass one function of the RPE, however, if improvements were seen then photoreceptors and retinal circuitry are still functional and restoration may be possible. At 3 days following $NaIO_3$ treatment an improvement in the scotopic ERG was only seen in half of the animals by chromophore supplementation and by 7 days 9-*cis* retinal treatment failed to show any improvements in the scotopic ERG. Interestingly, by 30 days after $NaIO_3$ administration, when the ERG has almost flatlined, 9-*cis* retinal was able to rescue a lot of retinal function and significantly increased the a- and b-wave amplitude. It is unknown why chromophore did not improve the ERG at earlier time points. Although, improvements to the RPE and retinal function have been reported 1-3 months following $NaIO_3$ administration (Franco et al., 2009, Kiuchi et al., 2002, Machalinska et al., 2013, Redfern et al., 2011).

Given these results, it was decided to transplant RPE cells at 3 weeks following $NaIO_3$-treatment, in the hope that a delay in treatment, may be a favourable environment for retinal recovery. Carido and colleagues transplanted hESC-RPE cells 7 days after $NaIO_3$ treatment and saw RPE cell integration, but no functional recovery by ERG (Carido et al., 2014), which also guided the decision to transplant at a later timepoint. Unfortunately, eyes receiving hESC-RPE cells showed no improvements in ERG recordings 3 weeks after the transplant and no hESC-RPE cells were found to survive in the retina, although, it was shown that functional rescue was possible by chromophore supplementation.

Thus, as of yet, $NaIO_3$ has not proven to be a suitable model for studying functional benefits of RPE cell transplantation. However, an important factor to consider is the loss of choroid following RPE damage seen in AMD (McLeod et

al., 2009, McLeod et al., 2002). Without a healthy blood supply, it may be very difficult to recover retinal function, although, this is a factor seen in AMD and therefore an important factor to consider when treating AMD patients with RPE cell transplantation.

Interestingly, the melanopsin function does not appear to be as affected as the function of outer-retinal photoreceptors. The PLR in $NaIO_3$-treated animals is still quite robust at 1 month, although the constriction is reduced compared to WT. The greatest deficit in the PLR is seen at low light powers and the maximum constriction graph resembles that seen in *rd/rd cl* mice (Lucas et al., 2003), where melanopsin drives the PLR at high irradiances and cannot drive a constriction at lower irradiances of 11 log photons/cm^2/s, comparable to the 0.8 µW/cm^2/s used in this study. However, while the PLR at high light powers is still quite robust, the constriction does fall short of that seen in WT, suggesting that there may be a small loss to melanopsin function. Interestingly, ipRGCs that innervate the OPN core are Brn3b-positive and stratify in the on sublamina of IPL (Hattar et al., 2002, Morin et al., 2003, Hattar et al., 2003, Lucas et al., 2003, Chen et al., 2011, Baver et al., 2008, Guler et al., 2008), which corresponds to the loss of melanopsin expression seen in the on sublamina of IPL following ,$NaIO_3$ administration in chapter 3.

While the study of $NaIO_3$, may or may not prove to be useful for studying RPE cell transplantation, it could be a potentially important source of information for studying the effects of RPE cell loss, seen in AMD, particularly with reference to the melanopsin system.

6.3 *Rd12*: A model of LCA2

The second model studied in this thesis is the *rd12* mouse. This is a naturally occurring mouse model of LCA2 (Pang et al., 2005), which has a mutation in the gene for RPE65, also seen in LCA2 patients (refSNP cluster report: rs368088025), making it a clinically relevant model. LCA2 is characterised by early onset of central vision loss, sensory nystagmus, amaurotic pupils and absent signals on electroretinography (ERG). It is one of the earliest and severe forms of inherited retinal dystrophies. The *rd12* mice were repeatedly backcrossed to a WT, C57BL/6J, to make a congenic inbred strain and C57BL/6J are accepted as a WT control when assessing *rd12* mice (Pang et al., 2005). The *rd12* mouse has a very similar phenotype to the previously described *rpe65*$^{-/-}$, except that the *rd12* develops distinctive white dots throughout the retina that become apparent at around 5 months of age, similar to those seem in LCA2 patients (Pang et al., 2005). This characteristic of the *rd12* mouse makes it a better model for human LCA2, as they are more likely to simulate the actual disease mechanism.

While the *rd12* mouse has significant loss of retinal function from an early age, it also exhibits a slow retinal degeneration, which are ideal features for attempting to recover retinal function. The first sign of the *rd12* morphology has been reported at 3 weeks when lipid-like droplets are found in the RPE. At 6 weeks, occasional voids start to appear in the POS and by 3 months these voids become obvious, and much larger lipid-like droplets appear (Pang et al., 2005). In this thesis rhodopsin was found located in the POS in *rd12* at 3 months. It has been published that rhodopsin spectral absorbance is not detected in the *rd12* mouse (Pang et al., 2005), however, rhodopsin protein presence and location have not been previously reported in *rd12* mice by immunohistochemistry.

While rods have a slow degeneration, cones are reported to be lost early in the *rd12* mouse; by P21, the PNA-lectin positive cone count was reportedly reduced to 55% of that seen in WT, however, cones lose opsin before cone death (Li et al., 2011), so the surviving cones may no longer be functional. By P90 PNA-positive cone counts were reportedly reduced to 16% that of WT, and only 15% of these express M/L-opsin, while no S-opsin was seen (Li et al., 2011). However, in this thesis, no M/L cones opsin was seen at 3 months and S-opsin was detected although it was mislocalised to the PIS and ONL. These discrepancies may be due to different techniques used (flatmount and retinal section) and/or different antibodies used.

This mislocation of cone opsin and cone loss may be due to the requirement of chromophore for correct opsin folding and trafficking (Bandyopadhyay et al., 2013). And, the timeline of cone loss observed in the literature (Li et al., 2011, Pang et al., 2010) coincides with WT development of peak expression of RPE65 (Bowes et al., 1988, Manes et al., 1998, Hamel et al., 1993) and the development of the ERG (Bakall et al., 2003). It has been reported that the scotopic ERG starts to diminish as early as 3 weeks in the *rd12* mouse with both scotopic and photopic ERGs decreasing with age (Pang et al., 2005, Pang et al., 2006). In this thesis, only a small scotopic b-wave was recorded at high light intensities in the 3-month old *rd12.* A more robust photopic ERG was recorded, although, it is known that this is rod driven (Seeliger et al., 2001, Cachafeiro et al., 2010, Dai et al., 2015). The lack of RPE65 in *rd12* mice allows rods to function at brighter light intensities without bleaching. Interestingly, patients with mutations in *rpe65* have similar ERG patterns (Lorenz et al., 2000).

The *rd12* mutation also influences the melanopsin system. This was first indicated by the absence of a negative masking effect in *rd12* mice (Thompson et al.,

2008). It has also been shown that *rpe65*$^{-/-}$ mice have a shifted circadian behaviour, which was corrected when exposed to increased illumination (Doyle et al., 2006). In this thesis, a loss of melanopsin^{+}-cells and a loss in melanopsin expression was recorded in 1-month old *rd12* mice. Also, melanopsin function is significantly reduced. The BLA response which is driven by both outer-retinal photoreceptors and ipRGCs is present at 1 month, but is lost by 3 months. The PLR, which is also driven by outer-retinal photoreceptors and melanopsin (Lucas et al., 2003), was shown to be significantly reduced in the 3-month old *rd12* mouse. A response is only seen at high light levels, where the WT has an almost total pupil constriction. Comparing these results to those published by Lucas et al, it suggests that both outer-retinal photoreceptors and ipRGC have reduced function in the *rd12* (Lucas et al., 2003). The iPLR is a functional readout selective for melanopsin function (Semo et al., 2014, Xue et al., 2011) and was also significantly reduced in the 3-month *rd12* mouse, where it only produces a small constriction.

The effects of the *rd12* mutation and $NaIO_3$ are similar when studying outer-retinal photoreceptors; cones are lost early, their opsin becomes mislocated to PIs and ONL, rods survive longer but their function is severely reduced. Scotopic ERGs are severely diminished but photopic ERGs are more robust, thus, a lot of this can be attributed to the loss of chromophore. However, the severe loss of melanopsin function in the *rd12* mouse is in contrast to results seen in the $NaIO_3$ model, while some loss to melanopsin function was seen, the PLR results suggested that the melanopsin function remains quite robust 1 month after $NaIO_3$-treatment. One possible explanation is that $NaIO_3$ has its strongest effect at the posterior pole and it is possible that melanopsin at the retinal rim is less

affected and driving the PLR, while the ERG is a whole field recording of the outer-retinal photoreceptors.

The *rd12* mouse has been used as a model for retinal rescue in many studies, however, most of these are by gene therapy (Nusinowitz et al., 2006, Li et al., 2011, Pang et al., 2010). While testing gene therapy was not the objective of this thesis, these positive results by other groups reassure that retinal rescue is achievable in this model. Pang et al initiated gene therapy at P14 with a rAAV5-CBA-hRPE65 vector, which resulted in RPE65 expression over large areas of the RPE, rhodopsin levels (measured by spectral absorbance) restored to 70% of WT levels and ERG signals restored to approximately 66% that of normal values when assayed at 7-months of age (Pang et al., 2006). Early treatment with gene therapy has been shown to keep remaining cones alive and to rescue opsin expression in these cones (Li et al., 2011). In animal models of RPE65 deficiency, rods undergo a slow progressive degeneration, and restoration of rod vision appears to be possible over a broad range of ages.

In contrast to the widespread usage of this model in gene therapy studies, the *rd12* mouse is an under-utilised animal for cellular therapies. Even though *rd12* is a model of LCA, stem cell work on this model can be translated to many other forms of retinopathy, such as testing RPE cell transplantation for application in age-related macular degeneration. Li and colleagues injected iPSC-derived RPE cells subretinally into 2-day old albino *rd12* mice and showed the presence of pigment in the RPE at 5 months, unfortunately, this does not confirm integration as host RPE cells could phagocytose melanin from dead iPSC-RPE cells and these pigmented RPE cells were not labelled for any human markers. iPSC-RPE cells were also injected into *rd12* mice crossed with *Prkdc*^{scid}/*Prkdc*^{scid} mice for a double homozygous with both SCID and *rpe65* mutation. While increased b-wave

amplitude was seen, the a-wave was still absent and the presence of grafted RPE was not shown in these animals (Li et al., 2012b).

In this thesis, functional recovery was tested, prior to RPE cell transplantation, by providing chromophore in the form of 9-*cis* retinal, to determine if the remaining photoreceptors were functional. Rod function was examined by scotopic ERG and ipRGC function was assessed by analysing the iPLR, this allowed separation from cone function, which is likely to be the most difficult function to restore (as they undergo a faster degeneration). Supplementation with 9-*cis* retinal provided a significant increase in both scotopic a- and b-wave amplitudes, although this was at the cost of longer latency and implicit time. The amplitudes were significantly lower than WT. The loss of amplitude signifies the level of rod degeneration at 3 months in the *rd12* retina. The longer latencies could indicate problems with remaining photoreceptor function and synaptic connections in the retina. Interestingly, these longer latencies were also seen in the $NaIO_3$ model, which also has a primary pathology in the RPE.

Interestingly, while 9-*cis* retinal only partially recovered the *rd12* scotopic ERG, the synthetic chromophore produced a super constricted iPLR. Normal *rd12* mice have a significantly diminished iPLR, however, 9-*cis* retinal drives this constriction to surpass that of WT and with at a significantly shorter latency. This suggests that the pathway of the iPLR is fully developed and intact in *rd12* mice. This was unexpected as the melanopsin expression is significantly lower in the *rd12* retina and the response from the rods in the scotopic ERG in *rd12* with 9-*cis* retinal was not as strong as untreated WT. This suggests that the iPLR function is only diminished due to the lack of chromophore and an increase in chromophore results in an increased constriction. This ability of 9-*cis* retinal to recover the iPLR was still seen at 12 months, suggesting a strong preservation of this functional

pathway. Interestingly, latency is increased in the *rd12* iPLR with age and pupil re-dilation after lights-off was lost in aged mice. However, as the mechanism of the iPLR is largely unknown, it is difficult to speculate why this effect of age is seen, especially when this was not reported in aged WT or *rd* mice (Vugler et al., 2015). However, these mice were only 9-months old and this may count for a difference, when comparing them to mice used in this study, which were 12 months old.

Given the improvements seen in the scotopic ERG following injection of 9-*cis* retinal, hESC-RPE cells were transplanted into the subretinal space and some improvements were seen in the scotopic ERG and the PLR. It is difficult to determine if the PLR improvements seen were from outer-retinal photoreceptors or ipRGCs. While the iPLR distinguishes these two, it was not recorded on these animals as it was decided that fixation of tissue by perfusion is ideal for preservation of grafted cells. Unfortunately, no hESC-RPE cells were found in the subretinal space of eyes which received the graft. A pigmented mass was found in many transplanted eyes; however, this did not stain positive for human mitochondria. The *rd12* mouse is an interesting alternative to the RCS rat as a model for studying RPE cell transplantation. Due to the severely reduced retinal function, chromophore-mediated improvements can be detected. However, more research needs to be carried out to improve RPE cell graft integration and survival in this model. The possibility of combining the *rd12* and the $NaIO_3$ models was not explored in this thesis, due to limitations on time and the number of animals, although, smaller doses of $NaIO_3$ would need to be explored and it is still unclear if normal retinal function can be restored following $NaIO_3$ insult.

6.4 Does the RPE supply chromophore for ipRGCs

The reliance of outer-retinal photoreceptors on the RPE and the visual cycle is very clear. Without the visual cycle outer-retinal photoreceptors have severely reduced function and start to degenerate. This relationship is less clear with ipRGCs. In the *rd12* mouse, melanopsin function is significantly reduced, however, removal of the RPE with $NaIO_3$, reveals a much more robust melanopsin driven PLR. A key difference in these two models may lie in the development of the melanopsin system. The PLR becomes fully developed around P10 (McNeill et al., 2011), which is when RPE65 expression becomes stable in mice (Bowes et al., 1988). The reduction of melanopsin^{+}-cells and melanopsin labelling in *rd12* mice did not significantly change from 1 to 8 months, thus this reduction appears most likely to occur during development.

Mice without a functioning visual cycle have a PLR less sensitive than that of *rdta or rd1 mice* (Tu et al., 2006), this shows that melanopsin function is reduced by the loss of chromophore and not just the loss of outer-retinal photoreceptors. In fact, the loss of outer-retinal photoreceptors can improve melanopsin function. *Rdta* mice, with selective deletion of rods exhibited an increased magnitude of circadian phase shift compared to WT controls and displayed tonic activation of RGCs (Lupi et al., 1999). Furthermore, selectively knocking out rods along with visual cycle (*rpe65*$^{-/-}$*:rdta* or *lrat*$^{-/-}$: *rd/rd*) improves circadian photosensitivity (Doyle et al., 2006) and knocking out rods and *rpe65* or *lrat* improves the PLR compared to *rpe65*$^{-/-}$ or *lrat*$^{-/-}$ alone (Tu et al., 2006). Perhaps these effects are seen following an increase in chromophore, which otherwise would be taken up by rods. Evidence of competition for chromophore is also seen in R91W knock-in mice, which can only produce small amounts of 11-*cis* retinal, with selective ablation of rhodopsin resulting in the correction of cone opsin localisation

(Samardzija et al., 2009). Rods are more numerous and contain more opsin, thus, they compete favourably for chromophore.

It is not clear how ipRGCs get 11-*cis* retinal, as they are located in the inner retina and are separated by several layers of cells from the RPE in the outer retina, the classic site of 11-*cis* retinal isomerisation. Perhaps, 11-*cis* retinal diffuses through the retina. Another possible theory is that Müller cells, which have been recognised to play a role in opsin cycling for cones (Wang and Kefalov, 2011), regenerate chromophore and/or transport chromophore to the inner retina. There is evidence to support the ability of 11-*cis* retinal production in Müller cells (Das et al., 1992, Fleisch and Neuhauss, 2010). Müller cells span the thickness of the retina and have been reported to be closely associated with ipRGCs but not non-melanopsin ganglion cells (Viney et al., 2007). It has also been shown that photoresponses from ipRGCs in isolated retina are less sustained when Müller glia are poisoned with a specific gliotoxin (Zhao et al., 2016).

Melanopsin has also been reported to work as a bi-stable pigment, with photoisomerase capacity generating 11-*cis* retinaldehyde from all-*trans* retinaldehyde upon exposure to long wavelength light (Melyan et al., 2005, Fu et al., 2005). However, this would appear insufficient for driving normal melanopsin function in *rd12* mice, albeit that these mice have significantly reduced levels of melanopsin protein (assessed by immunostaining).

Different ipRGC subclasses also have a different reliance on chromophore directly, as some ipRGCs rely more on extrinsic responses and input from the outer-retinal photoreceptors (Zhao et al., 2014, Dacey et al., 2005, Schmidt et al., 2008, Weng et al., 2013, Zhang et al., 2008). These extrinsic inputs allow ipRGCs to activate the correct brain regions even in the absence of melanopsin, where ipRGCs lose their intrinsic photosensitivity (Lucas et al., 2003, Wong et al., 2007).

IpRGCs can be subdivided into five subtypes, M1, M2, M3, M4 and M5. M1 ipRGCs, express the highest level of melanopsin and rely on intrinsic responses more than extrinsic (Schmidt and Kofuji, 2010). They are the only sub-type to stratify exclusively in the off sublamina of the IPL (Zhang et al., 2012, Zhang et al., 2008). M1 ipRGCs also have projections from the retina into the ciliary body in mice, which, may mediate the iPLR (Semo et al., 2014). M2-M5 express lower levels of melanopsin and rely on extrinsic synaptic responses more than intrinsic (Schmidt and Kofuji, 2010), sending axons to the OPN, which control the PLR (Chen et al., 2011, Hattar et al., 2002, Morin et al., 2003, Hattar et al., 2003, Lucas et al., 2003, Baver et al., 2008, Guler et al., 2008). Cones bleach and compensate for high levels of light, this means that they do not communicate irradiance levels. Melanopsin can communicate high irradiance levels much more accurately and is necessary for a complete PLR (Lucas et al., 2003).

An intrinsic pathway also controls the PLR in rodents, bypassing the OPN. Melanopsin and an intact CMZ are necessary for a complete iPLR response (Semo et al., 2014, Xue et al., 2011). The iPLR cannot be generated by cones and is unaffected by cone loss, however rod function and pigmentation appear to be essential for normal iPLR development in mice (Vugler et al., 2015). The iPLR develops progressively from P21-49 in mice (Vugler et al., 2015), much later than the PLR (McNeill et al., 2011). This may be due to late maturation of Brn3b-negative M1 ipRGCs, which innervate the ciliary body, as it is known that these Brn3b-negative M1 ipRGCs mature their projections into the SCN around P21 (McNeill et al., 2011).

The effect of chromophore supplementation on ipRGC function has been shown in single cell recordings (Fu et al., 2005) and also in this thesis by the super constriction recorded in chromophore-supplemented isolated *rd12* eyes. It is

known that the iPLR requires melanopsin to function (Semo et al., 2014, Xue et al., 2011) and therefore the supplemented chromophore, which created a super constriction in the *rd12* mouse, most likely acted on melanopsin directly. Importantly, supplementary chromophore was only able to improve the iPLR when retina remained attached to the anterior chamber, being unable to drive the iPLR in an isolated anterior chamber. Thus, it was shown that the chromophore was most likely acting on ipRGCs in the retina.

As the importance of chromophore for ipRGC function and the iPLR was established, the source of that chromophore was then investigated. As it is known that RPE65 is required for chromophore production in normal mice, the location of RPE65 was examined and there was no evidence of RPE65 labelling outside the RPE in WT retina. As ipRGCs lie on the vitreous side of the retina, and the RPE is located in the outer retina, by placing the *rpe65* gene into the vitreous of *rd12* mice and comparing melanopsin function with that from *rd12* receiving the *rpe65* gene subretinally (adjacent to the RPE), it was determined that *rpe65* in the RPE drove melanopsin function and the iPLR. R*pe65* placed into the vitreous, closer to ipRGCs, did not have a significant improvement on melanopsin function compared to a control virus. These results are further supported by recent in *vitro* studies showing that ipRGCs need the RPE visual cycle for prolonged light exposure and firing, with the removal of the RPE reducing the length of time that the response can be sustained (Zhao et al., 2016). The improvements in ipRGC function seen here in *rd12* mice treated with the *rpe65* gene delivered subretinally were not accompanied by significant increases in outer-retinal photoreceptor function as recorded by ERG. Labelling of RPE65 was only seen in eyes that received a subretinal injection of virus encoding *rpe65* and its expression was restricted to the RPE. Delivery of the virus intravitreally was unsuccessful in

transfecting the RPE, a result in agreement with findings from the study by Li and colleagues (Li et al., 2009).

Interestingly, an increase in melanopsin expression was seen in the off sublamina in areas of the retina that had RPE65 expression in the RPE. These dendrites are from M1 ipRGCs, which are likely to drive the retinal input of the iPLR (Semo et al., 2014) and are less reliant on outer-retinal photoreceptor input (Schmidt and Kofuji, 2010).

The melanopsin system is often not considered when assessing visual function in retinal degeneration. However, it has been shown in this thesis that the melanopsin system relies on chromophore from the RPE and melanopsin function could therefore provide additional readouts of RPE-driven retinal function. These results also have important implications for diseases of the RPE such as AMD (Maynard et al., 2017) and LCA (Charng et al., 2017), where melanopsin function is also disrupted and it is important to consider this when developing potential therapies.

References

ADAMIS, A. P., SHIMA, D. T., YEO, K. T., YEO, T. K., BROWN, L. F., BERSE, B., D'AMORE, P. A. & FOLKMAN, J. 1993. Synthesis and secretion of vascular permeability factor/vascular endothelial growth factor by human retinal pigment epithelial cells. *Biochem Biophys Res Commun,* 193**,** 631-8.

AGARWAL, N., NIR, I. & PAPERMASTER, D. S. 1992. Expression of opsin and IRBP genes in mutant RCS rats. *Exp Eye Res,* 54**,** 545-54.

AHMADO, A., CARR, A. J., VUGLER, A. A., SEMO, M., GIAS, C., LAWRENCE, J. M., CHEN, L. L., CHEN, F. K., TUROWSKI, P., DA CRUZ, L. & COFFEY, P. J. 2011. Induction of differentiation by pyruvate and DMEM in the human retinal pigment epithelium cell line ARPE-19. *Invest Ophthalmol Vis Sci,* 52**,** 7148-59.

AJAMI, B., BENNETT, J. L., KRIEGER, C., TETZLAFF, W. & ROSSI, F. M. 2007. Local self-renewal can sustain CNS microglia maintenance and function throughout adult life. *Nat Neurosci,* 10**,** 1538-43.

ALBINI, T. A., WANG, R. C., REISER, B., ZAMIR, E., WU, G. S. & RAO, N. A. 2005. Microglial stability and repopulation in the retina. *Br J Ophthalmol,* 89**,** 901-3.

ALEMAN, T. S., JACOBSON, S. G., CHICO, J. D., SCOTT, M. L., CHEUNG, A. Y., WINDSOR, E. A., FURUSHIMA, M., REDMOND, T. M., BENNETT, J., PALCZEWSKI, K. & CIDECIYAN, A. V. 2004. Impairment of the transient pupillary light reflex in Rpe65(-/-) mice and humans with leber congenital amaurosis. *Invest Ophthalmol Vis Sci,* 45**,** 1259-71.

ALLEN, A. E., STORCHI, R., MARTIAL, F. P., PETERSEN, R. S., MONTEMURRO, M. A., BROWN, T. M. & LUCAS, R. J. 2014. Melanopsin-driven light adaptation in mouse vision. *Curr Biol,* 24**,** 2481-90.

AMIRPOUR, N., KARAMALI, F., RABIEE, F., REZAEI, L., ESFANDIARI, E., RAZAVI, S., DEHGHANI, A., RAZMJU, H., NASR-ESFAHANI, M. H. & BAHARVAND, H. 2012. Differentiation of human embryonic stem cell-derived retinal progenitors into retinal cells by Sonic hedgehog and/or retinal pigmented epithelium and transplantation into the subretinal space of sodium iodate-injected rabbits. *Stem Cells Dev,* 21**,** 42-53.

APPLEBURY, M. L., ANTOCH, M. P., BAXTER, L. C., CHUN, L. L., FALK, J. D., FARHANGFAR, F., KAGE, K., KRZYSTOLIK, M. G., LYASS, L. A. & ROBBINS, J. T. 2000. The murine cone photoreceptor: a single cone type expresses both S and M opsins with retinal spatial patterning. *Neuron,* 27**,** 513-23.

ATMACA-SONMEZ, P., LI, Y., YAMAUCHI, Y., SCHANIE, C. L., ILDSTAD, S. T., KAPLAN, H. J. & ENZMANN, V. 2006. Systemically transferred hematopoietic stem cells home to the subretinal space and express RPE-65 in a mouse model of retinal pigment epithelium damage. *Exp Eye Res,* 83**,** 1295-302.

BAEHR, W., DEVLIN, M. J. & APPLEBURY, M. L. 1979. Isolation and characterization of cGMP phosphodiesterase from bovine rod outer segments. *J Biol Chem,* 254**,** 11669-77.

BAICH, A. & ZIEGLER, M. 1992. The effect of sodium iodate and melanin on the formation of glyoxylate. *Pigment Cell Res,* 5**,** 394-5.

BAILEY, M. J., BEREMAND, P. D., HAMMER, R., REIDEL, E., THOMAS, T. L. & CASSONE, V. M. 2004. Transcriptional profiling of circadian patterns of mRNA expression in the chick retina. *J Biol Chem,* 279**,** 52247-54.

BAKALL, B., MARMORSTEIN, L. Y., HOPPE, G., PEACHEY, N. S., WADELIUS, C. & MARMORSTEIN, A. D. 2003. Expression and localization of bestrophin during normal mouse development. *Invest Ophthalmol Vis Sci,* 44**,** 3622-8.

BANDYOPADHYAY, M., KONO, M. & ROHRER, B. 2013. Explant cultures of Rpe65-/- mouse retina: a model to investigate cone opsin trafficking. *Mol Vis,* 19**,** 1149-57.

BARLOW, H. B. 1953. Summation and inhibition in the frog's retina. *J Physiol,* 119**,** 69-88.

BARR, L. & ALPERN, M. 1963. Photosensitivity of the frog iris. *J Gen Physiol,* 46**,** 1249-65.

BAVER, S. B., PICKARD, G. E., SOLLARS, P. J. & PICKARD, G. E. 2008. Two types of melanopsin retinal ganglion cell differentially innervate the hypothalamic suprachiasmatic nucleus and the olivary pretectal nucleus. *Eur J Neurosci,* 27**,** 1763-70.

BAYLOR, D. A., LAMB, T. D. & YAU, K. W. 1979. Responses of retinal rods to single photons. *J Physiol,* 288**,** 613-34.

BEATRICE, J., WENZEL, A., REME, C. E. & GRIMM, C. 2003. Increased light damage susceptibility at night does not correlate with RPE65 levels and rhodopsin regeneration in rats. *Exp Eye Res,* 76**,** 695-700.

BERNAL, S., CALAF, M., GARCIA-HOYOS, M., GARCIA-SANDOVAL, B., ROSELL, J., ADAN, A., AYUSO, C. & BAIGET, M. 2003. Study of the involvement of the RGR, CRPB1, and CRB1 genes in the pathogenesis of autosomal recessive retinitis pigmentosa. *J Med Genet,* 40**,** e89.

BERSON, D. M., CASTRUCCI, A. M. & PROVENCIO, I. 2010. Morphology and mosaics of melanopsin-expressing retinal ganglion cell types in mice. *J Comp Neurol,* 518**,** 2405-22.

BERSON, D. M., DUNN, F. A. & TAKAO, M. 2002. Phototransduction by retinal ganglion cells that set the circadian clock. *Science,* 295**,** 1070-3.

BOBU, C. & HICKS, D. 2009. Regulation of retinal photoreceptor phagocytosis in a diurnal mammal by circadian clocks and ambient lighting. *Invest Ophthalmol Vis Sci,* 50**,** 3495-502.

BOWES, C., LI, T., DANCIGER, M., BAXTER, L. C., APPLEBURY, M. L. & FARBER, D. B. 1990. Retinal degeneration in the rd mouse is caused by a defect in the beta subunit of rod cGMP-phosphodiesterase. *Nature,* 347**,** 677-80.

BOWES, C., VAN VEEN, T. & FARBER, D. B. 1988. Opsin, G-protein and 48-kDa protein in normal and rd mouse retinas: developmental expression of mRNAs and proteins and light/dark cycling of mRNAs. *Exp Eye Res,* 47**,** 369-90.

BROWN, K. T. 1968. The eclectroretinogram: its components and their origins. *Vision Res,* 8**,** 633-77.

BROWN, T. M., GIAS, C., HATORI, M., KEDING, S. R., SEMO, M., COFFEY, P. J., GIGG, J., PIGGINS, H. D., PANDA, S. & LUCAS, R. J. 2010. Melanopsin contributions to irradiance coding in the thalamo-cortical visual system. *PLoS Biol,* 8**,** e1000558.

BROWN, T. M., TSUJIMURA, S., ALLEN, A. E., WYNNE, J., BEDFORD, R., VICKERY, G., VUGLER, A. & LUCAS, R. J. 2012. Melanopsin-based brightness discrimination in mice and humans. *Curr Biol,* 22**,** 1134-41.

BUCHNER, D. A., SEBURN, K. L., FRANKEL, W. N. & MEISLER, M. H. 2004. Three ENU-induced neurological mutations in the pore loop of sodium channel Scn8a (Na(v)1.6) and a genetically linked retinal mutation, rd13. *Mamm Genome,* 15**,** 344-51.

CACHAFEIRO, M., BEMELMANS, A. P., CANOLA, K., PIGNAT, V., CRIPPA, S. V., KOSTIC, C. & ARSENIJEVIC, Y. 2010. Remaining rod activity mediates visual behavior in adult Rpe65-/- mice. *Invest Ophthalmol Vis Sci,* 51**,** 6835-42.

CAMERON, M. A., POZDEYEV, N., VUGLER, A. A., COOPER, H., IUVONE, P. M. & LUCAS, R. J. 2009. Light regulation of retinal dopamine that is independent of melanopsin phototransduction. *Eur J Neurosci,* 29**,** 761-7.

CARIDO, M., ZHU, Y., POSTEL, K., BENKNER, B., CIMALLA, P., KARL, M. O., KURTH, T., PAQUET-DURAND, F., KOCH, E., MUNCH, T. A., TANAKA, E. M. & ADER, M. 2014. Characterization of a mouse model with complete RPE loss and its use for RPE cell transplantation. *Invest Ophthalmol Vis Sci,* 55**,** 5431-44.

CARR, A. J., SMART, M. J., RAMSDEN, C. M., POWNER, M. B., DA CRUZ, L. & COFFEY, P. J. 2013. Development of human embryonic stem cell therapies for age-related macular degeneration. *Trends Neurosci,* 36**,** 385-95.

CARR, A. J., VUGLER, A. A., HIKITA, S. T., LAWRENCE, J. M., GIAS, C., CHEN, L. L., BUCHHOLZ, D. E., AHMADO, A., SEMO, M., SMART, M. J., HASAN, S., DA CRUZ, L., JOHNSON, L. V., CLEGG, D. O. & COFFEY, P. J. 2009. Protective effects of human iPS-derived retinal pigment epithelium cell transplantation in the retinal dystrophic rat. *PLoS One,* 4**,** e8152.

CARTER-DAWSON, L. D. & LAVAIL, M. M. 1979. Rods and cones in the mouse retina. I. Structural analysis using light and electron microscopy. *J Comp Neurol,* 188**,** 245-62.

CAYOUETTE, M., SMITH, S. B., BECERRA, S. P. & GRAVEL, C. 1999. Pigment epithelium-derived factor delays the death of photoreceptors in mouse models of inherited retinal degenerations. *Neurobiol Dis,* 6**,** 523-32.

CHANG, B. 2016. Mouse Models as Tools to Identify Genetic Pathways for Retinal Degeneration, as Exemplified by Leber's Congenital Amaurosis. *Methods Mol Biol,* 1438**,** 417-30.

CHANG, B., HAWES, N. L., PARDUE, M. T., GERMAN, A. M., HURD, R. E., DAVISSON, M. T., NUSINOWITZ, S., RENGARAJAN, K., BOYD, A. P., SIDNEY, S. S., PHILLIPS, M. J., STEWART, R. E., CHAUDHURY, R., NICKERSON, J. M., HECKENLIVELY, J. R. & BOATRIGHT, J. H. 2007. Two mouse retinal degenerations caused by missense mutations in the beta-subunit of rod cGMP phosphodiesterase gene. *Vision Res,* 47**,** 624-33.

CHANG, B., HECKENLIVELY, J. R., HAWES, N. L. & RODERICK, T. H. 1993. New mouse primary retinal degeneration (rd-3). *Genomics,* 16**,** 45-9.

CHARNG, J., JACOBSON, S. G., HEON, E., ROMAN, A. J., MCGUIGAN, D. B., 3RD, SHEPLOCK, R., KOSYK, M. S., SWIDER, M. & CIDECIYAN, A. V. 2017. Pupillary Light Reflexes in Severe Photoreceptor Blindness Isolate the Melanopic Component of Intrinsically Photosensitive Retinal Ganglion Cells. *Invest Ophthalmol Vis Sci,* 58**,** 3215-3224.

CHAUDHRY, G. R., FECEK, C., LAI, M. M., WU, W. C., CHANG, M., VASQUEZ, A., PASIERB, M. & TRESE, M. T. 2009. Fate of embryonic stem cell derivatives implanted into the vitreous of a slow retinal degenerative mouse model. *Stem Cells Dev,* 18**,** 247-58.

CHAURASIA, S. S., ROLLAG, M. D., JIANG, G., HAYES, W. P., HAQUE, R., NATESAN, A., ZATZ, M., TOSINI, G., LIU, C., KORF, H. W., IUVONE, P. M. & PROVENCIO, I. 2005. Molecular cloning, localization and circadian expression of chicken melanopsin (Opn4): differential regulation of expression in pineal and retinal cell types. *J Neurochem,* 92**,** 158-70.

CHEN, C., NAKATANI, K. & KOUTALOS, Y. 2003. Free magnesium concentration in salamander photoreceptor outer segments. *J Physiol,* 553**,** 125-35.

CHEN, J., WU, M., SEZATE, S. A. & MCGINNIS, J. F. 2007. Light threshold-controlled cone alpha-transducin translocation. *Invest Ophthalmol Vis Sci,* 48**,** 3350-5.

CHEN, S. K., BADEA, T. C. & HATTAR, S. 2011. Photoentrainment and pupillary light reflex are mediated by distinct populations of ipRGCs. *Nature,* 476**,** 92-5.

CHEN, W., YU, M., WANG, Y., PENG, Y., LI, X., LAM, D. M., CHEN, X. & LIU, X. 2009. Non-mitogenic human acidic fibroblast growth factor reduces retinal degeneration induced by sodium iodate. *J Ocul Pharmacol Ther,* 25**,** 315-20.

CHOWERS, G., COHEN, M., MARKS-OHANA, D., STIKA, S., EIJZENBERG, A., BANIN, E. & OBOLENSKY, A. 2017. Course of Sodium Iodate-Induced Retinal Degeneration in Albino and Pigmented Mice. *Invest Ophthalmol Vis Sci,* 58**,** 2239-2249.

COFFEY, P. J., GIRMAN, S., WANG, S. M., HETHERINGTON, L., KEEGAN, D. J., ADAMSON, P., GREENWOOD, J. & LUND, R. D. 2002. Long-term preservation of cortically dependent visual function in RCS rats by transplantation. *Nat Neurosci,* 5**,** 53-6.

COLEMAN, J. E. & SEMPLE-ROWLAND, S. L. 2005. GC1 deletion prevents light-dependent arrestin translocation in mouse cone photoreceptor cells. *Invest Ophthalmol Vis Sci,* 46**,** 12-6.

COWAN, C. W., FARISS, R. N., SOKAL, I., PALCZEWSKI, K. & WENSEL, T. G. 1998. High expression levels in cones of RGS9, the predominant GTPase accelerating protein of rods. *Proc Natl Acad Sci U S A,* 95**,** 5351-6.

CURCIO, C. A., ALLEN, K. A., SLOAN, K. R., LEREA, C. L., HURLEY, J. B., KLOCK, I. B. & MILAM, A. H. 1991. Distribution and morphology of human cone photoreceptors stained with anti-blue opsin. *J Comp Neurol,* 312**,** 610-24.

D'CRUZ, P. M., YASUMURA, D., WEIR, J., MATTHES, M. T., ABDERRAHIM, H., LAVAIL, M. M. & VOLLRATH, D. 2000. Mutation of the receptor tyrosine kinase gene Mertk in the retinal dystrophic RCS rat. *Hum Mol Genet,* 9**,** 645-51.

DA CRUZ, L., CHEN, F. K., AHMADO, A., GREENWOOD, J. & COFFEY, P. 2007. RPE transplantation and its role in retinal disease. *Prog Retin Eye Res,* 26**,** 598-635.

DA CRUZ, L., FYNES, K., GEORGIADIS, O., KERBY, J., LUO, Y. H., AHMADO, A., VERNON, A., DANIELS, J. T., NOMMISTE, B., HASAN, S. M., GOOLJAR, S. B., CARR, A. F., VUGLER, A., RAMSDEN, C. M., BICTASH, M., FENSTER, M., STEER, J., HARBINSON, T., WILBREY, A., TUFAIL, A., FENG, G., WHITLOCK, M., ROBSON, A. G., HOLDER, G. E., SAGOO, M. S., LOUDON, P. T., WHITING, P. & COFFEY, P. J. 2018. Phase 1 clinical study of an embryonic stem cell-derived retinal pigment epithelium patch in age-related macular degeneration. *Nat Biotechnol*.

DACEY, D. M., LIAO, H. W., PETERSON, B. B., ROBINSON, F. R., SMITH, V. C., POKORNY, J., YAU, K. W. & GAMLIN, P. D. 2005. Melanopsin-expressing ganglion cells in primate retina signal colour and irradiance and project to the LGN. *Nature,* 433**,** 749-54.

DAI, X., ZHANG, H., HE, Y., QI, Y., CHANG, B. & PANG, J. J. 2015. The frequency-response electroretinogram distinguishes cone and abnormal rod function in rd12 mice. *PLoS One,* 10**,** e0117570.

DAS, S. R., BHARDWAJ, N., KJELDBYE, H. & GOURAS, P. 1992. Muller cells of chicken retina synthesize 11-cis-retinol. *Biochem J,* 285 (Pt 3)**,** 907-13.

DEL PRIORE, L. V. 2005. Effect of sham surgery on retinal function after subretinal transplantation of the artificial silicone retina. *Arch Ophthalmol,* 123**,** 1156; author reply 1156-7.

DEL PRIORE, L. V., ISHIDA, O., JOHNSON, E. W., SHENG, Y., JACOBY, D. B., GENG, L., TEZEL, T. H. & KAPLAN, H. J. 2003. Triple immune suppression increases short-term survival of porcine fetal retinal pigment epithelium xenografts. *Invest Ophthalmol Vis Sci,* 44**,** 4044-53.

DEL PRIORE, L. V., TEZEL, T. H. & KAPLAN, H. J. 2006. Maculoplasty for age-related macular degeneration: reengineering Bruch's membrane and the human macula. *Prog Retin Eye Res,* 25**,** 539-62.

DIZHOOR, A. M., OLSHEVSKAYA, E. V. & PESHENKO, I. V. 2016. The R838S Mutation in Retinal Guanylyl Cyclase 1 (RetGC1) Alters Calcium Sensitivity of cGMP Synthesis in the Retina and Causes Blindness in Transgenic Mice. *J Biol Chem,* 291**,** 24504-24516.

DOWLING, J. E. & SIDMAN, R. L. 1962. Inherited retinal dystrophy in the rat. *J Cell Biol,* 14**,** 73-109.

DOYLE, S. E., CASTRUCCI, A. M., MCCALL, M., PROVENCIO, I. & MENAKER, M. 2006. Nonvisual light responses in the Rpe65 knockout mouse: rod loss restores sensitivity to the melanopsin system. *Proc Natl Acad Sci U S A,* 103**,** 10432-7.

DULAI, K. S., VON DORNUM, M., MOLLON, J. D. & HUNT, D. M. 1999. The evolution of trichromatic color vision by opsin gene duplication in New World and Old World primates. *Genome Res,* 9**,** 629-38.

ECKER, J. L., DUMITRESCU, O. N., WONG, K. Y., ALAM, N. M., CHEN, S. K., LEGATES, T., RENNA, J. M., PRUSKY, G. T., BERSON, D. M. & HATTAR, S. 2010. Melanopsin-expressing retinal ganglion-cell photoreceptors: cellular diversity and role in pattern vision. *Neuron,* 67**,** 49-60.

EDWARDS, R. B. & SZAMIER, R. B. 1977. Defective phagocytosis of isolated rod outer segments by RCS rat retinal pigment epithelium in culture. *Science,* 197**,** 1001-3.

ELIAS, R. V., SEZATE, S. S., CAO, W. & MCGINNIS, J. F. 2004. Temporal kinetics of the light/dark translocation and compartmentation of arrestin and alpha-transducin in mouse photoreceptor cells. *Mol Vis,* 10**,** 672-81.

ENZMANN, V., LECAUDE, S., KRUSCHINSKI, A. & VATER, A. 2017. CXCL12/SDF-1-Dependent Retinal Migration of Endogenous Bone Marrow-Derived Stem Cells Improves Visual Function after Pharmacologically Induced Retinal Degeneration. *Stem Cell Rev,* 13**,** 278-286.

ENZMANN, V., ROW, B. W., YAMAUCHI, Y., KHEIRANDISH, L., GOZAL, D., KAPLAN, H. J. & MCCALL, M. A. 2006. Behavioral and anatomical abnormalities in a sodium iodate-induced model of retinal pigment epithelium degeneration. *Exp Eye Res,* 82**,** 441-8.

FADOK, V. A., DE CATHELINEAU, A., DALEKE, D. L., HENSON, P. M. & BRATTON, D. L. 2001. Loss of phospholipid asymmetry and surface exposure of phosphatidylserine is required for phagocytosis of apoptotic cells by macrophages and fibroblasts. *J Biol Chem,* 276**,** 1071-7.

FAN, J., ROHRER, B., FREDERICK, J. M., BAEHR, W. & CROUCH, R. K. 2008. Rpe65-/- and Lrat-/- mice: comparable models of leber congenital amaurosis. *Invest Ophthalmol Vis Sci,* 49**,** 2384-9.

FAN, J., ROHRER, B., MOISEYEV, G., MA, J. X. & CROUCH, R. K. 2003. Isorhodopsin rather than rhodopsin mediates rod function in RPE65 knock-out mice. *Proc Natl Acad Sci U S A,* 100**,** 13662-7.

FINNEMANN, S. C. 2003. Focal adhesion kinase signaling promotes phagocytosis of integrin-bound photoreceptors. *Embo j,* 22**,** 4143-54.

FINNEMANN, S. C., BONILHA, V. L., MARMORSTEIN, A. D. & RODRIGUEZ-BOULAN, E. 1997. Phagocytosis of rod outer segments by retinal pigment epithelial cells requires alpha(v)beta5 integrin for binding but not for internalization. *Proc Natl Acad Sci U S A,* 94**,** 12932-7.

FLEISCH, V. C. & NEUHAUSS, S. C. 2010. Parallel visual cycles in the zebrafish retina. *Prog Retin Eye Res,* 29**,** 476-86.

FRANCO, L. M., ZULLIGER, R., WOLF-SCHNURRBUSCH, U. E., KATAGIRI, Y., KAPLAN, H. J., WOLF, S. & ENZMANN, V. 2009. Decreased visual function after patchy loss of retinal pigment epithelium induced by low-dose sodium iodate. *Invest Ophthalmol Vis Sci,* 50**,** 4004-10.

FRAZAO, R., MCMAHON, D. G., SCHUNACK, W., DATTA, P., HEIDELBERGER, R. & MARSHAK, D. W. 2011. Histamine elevates free intracellular calcium in mouse retinal dopaminergic cells via H1-receptors. *Invest Ophthalmol Vis Sci,* 52**,** 3083-8.

FREDERICK, J. M., RAYBORN, M. E., LATIES, A. M., LAM, D. M. & HOLLYFIELD, J. G. 1982. Dopaminergic neurons in the human retina. *J Comp Neurol,* 210**,** 65-79.

FREED, M. A., SMITH, R. G. & STERLING, P. 1987. Rod bipolar array in the cat retina: pattern of input from rods and GABA-accumulating amacrine cells. *J Comp Neurol,* 266**,** 445-55.

FRIEDMAN, J. S., CHANG, B., KRAUTH, D. S., LOPEZ, I., WASEEM, N. H., HURD, R. E., FEATHERS, K. L., BRANHAM, K. E., SHAW, M., THOMAS, G. E., BROOKS, M. J., LIU, C., BAKERI, H. A., CAMPOS, M. M., MAUBARET, C., WEBSTER, A. R., RODRIGUEZ, I. R., THOMPSON, D. A., BHATTACHARYA, S. S., KOENEKOOP, R. K., HECKENLIVELY, J. R. & SWAROOP, A. 2010. Loss of lysophosphatidylcholine acyltransferase 1 leads to photoreceptor degeneration in rd11 mice. *Proc Natl Acad Sci U S A,* 107**,** 15523-8.

FU, Y., ZHONG, H., WANG, M. H., LUO, D. G., LIAO, H. W., MAEDA, H., HATTAR, S., FRISHMAN, L. J. & YAU, K. W. 2005. Intrinsically photosensitive retinal ganglion cells detect light with a vitamin A-based photopigment, melanopsin. *Proc Natl Acad Sci U S A,* 102**,** 10339-44.

FUNG, B. K., LIEBERMAN, B. S. & LEE, R. H. 1992. A third form of the G protein beta subunit. 2. Purification and biochemical properties. *J Biol Chem,* 267**,** 24782-8.

GAO, S. Q., MAEDA, T., OKANO, K. & PALCZEWSKI, K. 2012. A microparticle/hydrogel combination drug-delivery system for sustained release of retinoids. *Invest Ophthalmol Vis Sci,* 53**,** 6314-23.

GARCIA-LAYANA, A., VASQUEZ, G., SALINAS-ALAMAN, A., MORENO-MONTANES, J., RECALDE, S. & FERNANDEZ-ROBREDO, P. 2009. Development of laser-induced choroidal neovascularization in rats after retinal damage by sodium iodate injection. *Ophthalmic Res,* 42**,** 205-12.

GASTINGER, M. J., O'BRIEN, J. J., LARSEN, N. B. & MARSHAK, D. W. 1999. Histamine immunoreactive axons in the macaque retina. *Invest Ophthalmol Vis Sci,* 40**,** 487-95.

GINHOUX, F., GRETER, M., LEBOEUF, M., NANDI, S., SEE, P., GOKHAN, S., MEHLER, M. F., CONWAY, S. J., NG, L. G., STANLEY, E. R., SAMOKHVALOV, I. M. & MERAD, M. 2010. Fate mapping analysis reveals that adult microglia derive from primitive macrophages. *Science,* 330**,** 841-5.

GIRMAN, S. V., WANG, S. & LUND, R. D. 2005. Time course of deterioration of rod and cone function in RCS rat and the effects of subretinal cell grafting: a light- and dark-adaptation study. *Vision Res,* 45**,** 343-54.

GLICKMAN, R. D. 2011. Ultraviolet phototoxicity to the retina. *Eye Contact Lens,* 37**,** 196-205.

GOLDMAN, A. I., TEIRSTEIN, P. S. & O'BRIEN, P. J. 1980. The role of ambient lighting in circadian disc shedding in the rod outer segment of the rat retina. *Invest Ophthalmol Vis Sci,* 19**,** 1257-67.

GOLDSTEIN, E. B. & WOLF, B. M. 1973. Regeneration of the green-rod pigment in the isolated frog retina. *Vision Res,* 13**,** 527-34.

GONG, L., WU, Q., SONG, B., LU, B. & ZHANG, Y. 2008. Differentiation of rat mesenchymal stem cells transplanted into the subretinal space of sodium iodate-injected rats. *Clin Experiment Ophthalmol,* 36**,** 666-71.

GOSLINGS, W. R., PRODEUS, A. P., STREILEIN, J. W., CARROLL, M. C., JAGER, M. J. & TAYLOR, A. W. 1998. A small molecular weight factor in aqueous humor acts on C1q to prevent antibody-dependent complement activation. *Invest Ophthalmol Vis Sci,* 39**,** 989-95.

GOURAS, P., FLOOD, M. T., KJEDBYE, H., BILEK, M. K. & EGGERS, H. 1985. Transplantation of cultured human retinal epithelium to Bruch's membrane of the owl monkey's eye. *Curr Eye Res,* 4**,** 253-65.

GRANIT, R. 1933. The components of the retinal action potential in mammals and their relation to the discharge in the optic nerve. *J Physiol,* 77**,** 207-39.

GRISANTI, S., ISHIOKA, M., KOSIEWICZ, M. & JIANG, L. Q. 1997. Immunity and immune privilege elicited by cultured retinal pigment epithelial cell transplants. *Invest Ophthalmol Vis Sci,* 38**,** 1619-26.

GU, S. M., THOMPSON, D. A., SRIKUMARI, C. R., LORENZ, B., FINCKH, U., NICOLETTI, A., MURTHY, K. R., RATHMANN, M., KUMARAMANICKAVEL, G., DENTON, M. J. & GAL, A. 1997. Mutations in RPE65 cause autosomal recessive childhood-onset severe retinal dystrophy. *Nat Genet,* 17**,** 194-7.

GUERIN, K., GREGORY-EVANS, C. Y., HODGES, M. D., MOOSAJEE, M., MACKAY, D. S., GREGORY-EVANS, K. & FLANNERY, J. G. 2008. Systemic aminoglycoside treatment in rodent models of retinitis pigmentosa. *Exp Eye Res,* 87**,** 197-207.

GULER, A. D., ECKER, J. L., LALL, G. S., HAQ, S., ALTIMUS, C. M., LIAO, H. W., BARNARD, A. R., CAHILL, H., BADEA, T. C., ZHAO, H., HANKINS, M. W., BERSON, D. M., LUCAS, R. J., YAU, K. W. & HATTAR, S. 2008. Melanopsin cells are the principal conduits for rod-cone input to non-image-forming vision. *Nature,* 453**,** 102-5.

HAGINS, W. A., PENN, R. D. & YOSHIKAMI, S. 1970. Dark current and photocurrent in retinal rods. *Biophys J,* 10**,** 380-412.

HALL, M. O., OBIN, M. S., HEEB, M. J., BURGESS, B. L. & ABRAMS, T. A. 2005. Both protein S and Gas6 stimulate outer segment phagocytosis by cultured rat retinal pigment epithelial cells. *Exp Eye Res,* 81**,** 581-91.

HALL, M. O., PRIETO, A. L., OBIN, M. S., ABRAMS, T. A., BURGESS, B. L., HEEB, M. J. & AGNEW, B. J. 2001. Outer segment phagocytosis by cultured retinal pigment epithelial cells requires Gas6. *Exp Eye Res,* 73**,** 509-20.

HAMEL, C. P., TSILOU, E., HARRIS, E., PFEFFER, B. A., HOOKS, J. J., DETRICK, B. & REDMOND, T. M. 1993. A developmentally regulated microsomal protein specific for the pigment epithelium of the vertebrate retina. *J Neurosci Res,* 34**,** 414-25.

HANAYAMA, R., TANAKA, M., MIWA, K., SHINOHARA, A., IWAMATSU, A. & NAGATA, S. 2002. Identification of a factor that links apoptotic cells to phagocytes. *Nature,* 417**,** 182-7.

HANEIN, S., PERRAULT, I., GERBER, S., TANGUY, G., BARBET, F., DUCROQ, D., CALVAS, P., DOLLFUS, H., HAMEL, C., LOPPONEN, T., MUNIER, F., SANTOS, L., SHALEV, S., ZAFEIRIOU, D., DUFIER, J. L., MUNNICH, A., ROZET, J. M. & KAPLAN, J. 2004. Leber congenital amaurosis: comprehensive survey of the genetic heterogeneity, refinement of the clinical definition, and genotype-phenotype correlations as a strategy for molecular diagnosis. *Hum Mutat,* 23**,** 306-17.

HANNIBAL, J. & FAHRENKRUG, J. 2004. Melanopsin containing retinal ganglion cells are light responsive from birth. *Neuroreport,* 15**,** 2317-20.

HANNIBAL, J., VRANG, N., CARD, J. P. & FAHRENKRUG, J. 2001. Light-dependent induction of cFos during subjective day and night in PACAP-containing ganglion cells of the retinohypothalamic tract. *J Biol Rhythms,* 16**,** 457-70.

HANZLICEK, B. W., PEACHEY, N. S., GRIMM, C., HAGSTROM, S. A. & BALL, S. L. 2004. Probing inner retinal circuits in the rod pathway: a comparison of c-fos activation in mutant mice. *Vis Neurosci,* 21**,** 873-81.

HAO, W. & FONG, H. K. 1999. The endogenous chromophore of retinal G protein-coupled receptor opsin from the pigment epithelium. *J Biol Chem,* 274**,** 6085-90.

HARIRI, S., TAM, M. C., LEE, D., HILEETO, D., MOAYED, A. A. & BIZHEVA, K. 2013. Noninvasive imaging of the early effect of sodium iodate toxicity in a rat model of outer retina degeneration with spectral domain optical coherence tomography. *J Biomed Opt,* 18**,** 26017.

HARRIS, J. R., BROWN, G. A., JORGENSEN, M., KAUSHAL, S., ELLIS, E. A., GRANT, M. B. & SCOTT, E. W. 2006. Bone marrow-derived cells home to and regenerate retinal pigment epithelium after injury. *Invest Ophthalmol Vis Sci,* 47**,** 2108-13.

HARTWICK, A. T., BRAMLEY, J. R., YU, J., STEVENS, K. T., ALLEN, C. N., BALDRIDGE, W. H., SOLLARS, P. J. & PICKARD, G. E. 2007. Light-evoked calcium responses of isolated melanopsin-expressing retinal ganglion cells. *J Neurosci,* 27**,** 13468-80.

HASCOET, M., BOURIN, M. & NIC DHONNCHADHA, B. A. 2001. The mouse light-dark paradigm: a review. *Prog Neuropsychopharmacol Biol Psychiatry,* 25**,** 141-66.

HASEGAWA, T., IKEDA, H. O., NAKANO, N., MURAOKA, Y., TSURUYAMA, T., OKAMOTO-FURUTA, K., KOHDA, H. & YOSHIMURA, N. 2016. Changes in morphology and visual function over time in mouse models of retinal degeneration: an SD-OCT, histology, and electroretinography study. *Jpn J Ophthalmol,* 60**,** 111-25.

HATTAR, S., LIAO, H. W., TAKAO, M., BERSON, D. M. & YAU, K. W. 2002. Melanopsin-containing retinal ganglion cells: architecture, projections, and intrinsic photosensitivity. *Science,* 295**,** 1065-70.

HATTAR, S., LUCAS, R. J., MROSOVSKY, N., THOMPSON, S., DOUGLAS, R. H., HANKINS, M. W., LEM, J., BIEL, M., HOFMANN, F., FOSTER, R. G. & YAU, K. W. 2003. Melanopsin and rod-cone photoreceptive systems account for all major accessory visual functions in mice. *Nature,* 424**,** 76-81.

HAWES, N. L., CHANG, B., HAGEMAN, G. S., NUSINOWITZ, S., NISHINA, P. M., SCHNEIDER, B. S., SMITH, R. S., RODERICK, T. H., DAVISSON, M. T. & HECKENLIVELY, J. R. 2000. Retinal degeneration 6 (rd6): a new mouse model for human retinitis punctata albescens. *Invest Ophthalmol Vis Sci,* 41**,** 3149-57.

HAWES, N. L., HURD, R. E., WANG, J., DAVISSON, M. T., NUSINOWITZ, S., HECKENLIVELY, J. R. & CHANG, B. 2005. A New Mouse Model of Retinal Degeneration (rd15) With Retinal Outer Plexiform Dystrophy. *Investigative Ophthalmology & Visual Science,* 46**,** 3175-3175.

HECKENLIVELY, J. R., CHANG, B., ERWAY, L. C., PENG, C., HAWES, N. L., HAGEMAN, G. S. & RODERICK, T. H. 1995. Mouse model for Usher syndrome: linkage mapping suggests homology to Usher type I reported at human chromosome 11p15. *Proc Natl Acad Sci U S A,* 92**,** 11100-4.

HEIKE, M. & MARMOR, M. F. 1990. L-cystein protects the pigment epithelium from acute sodium iodate toxicity. *Doc Ophthalmol,* 75**,** 15-22.

HEYNEN, H. & VAN NORREN, D. 1985. Origin of the electroretinogram in the intact macaque eye--II. Current source-density analysis. *Vision Res,* 25**,** 709-15.

HOOD, D. C. & BIRCH, D. G. 1990. The A-wave of the human electroretinogram and rod receptor function. *Invest Ophthalmol Vis Sci,* 31**,** 2070-81.

HOOD, D. C. & BIRCH, D. G. 1995. Phototransduction in human cones measured using the alpha-wave of the ERG. *Vision Res,* 35**,** 2801-10.

HSU, Y. T. & MOLDAY, R. S. 1993. Modulation of the cGMP-gated channel of rod photoreceptor cells by calmodulin. *Nature,* 361**,** 76-9.

HULPIAU, P. & VAN ROY, F. 2009. Molecular evolution of the cadherin superfamily. *Int J Biochem Cell Biol,* 41**,** 349-69.

HURLEY, J. B. & STRYER, L. 1982. Purification and characterization of the gamma regulatory subunit of the cyclic GMP phosphodiesterase from retinal rod outer segments. *J Biol Chem,* 257**,** 11094-9.

IDELSON, M., ALPER, R., OBOLENSKY, A., BEN-SHUSHAN, E., HEMO, I., YACHIMOVICH-COHEN, N., KHANER, H., SMITH, Y., WISER, O., GROPP, M., COHEN, M. A., EVEN-RAM, S., BERMAN-ZAKEN, Y., MATZRAFI, L., RECHAVI, G., BANIN, E. & REUBINOFF, B. 2009. Directed differentiation of human embryonic stem cells into functional retinal pigment epithelium cells. *Cell Stem Cell,* 5**,** 396-408.

IMANISHI, Y., BATTEN, M. L., PISTON, D. W., BAEHR, W. & PALCZEWSKI, K. 2004. Noninvasive two-photon imaging reveals retinyl ester storage structures in the eye. *J Cell Biol,* 164**,** 373-83.

INGRAM, N. T., SAMPATH, A. P. & FAIN, G. L. 2016. Why are rods more sensitive than cones? *J Physiol*.

ISHIDA, K., PANJWANI, N., CAO, Z. & STREILEIN, J. W. 2003. Participation of pigment epithelium in ocular immune privilege. 3. Epithelia cultured from iris, ciliary body, and retina suppress T-cell activation by partially non-overlapping mechanisms. *Ocul Immunol Inflamm,* 11**,** 91-105.

JACKSON, G. R., OWSLEY, C. & CURCIO, C. A. 2002. Photoreceptor degeneration and dysfunction in aging and age-related maculopathy. *Ageing Res Rev,* 1**,** 381-96.

JACOBS, G. H., NEITZ, J. & DEEGAN, J. F., 2ND 1991. Retinal receptors in rodents maximally sensitive to ultraviolet light. *Nature,* 353**,** 655-6.

JENSEN, R. J. & DAW, N. W. 1986. Effects of dopamine and its agonists and antagonists on the receptive field properties of ganglion cells in the rabbit retina. *Neuroscience,* 17**,** 837-55.

JEON, C. J., STRETTOI, E. & MASLAND, R. H. 1998. The major cell populations of the mouse retina. *J Neurosci,* 18**,** 8936-46.

JIANG, L. Q. & HAMASAKI, D. 1994. Corneal electroretinographic function rescued by normal retinal pigment epithelial grafts in retinal degenerative Royal College of Surgeons rats. *Invest Ophthalmol Vis Sci,* 35**,** 4300-9.

JIANG, M., PANDEY, S. & FONG, H. K. 1993. An opsin homologue in the retina and pigment epithelium. *Invest Ophthalmol Vis Sci,* 34**,** 3669-78.

JIN, M., LI, S., MOGHRABI, W. N., SUN, H. & TRAVIS, G. H. 2005. Rpe65 is the retinoid isomerase in bovine retinal pigment epithelium. *Cell,* 122**,** 449-59.

JORGENSEN, A., WIENCKE, A. K., LA COUR, M., KAESTEL, C. G., MADSEN, H. O., HAMANN, S., LUI, G. M., SCHERFIG, E., PRAUSE, J. U., SVEJGAARD, A., ODUM, N., NISSEN, M. H. & ROPKE, C. 1998. Human retinal pigment epithelial cell-induced apoptosis in activated T cells. *Invest Ophthalmol Vis Sci,* 39**,** 1590-9.

KADKHODAEIAN, H. A., TIRAIHI, T., DAFTARIAN, N., AHMADIEH, H., ZIAEI, H. & TAHERI, T. 2016. Histological and Electrophysiological Changes in the Retinal Pigment Epithelium after Injection of Sodium Iodate in the Orbital Venus Plexus of Pigmented Rats. *J Ophthalmic Vis Res,* 11**,** 70-7.

KAMAO, H., MANDAI, M., OKAMOTO, S., SAKAI, N., SUGA, A., SUGITA, S., KIRYU, J. & TAKAHASHI, M. 2014. Characterization of human induced pluripotent stem cell-derived retinal pigment epithelium cell sheets aiming for clinical application. *Stem Cell Reports,* 2**,** 205-18.

KASSAI, H., AIBA, A., NAKAO, K., NAKAMURA, K., KATSUKI, M., XIONG, W. H., YAU, K. W., IMAI, H., SHICHIDA, Y., SATOMI, Y., TAKAO, T., OKANO, T. & FUKADA, Y. 2005. Farnesylation of retinal transducin underlies its translocation during light adaptation. *Neuron,* 47**,** 529-39.

KAWAZOE, Y., SUGITA, S., KEINO, H., YAMADA, Y., IMAI, A., HORIE, S. & MOCHIZUKI, M. 2012. Retinoic acid from retinal pigment epithelium induces T regulatory cells. *Exp Eye Res,* 94**,** 32-40.

KEEGAN, D. J., KENNA, P., HUMPHRIES, M. M., HUMPHRIES, P., FLITCROFT, D. I., COFFEY, P. J., LUND, R. D. & LAWRENCE, J. M. 2003. Transplantation of syngeneic Schwann cells to the retina of the rhodopsin knockout (rho(-/-)) mouse. *Invest Ophthalmol Vis Sci,* 44**,** 3526-32.

KITAMURA, E., DANCIGER, M., YAMASHITA, C., RAO, N. P., NUSINOWITZ, S., CHANG, B. & FARBER, D. B. 2006. Disruption of the gene encoding the beta1-subunit of transducin in the Rd4/+ mouse. *Invest Ophthalmol Vis Sci,* 47**,** 1293-301.

KIUCHI, K., YOSHIZAWA, K., SHIKATA, N., MORIGUCHI, K. & TSUBURA, A. 2002. Morphologic characteristics of retinal degeneration induced by sodium iodate in mice. *Curr Eye Res,* 25**,** 373-9.

KLASSEN, H., WHITELEY, S. J., YOUNG, M. J. & LUND, R. D. 2001. Graft location affects functional rescue following RPE cell transplantation in the RCS rat. *Exp Neurol,* 169**,** 114-21.

KLEIN, R., KLEIN, B. E., JENSEN, S. C. & MEUER, S. M. 1997. The five-year incidence and progression of age-related maculopathy: the Beaver Dam Eye Study. *Ophthalmology,* 104**,** 7-21.

KOENEKOOP, R. K., SUI, R., SALLUM, J., VAN DEN BORN, L. I., AJLAN, R., KHAN, A., DEN HOLLANDER, A. I., CREMERS, F. P., MENDOLA, J. D., BITTNER, A. K., DAGNELIE, G., SCHUCHARD, R. A. & SAPERSTEIN, D. A. 2014. Oral 9-cis retinoid for childhood blindness due to Leber congenital amaurosis caused by RPE65 or LRAT mutations: an open-label phase 1b trial. *Lancet,* 384**,** 1513-20.

KOLB, H. & WEST, R. W. 1977. Synaptic connections of the interplexiform cell in the retina of the cat. *J Neurocytol,* 6**,** 155-70.

KOPP, C., VOGEL, E. & MISSLIN, R. 1999. Comparative study of emotional behaviour in three inbred strains of mice. *Behav Processes,* 47**,** 161-74.

KRISPEL, C. M., CHEN, D., MELLING, N., CHEN, Y. J., MARTEMYANOV, K. A., QUILLINAN, N., ARSHAVSKY, V. Y., WENSEL, T. G., CHEN, C. K. & BURNS, M. E. 2006. RGS expression rate-limits recovery of rod photoresponses. *Neuron,* 51**,** 409-16.

KROHNE, T. U., WESTENSKOW, P. D., KURIHARA, T., FRIEDLANDER, D. F., LEHMANN, M., DORSEY, A. L., LI, W., ZHU, S., SCHULTZ, A., WANG, J., SIUZDAK, G., DING, S. & FRIEDLANDER, M. 2012. Generation of retinal pigment epithelial cells from small molecules and OCT4 reprogrammed human induced pluripotent stem cells. *Stem Cells Transl Med,* 1**,** 96-109.

KSANTINI, M., LAFONT, E., BOCQUET, B., MEUNIER, I. & HAMEL, C. P. 2012. Homozygous mutation in MERTK causes severe autosomal recessive retinitis pigmentosa. *Eur J Ophthalmol,* 22**,** 647-53.

KUHN, H. & WILDEN, U. 1987. Deactivation of photoactivated rhodopsin by rhodopsin-kinase and arrestin. *J Recept Res,* 7**,** 283-98.

LAVAIL, M. M. 1976. Rod outer segment disk shedding in rat retina: relationship to cyclic lighting. *Science,* 194**,** 1071-4.

LAVAIL, M. M. 1980. Circadian nature of rod outer segment disc shedding in the rat. *Invest Ophthalmol Vis Sci,* 19**,** 407-11.

LAWRENCE, J. M., SAUVE, Y., KEEGAN, D. J., COFFEY, P. J., HETHERINGTON, L., GIRMAN, S., WHITELEY, S. J., KWAN, A. S., PHEBY, T. & LUND, R. D. 2000. Schwann cell grafting into the retina of the dystrophic RCS rat limits functional deterioration. Royal College of Surgeons. *Invest Ophthalmol Vis Sci,* 41**,** 518-28.

LEE, R. H., LIEBERMAN, B. S., YAMANE, H. K., BOK, D. & FUNG, B. K. 1992. A third form of the G protein beta subunit. 1. Immunochemical identification and localization to cone photoreceptors. *J Biol Chem,* 267**,** 24776-81.

LESKOV, I. B., KLENCHIN, V. A., HANDY, J. W., WHITLOCK, G. G., GOVARDOVSKII, V. I., BOWNDS, M. D., LAMB, T. D., PUGH, E. N., JR. & ARSHAVSKY, V. Y. 2000. The gain of rod

phototransduction: reconciliation of biochemical and electrophysiological measurements. *Neuron,* 27**,** 525-37.

LI, L. & TURNER, J. E. 1991. Optimal conditions for long-term photoreceptor cell rescue in RCS rats: the necessity for healthy RPE transplants. *Exp Eye Res,* 52**,** 669-79.

LI, L. X. & TURNER, J. E. 1988. Inherited retinal dystrophy in the RCS rat: prevention of photoreceptor degeneration by pigment epithelial cell transplantation. *Exp Eye Res,* 47**,** 911-7.

LI, Q., MILLER, R., HAN, P. Y., PANG, J., DINCULESCU, A., CHIODO, V. & HAUSWIRTH, W. W. 2008. Intraocular route of AAV2 vector administration defines humoral immune response and therapeutic potential. *Mol Vis,* 14**,** 1760-9.

LI, W., KONG, F., LI, X., DAI, X., LIU, X., ZHENG, Q., WU, R., ZHOU, X., LU, F., CHANG, B., LI, Q., HAUSWIRTH, W. W., QU, J. & PANG, J. J. 2009. Gene therapy following subretinal AAV5 vector delivery is not affected by a previous intravitreal AAV5 vector administration in the partner eye. *Mol Vis,* 15**,** 267-75.

LI, X., LI, W., DAI, X., KONG, F., ZHENG, Q., ZHOU, X., LU, F., CHANG, B., ROHRER, B., HAUSWIRTH, W. W., QU, J. & PANG, J. J. 2011. Gene therapy rescues cone structure and function in the 3-month-old rd12 mouse: a model for midcourse RPE65 leber congenital amaurosis. *Invest Ophthalmol Vis Sci,* 52**,** 7-15.

LI, Y., LI, C., CHEN, Z., HE, J., TAO, Z. & YIN, Z. Q. 2012a. A microRNA, mir133b, suppresses melanopsin expression mediated by failure dopaminergic amacrine cells in RCS rats. *Cell Signal,* 24**,** 685-98.

LI, Y., TSAI, Y. T., HSU, C. W., EROL, D., YANG, J., WU, W. H., DAVIS, R. J., EGLI, D. & TSANG, S. H. 2012b. Long-term safety and efficacy of human-induced pluripotent stem cell (iPS) grafts in a preclinical model of retinitis pigmentosa. *Mol Med,* 18**,** 1312-9.

LIOU, G. I., BRIDGES, C. D., FONG, S. L., ALVAREZ, R. A. & GONZALEZ-FERNANDEZ, F. 1982. Vitamin A transport between retina and pigment epithelium--an interstitial protein carrying endogenous retinol (interstitial retinol-binding protein). *Vision Res,* 22**,** 1457-67.

LITTLE, C. W., CASTILLO, B., DILORETO, D. A., COX, C., WYATT, J., DEL CERRO, C. & DEL CERRO, M. 1996. Transplantation of human fetal retinal pigment epithelium rescues photoreceptor cells from degeneration in the Royal College of Surgeons rat retina. *Invest Ophthalmol Vis Sci,* 37**,** 204-11.

LONG, K. O., FISHER, S. K., FARISS, R. N. & ANDERSON, D. H. 1986. Disc shedding and autophagy in the cone-dominant ground squirrel retina. *Exp Eye Res,* 43**,** 193-205.

LONGBOTTOM, R., FRUTTIGER, M., DOUGLAS, R. H., MARTINEZ-BARBERA, J. P., GREENWOOD, J. & MOSS, S. E. 2009. Genetic ablation of retinal pigment epithelial cells reveals the adaptive response of the epithelium and impact on photoreceptors. *Proc Natl Acad Sci U S A,* 106**,** 18728-33.

LORENZ, B., GYURUS, P., PREISING, M., BREMSER, D., GU, S., ANDRASSI, M., GERTH, C. & GAL, A. 2000. Early-onset severe rod-cone dystrophy in young children with RPE65 mutations. *Invest Ophthalmol Vis Sci,* 41**,** 2735-42.

LU, B., MALCUIT, C., WANG, S., GIRMAN, S., FRANCIS, P., LEMIEUX, L., LANZA, R. & LUND, R. 2009. Long-term safety and function of RPE from human embryonic stem cells in preclinical models of macular degeneration. *Stem Cells,* 27**,** 2126-35.

LUCAS, R. J., DOUGLAS, R. H. & FOSTER, R. G. 2001. Characterization of an ocular photopigment capable of driving pupillary constriction in mice. *Nat Neurosci,* 4**,** 621-6.

LUCAS, R. J., HATTAR, S., TAKAO, M., BERSON, D. M., FOSTER, R. G. & YAU, K. W. 2003. Diminished pupillary light reflex at high irradiances in melanopsin-knockout mice. *Science,* 299**,** 245-7.

LUPI, D., COOPER, H. M., FROEHLICH, A., STANDFORD, L., MCCALL, M. A. & FOSTER, R. G. 1999. Transgenic ablation of rod photoreceptors alters the circadian phenotype of mice. *Neuroscience,* 89**,** 363-74.

MA, J., XU, L., OTHERSEN, D. K., REDMOND, T. M. & CROUCH, R. K. 1998. Cloning and localization of RPE65 mRNA in salamander cone photoreceptor cells1. *Biochim Biophys Acta,* 1443**,** 255-61.

MA, J., ZHANG, J., OTHERSEN, K. L., MOISEYEV, G., ABLONCZY, Z., REDMOND, T. M., CHEN, Y. & CROUCH, R. K. 2001. Expression, purification, and MALDI analysis of RPE65. *Invest Ophthalmol Vis Sci,* 42**,** 1429-35.

MACHALINSKA, A., KAWA, M. P., PIUS-SADOWSKA, E., ROGINSKA, D., KLOS, P., BAUMERT, B., WISZNIEWSKA, B. & MACHALINSKI, B. 2013. Endogenous regeneration of damaged retinal pigment epithelium following low dose sodium iodate administration: an insight into the role of glial cells in retinal repair. *Exp Eye Res,* 112**,** 68-78.

MACHALINSKA, A., KLOS, P., BAUMERT, B., BASKIEWICZ, M., KAWA, M., RUDNICKI, M., LUBINSKI, W., WISZNIEWSKA, B., KARCZEWICZ, D. & MACHALINSKI, B. 2011. Stem Cells are mobilized from the bone marrow into the peripheral circulation in response to retinal pigment epithelium damage--a pathophysiological attempt to induce endogenous regeneration. *Curr Eye Res,* 36**,** 663-72.

MACHALINSKA, A., LUBINSKI, W., KLOS, P., KAWA, M., BAUMERT, B., PENKALA, K., GRZEGRZOLKA, R., KARCZEWICZ, D., WISZNIEWSKA, B. & MACHALINSKI, B. 2010. Sodium iodate selectively injuries the posterior pole of the retina in a dose-dependent manner: morphological and electrophysiological study. *Neurochem Res,* 35**,** 1819-27.

MAEDA, A., MAEDA, T. & PALCZEWSKI, K. 2006. Improvement in rod and cone function in mouse model of Fundus albipunctatus after pharmacologic treatment with 9-cis-retinal. *Invest Ophthalmol Vis Sci,* 47**,** 4540-6.

MAEDA, T., MAEDA, A., CASADESUS, G., PALCZEWSKI, K. & MARGARON, P. 2009a. Evaluation of 9-cis-retinyl acetate therapy in Rpe65-/- mice. *Invest Ophthalmol Vis Sci,* 50**,** 4368-78.

MAEDA, T., MAEDA, A., LEAHY, P., SAPERSTEIN, D. A. & PALCZEWSKI, K. 2009b. Effects of long-term administration of 9-cis-retinyl acetate on visual function in mice. *Invest Ophthalmol Vis Sci,* 50**,** 322-33.

MANES, G., LEDUCQ, R., KUCHARCZAK, J., PAGES, A., SCHMITT-BERNARD, C. F. & HAMEL, C. P. 1998. Rat messenger RNA for the retinal pigment epithelium-specific protein RPE65 gradually accumulates in two weeks from late embryonic days. *FEBS Lett,* 423**,** 133-7.

MARLHENS, F., BAREIL, C., GRIFFOIN, J. M., ZRENNER, E., AMALRIC, P., ELIAOU, C., LIU, S. Y., HARRIS, E., REDMOND, T. M., ARNAUD, B., CLAUSTRES, M. & HAMEL, C. P. 1997. Mutations in RPE65 cause Leber's congenital amaurosis. *Nat Genet,* 17**,** 139-41.

MATTAPALLIL, M. J., WAWROUSEK, E. F., CHAN, C. C., ZHAO, H., ROYCHOUDHURY, J., FERGUSON, T. A. & CASPI, R. R. 2012. The Rd8 mutation of the Crb1 gene is present in vendor lines of C57BL/6N mice and embryonic stem cells, and confounds ocular induced mutant phenotypes. *Invest Ophthalmol Vis Sci,* 53**,** 2921-7.

MAYNARD, M. L., ZELE, A. J., KWAN, A. S. & FEIGL, B. 2017. Intrinsically Photosensitive Retinal Ganglion Cell Function, Sleep Efficiency and Depression in Advanced Age-Related Macular Degeneration. *Invest Ophthalmol Vis Sci,* 58**,** 990-996.

MCCALL, M. A., GREGG, R. G., MERRIMAN, K., GOTO, Y., PEACHEY, N. S. & STANFORD, L. R. 1996. Morphological and physiological consequences of the selective elimination of rod photoreceptors in transgenic mice. *Exp Eye Res,* 63**,** 35-50.

MCLEOD, D. S., GREBE, R., BHUTTO, I., MERGES, C., BABA, T. & LUTTY, G. A. 2009. Relationship between RPE and choriocapillaris in age-related macular degeneration. *Invest Ophthalmol Vis Sci,* 50**,** 4982-91.

MCLEOD, D. S., TAOMOTO, M., OTSUJI, T., GREEN, W. R., SUNNESS, J. S. & LUTTY, G. A. 2002. Quantifying changes in RPE and choroidal vasculature in eyes with age-related macular degeneration. *Invest Ophthalmol Vis Sci,* 43**,** 1986-93.

MCNEILL, D. S., SHEELY, C. J., ECKER, J. L., BADEA, T. C., MORHARDT, D., GUIDO, W. & HATTAR, S. 2011. Development of melanopsin-based irradiance detecting circuitry. *Neural Dev,* 6**,** 8.

MEAD, B., THOMPSON, A., SCHEVEN, B. A., LOGAN, A., BERRY, M. & LEADBEATER, W. 2014. Comparative evaluation of methods for estimating retinal ganglion cell loss in retinal sections and wholemounts. *PLoS One,* 9**,** e110612.

MEDAWAR, P. B. 1948. Immunity to homologous grafted skin; the fate of skin homografts transplanted to the brain, to subcutaneous tissue, and to the anterior chamber of the eye. *Br J Exp Pathol,* 29**,** 58-69.

MELYAN, Z., TARTTELIN, E. E., BELLINGHAM, J., LUCAS, R. J. & HANKINS, M. W. 2005. Addition of human melanopsin renders mammalian cells photoresponsive. *Nature,* 433**,** 741-5.

MILAM, A. H., ROSE, L., CIDECIYAN, A. V., BARAKAT, M. R., TANG, W. X., GUPTA, N., ALEMAN, T. S., WRIGHT, A. F., STONE, E. M., SHEFFIELD, V. C. & JACOBSON, S. G. 2002. The nuclear receptor NR2E3 plays a role in human retinal photoreceptor differentiation and degeneration. *Proc Natl Acad Sci U S A,* 99**,** 473-8.

MILLER, R. F. & DOWLING, J. E. 1970. Intracellular responses of the Muller (glial) cells of mudpuppy retina: their relation to b-wave of the electroretinogram. *J Neurophysiol,* 33**,** 323-41.

MISSLIN, R., BELZUNG, C. & VOGEL, E. 1989. Behavioural validation of a light/dark choice procedure for testing anti-anxiety agents. *Behav Processes,* 18**,** 119-32.

MIYAMOTO, Y. & DEL MONTE, M. A. 1994. Na(+)-dependent glutamate transporter in human retinal pigment epithelial cells. *Invest Ophthalmol Vis Sci,* 35**,** 3589-98.

MOISEYEV, G., CHEN, Y., TAKAHASHI, Y., WU, B. X. & MA, J. X. 2005. RPE65 is the isomerohydrolase in the retinoid visual cycle. *Proc Natl Acad Sci U S A,* 102**,** 12413-8.

MONES, J., LEIVA, M., PENA, T., MARTINEZ, G., BIARNES, M., GARCIA, M., SERRANO, A. & FERNANDEZ, E. 2016. A Swine Model of Selective Geographic Atrophy of Outer Retinal Layers Mimicking Atrophic AMD: A Phase I Escalating Dose of Subretinal Sodium Iodate. *Invest Ophthalmol Vis Sci,* 57**,** 3974-83.

MORIMURA, H., FISHMAN, G. A., GROVER, S. A., FULTON, A. B., BERSON, E. L. & DRYJA, T. P. 1998. Mutations in the RPE65 gene in patients with autosomal recessive retinitis pigmentosa or leber congenital amaurosis. *Proc Natl Acad Sci U S A,* 95**,** 3088-93.

MORIMURA, H., SAINDELLE-RIBEAUDEAU, F., BERSON, E. L. & DRYJA, T. P. 1999. Mutations in RGR, encoding a light-sensitive opsin homologue, in patients with retinitis pigmentosa. *Nat Genet,* 23**,** 393-4.

MORIN, L. P., BLANCHARD, J. H. & PROVENCIO, I. 2003. Retinal ganglion cell projections to the hamster suprachiasmatic nucleus, intergeniculate leaflet, and visual midbrain: bifurcation and melanopsin immunoreactivity. *J Comp Neurol,* 465**,** 401-16.

MOSELEY, H., FOULDS, W. S., ALLAN, D. & KYLE, P. M. 1984. Routes of clearance of radioactive water from the rabbit vitreous. *Br J Ophthalmol,* 68**,** 145-51.

MROSOVSKY, N., FOSTER, R. G. & SALMON, P. A. 1999. Thresholds for masking responses to light in three strains of retinally degenerate mice. *J Comp Physiol A,* 184**,** 423-8.

MROSOVSKY, N. & HATTAR, S. 2003. Impaired masking responses to light in melanopsin-knockout mice. *Chronobiol Int,* 20**,** 989-99.

NADAL-NICOLAS, F. M., JIMENEZ-LOPEZ, M., SOBRADO-CALVO, P., NIETO-LOPEZ, L., CANOVAS-MARTINEZ, I., SALINAS-NAVARRO, M., VIDAL-SANZ, M. & AGUDO, M. 2009. Brn3a as a marker of retinal ganglion cells: qualitative and quantitative time course studies in naive and optic nerve-injured retinas. *Invest Ophthalmol Vis Sci,* 50**,** 3860-8.

NAGAI, T., IBATA, K., PARK, E. S., KUBOTA, M., MIKOSHIBA, K. & MIYAWAKI, A. 2002. A variant of yellow fluorescent protein with fast and efficient maturation for cell-biological applications. *Nat Biotechnol,* 20**,** 87-90.

NAGATA, K., OHASHI, K., NAKANO, T., ARITA, H., ZONG, C., HANAFUSA, H. & MIZUNO, K. 1996. Identification of the product of growth arrest-specific gene 6 as a common ligand for Axl, Sky, and Mer receptor tyrosine kinases. *J Biol Chem,* 271**,** 30022-7.

NAGELHUS, E. A., HORIO, Y., INANOBE, A., FUJITA, A., HAUG, F. M., NIELSEN, S., KURACHI, Y. & OTTERSEN, O. P. 1999. Immunogold evidence suggests that coupling of K+ siphoning and

water transport in rat retinal Muller cells is mediated by a coenrichment of Kir4.1 and AQP4 in specific membrane domains. *Glia,* 26**,** 47-54.

NAKAMURA, Y., MCGUIRE, B. A. & STERLING, P. 1980. Interplexiform cell in cat retina: identification by uptake of gamma-[3H]aminobutyric acid and serial reconstruction. *Proc Natl Acad Sci U S A,* 77**,** 658-61.

NAKANO, T., ISHIMOTO, Y., KISHINO, J., UMEDA, M., INOUE, K., NAGATA, K., OHASHI, K., MIZUNO, K. & ARITA, H. 1997. Cell adhesion to phosphatidylserine mediated by a product of growth arrest-specific gene 6. *J Biol Chem,* 272**,** 29411-4.

NANDROT, E. F., KIM, Y., BRODIE, S. E., HUANG, X., SHEPPARD, D. & FINNEMANN, S. C. 2004. Loss of synchronized retinal phagocytosis and age-related blindness in mice lacking alphavbeta5 integrin. *J Exp Med,* 200**,** 1539-45.

NILSSON, S. E., KNAVE, B. & PERSSON, H. E. 1977. Changes in ultrastructure and function of the sheep pigment epithelium and retina induced by sodium iodate. II. Early effects. *Acta Ophthalmol (Copenh),* 55**,** 1007-26.

NIR, I., HAQUE, R. & IUVONE, P. M. 2000. Diurnal metabolism of dopamine in the mouse retina. *Brain Res,* 870**,** 118-25.

NISHIMURA, T., ZHU, Z. R. & RYAN, S. J. 1990. Effects of sodium iodate on experimental subretinal neovascularization in the primate. *Ophthalmologica,* 200**,** 28-38.

NOMMISTE, B., FYNES, K., TOVELL, V. E., RAMSDEN, C., DA CRUZ, L. & COFFEY, P. 2017. Stem cell-derived retinal pigment epithelium transplantation for treatment of retinal disease. *Prog Brain Res,* 231**,** 225-244.

NUSINOWITZ, S., RIDDER, W. H., 3RD, PANG, J. J., CHANG, B., NOORWEZ, S. M., KAUSHAL, S., HAUSWIRTH, W. W. & HECKENLIVELY, J. R. 2006. Cortical visual function in the rd12 mouse model of Leber Congenital Amarousis (LCA) after gene replacement therapy to restore retinal function. *Vision Res,* 46**,** 3926-34.

O'DAY, W. T. & YOUNG, R. W. 1978. Rhythmic daily shedding of outer-segment membranes by visual cells in the goldfish. *J Cell Biol,* 76**,** 593-604.

OHTAKA, K., MACHIDA, S., OHZEKI, T., TANAKA, M., KUROSAKA, D., MASUDA, T. & ISHII, T. 2006. Protective effect of hepatocyte growth factor against degeneration of the retinal pigment epithelium and photoreceptor in sodium iodate-injected rats. *Curr Eye Res,* 31**,** 347-55.

ORTIN-MARTINEZ, A., JIMENEZ-LOPEZ, M., NADAL-NICOLAS, F. M., SALINAS-NAVARRO, M., ALARCON-MARTINEZ, L., SAUVE, Y., VILLEGAS-PEREZ, M. P., VIDAL-SANZ, M. & AGUDO-BARRIUSO, M. 2010. Automated quantification and topographical distribution of the whole population of S- and L-cones in adult albino and pigmented rats. *Invest Ophthalmol Vis Sci,* 51**,** 3171-83.

ORTIN-MARTINEZ, A., NADAL-NICOLAS, F. M., JIMENEZ-LOPEZ, M., ALBURQUERQUE-BEJAR, J. J., NIETO-LOPEZ, L., GARCIA-AYUSO, D., VILLEGAS-PEREZ, M. P., VIDAL-SANZ, M. & AGUDO-BARRIUSO, M. 2014. Number and distribution of mouse retinal cone photoreceptors: differences between an albino (Swiss) and a pigmented (C57/BL6) strain. *PLoS One,* 9**,** e102392.

OSTWALD, T. J. & STEINBERG, R. H. 1980. Localization of frog retinal pigment epithelium Na+-K+ ATPase. *Exp Eye Res,* 31**,** 351-60.

OZAKI, K., NAGATANI, H., OZAKI, M. & TOKUNAGA, F. 1993. Maturation of major Drosophila rhodopsin, ninaE, requires chromophore 3-hydroxyretinal. *Neuron,* 10**,** 1113-9.

OZAWA, M., BARIBAULT, H. & KEMLER, R. 1989. The cytoplasmic domain of the cell adhesion molecule uvomorulin associates with three independent proteins structurally related in different species. *Embo j,* 8**,** 1711-7.

PANDA, S., NAYAK, S. K., CAMPO, B., WALKER, J. R., HOGENESCH, J. B. & JEGLA, T. 2005. Illumination of the melanopsin signaling pathway. *Science,* 307**,** 600-4.

PANG, J., BOYE, S. E., LEI, B., BOYE, S. L., EVERHART, D., RYALS, R., UMINO, Y., ROHRER, B., ALEXANDER, J., LI, J., DAI, X., LI, Q., CHANG, B., BARLOW, R. & HAUSWIRTH, W. W. 2010.

Self-complementary AAV-mediated gene therapy restores cone function and prevents cone degeneration in two models of Rpe65 deficiency. *Gene Ther,* 17**,** 815-26.

PANG, J. J., CHANG, B., HAWES, N. L., HURD, R. E., DAVISSON, M. T., LI, J., NOORWEZ, S. M., MALHOTRA, R., MCDOWELL, J. H., KAUSHAL, S., HAUSWIRTH, W. W., NUSINOWITZ, S., THOMPSON, D. A. & HECKENLIVELY, J. R. 2005. Retinal degeneration 12 (rd12): a new, spontaneously arising mouse model for human Leber congenital amaurosis (LCA). *Mol Vis,* 11**,** 152-62.

PANG, J. J., CHANG, B., KUMAR, A., NUSINOWITZ, S., NOORWEZ, S. M., LI, J., RANI, A., FOSTER, T. C., CHIODO, V. A., DOYLE, T., LI, H., MALHOTRA, R., TEUSNER, J. T., MCDOWELL, J. H., MIN, S. H., LI, Q., KAUSHAL, S. & HAUSWIRTH, W. W. 2006. Gene therapy restores vision-dependent behavior as well as retinal structure and function in a mouse model of RPE65 Leber congenital amaurosis. *Mol Ther,* 13**,** 565-72.

PAQUES, M., SIMONUTTI, M., AUGUSTIN, S., GOUPILLE, O., EL MATHARI, B. & SAHEL, J. A. 2010. In vivo observation of the locomotion of microglial cells in the retina. *Glia,* 58**,** 1663-8.

PARKER, R. O. & CROUCH, R. K. 2010. The interphotoreceptor retinoid binding (IRBP) is essential for normal retinoid processing in cone photoreceptors. *Adv Exp Med Biol,* 664**,** 141-9.

PARKER, R. O., FAN, J., NICKERSON, J. M., LIOU, G. I. & CROUCH, R. K. 2009. Normal cone function requires the interphotoreceptor retinoid binding protein. *J Neurosci,* 29**,** 4616-21.

PETRUS-REURER, S., BARTUMA, H., ARONSSON, M., WESTMAN, S., LANNER, F., ANDRE, H. & KVANTA, A. 2017. Integration of Subretinal Suspension Transplants of Human Embryonic Stem Cell-Derived Retinal Pigment Epithelial Cells in a Large-Eyed Model of Geographic Atrophy. *Invest Ophthalmol Vis Sci,* 58**,** 1314-1322.

PHILP, A. R., JIN, M., LI, S., SCHINDLER, E. I., IANNACCONE, A., LAM, B. L., WELEBER, R. G., FISHMAN, G. A., JACOBSON, S. G., MULLINS, R. F., TRAVIS, G. H. & STONE, E. M. 2009. Predicting the pathogenicity of RPE65 mutations. *Hum Mutat,* 30**,** 1183-8.

PITTLER, S. J. & BAEHR, W. 1991. Identification of a nonsense mutation in the rod photoreceptor cGMP phosphodiesterase beta-subunit gene of the rd mouse. *Proc Natl Acad Sci U S A,* 88**,** 8322-6.

POLANS, A., BAEHR, W. & PALCZEWSKI, K. 1996. Turned on by Ca2+! The physiology and pathology of Ca(2+)-binding proteins in the retina. *Trends Neurosci,* 19**,** 547-54.

PROVENCIO, I., JIANG, G., DE GRIP, W. J., HAYES, W. P. & ROLLAG, M. D. 1998. Melanopsin: An opsin in melanophores, brain, and eye. *Proc Natl Acad Sci U S A,* 95**,** 340-5.

PROVENCIO, I., RODRIGUEZ, I. R., JIANG, G., HAYES, W. P., MOREIRA, E. F. & ROLLAG, M. D. 2000. A novel human opsin in the inner retina. *J Neurosci,* 20**,** 600-5.

PURRIER, N., ENGELAND, W. C. & KOFUJI, P. 2014. Mice deficient of glutamatergic signaling from intrinsically photosensitive retinal ganglion cells exhibit abnormal circadian photoentrainment. *PLoS One,* 9**,** e111449.

RADU, R. A., HU, J., PENG, J., BOK, D., MATA, N. L. & TRAVIS, G. H. 2008. Retinal pigment epithelium-retinal G protein receptor-opsin mediates light-dependent translocation of all-trans-retinyl esters for synthesis of visual chromophore in retinal pigment epithelial cells. *J Biol Chem,* 283**,** 19730-8.

RAMRATTAN, R. S., VAN DER SCHAFT, T. L., MOOY, C. M., DE BRUIJN, W. C., MULDER, P. G. & DE JONG, P. T. 1994. Morphometric analysis of Bruch's membrane, the choriocapillaris, and the choroid in aging. *Invest Ophthalmol Vis Sci,* 35**,** 2857-64.

REARDON, S. & CYRANOSKI, D. 2014. Japan stem-cell trial stirs envy. *Nature,* 513**,** 287-8.

REDFERN, W. S., STOREY, S., TSE, K., HUSSAIN, Q., MAUNG, K. P., VALENTIN, J. P., AHMED, G., BIGLEY, A., HEATHCOTE, D. & MCKAY, J. S. 2011. Evaluation of a convenient method of assessing rodent visual function in safety pharmacology studies: effects of sodium iodate on visual acuity and retinal morphology in albino and pigmented rats and mice. *J Pharmacol Toxicol Methods,* 63**,** 102-14.

REDMOND, T. M., POLIAKOV, E., YU, S., TSAI, J. Y., LU, Z. & GENTLEMAN, S. 2005. Mutation of key residues of RPE65 abolishes its enzymatic role as isomerohydrolase in the visual cycle. *Proc Natl Acad Sci U S A,* 102**,** 13658-63.

REDMOND, T. M., YU, S., LEE, E., BOK, D., HAMASAKI, D., CHEN, N., GOLETZ, P., MA, J. X., CROUCH, R. K. & PFEIFER, K. 1998. Rpe65 is necessary for production of 11-cis-vitamin A in the retinal visual cycle. *Nat Genet,* 20**,** 344-51.

RIVAS, M. A. & VECINO, E. 2009. Animal models and different therapies for treatment of retinitis pigmentosa. *Histol Histopathol,* 24**,** 1295-322.

ROBERTS, W. G. & PALADE, G. E. 1995. Increased microvascular permeability and endothelial fenestration induced by vascular endothelial growth factor. *J Cell Sci,* 108 (Pt 6)**,** 2369-79.

RODERICK, T. H., CHANG, B., HAWES, N. L. & HECKENLIVELY, J. R. 1997. A new dominant retinal degeneration (Rd4) associated with a chromosomal inversion in the mouse. *Genomics,* 42**,** 393-6.

ROHRER, B., LOHR, H. R., HUMPHRIES, P., REDMOND, T. M., SEELIGER, M. W. & CROUCH, R. K. 2005. Cone opsin mislocalization in Rpe65-/- mice: a defect that can be corrected by 11-cis retinal. *Invest Ophthalmol Vis Sci,* 46**,** 3876-82.

ROORDA, A., METHA, A. B., LENNIE, P. & WILLIAMS, D. R. 2001. Packing arrangement of the three cone classes in primate retina. *Vision Res,* 41**,** 1291-306.

SAKAMOTO, K., LIU, C. & TOSINI, G. 2004. Classical photoreceptors regulate melanopsin mRNA levels in the rat retina. *J Neurosci,* 24**,** 9693-7.

SALINAS-NAVARRO, M., JIMENEZ-LOPEZ, M., VALIENTE-SORIANO, F. J., ALARCON-MARTINEZ, L., AVILES-TRIGUEROS, M., MAYOR, S., HOLMES, T., LUND, R. D., VILLEGAS-PEREZ, M. P. & VIDAL-SANZ, M. 2009. Retinal ganglion cell population in adult albino and pigmented mice: a computerized analysis of the entire population and its spatial distribution. *Vision Res,* 49**,** 637-47.

SAMARDZIJA, M., TANIMOTO, N., KOSTIC, C., BECK, S., OBERHAUSER, V., JOLY, S., THIERSCH, M., FAHL, E., ARSENIJEVIC, Y., VON LINTIG, J., WENZEL, A., SEELIGER, M. W. & GRIMM, C. 2009. In conditions of limited chromophore supply rods entrap 11-cis-retinal leading to loss of cone function and cell death. *Hum Mol Genet,* 18**,** 1266-75.

SANYAL, S., DE RUITER, A. & HAWKINS, R. K. 1980. Development and degeneration of retina in rds mutant mice: light microscopy. *J Comp Neurol,* 194**,** 193-207.

SCHMIDT, T. M., ALAM, N. M., CHEN, S., KOFUJI, P., LI, W., PRUSKY, G. T. & HATTAR, S. 2014. A role for melanopsin in alpha retinal ganglion cells and contrast detection. *Neuron,* 82**,** 781-8.

SCHMIDT, T. M., CHEN, S. K. & HATTAR, S. 2011. Intrinsically photosensitive retinal ganglion cells: many subtypes, diverse functions. *Trends Neurosci,* 34**,** 572-80.

SCHMIDT, T. M. & KOFUJI, P. 2010. Differential cone pathway influence on intrinsically photosensitive retinal ganglion cell subtypes. *J Neurosci,* 30**,** 16262-71.

SCHMIDT, T. M. & KOFUJI, P. 2011. Structure and function of bistratified intrinsically photosensitive retinal ganglion cells in the mouse. *J Comp Neurol,* 519**,** 1492-504.

SCHMIDT, T. M., TANIGUCHI, K. & KOFUJI, P. 2008. Intrinsic and extrinsic light responses in melanopsin-expressing ganglion cells during mouse development. *J Neurophysiol,* 100**,** 371-84.

SCHOLL, H. P., MOORE, A. T., KOENEKOOP, R. K., WEN, Y., FISHMAN, G. A., VAN DEN BORN, L. I., BITTNER, A., BOWLES, K., FLETCHER, E. C., COLLISON, F. T., DAGNELIE, G., DEGLI EPOSTI, S., MICHAELIDES, M., SAPERSTEIN, D. A., SCHUCHARD, R. A., BARNES, C., ZEIN, W., ZOBOR, D., BIRCH, D. G., MENDOLA, J. D. & ZRENNER, E. 2015. Safety and Proof-of-Concept Study of Oral QLT091001 in Retinitis Pigmentosa Due to Inherited Deficiencies of Retinal Pigment Epithelial 65 Protein (RPE65) or Lecithin:Retinol Acyltransferase (LRAT). *PLoS One,* 10**,** e0143846.

SCHWARTZ, S. D., HUBSCHMAN, J. P., HEILWELL, G., FRANCO-CARDENAS, V., PAN, C. K., OSTRICK, R. M., MICKUNAS, E., GAY, R., KLIMANSKAYA, I. & LANZA, R. 2012. Embryonic stem cell trials for macular degeneration: a preliminary report. *Lancet,* 379**,** 713-20.

SCHWARTZ, S. D., REGILLO, C. D., LAM, B. L., ELIOTT, D., ROSENFELD, P. J., GREGORI, N. Z., HUBSCHMAN, J. P., DAVIS, J. L., HEILWELL, G., SPIRN, M., MAGUIRE, J., GAY, R.,

BATEMAN, J., OSTRICK, R. M., MORRIS, D., VINCENT, M., ANGLADE, E., DEL PRIORE, L. V. & LANZA, R. 2015. Human embryonic stem cell-derived retinal pigment epithelium in patients with age-related macular degeneration and Stargardt's macular dystrophy: follow-up of two open-label phase 1/2 studies. *Lancet,* 385**,** 509-16.

SEATON, A. D. & TURNER, J. E. 1992. RPE transplants stabilize retinal vasculature and prevent neovascularization in the RCS rat. *Invest Ophthalmol Vis Sci,* 33**,** 83-91.

SEELIGER, M. W., GRIMM, C., STAHLBERG, F., FRIEDBURG, C., JAISSLE, G., ZRENNER, E., GUO, H., REME, C. E., HUMPHRIES, P., HOFMANN, F., BIEL, M., FARISS, R. N., REDMOND, T. M. & WENZEL, A. 2001. New views on RPE65 deficiency: the rod system is the source of vision in a mouse model of Leber congenital amaurosis. *Nat Genet,* 29**,** 70-4.

SEKARAN, S., LUPI, D., JONES, S. L., SHEELY, C. J., HATTAR, S., YAU, K. W., LUCAS, R. J., FOSTER, R. G. & HANKINS, M. W. 2005. Melanopsin-dependent photoreception provides earliest light detection in the mammalian retina. *Curr Biol,* 15**,** 1099-107.

SELIGER, H. H. 1962. Direct action of light in naturally pigmented muscle fibers. I. Action spectrum for contraction in eel iris sphincter. *J Gen Physiol,* 46**,** 333-42.

SEMO, M., GIAS, C., AHMADO, A., SUGANO, E., ALLEN, A. E., LAWRENCE, J. M., TOMITA, H., COFFEY, P. J. & VUGLER, A. A. 2010. Dissecting a role for melanopsin in behavioural light aversion reveals a response independent of conventional photoreception. *PLoS One,* 5**,** e15009.

SEMO, M., GIAS, C., AHMADO, A. & VUGLER, A. 2014. A role for the ciliary marginal zone in the melanopsin-dependent intrinsic pupillary light reflex. *Exp Eye Res,* 119**,** 8-18.

SENECHAL, A., HUMBERT, G., SURGET, M. O., BAZALGETTE, C., BAZALGETTE, C., ARNAUD, B., ARNDT, C., LAURENT, E., BRABET, P. & HAMEL, C. P. 2006. Screening genes of the retinoid metabolism: novel LRAT mutation in leber congenital amaurosis. *Am J Ophthalmol,* 142**,** 702-4.

SHEEDLO, H. J., GAUR, V., LI, L. X., SEATON, A. D. & TURNER, J. E. 1991. Transplantation to the diseased and damaged retina. *Trends Neurosci,* 14**,** 347-50.

SOKOLOV, M., LYUBARSKY, A. L., STRISSEL, K. J., SAVCHENKO, A. B., GOVARDOVSKII, V. I., PUGH, E. N., JR. & ARSHAVSKY, V. Y. 2002. Massive light-driven translocation of transducin between the two major compartments of rod cells: a novel mechanism of light adaptation. *Neuron,* 34**,** 95-106.

SORSBY, A. 1941. Experimental pigmentary degeneration of the retina by sodium iodate. *Br J Ophthalmol,* 25**,** 58-62.

STONE, E. M. 2007. Leber congenital amaurosis - a model for efficient genetic testing of heterogeneous disorders: LXIV Edward Jackson Memorial Lecture. *Am J Ophthalmol,* 144**,** 791-811.

STRICK, D. J., FENG, W. & VOLLRATH, D. 2009. Mertk drives myosin II redistribution during retinal pigment epithelial phagocytosis. *Invest Ophthalmol Vis Sci,* 50**,** 2427-35.

SUGITA, S., FUTAGAMI, Y., SMITH, S. B., NAGGAR, H. & MOCHIZUKI, M. 2006. Retinal and ciliary body pigment epithelium suppress activation of T lymphocytes via transforming growth factor beta. *Exp Eye Res,* 83**,** 1459-71.

SUGITA, S., HORIE, S., NAKAMURA, O., MARUYAMA, K., TAKASE, H., USUI, Y., TAKEUCHI, M., ISHIDOH, K., KOIKE, M., UCHIYAMA, Y., PETERS, C., YAMAMOTO, Y. & MOCHIZUKI, M. 2009. Acquisition of T regulatory function in cathepsin L-inhibited T cells by eye-derived CTLA-2alpha during inflammatory conditions. *J Immunol,* 183**,** 5013-22.

SWEENEY, M. O., MCGEE, T. L., BERSON, E. L. & DRYJA, T. P. 2007. Low prevalence of lecithin retinol acyltransferase mutations in patients with Leber congenital amaurosis and autosomal recessive retinitis pigmentosa. *Mol Vis,* 13**,** 588-93.

TACHIBANAKI, S., TSUSHIMA, S. & KAWAMURA, S. 2001. Low amplification and fast visual pigment phosphorylation as mechanisms characterizing cone photoresponses. *Proc Natl Acad Sci U S A,* 98**,** 14044-9.

TAKAHASHI, K. & YAMANAKA, S. 2006. Induction of pluripotent stem cells from mouse embryonic and adult fibroblast cultures by defined factors. *Cell,* 126**,** 663-76.

TANG, P. H., BUHUSI, M. C., MA, J. X. & CROUCH, R. K. 2011. RPE65 is present in human green/red cones and promotes photopigment regeneration in an in vitro cone cell model. *J Neurosci,* 31**,** 18618-26.

TANG, P. H., FAN, J., GOLETZ, P. W., WHELESS, L. & CROUCH, R. K. 2010. Effective and sustained delivery of hydrophobic retinoids to photoreceptors. *Invest Ophthalmol Vis Sci,* 51**,** 5958-64.

TAO, Z., DAI, J., HE, J., LI, C., LI, Y. & YIN, Z. Q. 2013. The influence of NaIO(3)-induced retinal degeneration on intra-retinal layer and the changes of expression profile/morphology of DA-ACs and mRGCS. *Mol Neurobiol,* 47**,** 241-60.

TAYLOR, A. W., STREILEIN, J. W. & COUSINS, S. W. 1992. Identification of alpha-melanocyte stimulating hormone as a potential immunosuppressive factor in aqueous humor. *Curr Eye Res,* 11**,** 1199-206.

TAYLOR, A. W., STREILEIN, J. W. & COUSINS, S. W. 1994. Immunoreactive vasoactive intestinal peptide contributes to the immunosuppressive activity of normal aqueous humor. *J Immunol,* 153**,** 1080-6.

TAYLOR, A. W. & YEE, D. G. 2003. Somatostatin is an immunosuppressive factor in aqueous humor. *Invest Ophthalmol Vis Sci,* 44**,** 2644-9.

TAYLOR, A. W., YEE, D. G. & STREILEIN, J. W. 1998. Suppression of nitric oxide generated by inflammatory macrophages by calcitonin gene-related peptide in aqueous humor. *Invest Ophthalmol Vis Sci,* 39**,** 1372-8.

TEXTORIUS, O., WELINDER, E. & NILSSON, S. E. 1985. Combined effects of DL-alpha-aminoadipic acid with sodium iodate, ethyl alcohol, or light stimulation on the ERG c-wave and on the standing potential of albino rabbit eyes. *Doc Ophthalmol,* 60**,** 393-400.

TEZEL, T. H. & DEL PRIORE, L. V. 1997. Reattachment to a substrate prevents apoptosis of human retinal pigment epithelium. *Graefes Arch Clin Exp Ophthalmol,* 235**,** 41-7.

TEZEL, T. H., DEL PRIORE, L. V. & KAPLAN, H. J. 2004. Reengineering of aged Bruch's membrane to enhance retinal pigment epithelium repopulation. *Invest Ophthalmol Vis Sci,* 45**,** 3337-48.

THOMPSON, D. A., KHAN, N. W., OTHMAN, M. I., CHANG, B., JIA, L., GRAHEK, G., WU, Z., HIRIYANNA, S., NELLISSERY, J., LI, T., KHANNA, H., COLOSI, P., SWAROOP, A. & HECKENLIVELY, J. R. 2012. Rd9 is a naturally occurring mouse model of a common form of retinitis pigmentosa caused by mutations in RPGR-ORF15. *PLoS One,* 7**,** e35865.

THOMPSON, S., MULLINS, R. F., PHILP, A. R., STONE, E. M. & MROSOVSKY, N. 2008. Divergent phenotypes of vision and accessory visual function in mice with visual cycle dysfunction (Rpe65 rd12) or retinal degeneration (rd/rd). *Invest Ophthalmol Vis Sci,* 49**,** 2737-42.

THOMSON, J. A., ITSKOVITZ-ELDOR, J., SHAPIRO, S. S., WAKNITZ, M. A., SWIERGIEL, J. J., MARSHALL, V. S. & JONES, J. M. 1998. Embryonic stem cell lines derived from human blastocysts. *Science,* 282**,** 1145-7.

TORNQUIST, P., ALM, A. & BILL, A. 1990. Permeability of ocular vessels and transport across the blood-retinal-barrier. *Eye (Lond),* 4 (Pt 2)**,** 303-9.

TU, D. C., BATTEN, M. L., PALCZEWSKI, K. & VAN GELDER, R. N. 2004. Nonvisual photoreception in the chick iris. *Science,* 306**,** 129-31.

TU, D. C., OWENS, L. A., ANDERSON, L., GOLCZAK, M., DOYLE, S. E., MCCALL, M., MENAKER, M., PALCZEWSKI, K. & VAN GELDER, R. N. 2006. Inner retinal photoreception independent of the visual retinoid cycle. *Proc Natl Acad Sci U S A,* 103**,** 10426-31.

VALIENTE-SORIANO, F. J., GARCIA-AYUSO, D., ORTIN-MARTINEZ, A., JIMENEZ-LOPEZ, M., GALINDO-ROMERO, C., VILLEGAS-PEREZ, M. P., AGUDO-BARRIUSO, M., VUGLER, A. A. & VIDAL-SANZ, M. 2014. Distribution of melanopsin positive neurons in pigmented and albino mice: evidence for melanopsin interneurons in the mouse retina. *Front Neuroanat,* 8**,** 131.

VAN HOOSER, J. P., ALEMAN, T. S., HE, Y. G., CIDECIYAN, A. V., KUKSA, V., PITTLER, S. J., STONE, E. M., JACOBSON, S. G. & PALCZEWSKI, K. 2000. Rapid restoration of visual pigment and

function with oral retinoid in a mouse model of childhood blindness. *Proc Natl Acad Sci U S A,* 97**,** 8623-8.

VAN MEURS, J. C. & VAN DEN BIESEN, P. R. 2003. Autologous retinal pigment epithelium and choroid translocation in patients with exudative age-related macular degeneration: short-term follow-up. *Am J Ophthalmol,* 136**,** 688-95.

VINEY, T. J., BALINT, K., HILLIER, D., SIEGERT, S., BOLDOGKOI, Z., ENQUIST, L. W., MEISTER, M., CEPKO, C. L. & ROSKA, B. 2007. Local retinal circuits of melanopsin-containing ganglion cells identified by transsynaptic viral tracing. *Curr Biol,* 17**,** 981-8.

VON LEITHNER, P. L., CIURTIN, C. & JEFFERY, G. 2010. Microscopic mammalian retinal pigment epithelium lesions induce widespread proliferation with differences in magnitude between center and periphery. *Mol Vis,* 16**,** 570-81.

VUGLER, A., CARR, A. J., LAWRENCE, J., CHEN, L. L., BURRELL, K., WRIGHT, A., LUNDH, P., SEMO, M., AHMADO, A., GIAS, C., DA CRUZ, L., MOORE, H., ANDREWS, P., WALSH, J. & COFFEY, P. 2008a. Elucidating the phenomenon of HESC-derived RPE: anatomy of cell genesis, expansion and retinal transplantation. *Exp Neurol,* 214**,** 347-61.

VUGLER, A., LAWRENCE, J., WALSH, J., CARR, A., GIAS, C., SEMO, M., AHMADO, A., DA CRUZ, L., ANDREWS, P. & COFFEY, P. 2007a. Embryonic stem cells and retinal repair. *Mech Dev,* 124**,** 807-29.

VUGLER, A., SEMO, M., ORTIN-MARTINEZ, A., ROJANASAKUL, A., NOMMISTE, B., VALIENTE-SORIANO, F. J., GARCIA-AYUSO, D., COFFEY, P., VIDAL-SANZ, M. & GIAS, C. 2015. A role for the outer retina in development of the intrinsic pupillary light reflex in mice. *Neuroscience,* 286**,** 60-78.

VUGLER, A. A., REDGRAVE, P., SEMO, M., LAWRENCE, J., GREENWOOD, J. & COFFEY, P. J. 2007b. Dopamine neurones form a discrete plexus with melanopsin cells in normal and degenerating retina. *Exp Neurol,* 205**,** 26-35.

VUGLER, A. A., SEMO, M., JOSEPH, A. & JEFFERY, G. 2008b. Survival and remodeling of melanopsin cells during retinal dystrophy. *Vis Neurosci,* 25**,** 125-38.

WANG, J., IACOVELLI, J., SPENCER, C. & SAINT-GENIEZ, M. 2014. Direct effect of sodium iodate on neurosensory retina. *Invest Ophthalmol Vis Sci,* 55**,** 1941-53.

WANG, J. S. & KEFALOV, V. J. 2011. The cone-specific visual cycle. *Prog Retin Eye Res,* 30**,** 115-28.

WANG, Q., CHEN, Q., ZHAO, K., WANG, L., WANG, L. & TRABOULSI, E. I. 2001. Update on the molecular genetics of retinitis pigmentosa. *Ophthalmic Genet,* 22**,** 133-54.

WANG, Q., YUE, W. W. S., JIANG, Z., XUE, T., KANG, S. H., BERGLES, D. E., MIKOSHIBA, K., OFFERMANNS, S. & YAU, K. W. 2017. Synergistic Signaling by Light and Acetylcholine in Mouse Iris Sphincter Muscle. *Curr Biol,* 27**,** 1791-1800.e5.

WANG, S., GIRMAN, S., LU, B., BISCHOFF, N., HOLMES, T., SHEARER, R., WRIGHT, L. S., SVENDSEN, C. N., GAMM, D. M. & LUND, R. D. 2008. Long-term vision rescue by human neural progenitors in a rat model of photoreceptor degeneration. *Invest Ophthalmol Vis Sci,* 49**,** 3201-6.

WANG, S., LU, B., WOOD, P. & LUND, R. D. 2005. Grafting of ARPE-19 and Schwann cells to the subretinal space in RCS rats. *Invest Ophthalmol Vis Sci,* 46**,** 2552-60.

WENG, S., ESTEVEZ, M. E. & BERSON, D. M. 2013. Mouse ganglion-cell photoreceptors are driven by the most sensitive rod pathway and by both types of cones. *PLoS One,* 8**,** e66480.

WENKEL, H. & STREILEIN, J. W. 1998. Analysis of immune deviation elicited by antigens injected into the subretinal space. *Invest Ophthalmol Vis Sci,* 39**,** 1823-34.

WENKEL, H. & STREILEIN, J. W. 2000. Evidence that retinal pigment epithelium functions as an immune-privileged tissue. *Invest Ophthalmol Vis Sci,* 41**,** 3467-73.

WILDEN, U., HALL, S. W. & KUHN, H. 1986. Phosphodiesterase activation by photoexcited rhodopsin is quenched when rhodopsin is phosphorylated and binds the intrinsic 48-kDa protein of rod outer segments. *Proc Natl Acad Sci U S A,* 83**,** 1174-8.

WOCH, G., ARAMANT, R. B., SEILER, M. J., SAGDULLAEV, B. T. & MCCALL, M. A. 2001. Retinal transplants restore visually evoked responses in rats with photoreceptor degeneration. *Invest Ophthalmol Vis Sci,* 42**,** 1669-76.

WONG, K. Y., DUNN, F. A., GRAHAM, D. M. & BERSON, D. M. 2007. Synaptic influences on rat ganglion-cell photoreceptors. *J Physiol,* 582**,** 279-96.

WRIGHT, C. B., CHRENEK, M. A., FENG, W., GETZ, S. E., DUNCAN, T., PARDUE, M. T., FENG, Y., REDMOND, T. M., BOATRIGHT, J. H. & NICKERSON, J. M. 2014. The Rpe65 rd12 allele exerts a semidominant negative effect on vision in mice. *Invest Ophthalmol Vis Sci,* 55**,** 2500-15.

XIA, H., KREBS, M. P., KAUSHAL, S. & SCOTT, E. W. 2011. Enhanced retinal pigment epithelium regeneration after injury in MRL/MpJ mice. *Exp Eye Res,* 93**,** 862-72.

XIAN, B. & HUANG, B. 2015. The immune response of stem cells in subretinal transplantation. *Stem Cell Res Ther,* 6**,** 161.

XU, X. & KARWOSKI, C. J. 1994. Current source density analysis of retinal field potentials. II. Pharmacological analysis of the b-wave and M-wave. *J Neurophysiol,* 72**,** 96-105.

XUE, T., DO, M. T., RICCIO, A., JIANG, Z., HSIEH, J., WANG, H. C., MERBS, S. L., WELSBIE, D. S., YOSHIOKA, T., WEISSGERBER, P., STOLZ, S., FLOCKERZI, V., FREICHEL, M., SIMON, M. I., CLAPHAM, D. E. & YAU, K. W. 2011. Melanopsin signalling in mammalian iris and retina. *Nature,* 479**,** 67-73.

YEE, R. & LIEBMAN, P. A. 1978. Light-activated phosphodiesterase of the rod outer segment. Kinetics and parameters of activation and deactivation. *J Biol Chem,* 253**,** 8902-9.

YOON, Y. H. & MARMOR, M. F. 1993. Retinal pigment epithelium adhesion to Bruch's membrane is weakened by hemicholinium-3 and sodium iodate. *Ophthalmic Res,* 25**,** 386-92.

YOUNG, R. W. 1967. The renewal of photoreceptor cell outer segments. *J Cell Biol,* 33**,** 61-72.

YOUNG, R. W. 1978. The daily rhythm of shedding and degradation of rod and cone outer segment membranes in the chick retina. *Invest Ophthalmol Vis Sci,* 17**,** 105-16.

YOUNG, R. W. & BOK, D. 1969. Participation of the retinal pigment epithelium in the rod outer segment renewal process. *J Cell Biol,* 42**,** 392-403.

YOUNG, R. W. & DROZ, B. 1968. The renewal of protein in retinal rods and cones. *J Cell Biol,* 39**,** 169-84.

ZHANG, D. Q., BELENKY, M. A., SOLLARS, P. J., PICKARD, G. E. & MCMAHON, D. G. 2012. Melanopsin mediates retrograde visual signaling in the retina. *PLoS One,* 7**,** e42647.

ZHANG, D. Q., WONG, K. Y., SOLLARS, P. J., BERSON, D. M., PICKARD, G. E. & MCMAHON, D. G. 2008. Intraretinal signaling by ganglion cell photoreceptors to dopaminergic amacrine neurons. *Proc Natl Acad Sci U S A,* 105**,** 14181-6.

ZHANG, J., HAWES, N. L., WANG, J., HARRIS, B. S., HURD, R. E., DAVISSON, M. T., HECKENLIVELY, J. R. & CHANG, B. 2005. A New Mouse Model of Retinal Degeneration (RD14) Associated With Neurological Defects. *Investigative Ophthalmology & Visual Science,* 46**,** 3170-3170.

ZHANG, X. & BOK, D. 1998. Transplantation of retinal pigment epithelial cells and immune response in the subretinal space. *Invest Ophthalmol Vis Sci,* 39**,** 1021-7.

ZHANG, X., WENSEL, T. G. & KRAFT, T. W. 2003. GTPase regulators and photoresponses in cones of the eastern chipmunk. *J Neurosci,* 23**,** 1287-97.

ZHAO, J., KIM, H. J. & SPARROW, J. R. 2017. Multimodal Fundus Imaging of Sodium Iodate-Treated Mice Informs RPE Susceptibility and Origins of Increased Fundus Autofluorescence. *Invest Ophthalmol Vis Sci,* 58**,** 2152-2159.

ZHAO, X., PACK, W., KHAN, N. W. & WONG, K. Y. 2016. Prolonged Inner Retinal Photoreception Depends on the Visual Retinoid Cycle. *J Neurosci,* 36**,** 4209-17.

ZHAO, X., STAFFORD, B. K., GODIN, A. L., KING, W. M. & WONG, K. Y. 2014. Photoresponse diversity among the five types of intrinsically photosensitive retinal ganglion cells. *J Physiol,* 592**,** 1619-36.

ZHENG, Q., REN, Y., TZEKOV, R., HUA, S., LI, M., PANG, J., QU, J. & LI, W. 2015. iTRAQ-Based Proteomic Analysis of Visual Cycle-Associated Proteins in RPE of rd12 Mice before and after RPE65 Gene Delivery. *J Ophthalmol,* 2015**,** 918473.

ZHU, Y., CARIDO, M., MEINHARDT, A., KURTH, T., KARL, M. O., ADER, M. & TANAKA, E. M. 2013. Three-dimensional neuroepithelial culture from human embryonic stem cells and its use for quantitative conversion to retinal pigment epithelium. *PLoS One,* 8**,** e54552.

ZNOIKO, S. L., CROUCH, R. K., MOISEYEV, G. & MA, J. X. 2002. Identification of the RPE65 protein in mammalian cone photoreceptors. *Invest Ophthalmol Vis Sci,* 43**,** 1604-9.

ZNOIKO, S. L., ROHRER, B., LU, K., LOHR, H. R., CROUCH, R. K. & MA, J. X. 2005. Downregulation of cone-specific gene expression and degeneration of cone photoreceptors in the Rpe65-/- mouse at early ages. *Invest Ophthalmol Vis Sci,* 46**,** 1473-9.